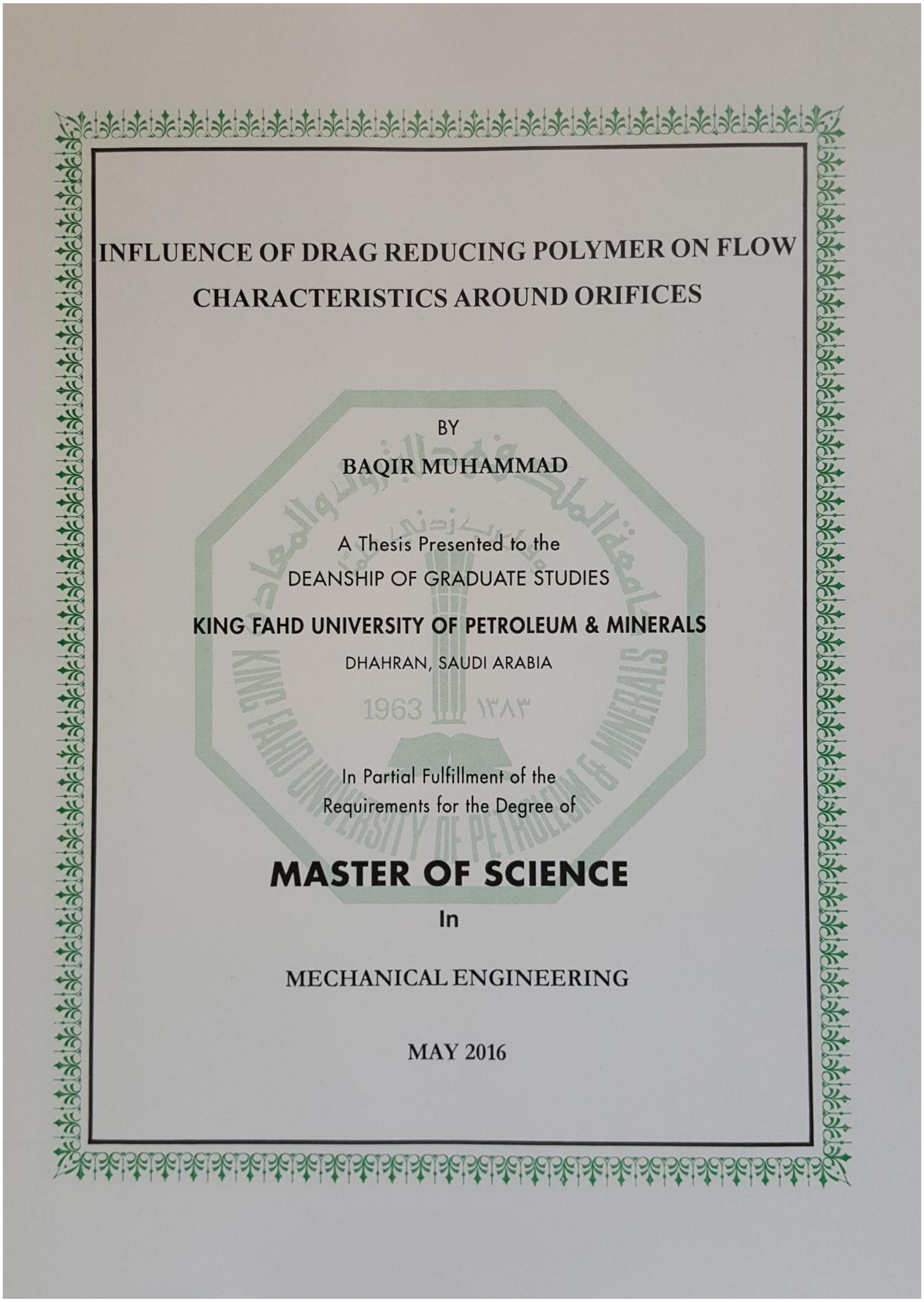

INFLUENCE OF DRAG REDUCING POLYMER ON FLOW CHARACTERISTICS AROUND ORIFICES

BY

BAQIR MUHAMMAD

A Thesis Presented to the
DEANSHIP OF GRADUATE STUDIES

KING FAHD UNIVERSITY OF PETROLEUM & MINERALS
DHAHRAN, SAUDI ARABIA

In Partial Fulfillment of the
Requirements for the Degree of

MASTER OF SCIENCE
In

MECHANICAL ENGINEERING

MAY 2016

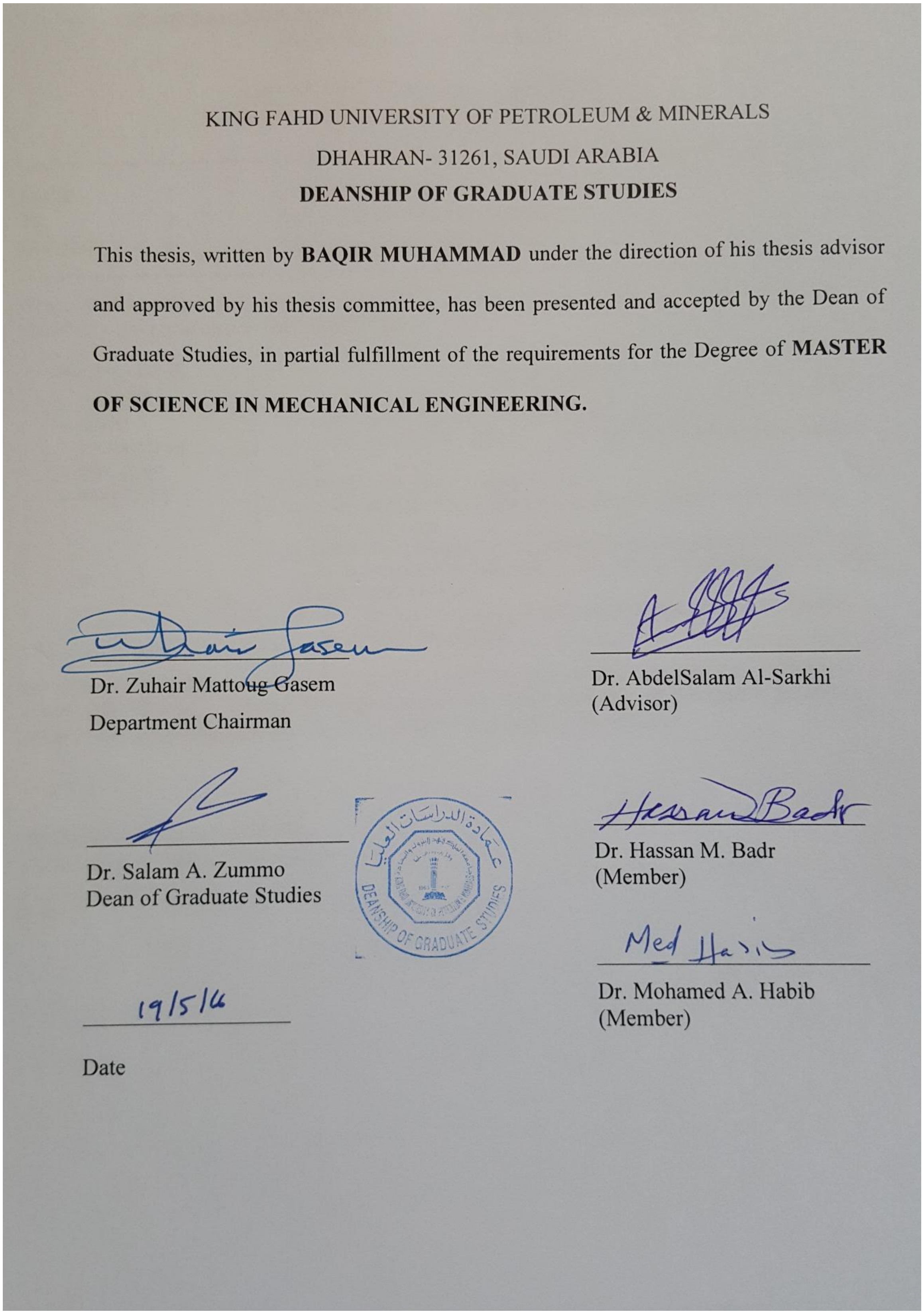

KING FAHD UNIVERSITY OF PETROLEUM & MINERALS
DHAHRAN- 31261, SAUDI ARABIA
DEANSHIP OF GRADUATE STUDIES

This thesis, written by **BAQIR MUHAMMAD** under the direction of his thesis advisor and approved by his thesis committee, has been presented and accepted by the Dean of Graduate Studies, in partial fulfillment of the requirements for the Degree of **MASTER OF SCIENCE IN MECHANICAL ENGINEERING.**

Zuhair Gasem

Dr. Zuhair Mattoug Gasem
Department Chairman

Dr. AbdelSalam Al-Sarkhi
(Advisor)

Dr. Salam A. Zummo
Dean of Graduate Studies

Hassan Badr

Dr. Hassan M. Badr
(Member)

Med Habib

Dr. Mohamed A. Habib
(Member)

19/5/16

Date

Dedicated to

My Beloved Parents.

ACKNOWLEDGMENTS

All gratitude and praises are to Almighty Allah who bestowed me the audacity to fulfill my commitment towards my thesis. Peace and blessings be upon the last and final messenger Prophet Muhammad (PBUH), his family and companions.

I wish to thank KFUPM for giving me the opportunity to pursue graduate studies and providing tremendous research facilities during the course of my MS degree.

I want to acknowledge my sincere gratitude to all those who have given their kind support towards the success of this study. It is matter of great pleasure and honor to express my deep sense of gratitude for the continuous guidance and precious advices given by my thesis advisor Dr. Abdelsalam Al-Sarkhi. He has been a constant source of enormous motivation and enthusiastic support throughout the span of the thesis. Due to his compassionate benefaction and competent coaching, I have been able to finish this thesis.

I am also thankful to my thesis committee members, Dr. Hassan M. Badr and Dr. Mohamed A. Habib, for their recommendations, productive criticism, and support which were of utmost significance. Their valuable suggestions and counseling helped me in achieving my objectives.

I owe ample credit to Mr. Bahaa Hasan, Mr. Ihab H. Alsurakji, and Mr. Abdulrazaq Adeniyi Araoye for their support and extended help during the research work. I also want to thank my friends for their continuous encouragement and support throughout my stay at KFUPM.

My parents and family deserves special appreciation for encouraging me to pursue my degree. Their love and affection made this journey very comfortable.

TABLE OF CONTENTS

LIST OF TABLES

LIST OF FIGURES

LIST OF NOTATIONS

Abbreviations

DR_T	Total Drag Reduction
DR_O	Drag Reduction across Orifice
DRAs	Drag Reducing Agents
DRP	Drag Reducing Polymer
PI	Polymer Injection
PIV	Particle Image Velocimetry
ANSI	American National Standard Institute
API	American Petroleum Institute
CCD	Charged Couple Device
CW	Continuous Wave
FOV	Field of View
IA	Interrogation Area
LED	Light Emitting Diode
PCC	Phantom Camera Control
SNR	Signal to Noise Ratio
C (ppm)	Concentration in parts per million.

Nomenclature

C_d	Coefficient of discharge
d	Orifice diameter
D	Pipe diameter
D_p	Particle diameter
D_r	Diameter ratio
f	Focal length
g	Acceleration due to gravity
M	Magnification
Re	Reynolds number based on inlet velocity
Δt	Time interval between successive exposure
Δx	Peak displacement
u	Average velocity
V_i	Flow inlet velocity
C_p	Coefficient of pressure
ρ	Density of fluid
ΔP_T	Total static pressure drop
ΔP_O	Pressure drop across orifice

ABSTRACT (ENGLISH)

Name: Baqir Muhammad

Title: Influence of Drag Reducing Polymer on Flow Characteristics around Orifices.

Major: Mechanical Engineering

Date: May 2016

The present study investigated the effect of drag reducing polymer (DRP) on flow characteristics in a serial arrangement of two similar bevel-edged thin orifices with same thickness but different diameter ratios and orifice spacing. The single and double orifice arrangements were experimentally investigated in one-inch diameter horizontal acrylic pipe with and without DRP using Particle Image Velocimetry (PIV) technique. The water-soluble drag reducing polymer (DRP) used was ZETAG® 8165 which is a synthetic high molecular weight polyacrylamide. Flows with DRP show comparatively less circulation zone and velocity values at low Reynolds number flows. It was found that pressure drop through orifice in case of flow with DRP was less than pressure drop without DRP and the percentage reduction in pressure drop was considerable in lower Re flows than higher Re flow. Also, the reduction in pressure drop was found to be independent of concentration of polymers. Two phase flow was also studied and little reduction in pressure drop was also observed.

Keywords: pressure drop, orifice, drag reducing polymer, two-phase flow, PIV.

ملخص الرسالة

الاسم الكامل: باقر محمد

عنوان الرسالة: تأثير البوليمر المقلل للاحتكاك على خصائص التدفق حول فتحات دائريه

التخصص: الهندسه الميكانيكيه

تاريخ الدرجة العلمية: مايو 2015

تم في هذا البحث دراسة تأثير البوليمر المقلل للاحتكاك (DRP) على خصائص التدفق من خلال فتحتان دائريتان رقيقتان متتاليتان و متماثلتان من حيث السماكة ومختلفتان من حيث نسبة القطر والمسافة بين الفتحتين. وقد تم التحقق مخبريا باستخدام فتحة واحدة وايضا فتحتين وذلك باستخدام انبوب شفاف افقي قطره بوصة واحدة بوجود البوليمر المقلل للاحتكاك تارة وبدون وجودة تارة اخرى وذلك باستخدام تقنية قياس سرعة الجسيمات بواسطة الصور (PIV) تقنية. تم استخدام البوليمر المقلل للاحتكاك والذي يذوب مع الماء (DRP) من نوع ZETAG® 8165 وهو عبارة عن مادة اصطناعية متعددة الاكريلاميد ذات وزن جزيئي عال. اظهرت النتائج انه في حالة الجريان المنخفض (رينولدز-منخفض) فان التدفق مع وجود البوليمر المقلل للاحتكاك يؤدي الى تقليل مناطق الدوامات. وقد تبين أن انخفاض الضغط من خلال فتحة في حالة تدفق بوجود البوليمر المقلل للاحتكاك كان أقل من هبوط الضغط دون وجود البوليمر المقلل للاحتكاك، وايضا تبين ان نسبة الانخفاض في نقصان الضغط كان ملحوظا في التدفقات ذات قيمة رينولدز قليلة من التدفقات ذات قيمة رينولدز عالية. أيضا، تبين ان النقصان في انخفاض الضغط مستقل عن تركيز البوليمرات. كما وتمت دراسة الجريان ثنائي الحالة ولوحظ أيضا نقصان طفيف في انخفاض الضغط.

الكلمات المفتاحية: انخفاض الضغط ، فتحه دائريه، البوليمر المقلل للاحتكاك، الجريان ثنائي الحالة، PIV

درجة الماجستير في العلوم الهندسية
جامعة الملك فهد للبترول والمعادن
الظهران – ٣١٢٦١
المملكة العربية السعودية

CHAPTER 1

INTRODUCTION

1.1. Introduction

The reduction of resistance of a liquid to a turbulent flow by the injection of certain high molecular weight polymers is a well-known phenomenon. This process of drag reduction (DR) is also observed with other substances such as surfactants and fibers. This research is only concerned with the usage of drag reducing polymers (DRP) as they have been most commonly used in industry because of their lesser usage in quantity as compared to surfactants and fibers.

Multiphase flow is often faced in numerous industrial applications such as distillation towers, pipelines, boilers, furnaces, heat exchangers, and chemical reactors. Offshore petroleum production requires transport of multiphase oil and gas flows over large distances before they are separated. This type of flow has several unique characteristics which must be investigated in each situation. One factor which is always present is the high axial pressure losses accompanying pipeline flows, hence finding sustainable solutions to increase the pumping capacity without any mechanical modification is necessary. Regarding its importance and applications, multiphase drag reduction has been investigated by many researchers. Polymers as a drag reducing agents (DRA) provide economic solution because drag reduction of about 80% can be achieved by adding a minute quantity of them. A well-known example of DRA use is the 800-mile Trans-Alaska pipeline where addition of DRA resulted in a considerable increase in the flow rate.

The phenomenon of drag reduction by using additives in Newtonian and Non-Newtonian fluids is also known as Toms phenomenon because it was discovered back in 1947 by Toms [1]. DRA's have been very beneficial in reducing frictional losses, allowing a greater production flow rate at an economical cost. The benefits of DRA use in existing systems are increased production, reduction of operating costs such as pumping power, reduction of pipeline pressure while maintaining throughput, and to facilitate refinery debottlenecking and loading unloading operations. The design benefits of DRA's in new systems are a reduction in pipeline diameter and pumping station capital costs. The deferment of capital expenditure is also of economic value where pumps are introduced at a later stage in the life of an oil field. The fields of firefighting, storm control, medicine, pipeline transportation, scale flow testing, racing and military sea going vessels have all taken an interest in the discovery.

It was proven that in the pipe flow, the DR increases with increasing concentration of DRAs and eventually reaches a knoll. Active ingredient in DRA as proposed by [2] is a high molecular weight linear poly-alpha-olefin.

The general chemical formula of the polymer is as follows:

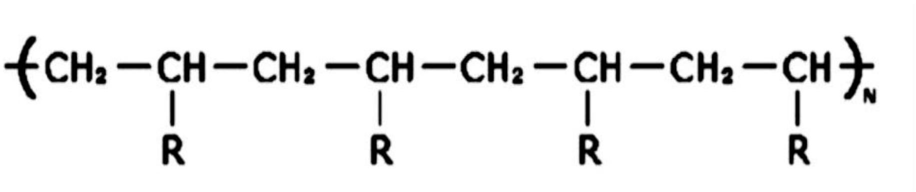

$$\left(CH_2 - \underset{\underset{R}{|}}{CH} - CH_2 - \underset{\underset{R}{|}}{CH} - CH_2 - \underset{\underset{R}{|}}{CH} - CH_2 - \underset{\underset{R}{|}}{CH} \right)_N$$

Figure 1-1 General Formula of a polymer

Where;

R: Carbon chains of various lengths.

N: Represents the repetition of the unit in parenthesis, e.g. It can range up to 1000 resulting in very high molecular weights.

Internal flows containing flow restrictions such as flowmeters are often encountered in certain engineering applications. Flowmeters are basically divided into two functional groups, positive displacement measures quantity and inferential measures rate of flow. Some of the most common quantity meters are rotating piston and vanes, reciprocating pistons and gear pumps etc. Orifice plate flow meters are grouped with flow nozzles, pitot tubes, venturi tubes and turbine meters as rate meters. Orifice plates have a number of industrial applications as flow meters and restricting orifices. Spray atomizers widely used in industries for coating, drying and fumigation purposes cannot achieve high level of atomization without cavitation induced by orifices even at large pressure difference. Pressure difference readings in liquid-gas flow through orifices and other pipe accessories is being utilized as control measures in HVAC, petrochemical industries. They are also used for metering of highly viscous liquids and quality control of products. Orifices either single or multi holes are also used to increase uniformity in flows, distribution and exchange of heat and mass. Some applications requires higher pressure drop without the occurrence of cavitation which cannot be achieved with single restricting orifices. Multiple orifices consisting of serial arrangements of restricting orifices are then employed.

The orifice is a restriction which operates by creating pressure difference between its upstream and downstream. The flow pressure decreases within the orifice, reaches its minimum at the ‘vena contracta’ and then gradually builds up towards the exit to a maximum point downward which is always lower than pressure upstream of the orifice. The pressure loss is because of friction and turbulence loss in the stream. The pressure drop is due to the increased velocity in reduced area of orifice. An orifice is said to be thick if its thickness to diameter ratio (t/d) also known as aspect ratio is greater than 0.5 otherwise, thin orifices [3]. The behavior of single phase flow passing through a thin orifice is such that it contracts to a region of minimum area downstream of the orifice known as vena contracta with minute loss of energy and irreversibly reattaches to the pipe wall further down the flow passage. In the case of a thick orifice plate, the vena contracta appears within the orifice opening with reattachment occurring twice; once with the orifice passage and second at the pipe wall downstream [4].

Orifice plate flowmeter is the most widely used flow measuring instrument because they are simple in design which gives room for flexibility in use, cheap and rugged. American Gas Association (AGA) and American Society of Mechanical Engineers (ASME) did a lot of research work between 1924 and 1935 to develop orifice meters coefficients and standards of construction. In 1935, they issued a joint report titled, “History of Orifice Meters and The Calibration, Construction, and Operation of Orifices for Metering” which is a basis for most present day orifice meters calculations. A.P.I issued its updated version in 1991. Orifice meter numerous applications are due to the wealth of data gathered over the years and documented in standards like ISO 5167, BS1042, ANSI, which allows design, construction and uncertainty calculations conveniently. Asides the simplicity in structure, reliability and longevity of the orifice plate, it differs from other inferentials such that in some applications it requires no calibration before use if manufactured and installed following standard procedures other than empirical correlation. However, results in high pressure loss which may lead to energy loss and non-linear characteristics which intensifies the effect of pulsation on readings [5], cavitation effects in liquids or critical flow in gases.

Different types of orifice plates in use are thin plate concentric, eccentric, segmental, quadrant edge and conical edge plates and there applications are guided by standard practices like the diameter ratio which must be within the limits recommended. Pressure taps formed on pipe walls provide route through which pressure measuring devices like manometers, pressure transducers access the flow. They must be made in such a way that the fluid will not be trapped in the openings. Some frequently used tap locations are flange taps in which taps are situated an inch either side of the orifice with +1/64 to +1/32 tolerance, pipe taps where taps are located 2.5D and 8D upstream and downstream respectively, vena-contracta taps at 1D upstream and at the vena contracta and corner taps having taps situated adjacently to the plate faces, upstream and downstream. Best practices for flow meter installation requires at least five diameters straight length pipe at both upstream and downstream.

The main drawback of orifice plate is the permanent loss in pressure of the stream flowing through it. Flow with drag reducing polymer can be considered as an alternate to minimize this problem. In light of this, this study is concerned with the flow through single and double orifice with and without drag reducing polymer. Pressure drop is investigated for both cases in single (water) and two phase (air-water) flow. Flow visualization is carried out using Particle Image Velocimetry (PIV) technique for single phase (water) flow. The resultant velocity profiles and streamlines are then compared.

1.2. Problem Description

The present study considered the effect of drag reducing polymer (DRP) on the flow characteristics downstream ANSI specified bevel-edged orifice/s of varying diameter ratios; 0.5, and 0.63 placed in a 1-inch ID horizontal pipe by visualization using Particle Image Velocimetry (PIV). The orifices were assumed to be placed in fully developed region of the flow by ensuring sufficient lengths of pipe upstream and downstream of the orifice plate. The upstream and the downstream pipe section had a length of about 40 and 30 times the pipe diameter respectively. In case of two orifices, orifice spacing of one and two pipe diameters were considered. The water-soluble drag reducing polymer (DRP) used was ZETAG® 8165 which is a synthetic high molecular weight polyacrylamide. Two phase (air-water) flow was also studied. The test section was fabricated with Plexiglas, fluid used was water at 303K and the orifice plates were made of Plexiglas.

1.3. Objectives

The specific objectives of this study are the following:

- To provide pressure drop (PD) data across the orifice plate(s) with and without drag reducing polymer (DRP) for single phase liquid (water) flow.
- To provide pressure drop (PD) variation across the orifice plate(s) with and without drag reducing polymer (DRP) for two phase (air-water) flow.
- To obtain the details of the flow field using Particle Image Velocimetry (PIV) for single phase with and without drag reducing polymer.
- To carry out detailed analysis of the obtained results.

CHAPTER 2

LITERATURE REVIEW

In this chapter, the principles of single and two phase flow are presented, followed by a discussion of some of the important works published in the field of drag reduction (DR) and flow through orifice, relevant to this study.

For the clarity of presentation, the literature review is divided into the following aspects:

- Drag Reduction in Pipeline
- Single Phase Flow through Orifice
- Two Phase Flow through Orifice
- Flow through Orifice with Drag Reducing Agents.

2.1. Drag Reduction in Pipeline

There has been considerable research in drag reduction in both single and two phase flows through pipelines. Two phase flow is often encountered in numerous industrial applications. Two-phase (gas-liquid) flow patterns are usually classified into three categories: Stratified flow (including smooth and wavy) is usually witnessed at low liquid and low gas velocities and is designated by two distinctive phases; liquid flowing along the bottom and gas along the top of the pipe. Intermittent flow is met at higher gas flow rates and includes both plug and slug flow. These are similar to the intermittent flow regimes seen in multiphase flow. Annular flow takes place at relatively high gas velocities and includes a core of gas flowing through the middle of the pipe surrounded by an annular film of liquid.

Experimental work has been conducted for several fluid mixtures and pipeline diameters to determine the flow regime transitions for horizontal flow. Baker [6] presented a flow regime map for small diameter pipes and for different fluids. Mandhane et al. [7] have shaped the most extensive set of experimentally determined flow regime maps. Mandhane's map is based on his 1178 flow observations for a two phase air-water flow system. Mandhane also standardized flow regime maps, plotting superficial liquid vs. superficial gas velocities.

Taitel et al. [8] suggested a physical model which can predict the transitions in flow regimes for two phase flow in horizontal pipes. Their mechanistic model considers five dimensionless groups including fluid properties, velocities, pipe diameter and inclination.

Lin et al. [9] found the pipe diameter has a crucial role in the determination of transition from stratified to slug and stratified to annular flow. He concluded that the transition from stratified to slug flow caused from the growth of small waves at gas velocities less than 3 m/s. As the gas velocity is further increased, slugs form if there is sufficient liquid in the stratified film. The diameter of pipe has a substantial effect on this transition. The transition from stratified-wavy to annular flow was revealed to be relatively independent of pipe diameter.

Jepson et al. [10] showed that the transitions from stratified to slug flow occur at relatively higher liquid velocities in larger diameter (30 cm) pipelines. The transition from slug to annular flow took place at lower gas velocities in the larger pipelines. They also have the opinion that the results from small pipe diameters could not be easily generalized to larger pipes.

Table 2-1 Two-Phase (Gas-Liquid) Flow

	Author's Name(s)/Year	Fluids type	Type of Flow Pattern	Pipe material/ geometry	Polymer used/quantity (ppm)	Parameter(s) investigated/ studied	Measurement technique(s)	Max DR (%)	Notice
Two-Phase (Gas-Liquid flow)	Greskovich, et al. [11]	Air-Water	Slug Flow	Acrylic Pipe ID=38.1mm L=6m	50 ppm polyethylene oxide coagulant (Polyox)	Pressure drop		50%	When 50 ppm Polyox is present in the liquid, the PDR tends to level off at approx. 40%
	Rosehart, et al. [12]	Air-Water	Slug Flow	ID=25.4 mm L=10.7m	68 ppm polyacrylamide (Polyhall 295)	Pressure drop	Manometer	33%	Two Phase DR was greater than single phase.
	Sylvester, et al. [13]	Air-Water	Annular Flow	Stainless steel Pipe ID= 12.7 mm L= 6.1 m	100 ppm polyethylene oxide.	Pressure drop	Pressure Transducer	37%	PDR increased with increase in liquid rate at a fixed gas rate.
	Al-Sarkhi, et al. [14]	Air-water	Annular Flow	Plexiglas Pipe ID=95.3 mm L= 10.7 m	10-15 ppm polyacrylamide & sodium-acrylate (Percol 727)	Pressure drop	U-tube Manometer	48%	At maximum DR, annular flow changed to a stratified flow.
	Al-Sarkhi, et al. [15]	Air-water	Annular Flow	ID=25.4 mm L=14 m	30 ppm Polyacrylamide & sodium-acrylate (Percol 727)	Pressure drop	U-tube Manometer	63%.	Higher concentration of DRP are required to obtain max DR.
	Soleimani, et al. [16]	Air-water	Stratified Flow	ID= 25.4 mm L=18.3 m	100 ppm polyacrylamide and sodium acrylate solution	Effect of DRP on flow patterns, Pressure drop, Hold up	Capacitance differential pressure transducer		As DRP added, the waves were decreased and liquid hold up increased.
	Baik, et al. [17]	Air-Water	Stratified Flow	Plexiglas pipe ID=95.3 mm L=23 m	50 ppm polyacrylamide (Magnafloc 101l)	Pressure drop	Differential pressure sensors	42%	Delaying the transition from stratified to slug flow.

	Al-Sarkhi, et al. [18]		Annular, Slug, and Pseudo-Slug Flow	ID= 25.4 mm L=17.0 m	50 ppm Polyacrylamide & sodium acrylate (Percol 727).	Effect of DRP on flow patterns, Pressure drop	Variable resistance differential pressure transducer		From annular, slug, or pseudo-slug to stratified flow
	Al-Sarkhi et al. [19]	Air-Water	Annular Flow	Plexiglas pipe ID = 12.7 mm L=7 m	40 ppm polyacrylamide (Magnafloc 101l)	Effect of DRP on flow patterns, Pressure drop		47%	The annular flow transferred to stratified flow pattern.
	Al-Sarkhi, et al. [20]	Air-Water	Annular Flow	1.28^0 inclined Plexiglas pipe ID = 12.7 mm L=7 m	100 ppm polyacrylamide (Magnafloc101l)	Pressure drop	U-tube manometer	71%	Annular flow was transferred to stratified or annular-stratified flow pattern.
	Wilkens et al. [21]	Air-Water	Slug Flow	PVC pipe ID=52 mm L=7m	400 ppm sodium dodecyl sulfate (SDS)	Pressure drop	Pressure Transducer	40%	Addition of SDS removed the occurrence of the slug flow.
	Fernandes, et al. [22]	Air-Water	Annular	Vertical polycarbonate pipe ID=25.4mm L=22.12 m	75 ppm polyacrylamide/ sodium acrylate (Magnaflox)	Hold-up, Pressure drop	Quick closing valve, pressure transducers	82%	An increase in the liquid holdup by 27%.
	Sylvester, et al. [23]	Natural gas-Hexane	Annular-mist	L=30.48 m ID=25.4mm, 50.8mm, 76.2mm	200 ppm Dowell APE (aluminum salt of an alkyl phosphate ester)	Effect of pipe diameter, gas & liquid flow rates, and DRA concentration	Pressure Transducer	34%	DR increased with decrease in gas rate at a fixed liquid rate

2.2. Single Phase Flow through Orifice

A great number of investigations on pipe orifice flow have been made so far. The most attended parameter for characterizing orifice flow has been the discharge coefficient. Some of other parameters are pressure drop and flow rate.

Johansen [24] did experimental investigation to calculate the discharge coefficient C_D of water through sharp edge circular orifice with the diameter ratio ranging from 0.1 to 0.75 for constant aspect ratio. The Reynolds No range was from less than 1 to 25000.

Medaugh et al. [25] built a test loop that had the capacity to measure flow rate and pressure drop across brass orifices of diameters ranging from 0.25 to 2 in. and pressure drops ranging from approximately 0.35 to 52 psi at various conditions using water as the test fluid. Orifices were constructed from 0.25 in. brass sheet.

Alvi et al. [26] did experiments for comparing flow characteristics of nozzles and sharp-edged orifices with quadrant-edged orifices. The diameter ratios are 0.2, 0.4, 0.6, and 0.8 for each geometry, and orifice Reynolds numbers were in the range of 1 to 10000. They found that at small Reynolds no, the pressure drops for sharp edge and quadrant edge orifices were similar. The quadrant edge orifices exhibit similar pressure drops as nozzles for high Reynolds no. They characterize the orifice flow in four regimes, fully laminar, critical Reynolds no, re-laminarizing, and turbulent flow regime.

Sahin et al. [27] examined incompressible flow through orifice both numerically and experimentally. The diameter ratio was 0.5 and aspect ratio was varied between 0.0625 and 1. The numerical analysis was conducted using 2-D Navier Stokes eqns. for axi-symmetric, viscous, incompressible flow across a square-edged orifice in a circular pipe.

Hasegawa et al. [28] examined thin orifices ranging from 1 mm to 10 µm in diameter. Experiments were conducted using distilled water, silicone oils, and glycerin solutions as the working fluids. The resulting pressure drop, flow rate relationship was examined for Reynolds numbers in the range of 1-1000. Additionally, numerical analysis was conducted for these same flow conditions.

Morris et al. [29] performed numerical analysis and compared the generated flow fields with laser-Doppler Velocimetry. They found good agreement between the data taken from the numerical simulation and the experimental data at Re greater than 8500 but not for Reynolds numbers of 2000 and 4000. They propose that this is due to not fully accounting for the effects of "laminar/semi-turbulent" flow fields in their model.

Mincks [30] did an experimental study to measure pressure drop characteristics of viscous fluid through small diameter orifices. He concluded that pressure drop across orifices can be shown as a function of aspect ratio (t/d), diameter ratio, and Re number. He also proposed a correlation for non-dimensional pressure drop (PD).

Mustafa [31] investigated the flow field downstream of orifice with variable aspect ratios inserted in a pipe in turbulent flow for Reynolds number ranging from 7400 to 37000 using Particle Image Velocimetry (PIV). The diameter ratio was kept constant at 0.6 while aspect ratio was varied from 1/8 to 1. The flow structure downstream of orifice plate in consecutive side view plane were presented using velocity vector maps, streamline patterns and vorticity contours.

Abdulrazaq [32] studied the erosion and flow characteristics in a serial arrangement of two similar bevel-edged thin orifice plates with different diameter ratios and orifice spacing. The single and double orifice arrangements were tested in one-inch-diameter carbon steel pipe. To verify the computational results, the flow velocity was measured using a 2D-2C PIV system. The location of vena contracta downstream of the first orifice was verified both computationally and experimentally, however the presence of vena contracta downstream of the second orifice was found to depend on the orifice spacing. Not only the flow structure between the two orifices and downstream the second orifice was found to depend on the orifice spacing but also the total pressure drop and hydraulic losses. The double orifice with one pipe diameter spacing was found to produce the least pressure drop due to reduced hydraulic losses.

Table 2-2 Single Phase Flow through Orifice

Author's Name(s)/Year	Fluids type/ Properties	Range of Re No.	Orifice geometry	Diameter Ratio (D_r=d/D)	Aspect Ratio (t/d)	Measurement technique(s)	Notice
Johansen [24]	Water, castor oil, lubricating oil	0-25000	Square-Edged with 45° Back Cut	0.1 to 0.75	≤0.083	Experimental, Visualization	Photos from dye test. Plots of C_d versus square root of Re for experiments.
Medaugh et al. [25]	Water	30,000 - 350,000	Square-Edged		≤1	Experimental	Plots of C_d versus pressure drop, plot of C_d vs. Re for high Re
Sahin et al. [27]	Oil	0-150	Square-Edged	0.5	0.0625, 1	Experimental, Computational	Numerical results agreed with the experimental ones.
Hasegawa et al. [28]	Distilled water, glycerin solution silicon oil	1-1000	Square-Edged	0.01 to 1.0	0.051-1.14	Experimental, Computational	As the dia of the orifice decreases below 0.065 mm, the numerical solution under predicts the pressure drop.
Morris et al. [29]		2000 - 23,000	Square-edged			Experimental, Visualization, Computational	Velocity profiles for various arrangements
Mincks [30]	Viscous hydraulic oil	8 – 7285	Square-edged	0.023, 0.044 and 0.137	0.33, 0.66, 1, 2, 4 and 6	Experimental	Proposed a correlation for non-dimensional pressure drop
Mustafa [31]	Water	7400-37000	Square-edged	0.6	0.125, 1	PIV	Velocity vector, streamlines, and vorticity contours are presented

2.3. Two Phase Flow through Orifice

The greater use of orifice in measuring the two phase flow is reflected in a number of papers. The main focus of the experimental work has been focused in quantifying the increase in pressure drop (PD) across the orifice as compared to single phase pressure drop. The pressure drop is then used to measure the flow rate across the orifice plate for the respective pipe geometries. Very little data exists concerning the two phase velocity distribution near the orifice.

Martha et al. [33] investigated the pressure drop through various obstructions in horizontal air water flow. Pressure loss coefficients and two phase multipliers were then developed. The test section constitutes 25.4 mm I.D. and 3 m long Lucite tube, headed by a honeycomb mixer and a 3m soothing length. The superficial air and water velocities were 29 and 0.59 m/s to get the annular flow regime. The resultant pressure distribution is shown in Figure 2-1.

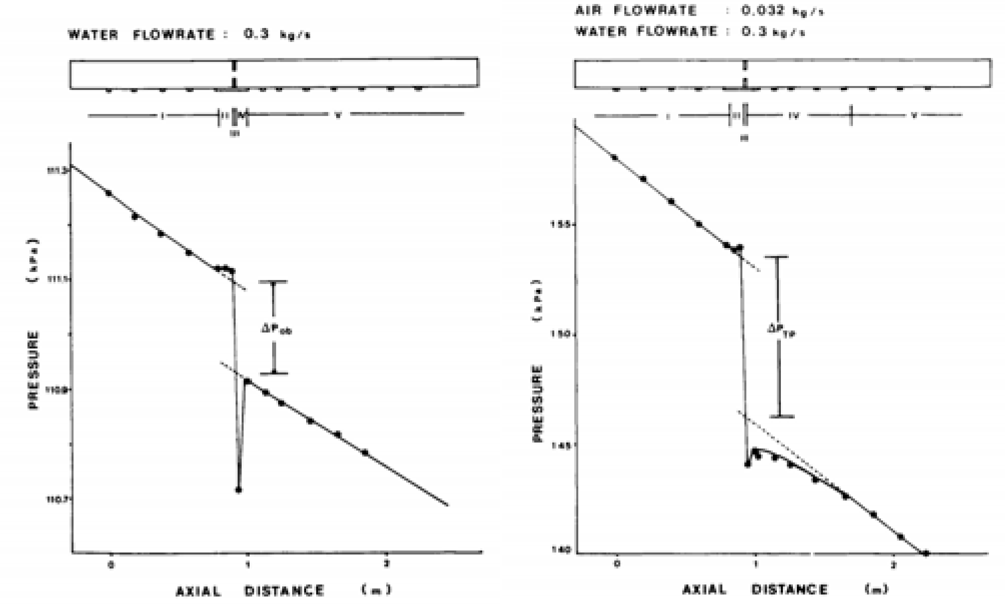

Figure 2-1 Pressure drop in single and two phase flow through orifice. [33]

Zhang et al. [34] performed the measurements for two phase (air-water) flow with sharp edged orifices for low quality mixtures. The air mass velocity varied from 0.9 to 9.1 kg/m^{2}s, while the water mass velocity varied from 840 to 1648 kg/m^{2}s. The quality was varied from 0.007 to 1%. The 25.36 and 21.42 mm diameter orifices were placed in a horizontal pipe of diameter 50.8mm. The resulting diameter ratios were 0.499 and 0.422 respectively.

Fossa et al. [35] investigated the pressure drop through thin and thick orifices. Gas superficial velocity ranged from 0.3 to 4 m/s whereas liquid superficial velocity was in range of 0.6 to 2 m/s. The test section was 12 m long having diameters equal to 60 and 40 mm. Three different aspect ratios were considered as 0.025, 0.20 and 0.59. Plug flow was witnessed at gas superficial velocity of 0.7 m/s and slug flow for higher gas flow rate. The pressure drop was decreased as the aspect ratio increases.

Arun Kamar et al. [36] did an investigation to measure the pressure drop (PD) for gas non-Newtonian liquid flow across orifices. The liquid used was the sodium salt of carboxy methyl cellulose (SCMC). The test section had internal diameter of 0.0127 m and was 2.30 m long. The liquid and gas flow rates were 4.05×10^{-5} to 16.17×10^{-5} and 3.762×10^{-5} to 37.151×10^{-5} m^3/s respectively. The flow patterns were mainly in slug and plug flow regimes. An increase in pressure drop was observed for two phase flow as the concentration of aqueous solution of SCMC increases from 0.2 to 0.8 kg/m^3.

Jorge et al. [37] performed measurements on two phase flow to measure the liquid and gas flow rate. Annular, bubbly, slug and churn flow were observed during horizontal and vertical flow. The mass flow rate of air was up to 50 kg/h, while that of water was up to 4000 kg/h. Void fraction ranged from 2 to 85%. It was observed that by increasing the air flow rate for given water flow rate, the pressure drop increases.

Alimonti et al. [38] did experimental work to investigate the two phase flow characteristics through multiple orifice valves (MOV). Three values of aspect ratios were considered as 1.41, 1.66 and 2.21. Test section was 4m long with diameter of 0.05. The water flow rate was varied from 0.00027 to 0.00081 m^3/s. The void fraction was kept fixed by setting the void fraction from 5% to 35%. The flow patterns were predominantly bubbly and slug. The authors proposed a correlation for two phase (gas-liquid) flow pressure drop multiplier through a multiple orifice valve (MOV).

Manmatha et al. [39] performed numerical investigation on air-water flows in 40 and 60mm diameter horizontal pipes. The water superficial velocity ranged from 0.3 to 4 m/s whereas air superficial velocity was varied from 0.6 to 2 m/s. Two area (0.73 and 0.54) and four aspect (0.025-0.59) ratios were considered. The result obtained were compared with experimental results of Fossa et al. [35] and found to be in good agreement. They found the maximum value of void fraction just after the restriction.

2.4. Flow through Orifice with Drag Reducing Agents.

Nobuyuki [40] measured the loss, discharge coefficient and pressure distribution of polyacrylamide solution through orifice having diameter ratio varying from 0.562, 0.667, and 0.771 for both laminar and turbulent flow. It has been observed that loss observed is reduced in turbulent region. The pipe Reynolds no ranged from 1000 to 5000.

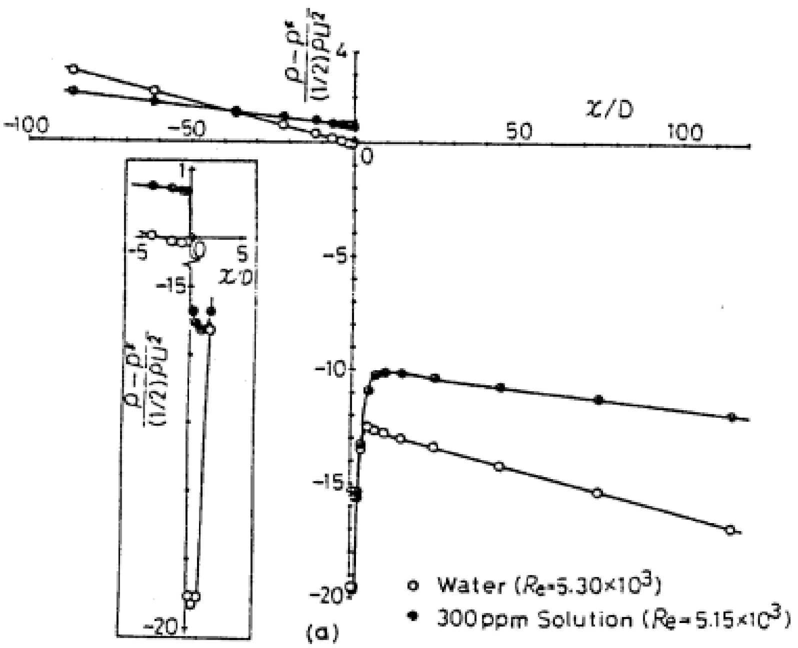

Figure 2-2 Pressure distribution of flow through orifice [39]

Tomiichi et al. [41] studied the pressure drop through various sizes of orifices. Three different solutions; water, a 50/50 glycol/water mixture, and a 0.1% solution of polyethylene oxide (PEO) 8000 at high velocity were considered. The range of Reynolds number was from 1 to 10000. The measured pressure drop of water and glycol/water mixture was in agreement with the result obtained from Navier-stokes equation for orifice having diameter 100 and 400 µm. However it was lesser for orifices having diameter less than 50 µm. The aqueous solution of polyethylene oxide (PEO) made a lower pressure drop than the other two solutions except for orifice having diameter 400 µm. The authors suggested that reduced pressure drop may be due to slip at the wall and elasticity induced in an elongated flow.

Akiomi et al. [42] measured the pressure drop for silicon oils, aqueous solutions of polyethylene glycol (PEG) and surfactant solutions. The diameter of orifice varied from 5 to 400 µm whereas the thickness was kept constant at 20 µm. The range of Reynolds number was from 1 to 10000. Silicon oils produced similar drag reduction as that of water and glycol/water mixture. It was observed that PEG20000 produced almost the same pressure drop as that of PEG8000 for the 400 to 15 µm orifices, but a greater pressure drop than that of PEG8000 for the 10 to 5 µm orifices.

Akiomi et al. [43] measured the pressure drop and jet thrust for several aqueous solutions of polymers and surfactants in orifices having diameter ranging from 15 to 100 µm. The orifice thickness was maintained at 20 µm. The range of Reynolds number was from 1 to more than 1000. The results showed that PD for PEG20000 was same as that of PEG8000.The authors suggested that pressure drop reduction (PDR) was due to the existence of viscoelasticity.

Akiomi et al. [44] measured the pressure drop of several types of mixtures through orifice diameter of 20, 50 and 100 µm. The solutions include polymer and surfactant solutions with and without nanobubbles. The range of Reynolds number was from 1 to more than 1000. The pressure drop for polyethylene glycol was lower than the NB and NB/polymer mixture. The authors proposed that elasticity of PEG due to entanglement of polymer chains is disturbed by nanobubbles in NB/PEG and hence pressure drop increased in these solutions.

Takahiro et al. [45] performed the DNS and PIV measurements of viscoelastic fluids through rectangular orifices. A surfactant solution of CTAC (cetytrimethyl ammonium chloride) was used as the viscoelastic fluid. It was observed that the vortices originating from the orifice edge in viscoelastic fluid was reduced compared to Newtonian fluid resulting in the suppression of turbulent eddies and Reynolds shear stress downstream of the orifice. Drag reduction effect was observed in limited cases of low Reynolds number flows. The experimental and numerical results were found to be in qualitative agreement.

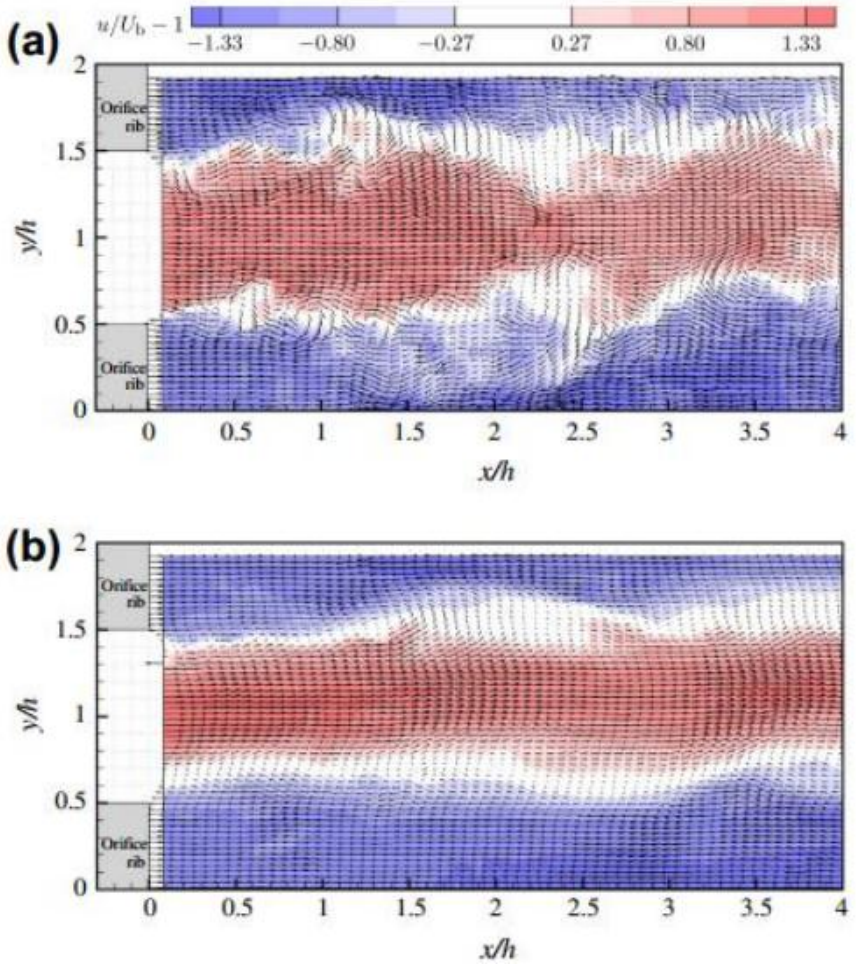

Figure 2-3 Snapshot of flow fields behind the orifice by PIV; a) Water, b) CTAC 150ppm [45]

CHAPTER 3

RESEARCH METHODOLOGY

In the present study, experiments were carried out to investigate the flow characteristics around single or double orifice with the aid of Particle Image Velocimetry (PIV) with and without drag reducing polymer. Pressure readings were measured with the help of Piezometric tubes.

3.1 Experimental Set-Up

Experiments were carried out with a flow loop designed for two phase flows whose schematic is represented by Figure 3-1. The line which connected different components in the flow loop was mostly made of Acrylic pipe having an inner diameter of 25.4 mm and outer diameter of 38.3 mm. Flexible hose was used at some portions to assist adjustments during orifice replacement. Negligible leakage was maintained and flow direction was anticlockwise. A tank of 100 liters capacity was used as a source of water. The centrifugal pump was used to drive water from the tank through the loop. The water flow rate was controlled by gate valve installed on the discharge side of the pump. Atmospheric air at 2 bar pressure was used in the gas-phase. Properties of air were determined at each time during the experiment based on temperature and pressure in the laboratory.

A turbine flow meter with digital display of specifications SN: 503399, MODEL: FTB791 and K/F: 2562ppg in combination with a gap meter with SN: 0100100158847 and MODEL: FL-1504A fitted in the straight pipe section upstream of the orifice inlet was used to measure the flow rate of the liquid. The total length of the straight pipe section upstream was more than 60D to ensure fully-developed flow. The test section of the setup is labelled (5) which contained the orifices and served as the main focus of the PIV measurement.

The laser was placed to illuminate the test section from below and the camera, which was placed at right angles to the laser sheet, captured images of the seeded flow fields to be processed and analyzed using PIV software. The test section was designed in a way to accommodate multiple orifices and allow flexibility in varying the distance between the orifices as shown in Figure 3-3. The parts were machined form Plexiglas with the 4D parts upstream and downstream attached to the 2D or 1D parts separating the orifices for multiple orifice set up. In order to prevent leakages, O-rings were fitted to the faces. The orifices were manufactured to ANSI standard for D_r =0.5 and 0.63 with dimensions shown in Figure 3-4(a). The orifices were made form of square sheets of 3mm thickness and matching sizing with other parts to ensure uniformity and to avoid misalignment which might cause leakage. Holes of sizes M3 were bored at the four edges of the orifices and other parts of the test sections for fastening purpose. Four threaded rods of diameter 3mm were slotted through the length of the test section and tightened with nuts at flanges on the setup. Bolts and nuts were other fasteners that were used to fasten the flanges on both 4D upstream and downstream parts of the test section to the flanges on the test rig. A portion of flexible hose with inner diameter of 25.4 mm was used downstream to aid easy adjustment during assembling and disassembling of the test section from the setup.

Pressure taps were drilled upstream and downstream of the orifice through which pressure readings were taken with piezometers. Drag reducing polymer was injected at a distance of 1m before the orifice to ensure proper mixing before reaching the orifice. Polymer injection (PI) point is shown in Figure 3-2. P4 was the point to measure pressure downstream of the orifice.

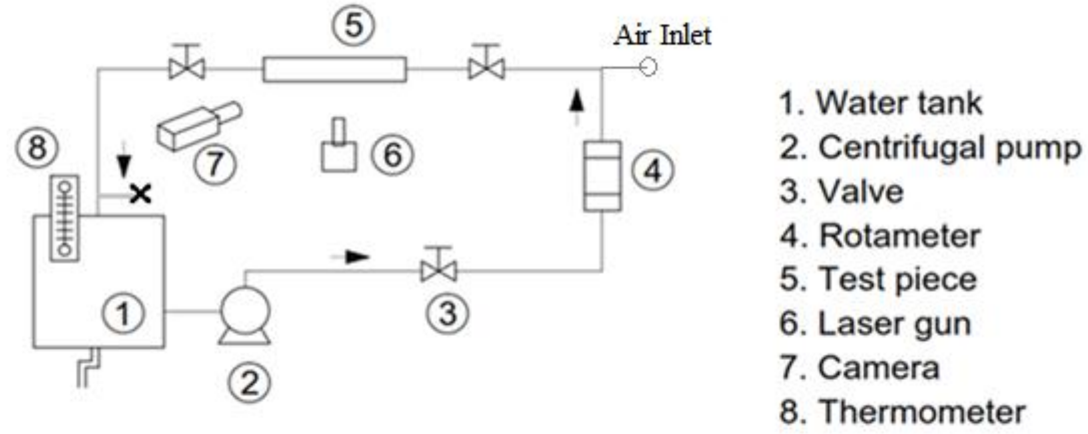

Figure 3-1 Flow loop schematics

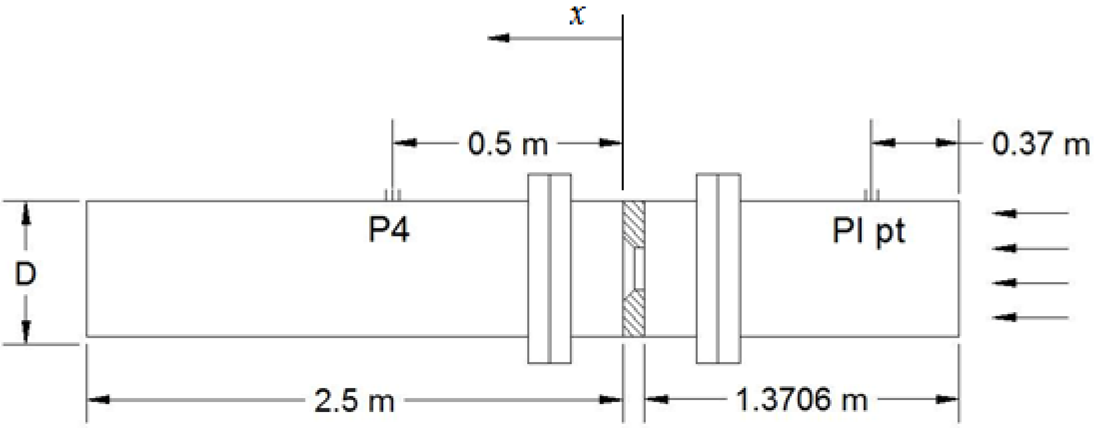

Figure 3-2 Schematics of flow domain around the orifice

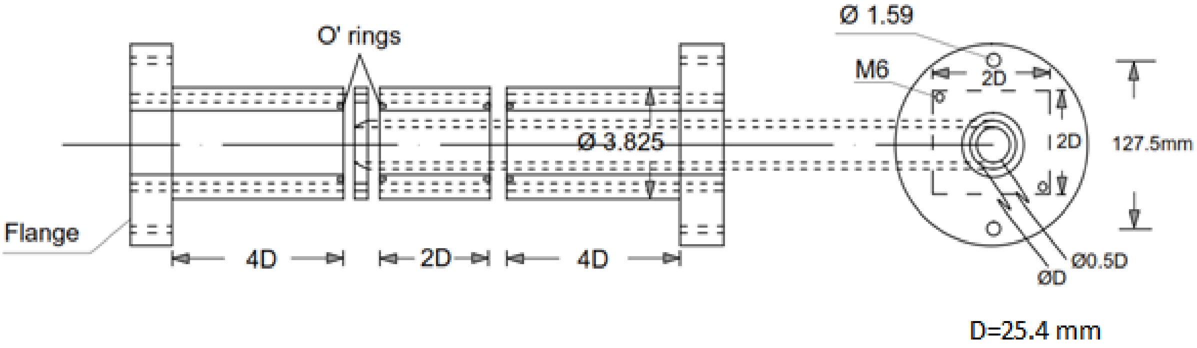

Figure 3-3 Test Section sectional view

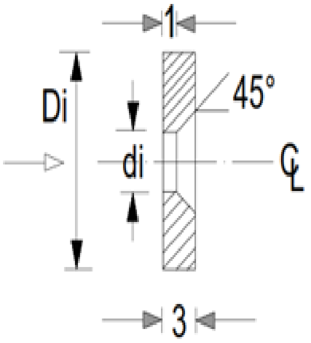

a) ANSI standard orifice dimensions

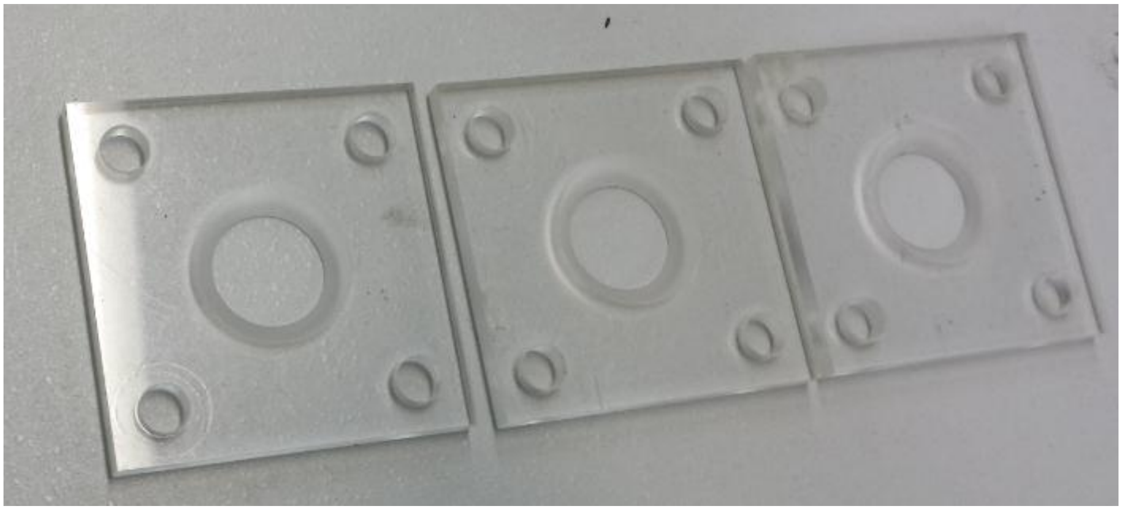

b) Orifices having D_r=0.63

Figure 3-4 a) ANSI standard orifice dimensions b) Orifices having Dr=0.63

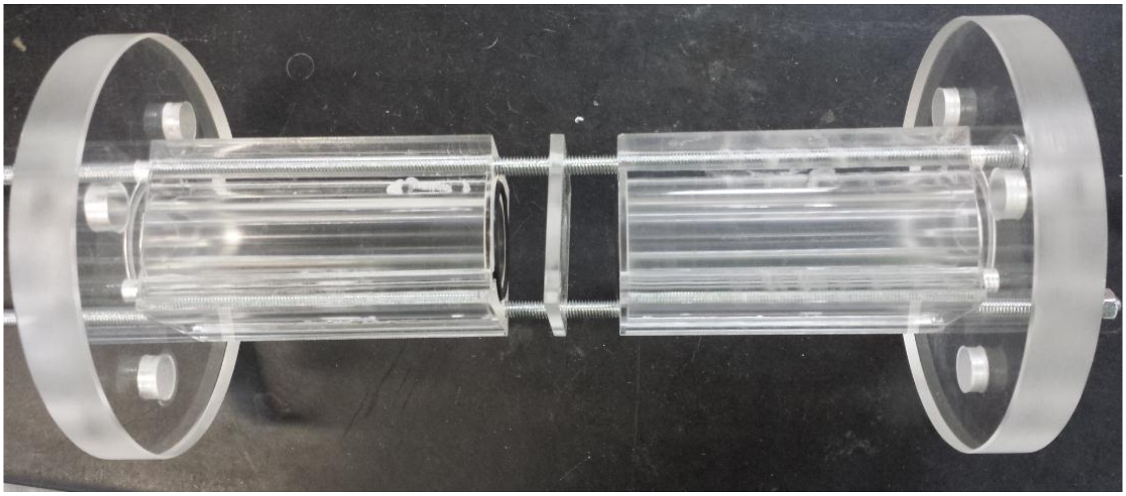

Figure 3-5 Test section having single orifice

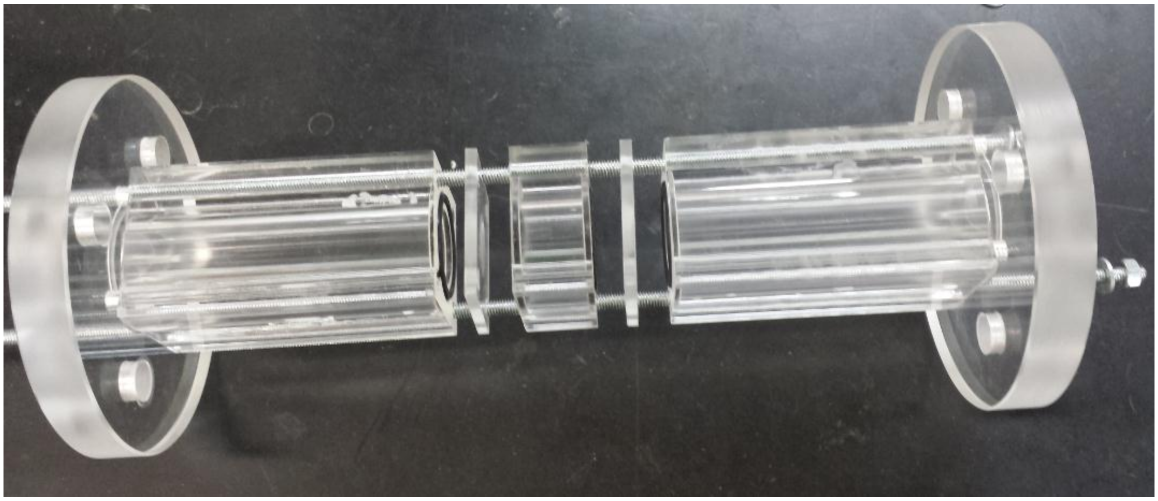

Figure 3-6 Test section having double orifice with 1D spacing

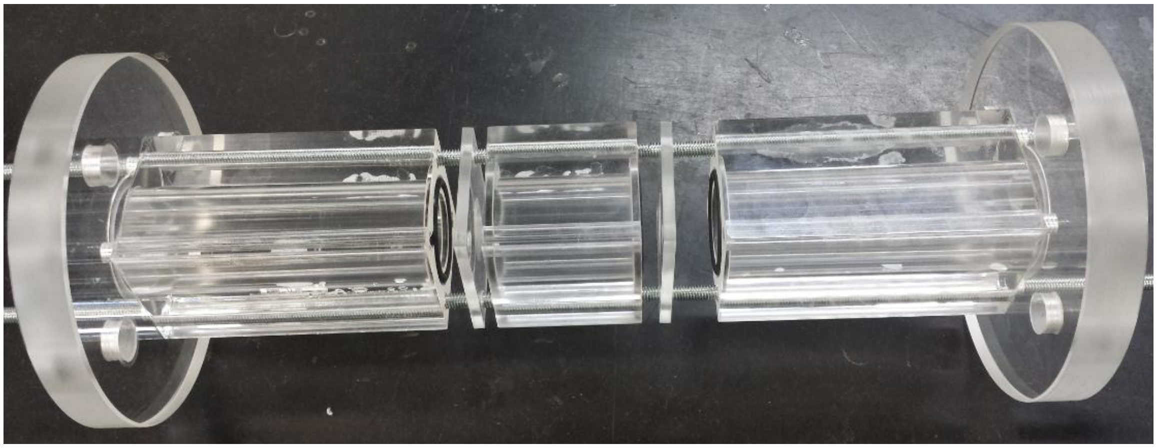

Figure 3-7 Test section having double orifice with 2D spacing

Pressure head was measured upstream, adjacent to and downstream of orifice plate using piezometers. The location of pressure taps for single orifice is shown in Figure 3-8. One pressure reading was measured further downstream at a length of 0.5m from the orifice as shown in Figure 3-2.

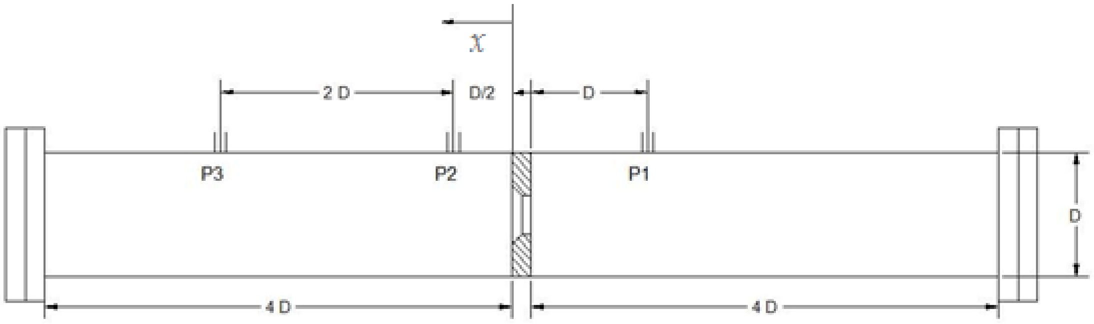

Figure 3-8 Location of Pressure Taps for single orifice

For double orifice with 1D spacing, the location of pressure taps is shown in Figure 3-9. P4 is the pressure port at a distance of 50cm downstream of the second orifice.

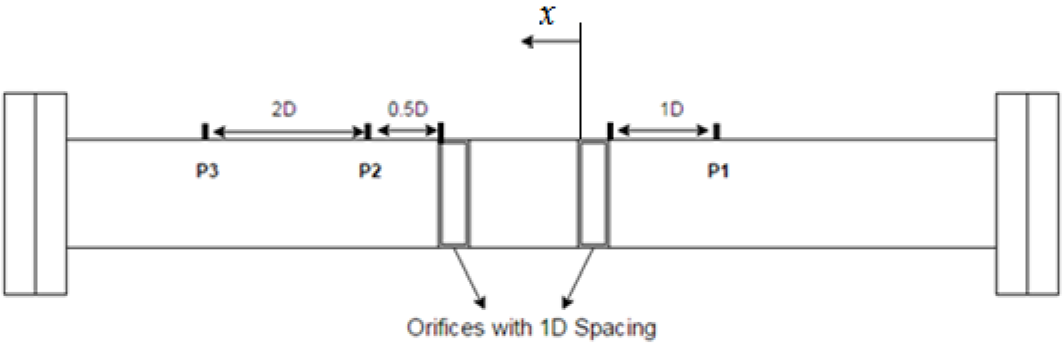

Figure 3-9 Location of Pressure Taps for double orifice with 1D spacing

For double orifice with 2D spacing, the location of pressure taps is shown in Figure 3-10. P6 is the pressure port at a distance of 50cm downstream of the second orifice.

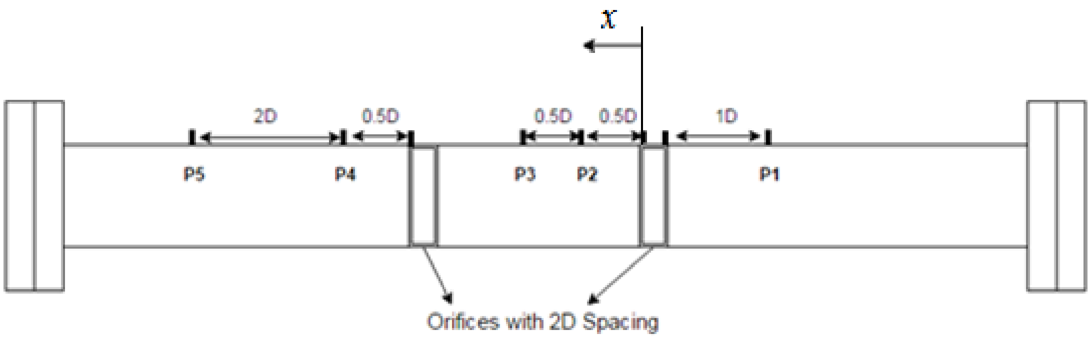

Figure 3-10 Location of Pressure Taps for double orifice with 2D spacing

The water-soluble Drag Reducing Polymer (DRP) used was ZETAG® 8165 which is a member of Cationic Powder-Solid Grade flocculants family produced by BASF chemical company. ZETAG® 8165 is a synthetic high molecular weight polyacrylamide and it is supplied as a free flowing white powder. Table 3-1 shows specifications of the selected water-soluble DRP as obtained from the manufacturer.

Table 3-1 Properties of ZETAG® 8165

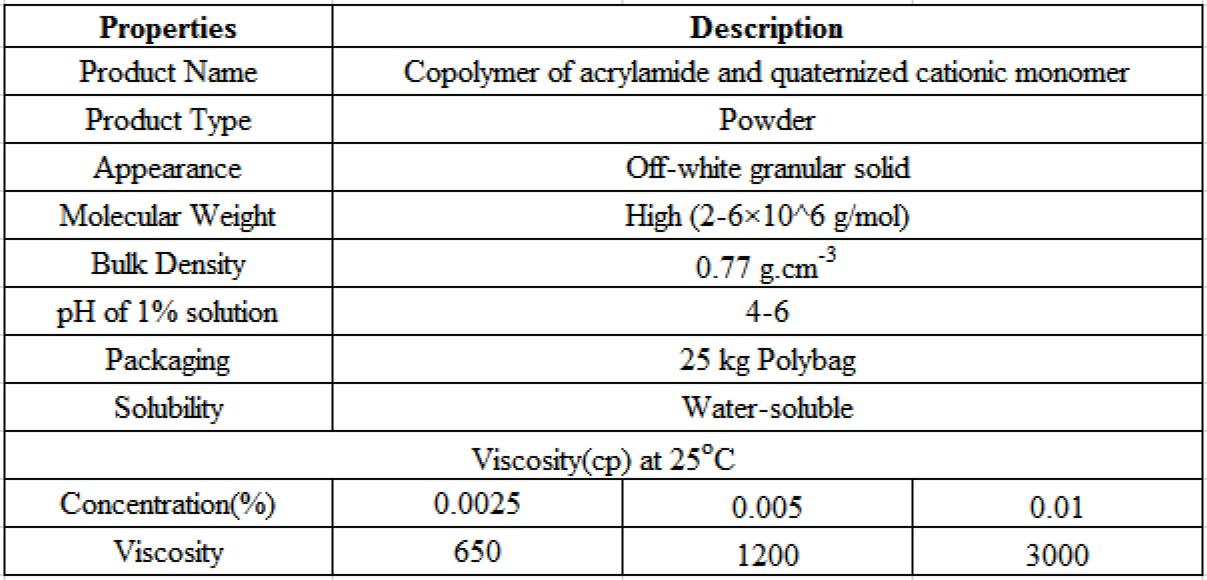

Properties	**Description**		
Product Name	Copolymer of acrylamide and quaternized cationic monomer		
Product Type	Powder		
Appearance	Off-white granular solid		
Molecular Weight	High (2-6×10^6 g/mol)		
Bulk Density	0.77 $g.cm^{-3}$		
pH of 1% solution	4-6		
Packaging	25 kg Polybag		
Solubility	Water-soluble		
Viscosity(cp) at 25°C			
Concentration(%)	0.0025	0.005	0.01
Viscosity	650	1200	3000

Drag reducing polymer (DRP) was mixed, shifted and injected as shown in Figure 3-11. To assure homogenous solution at the mixing stage, the DRP was stirred with water by using low speed mixer. 1000 ppm master solution of DRP was made in each case. The concentration of master solution of drag reducing polymer is calculated as shown in Table 3-2. After thorough mixing, the DRP was shifted to another tank by the help of gravity. This precaution was done to prevent polymer degradation. The tank was pressurized to 2 bars with air after completing the whole quantity. The DRP was then ready to be injected. Figure 3-11 shows schematics of the method by which the drag reducing polymers was introduced in the flow loop. A rotameter of MODEL: FL-50000 was used to measure the quantity of drag reducing polymer being injected into the main flow.

Table 3-2 Concentration of Master solution of DRP

DRP(kg)	Water(litre)	Concentration (ppm)
0.013	13	1000

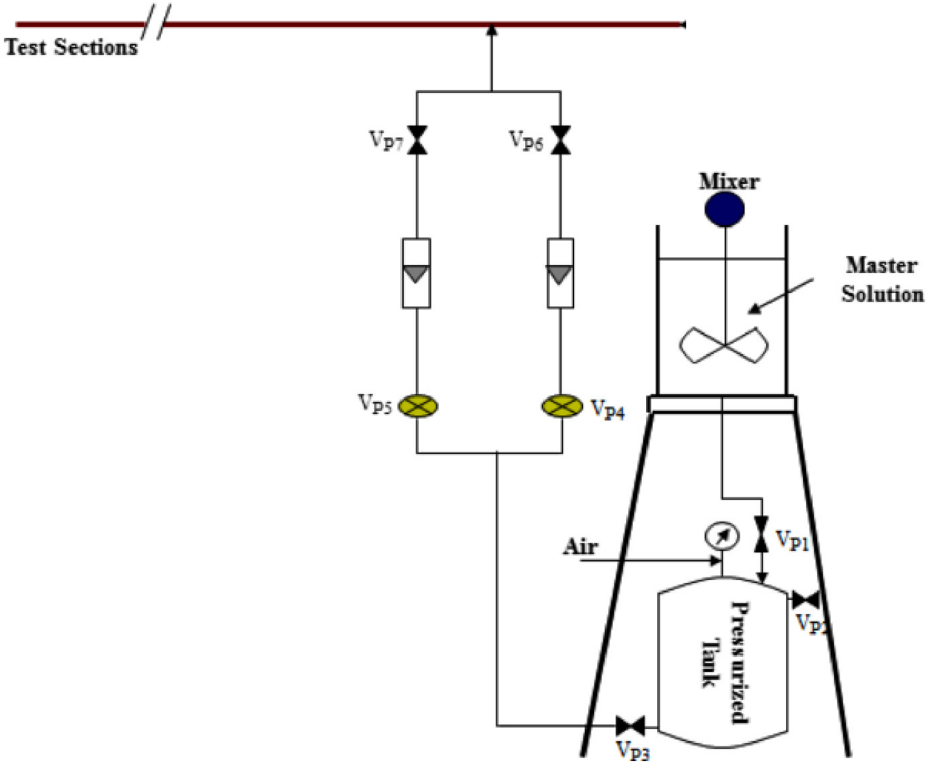

Figure 3-11 Polymer Injection Mechanism [46]

3.2 Measurement Technique

A 2D2C PIV measuring technique was used to study flow characteristics downstream of the orifice. Laser, which was used as a light source was installed in such a way that it illuminated the test section from below and camera was placed at right angle to the laser sheet to capture the seeded flow field. The test section was made in a square shape to minimize optical distortion during capturing of the images. A better way to avoid it is to locate the test section in the rectangular basin containing the same fluid as flowing through the test section. This study was concerned with the downstream section of orifice and an axial length of 2-2.5D was investigated due to the limitation of the light sheet width.

Particle Image Velocimetry (PIV) provides instantaneous, non-intrusive and quantitative measurement of flow field characteristics. It is a well-established technique in many areas of modern fluid mechanic applications. PIV has been used to measure velocity vector field from slow to supersonic fluids during the last two decades [47]. This technique includes seeding the flow under study, illuminating the region under investigation, and successively capturing the images of that region. A velocity vector map can be calculated in the flow field from the displacement of the tracer particles and the time interval between the two images. Adrian [47] introduced the concept of PIV in late 1980s with initial experimentation followed shortly afterwards. Due to the limitations of the hardware at that time, a single photographic frame was multiply exposed and analyzed using a correlation technique.

The non-intrusive approach of PIV has an edge over other probing techniques that it does not require any probing. Hence errors induced by probing in the flow field are thus eliminated. Also, it has the ability to determine whole field measurements rather than single point measurements. The main flow property measured by PIV is the instantaneous velocity, other properties can then be measured from the derivatives of velocity.

Figure 3-12 briefly explains the typical arrangement for PIV recordings. Small seeding or tracer particles are added to the flow, the light sheet plane within the flow field is illuminated by a light source (laser), and the light reflected from the area of interest is captured by a digital camera as image pairs. The digital images are then analyzed using PIV software by different correlation techniques. The PIV technique is also known as an indirect method of velocity measurement as the actual velocity is determined from the velocity of the seeding particles.

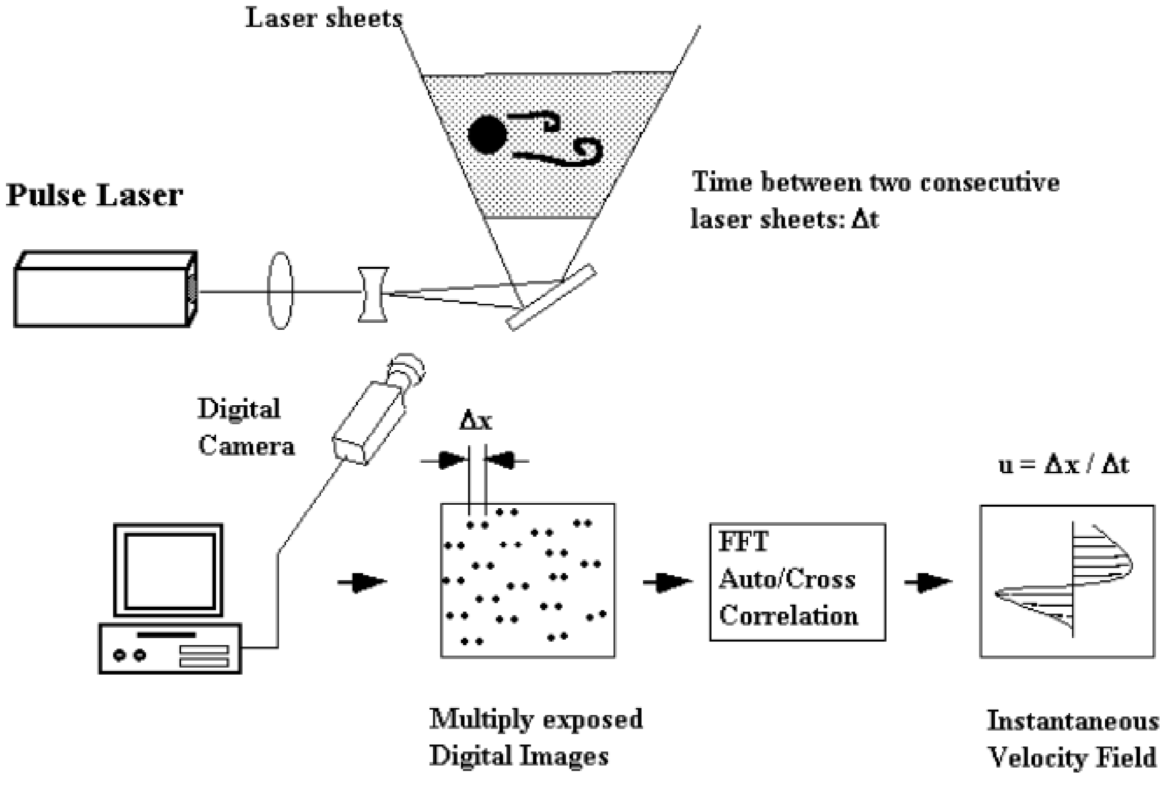

Figure 3-12 Schematic configuration of PIV system [31]

3.2.1 Principle of PIV

Particle image velocimetry techniques is based on the basic equation as given below:

Speed (u) = Distance (Δx) / Time (Δt)

In PIV, the main aspect of the flow measured is the distance between the two images of particles that travel in the direction of the flow field with known time period. These particles are deliberately added to the flow and known as seeding. The seeding particle is selected to follow the flow, and an area of flow field is illuminated by a laser light sheet in order to detect their movement. To detect the position of the illuminated seeding particles, a CCD camera is positioned at right angles to the laser light sheet and the particles appears as light spots on a dark background on each camera frame.

Calibrated images are divided into desirable interrogation areas (IA) with lesser particles to process cross-correlation techniques. For each of these interrogation areas, the image 1 and 2 of an image pair are correlated to produce an average particle displacement vector. Repeating the same process for all interrogation areas produces a vector map of average particle displacements. Displacements vectors are then divided by known time between the two images to generate a map of velocity vectors. Further analysis can produce streamlines and other fluid properties. Following topics of PIV arises from its basic principle:

- Seeding
- Illumination (Light sources)
- Cameras (Image Capturing)
- Correlations and Data processing (Image Evaluation)
- Application of PIV

3.2.2 Seeding

As stated earlier, the PIV actually measures the velocity of the seeding particles. Therefore, for successful seeding, some factors have to be considered such as flow medium (air/water), volume of the fluid to be seeded, light scattering, fluid flow rate, particle image size etc. Particle size and density along with fluid density and viscosity determine the effects of buoyancy and inertia. Exact neutral buoyancy is almost difficult to gain but particles should remain suspended throughout an experiment. The primary source of error is due to gravity which may arise due to the large differences in density between seeding particles and the fluid. Hence, proper selection of seeding particle that matches with density of the fluid is very crucial. Along with density, there are certain other parameters which must be considered like the clear visibility of the particles, and minimum interaction of particles with each other. Also, they should be chemically inert.

Proper selection of seeding particles are an important and economical way of getting a better image. There are variety of seeding particles available that are suitable for liquid flows. The injection of seeding particles into the main flow to get a homogenous mixture is another important aspect to be considered. For the study under consideration, Polyamide was selected as seeding particle as its density (1.03g/cm^3) is close to the density of water and it is easily available.

3.2.3 Illumination (Light Sources)

For the illumination of the flow region, Particle image velocimetry technique requires a light source. The light sheet should have minimum divergence. The thickness of the light sheet depends upon the application and it can be controlled. Although there are variety of sources of light sheet like LED, laser etc. but usually laser is preferred because laser beam is easy to form into a sheet by a cylindrical lens. They have been mostly used for PIV recordings. Laser light sources give high energy density monochromatic light along with sharp brightness and almost constant converging thickness and when combined with sheet optics of cylindrical lenses makes it easy to record tracer particles devoid of chromatic aberration. [49]

Laser light sources for PIV measurements are usually classified into three major groups as, continuous wave (CW), pulsating and semiconductor lasers. Continuous wave laser generates a good laser beam of low power light within short intervals together with little amount of heat, pulsating lasers gives high light energy during a very short time interval which makes the particle image practically frozen and enable them for high speed flows, semiconductor lasers give energy lower than pulsating lasers and are used for small scale experiments. For the current experiments, Continuous wave (CW) Raypower 2000 laser provided by Dantec Dynamics shown in Figure 3-13 was used. Its specifications are stated in Table 3-3.

Table 3-3 Laser Specifications

Specifications	Raypower 2000
Lasing medium	Gas
Wavelength	532 ± 1nm
Output power	>2000mW
Operating mode	CW
Transverse mode	Near TEM00
Beam diameter at the aperture	3.0nm
Polarization ratio	>100:1
Operating temperature	10-35^{o}C
Mains supply	100-240 VAC
	3A max, 50-60Hz
TTL modulation frequency	max 10kHz

Figure 3-13 PIV laser

3.2.4 Cameras (Image Capturing)

In order to get to single exposed images with a time interval of order of microseconds, one has to use a cross-correlation CCD camera. The basic concept is that initial image exposed by the laser is transferred very rapidly to light hidden regions on CCD chip. This is accomplished on a pixel by pixel basis, which means that each pixel has its own storage site in close vicinity of the light sensitive pixel area. After the next exposure, both images are transferred to the computer storage.

A very important consideration for obtaining accurate PIV measurements is the proper seeding of the flow with the seeding particles. Cameras with large apertures and high quality lenses are needed for PIV recordings because of the weak light reflected by the tracer particles. Now a days, digital recording cameras are available, which contain charged couple devices (CCD) arrays with large pixels to convert light into electric charges and hence avoiding photographic processing, getting instant images of flow fields along with allowing review of incidences [48]. The experimental investigations done in the current case were carried out by Dantec Speedsense Camera 9040, and lens having specifications shown in Table 3-4 and Table 3-5 respectively.

Table 3-4 Camera specifications

Specifications	Speedsense Camera 9040
Sensor Type	CCD progressive scan monochrome
Chip size (mm)	18.77 × 13.8
Resolution (pixels)	1632 × 1200
Pixel size (µm)	11.5
Bit depth	8, 12, 14
Max exposure time (µs)	2
Fps (full frame)	1016/508

Table 3-5 Lens specification

Specifications	Nikon AF Micro Nikkor 60mm f/2.8D
Focal length	60
f-number	2.8-32
Distance scale (m)	0.219 – infinity

3.2.5 Correlations and Data processing (Image Evaluation)

Ever since from the invention of first PIV image evaluation method, many alternative analysis algorithms have been developed. Also error correction and post-processing methods have been designed to enhance speed and accuracy of PIV measuring technique.

During the PIV experimentation, two important phenomenon arise which affect the images of the seeding particles. They are the refraction through the curved surfaces and diffraction limited imaging. Distortion of the images of the seeding particles arises because of the different refractive indices of the water, glass, and air, also because of the curvature of the interfaces. In order to eradicate or minimize this problem of optical distortion, several solutions have been proposed. The best possible method is to place the cylindrical pipe in a rectangular tank filled with same liquid flowing through the pipe. In our case, outer surfaces were made rectangular in order to avoid this problem as proposed by Agrawal et al. [50].

Correlation methods are used to evaluate the images. In order to perform any correlation method, the image map is first divided into interrogation areas (IA). Most common sizes of the IA used are 16 × 16 pixels or 32 × 32 pixels. The selection of the size of IA depends upon required accuracy, resolution and quality of the images. 8-25 particles should be present in an IA in order to achieve optimum results. Statistical techniques applied by either digitally performed Fourier algorithms or optical techniques are then applied in order to determine the peak displacement vector of each IA. The heart of the PIV technique is the correlation of regions (interrogation areas) with each other to determine the displacement vector in that part. The correlation techniques can be used for a single frame multiple exposed (auto-correlation) or multiple frame single exposed (cross-correlation). To increase the speed of the convolution process, correlations of pairs of IAs are carried out in Fourier space. After the interrogation of the images in this way and generating the vector maps, post processing is done to validate the data and to enhance the vector map resolution and accuracy. Using the same vector map, streamline patterns can be obtained.

3.2.6 Application of PIV

The most important step in PIV recording is its accurate application. For this purpose, certain rules should be followed to achieve optimum results;

- Seeding should be well enough for valid detection of particles. 15 number of particles should be present in an interrogation areas to achieve maximum detection of tracer particles
- One quarter rule should be followed which states that maximum displacement of seeding particles between consecutive images should be one quarter of interrogation size.
- The time interval between pulses of the laser should be selected in such a way that it is not lesser than equivalence of 8 pixels to avoid a reduction in velocity dynamic range.

Typical sizes of interrogation areas usually selected are 32 × 32 and 64 × 64 pix^2. Once the size of interrogation area and time interval is chosen, the light intensity distribution of each pixel in an IA is cross correlated between image exposures. The displacement vector is derived from the displacement between the correlation peak and center of IA. The same procedure is applied for the whole field to get velocity vector map.

Now, the complete procedure of setting up the PIV experimentation for studying the flow field in the downstream section on an orifice is described. Apparatus set-up, flow optimization, experimental runs, data gathering and analyzing are discussed in detail.

3.2.6.1 Apparatus set-up

We have to know the suitable distance between the camera and the test section for setting up the PIV system. We used a camera resolution of 1152 × 480 pixels, and camera chip's pixel size of 11.5 microns, the size in metric units is 13.248 × 5.52 mm. We can then able to calculate the field of view (FOV) which is defined as the portion visible to the camera based on orientation and position of the camera. It also depends on focal length, sensor size and distance from the object. The distance scale of the lens in which object can be captured is 219mm-infinity depending upon the diameter of the pipe i.e. 25.4mm. The test piece was fixed at 280mm. Then field of view (FOW) based on the above values is 61.69 × 25.70 mm^2.

The exposure time and frame rate was determined based on the flow rate of the flow. The exposure time is the time interval between pulses of the laser. In our case, we don't have a synchronizer and a time boxer, hence the value was added when importing images to the Dantec Dynamic studio. Moreover, sample rate should not exceed the maximum allowable frame rate of the camera.

The second step is the alignment of the laser with the test piece. The distance from the laser board to the pipe center was 6.61 cm. The thickness of the laser board was 2.21 cm. The laser board or the platform was made to allow the axial movement of the laser with the pipe centerline. The laser was connected to a power source of 110V and it was set to low current to check the alignment of laser with pipe centerline.

For setting up the camera, tripod was placed at a distance within the depth of field that allows a clear view of pipe centerline. In our case, we had placed it at a distance of 278-

280mm based on the specification of the lens. Bubble gauge on the tripod was used to achieve the alignment of the camera. PCC camera program was used in the computer system for the capturing of the images. Camera was adjusted to focus on the test piece and then covered with the cap to perform intensity calibration. Cap was then removed and continuous grab mode was then selected to record the videos of the flow field.

Flow was optimized by preparing a homogenous mixture of tracer particles and the working fluid. Flow was kept running for some time to check for any possible leakages. Desired flow rate was then selected using the valve in the loop.

For recording of the images, the sample time and exposure time was added into the PCC camera program and laser was switched on at its highest current value (5.9A). Laser light was then adjusted to check for the saturation of the flow field. Images were then recorded, previewed to ensure the image density, particle drift, and out of the plane motions. Necessary adjustments were then made to enhance the image quality. Image density should be suitable for PIV technique which means that 8-15 particles should be present in 32 × 32 pixel interrogation area. Number of seeding particles can be counted in a cross hair, whose size is approximately 32 × 32 pixels. Number of seeding can then be adjusted to achieve this condition.

Experimental runs were then conducted to capture the images of the flow field. Camera mode was selected to Record mode and desired number of images in the TIFF format were saved. Images were obtained as single frame images using the PCC studio software. For the analysis of the images using the Dantec Dynamic studio, they were imported as normal images. Calibration of the field of view was done on change the scale factor by stating the diameter of the pipe as the height or by specifying the length of FOV.

3.2.6.2 Analysis Sequence

Once the images were stored in database and scale factor was applied, analysis sequence was done as shown in Figure 3-14.

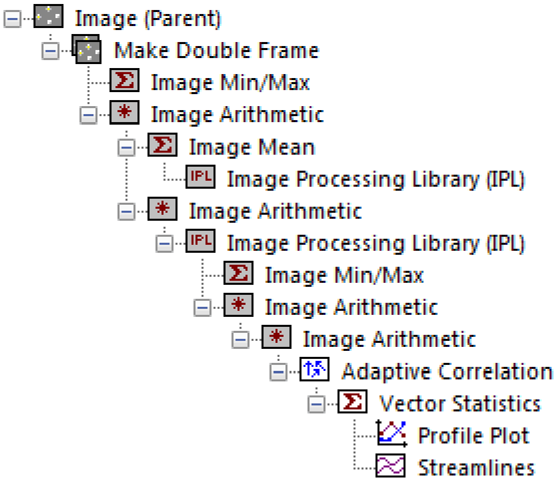

- Image (Parent)
  - Make Double Frame
    - Image Min/Max
    - Image Arithmetic
      - Image Mean
        - Image Processing Library (IPL)
      - Image Arithmetic
        - Image Processing Library (IPL)
          - Image Min/Max
          - Image Arithmetic
            - Image Arithmetic
              - Adaptive Correlation
                - Vector Statistics
                  - Profile Plot
                  - Streamlines

Figure 3-14 Analysis Sequence

The analysis was done in the following sequence:

- Make Double Frame: This step was done on the raw images stored in the database in order to convert them from single frame to double frame images by specifying N/2 double images from the option i.e. merging them in twos.
- Image Min and Max: This step is a subset of Image Processing Library (IPL) used to find the field of minima and maxima of the chain of the images. We used this method to determine the field of minima from the images from the previous step. It yields one image.
- Image Arithmetic: This step performs arithmetic operations like addition, subtraction, multiplication and division on the pixel values of the image. We utilized this procedure to subtract the minima image obtained from the previous step from the images in initial

step (Double frames). This is kind of background method to eliminate background noises from the raw images.

- Image Mean: This method calculates the mean intensity of pixels having same coordinates in all selected images. The images should be well-matched in terms of dimensions and grayscales. This step takes inputs from the previous step and generates a single map.
- Image Processing Library (IPL): This procedure uses different filters like low-pass, high-pass, morphology, signal processing etc. to smooth images, detect edges, improve contrast etc. We used this technique to reduce the particle image intensity of the image from the previous step by utilizing blurring option.
- Image Arithmetic: This step was performed to do the subtraction of images obtained from the previous step from the raw images got from previous arithmetic operation. The main aim of this procedure is to decrease the intensity of images in the collection.
- Image Processing Library (IPL): Here this technique was performed to the images from the previous step using Gaussian filters (5×5) twice. The aim was to make the images smooth and more visible.
- Image Min and Max: We used this method to determine the field of minima from the images from the previous step. It yields one image.
- Image Arithmetic: This techniques was used to check the occurrence of numeric diffusion that can arise by the application of filters. Here it was done by the subtraction of image from previous step to the raw images in its previous step.
- Adaptive Correlation: This technique was used to generate vector maps. It was applied on the images in the previous step. It is form cross-correlation technique with additional

post-processing algorithms like local validation. It determines the velocity vectors by starting from an IA area of larger size (256 × 256) and finishes at an IA of desired size (32 × 32) with its size multiples i.e. refinement steps by using the intermediate results as input for the succeeding smaller size. Also, to detect erroneous vectors, different processes like local validation was done using the same correlation. Local validation was conducted through peak validation and local neighborhood validation. The overlap of IA was applied to compensate for the loss of vector field resolution by 50% overlap between IA sets in both vertical and horizontal dimensions. From the displacement vectors and time period, velocity vectors were obtained by applying Central Difference Scheme.

- Vector Statistics: This is the last step of the analysis. It determines statistics from multiple vector maps and reveals the results of mean velocity vectors in the form of a vector map. Other statistical quantities are also calculated like standard deviations, variances, and covariance among velocity components.

CHAPTER 4

RESULTS AND DISCUSSION

In this section, main results of experimental study are presented. Single phase pressure drop is discussed in detail followed by a brief discussion on two phase pressure drop. The streamline patterns and velocity profiles obtained from PIV analysis are then analyzed.

Total drag reduction ($\mathrm{DR_T}$) is calculated by the given formula:

$$\mathrm{DR_T} = \frac{\Delta \mathrm{P_{T,without\ DRP}} - \Delta \mathrm{P_{T,with\ DRP}}}{\Delta \mathrm{P_{T,without\ DRP}}} \tag{4-1}$$

Where,

$\Delta \mathrm{P_{T,without\ DRP}}$= Total static pressure drop including orifice without drag reducing polymer

$\Delta \mathrm{P_{T,with\ DRP}}$= Total static pressure drop including orifice with drag reducing polymer

$\Delta \mathrm{P_T}$= P1-P4 for single and double orifice with 1D spacing as shown in Figure 3-2, Figure 3-8, and Figure 3-9

$\Delta \mathrm{P_T}$= P1-P6 for double orifice with 2D spacing as shown in Figure 3-10

Drag Reduction ($\mathrm{DR_O}$) across orifice is defined as:

$$\mathrm{DR_O} = \frac{\Delta \mathrm{P_{O,without\ DRP}} - \Delta \mathrm{P_{O,with\ DRP}}}{\Delta \mathrm{P_{O,without\ DRP}}} \tag{4-2}$$

Where,

$\Delta \mathrm{P_{O,without\ DRP}}$= Static pressure drop across orifice without drag reducing polymer

$\Delta \mathrm{P_{O,with\ DRP}}$= Static pressure drop across orifice with drag reducing polymer

In case of double orifice, it is the pressure drop across double orifice.

ΔP_O= P1-P2 for single and double orifice with 1D spacing as shown in Figure 3-8 and Figure 3-9.

ΔP_O= P1-P4 for double orifice with 2D spacing as shown in Figure 3-10.

Quantity of drag reducing polymers was maintained at the lowest and hence the minimum concentration of drag reducing polymer was maintained in every case.

Concentration of drag reducing polymer in the pipe is defined as:

$$C(\text{ppm}) = \frac{Q_{DRP}}{Q_{Total}} \times 1000 \qquad (4\text{-}3)$$

Where,

$C(\text{ppm})$= Concentration of drag reducing polymer in the pipe in ppm.

Q_{DRP}= Flow rate of drag reducing polymer in litres/min.

Q_{Total}= Total flow rate of liquid including drag reducing polymer in litres/min.

Also, the pressure coefficient (C_p) is defined as:

$$C_p = \frac{\Delta P}{\frac{1}{2}\rho u^2} \qquad (4\text{-}4)$$

Where,

ΔP= Static pressure difference at any point with respect to pressure upstream of the orifice

ρ= density of the fluid

u= Average velocity of the fluid.

Pressure readings were taken with the help of piezometer tubes. Appendix A shows the pressure readings at different Reynolds numbers for single and two phase flows. It should be mentioned that there is a plastic tube connecting two pipe sections in between last two pressure taps that may have caused some additional losses.

Also, in order to investigate the effect of drag reducing polymer on the flow field characteristics downstream of different orifice arrangements, a Particle Image Velocimetry (PIV) technique was used on one or two bevel edged orifice plates of diameter ratio 0.5 and 0.63 having a thickness of 3mm in a pipe with internal diameter of 25.4mm. Experimental measurements were performed for single and double orifice configuration for flows with and without drag reducing polymer (DRP).

The area of interest where the flow field was examined is the downstream section of the orifice having length 4D, and the spacing (1D and 2D) between the two orifices in the double orifice configuration. The orifice used in single and double orifice arrangements had exactly the same dimensions. The length of the 4D downstream section covered by the optical width of laser light differs between 2D and 2.5D. This limitation is due to the limited distance between laser and test section. Table 4-1 shows a summary of the parameters used in the PIV recordings and analysis was performed based on the sequence shown in Figure 3-14.

Around 4000 images were taken on average at different frame rates and exposure time depending on the Reynolds number. The PIV velocity vectors were acquired at 340 × 50 points approximately in axial and vertical directions of the downstream plane. The validation of the results obtained through PIV analysis was done by doing numerical integration of the velocity profiles and then compared it with measured flow rate.

Table 4-1 Parameters used in PIV measurements

Flow Properties	Reynolds Number.	3972, 5958
Test Section	Pipe ID, and OD	25.4 mm, 38.6mm
	Orifice size (D_r=d/D)	0.5, 0.63
	Test piece material	Acrylic
	Fluid	Water
	Drag Reducing Polymer	ZETAG® 8165
Seeding	Type	Polyamide
	Density	1.03 g/cm^3
	Mean diameter	20 µm
Light sheet (Laser)	Type	Continuous wave (CW)
	Beam max. output	4 W
	Wavelength	532 nm
	Beam diameter at aperture	4 nm
Camera	Type	Charged Coupled Device(CCD)
	Chip size	1632 × 1200 pixels
	Discretization	8 bit
	Pixel size	11.5 µm
	Lens focal length	60 mm
Capturing	f-number	2.8
	Viewing Angle	Right Angle
	Image Magnification	0.217
	Measurement Area size	1152 × 480
	Real viewing area	61.70 × 25.70 mm^2
	Pulse separation	100-500 based on Re and D_r
	Max. particle displacement	10 pixels
PIV Analysis	Interrogation area size	32 × 32 pixels
	Overlap ratio	50% overlap
	Number of iterations	3 iterations

4.1. Single Phase Pressure Drop

Figure 4-1 shows the total static pressure drop (ΔP_T) as defined in page (44) for single orifice having a diameter ratio of 0.63 at different Reynolds numbers ranging from 2300 to 12000. The flow rate of water in polymeric solution was reduced according to the quantity of drag reducing polymer used. It is clear that pressure drop is higher at higher Reynolds numbers. The percentage drag reduction is considerable in lower Reynolds number flows. This reduction is less prominent at higher Reynolds numbers. Similar trend was observed in the case of double orifices having same diameter ratio with 1 pipe diameter and 2 pipe diameter spacing as shown in Figure 4-2 and Figure 4-3. However, it is also found that pressure drop is less in case of double orifice with 1D spacing than single and double orifice with 2D spacing. Double orifice with 2D spacing experienced largest pressure drop in most of the cases. Similar kind of behavior was observed in 0.5 diameter ratio orifice as shown in Figure 4-4, Figure 4-5, and Figure 4-6, however pressure drop was quite greater than respective 0.63 diameter ratio orifices.

Figure 4-7 shows the pressure drop (ΔP_O) across single orifice having D_r=0.63 with and without drag reducing polymer. A reduction in pressure drop can be observed in flows with drag reducing polymer. Figure 4-8 and Figure 4-9 shows the pressure drop across double orifice configuration with 1D and 2D spacing respectively at the same Reynolds numbers. While, Figure 4-10, Figure 4-11, and Figure 4-12 shows the pressure drop across single orifice, double orifice with 1D spacing, and double orifice with 2D spacing having D_r=0.5 respectively. Similar kind of behavior is observed in these orifice arrangements. The variation of pressure coefficient with normalized axial distance for each case is now briefly described.

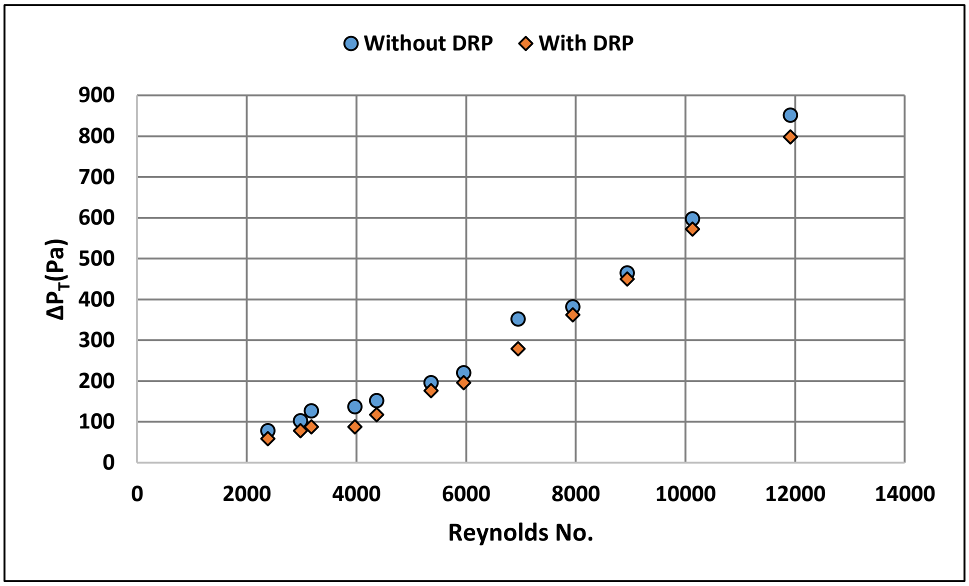

Figure 4-1 Comparison of total static pressure drop (ΔP_T) for a single orifice with $D_r = 0.63$ at different Reynolds numbers.

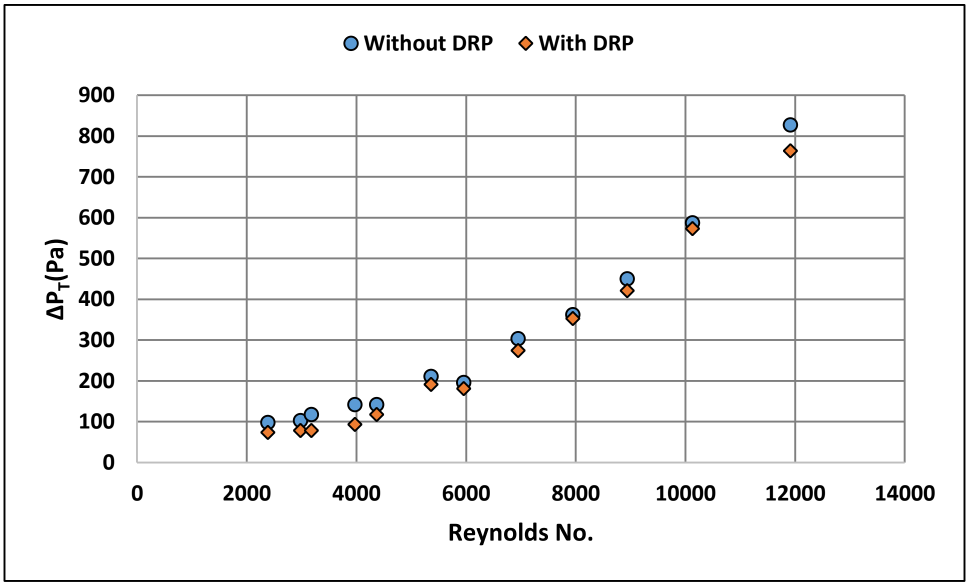

Figure 4-2 Comparison of total static pressure drop (ΔP_T) for double orifice-1D-spacing with $D_r = 0.63$ at different Reynolds numbers.

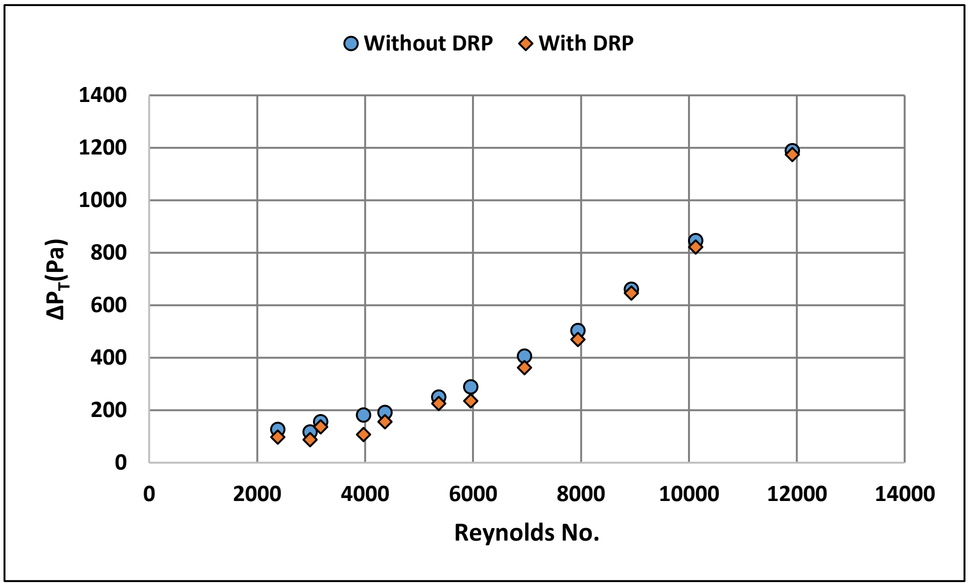

Figure 4-3 Comparison of total static pressure drop (ΔP_T) for double orifice-2D-spacing with $D_r = 0.63$ at different Reynolds numbers.

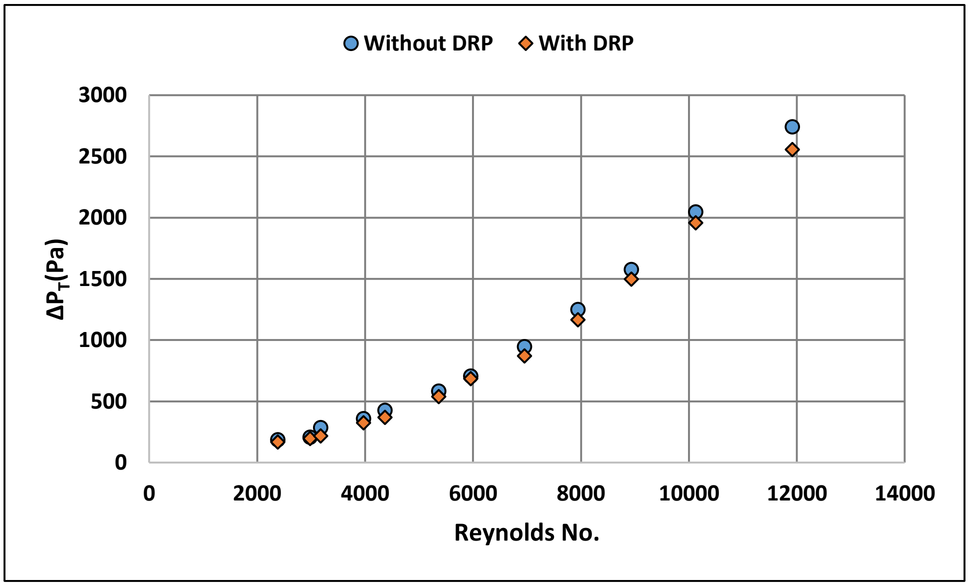

Figure 4-4 Comparison of total static pressure drop (ΔP_T) for single orifice with $D_r = 0.5$ at different Reynolds numbers.

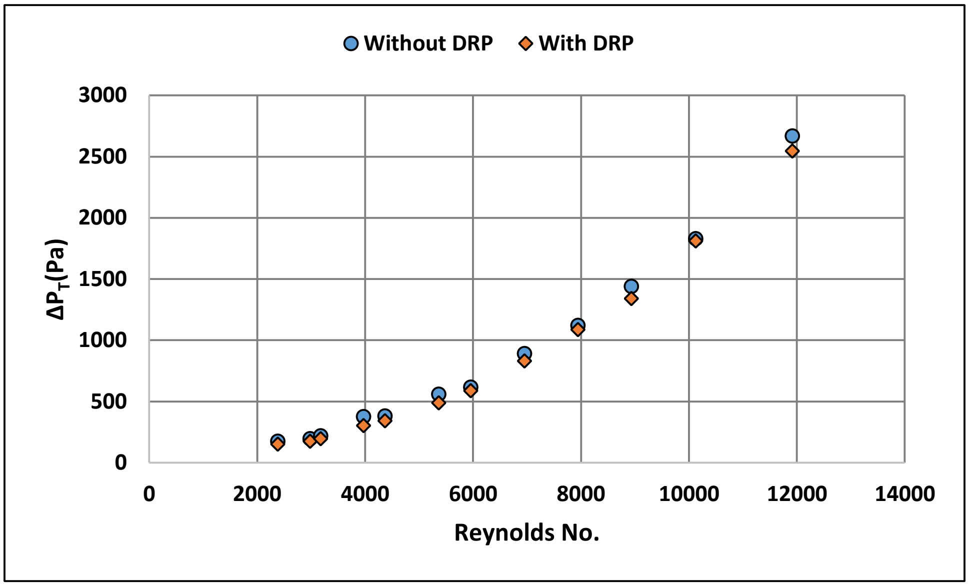

Figure 4-5 Comparison of total static pressure drop (ΔP_T) for double orifice-1D-spacing with D_r = 0.5 at different Reynolds numbers.

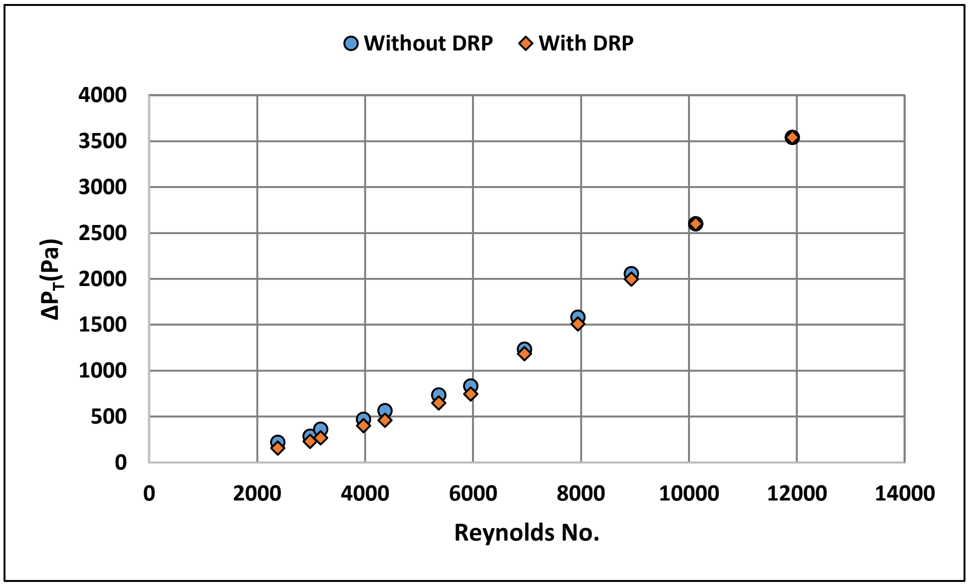

Figure 4-6 Comparison of total static pressure drop (ΔP_T) for double orifice-2D-spacing with D_r = 0.5 at different Reynolds numbers.

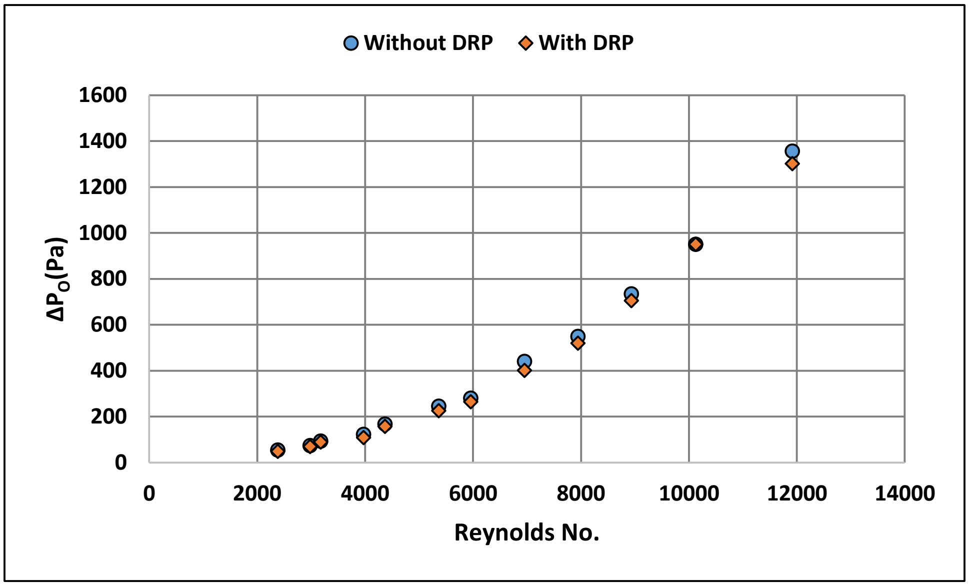

Figure 4-7 Comparison of pressure drop (ΔP_O) across single orifice having D_r = 0.63 at different Reynolds numbers.

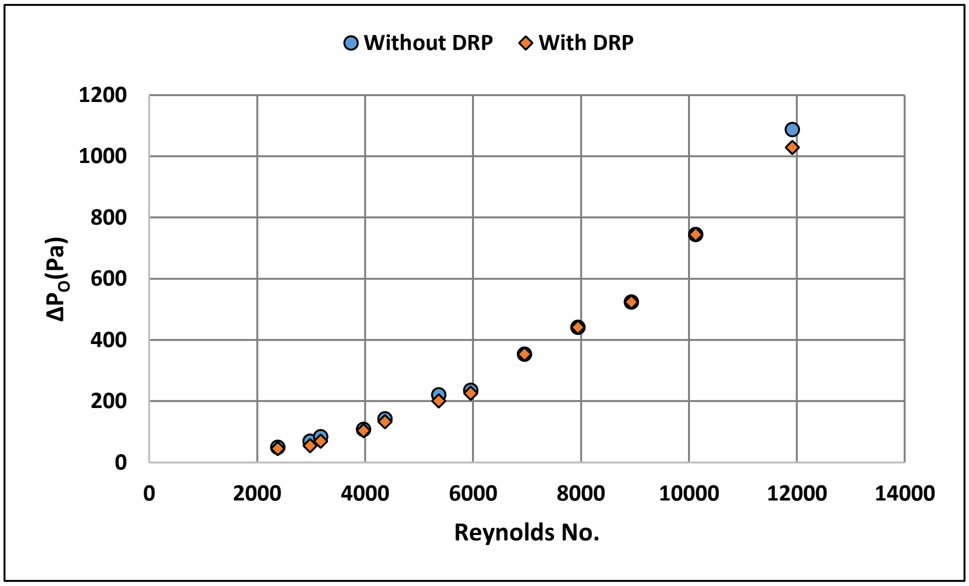

Figure 4-8 Comparison of pressure drop (ΔP_O) across double orifice with 1D spacing having D_r = 0.63 at different Reynolds numbers.

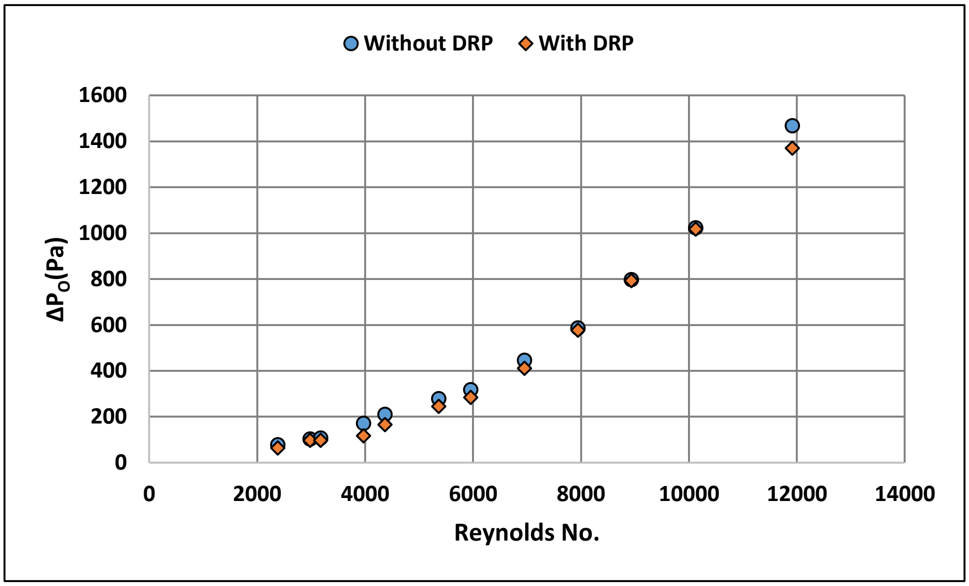

Figure 4-9 Comparison of pressure drop (ΔP_O) across double orifice with 2D spacing having $D_r = 0.63$ at different Reynolds numbers.

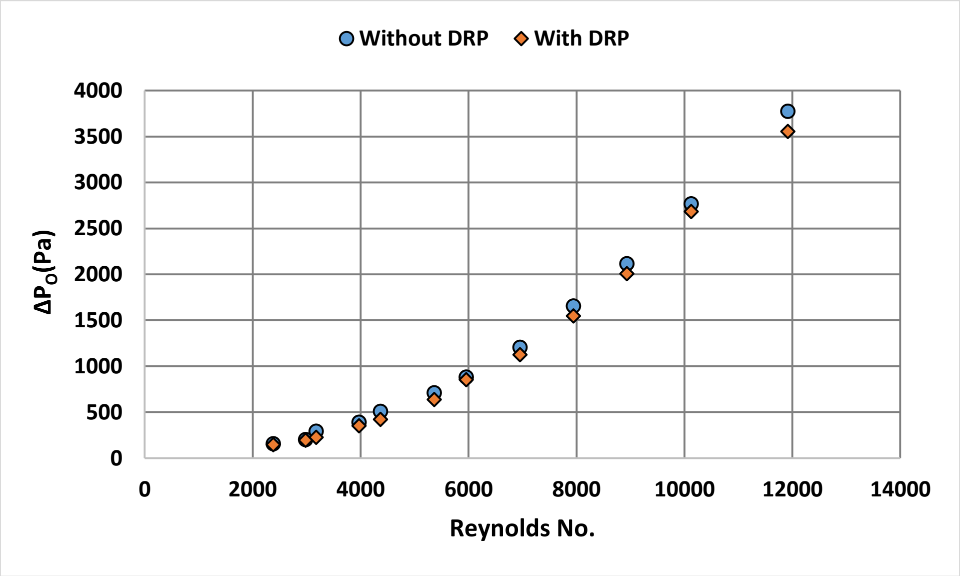

Figure 4-10 Comparison of pressure drop (ΔP_O) across single orifice having $D_r = 0.5$ at different Reynolds numbers.

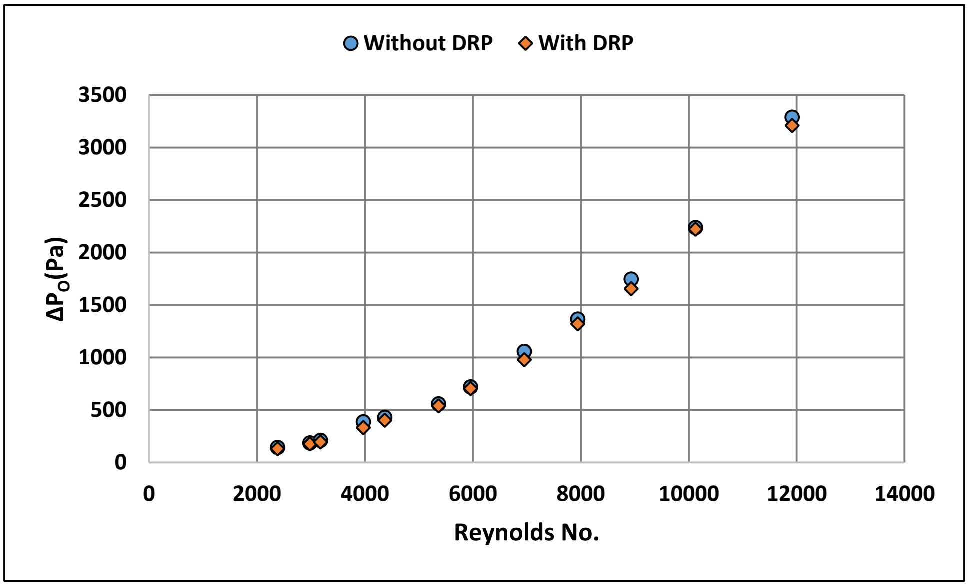

Figure 4-11 Comparison of pressure drop (ΔP_O) across double orifice with 1D spacing having $D_r = 0.5$ at different Reynolds numbers.

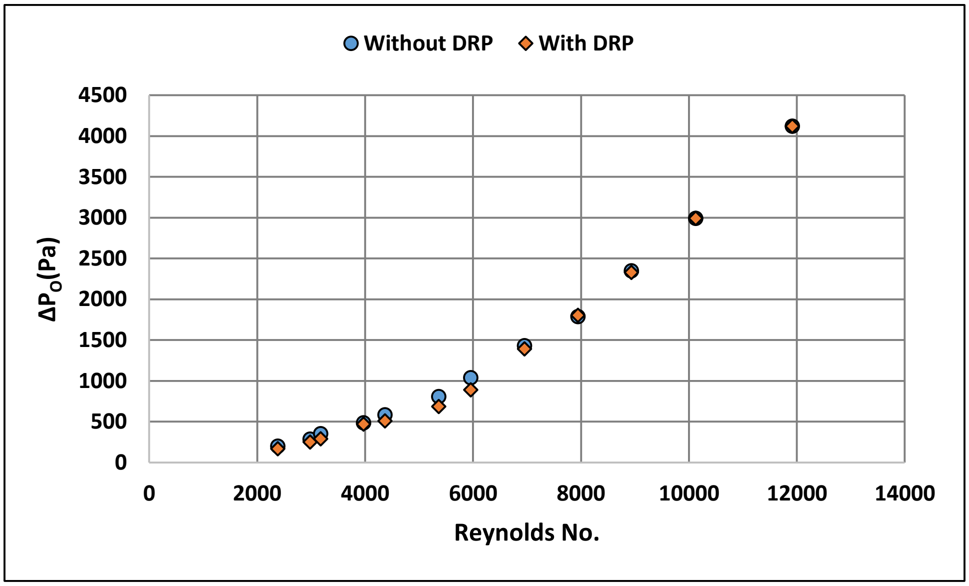

Figure 4-12 Comparison of pressure drop (ΔP_O) across double orifice with 2D spacing having $D_r = 0.5$ at different Reynolds numbers.

4.1.1. Re=2383

The Reynolds number in non-polymeric solution was 2383 and the concentration of drag reducing polymers (DRP) in polymeric solution was maintained at 196ppm. Figure 4-13 shows the pressure coefficient profile for the case of flow through orifice having $D_r = 0.63$ for different arrangements of orifices. Pressure upstream of the orifice is taken as reference pressure. It should be mentioned that in these figures, x/D is measured from first orifice plate in both single and double orifice configurations which means that the first orifice is located at x=0 as shown in Figure 3-2. Also the minimum pressure shown in case of double orifice with 1D spacing is the pressure downstream of the second orifice. 25% total drag reduction (DR_T) was observed in flow through both single and double orifice with 1D spacing while 23.1% total drag reduction was found in double orifice with 2D spacing. Also a decrease in pressure drop across the orifice is observed in all the case. 9.1%, 10%, and 18.8% drag reduction across orifice (DR_O) were observed for the respective three arrangements of orifices. Figure 4-14 shows the pressure coefficient profile for the case of flow through orifice having $D_r = 0.5$ for different arrangements of orifices at the same Reynolds no and same concentration of drag reducing polymer. 10.5, 13.9 and 28.9% total drag reduction (DR_T) was observed in single, double orifice with 1D spacing, and double orifice with 2D spacing respectively. Also 6.3, 6.9, and 17.1% drag reduction across orifices (DR_O) were observed across these three orifice configurations. The pressure drop through $D_r = 0.5$ is quite larger than $D_r = 0.63$ orifices.

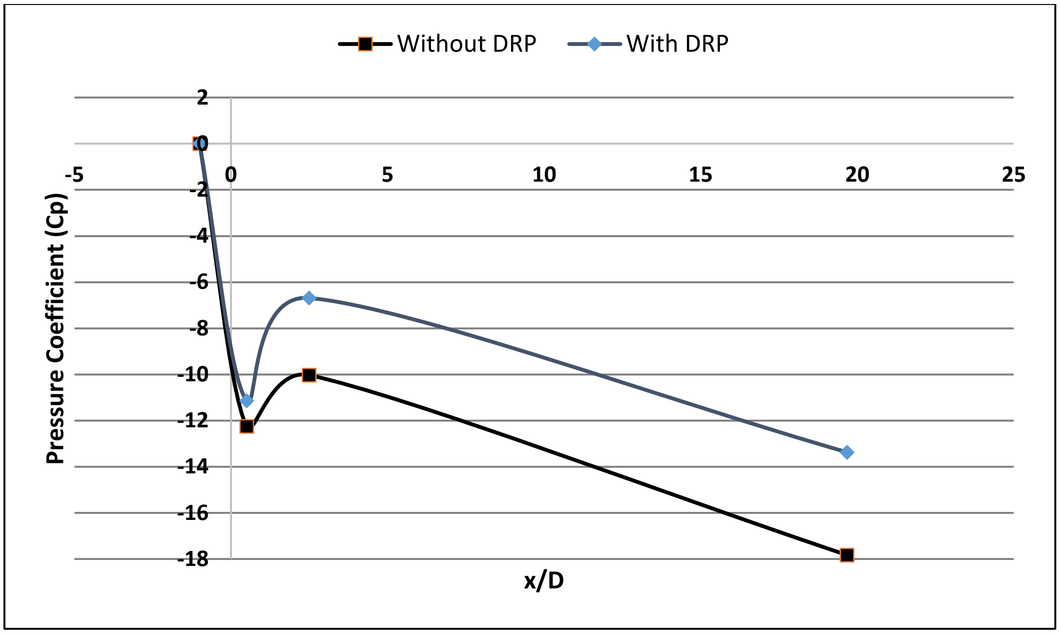

a) Single Orifice

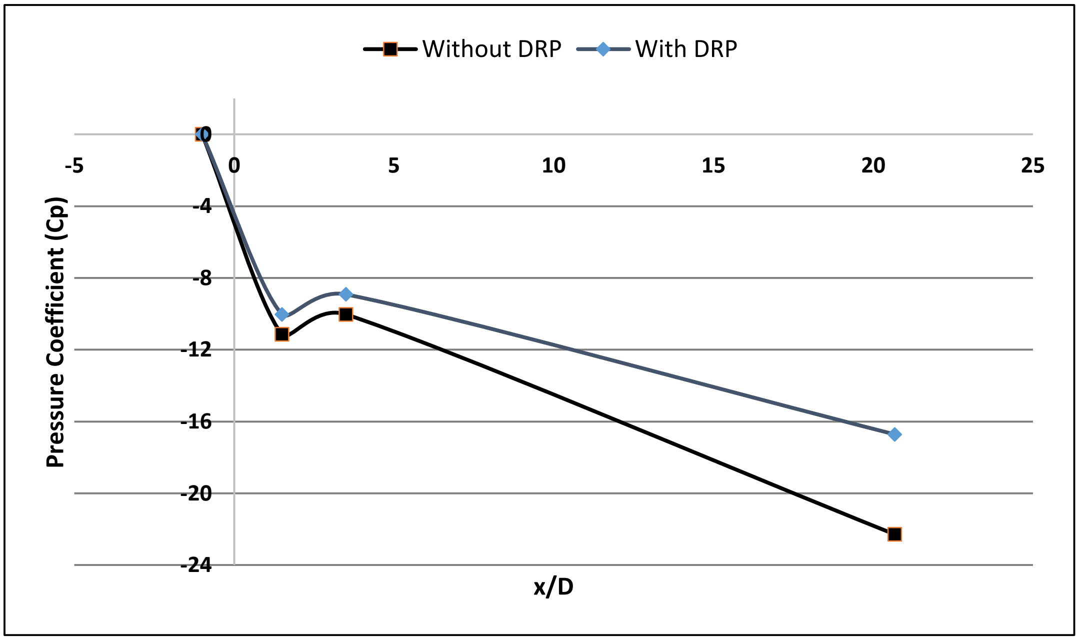

b) Double orifice with 1D spacing

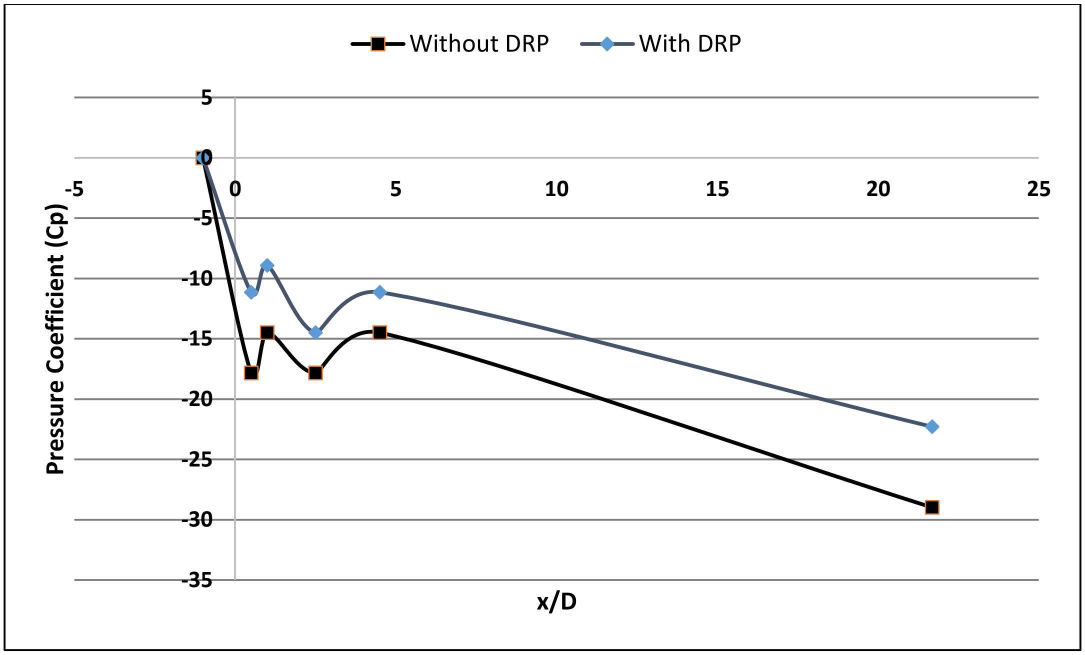

c) Double orifice with 2D spacing

Figure 4-13 Variation of pressure coefficient with normalized axial distance for the case of D_r = 0.63, Re= 2383 at 196ppm DRP; a) single orifice, b) double orifice with 1D spacing, c) double orifice with 2D spacing

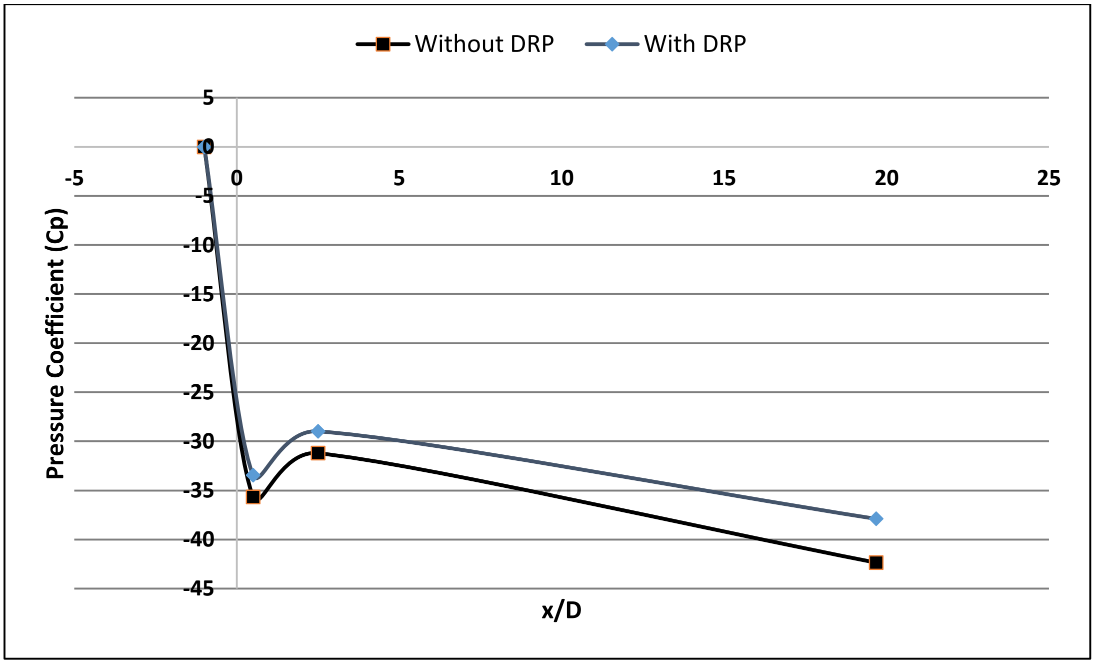

a) Single Orifice

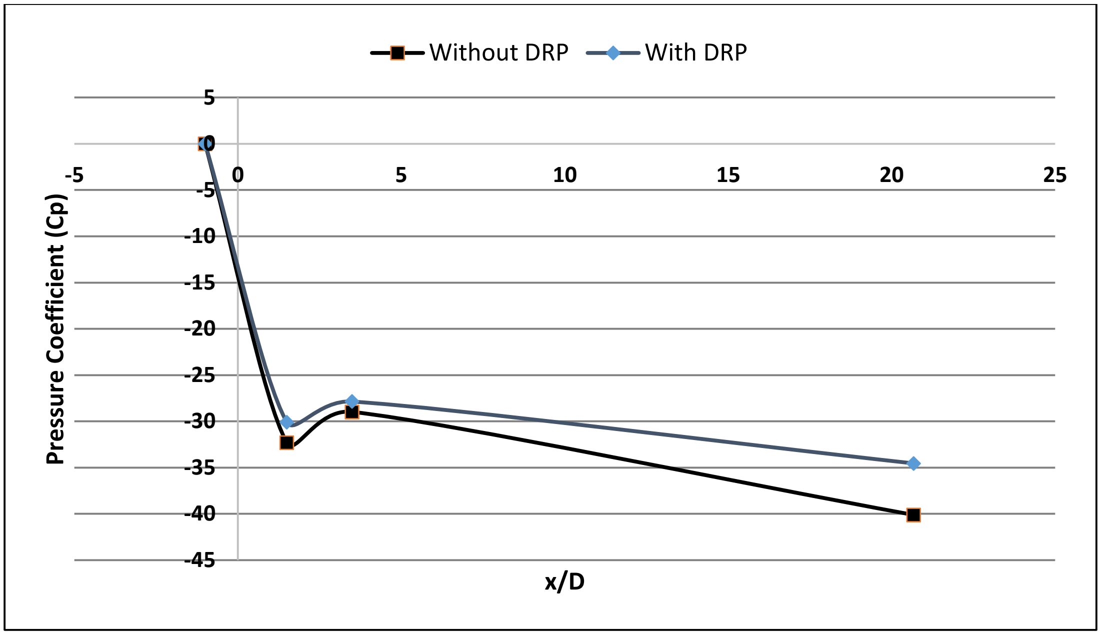

b) Double orifice with 1D spacing

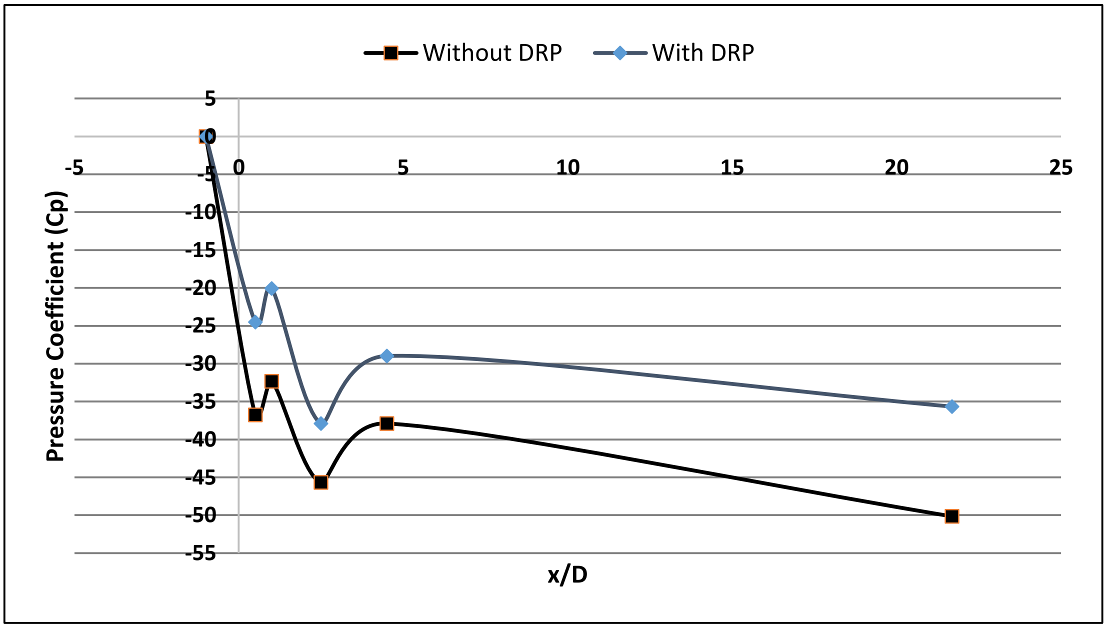

c) Double orifice with 2D spacing

Figure 4-14 Variation of pressure coefficient with normalized axial distance for the case of D_r = 0.5, Re= 2383 at 196ppm DRP; a) single orifice, b) double orifice with 1D spacing, c) double orifice with 2D spacing

4.1.2. Re=2979

In this case, the Reynolds number in non-polymeric solution was 2979 whereas the concentration of drag reducing polymers in polymeric solution was 158ppm. Figure 4-15 shows the profile of pressure coefficient for flow with and without drag reducing polymers through different arrangements of orifice having diameter ratio 0.63. 23.8% DR_T was observed in single orifice while 23.8 and 25% reduction in total drag was observed in double orifice with 1D and 2D spacing respectively. Also 6.7%, 21.4%, and 4.7% drag reductions (DR_O) were observed across these orifices. Figure 4-16 shows the corresponding pressure coefficient profiles through D_r=0.5 orifice. The reduction in drag was comparatively less than 0.63 diameter ratio orifice. 4.8, 10, and 19% total drag reduction (DR_T) was seen in corresponding three cases respectively. Similarly, 2.4, 5.3, and 12.1% DR_O were observed in these three arrangements of D_r = 0.5 orifices respectively.

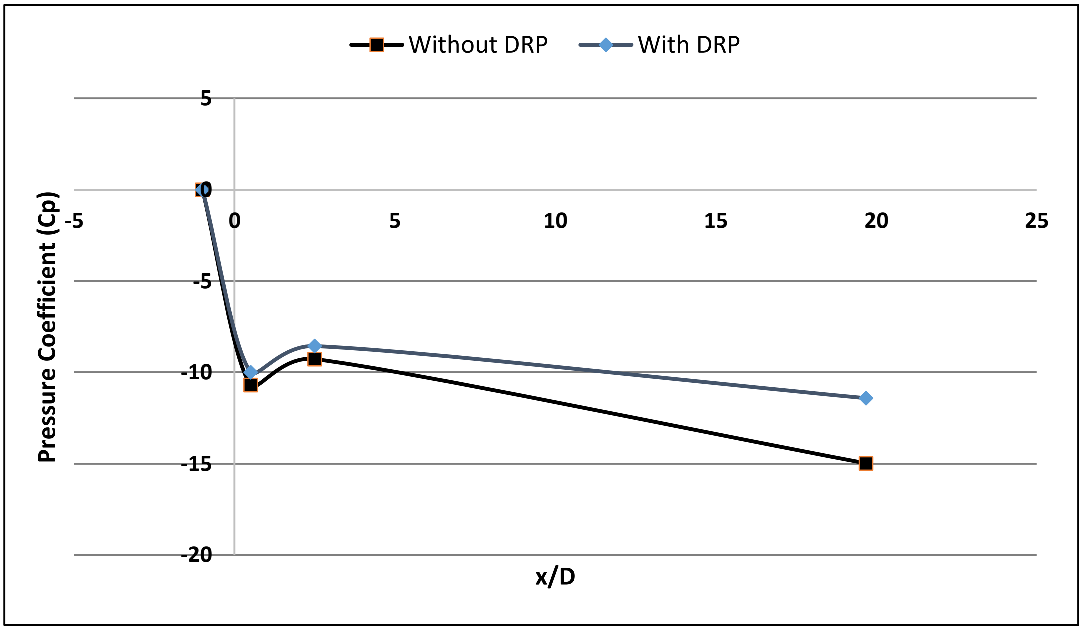

a) Single orifice

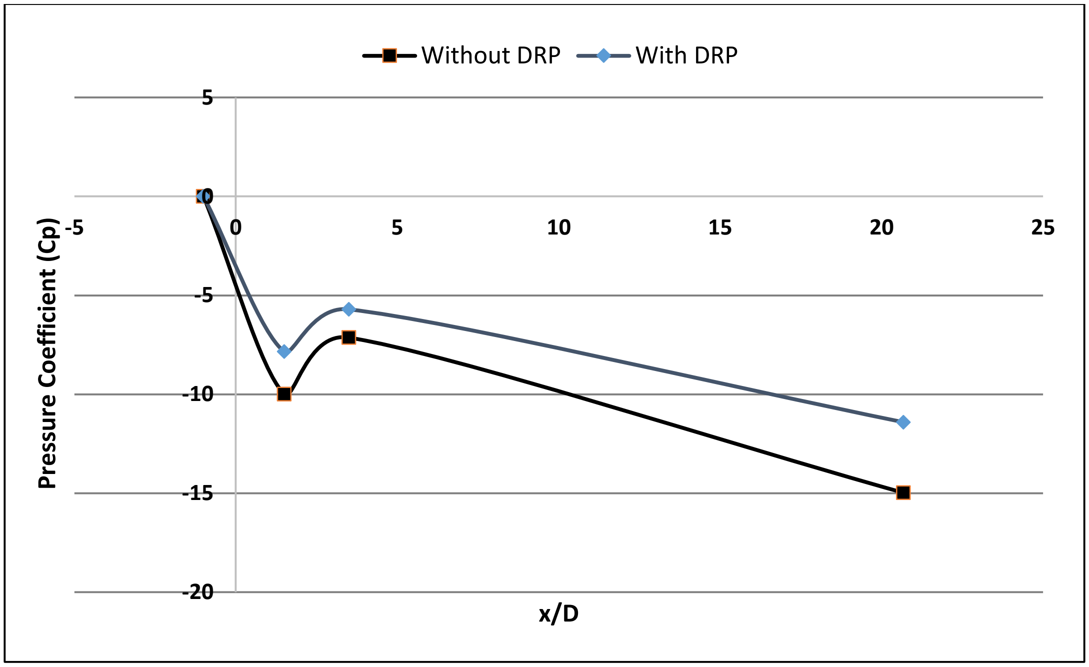

b) Double orifice with 1D spacing

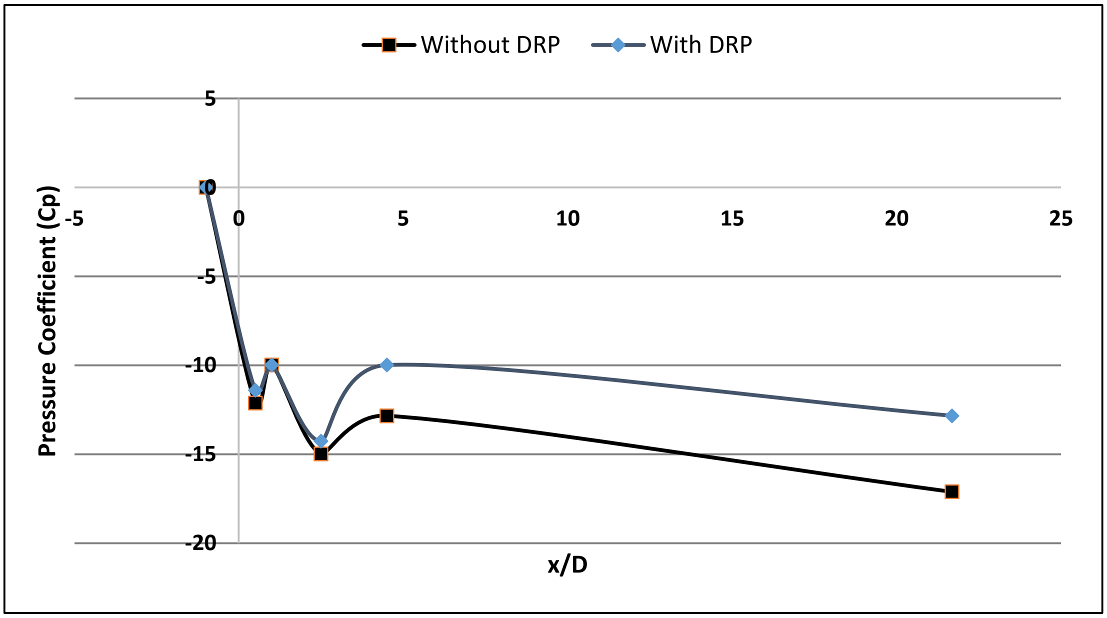

c) Double orifice with 2D spacing

Figure 4-15 Variation of pressure coefficient with normalized axial distance for the case of D_r = 0.63, Re= 2980 at 158ppm DRP; a) single orifice, b) double orifice with 1D spacing, c) double orifice with 2D spacing

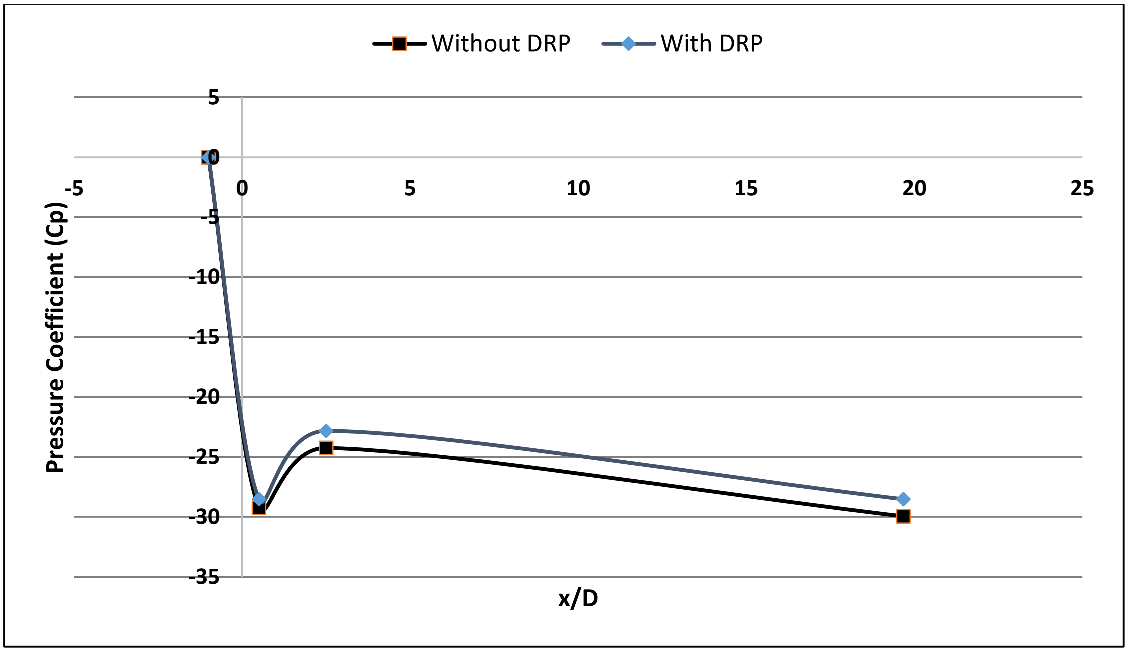

a) Single Orifice

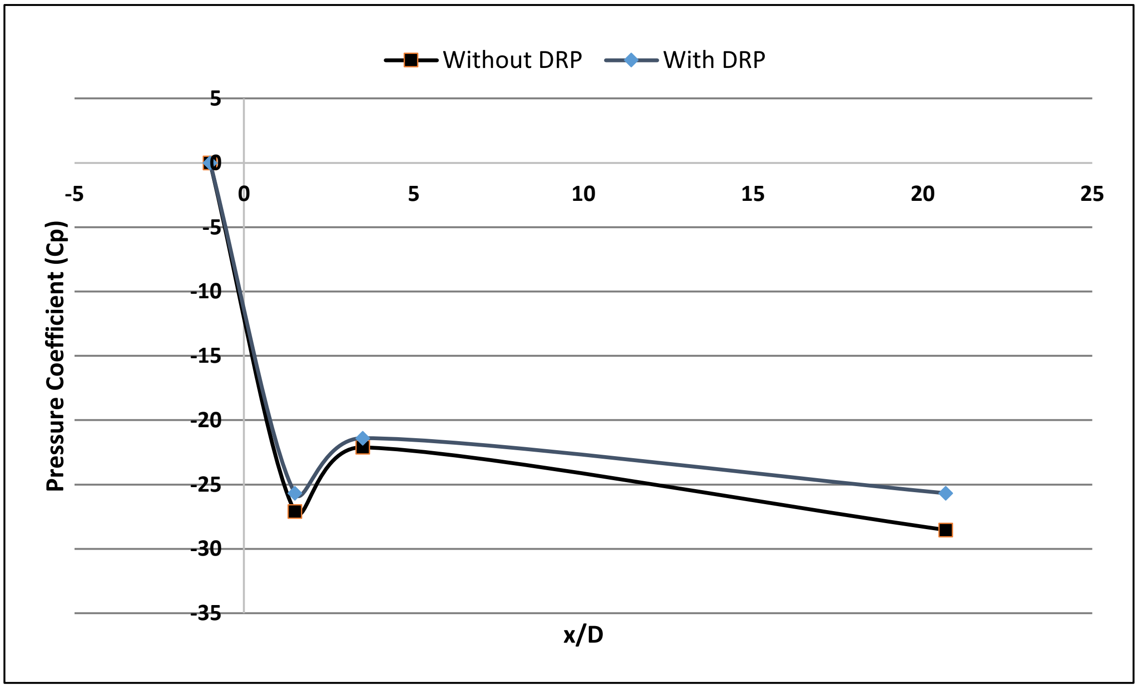

b) Double orifice with 1D spacing

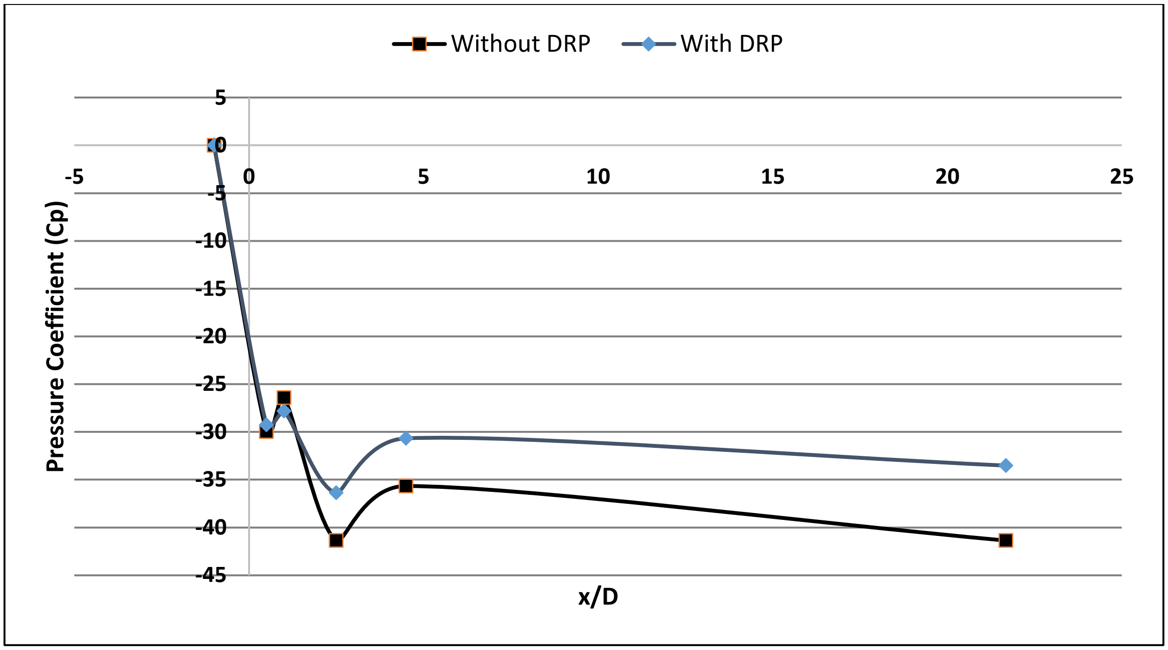

c) Double orifice with 2D spacing

Figure 4-16 Variation of pressure coefficient with normalized axial distance for the case of D_r = 0.5, Re= 2980 at 158ppm DRP; a) single orifice, b) double orifice with 1D spacing, c) double orifice with 2D spacing

4.1.3. Re=3177

The Reynolds number of water in non-polymeric solution in this case was 3177 and the concentration of polymer in polymeric solution was kept at 148ppm. Figure 4-17 and Figure 4-18 shows the profiles of pressure coefficients through 0.5 and 0.63 diameter ratio orifices at this Reynolds no. 30.8, 33.3 and 12.5% DR_T was observed in D_r = 0.63 orifices in single, double with 1D spacing, and double with 2D spacing configuration. Also, 5.3%, 17.6 and 9.1% DR_O was found in the respective three arrangements of D_r = 0.63 orifices. On the other hand, 24.1, 11.1, and 25.7% DR_T was observed in case of 0.5 diameter ratio orifices. Similarly 23.3, 7 and 18.1% DR_O was observed in 0.5 diameter ratio orifices respectively.

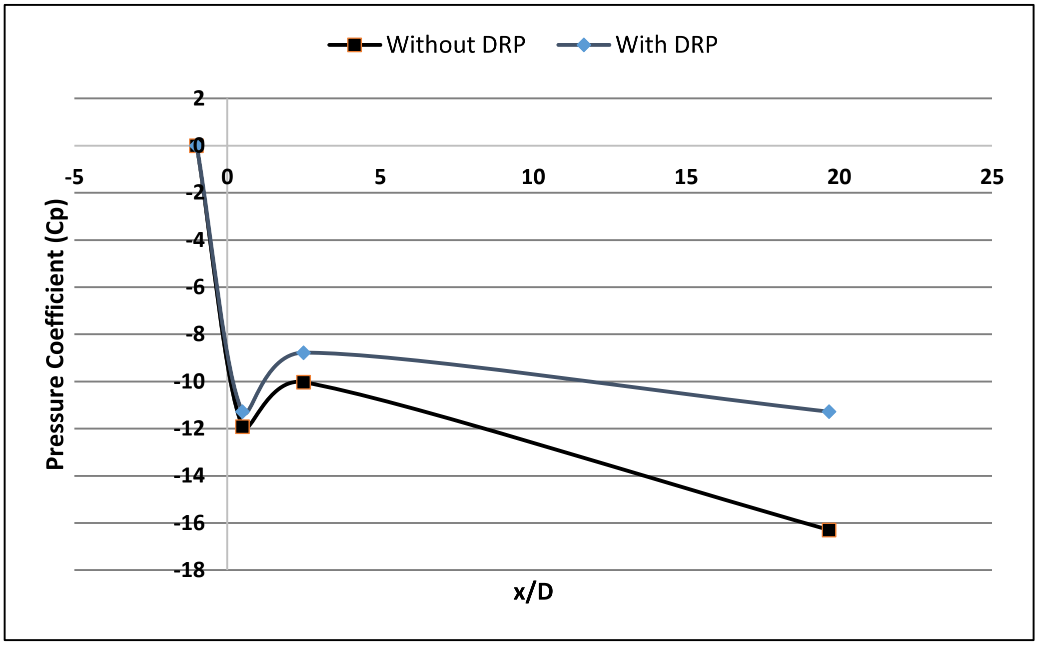

a) Single Orifice

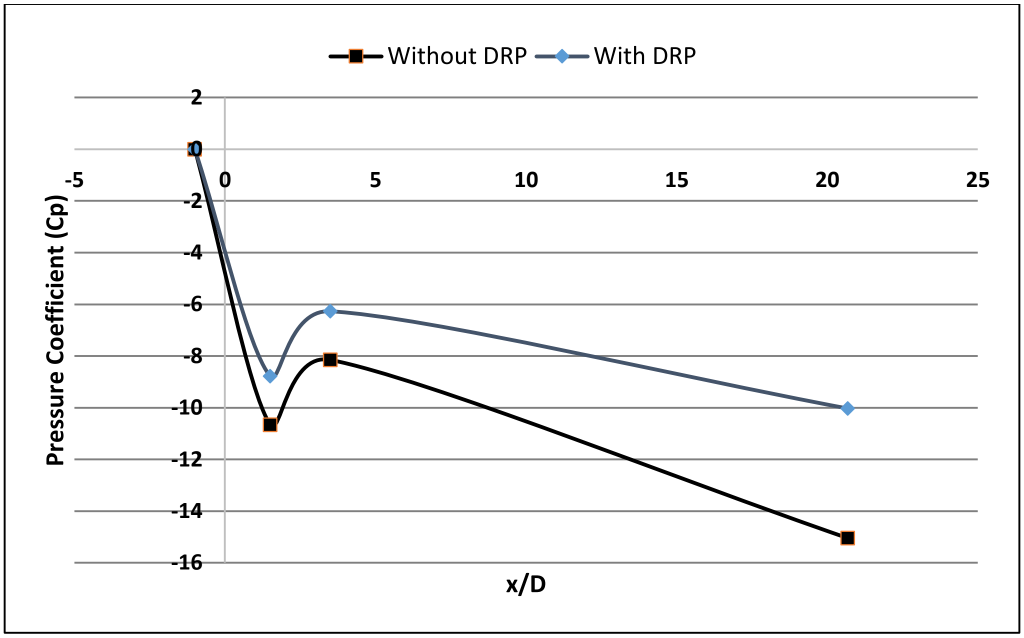

b) Double orifice with 1D spacing

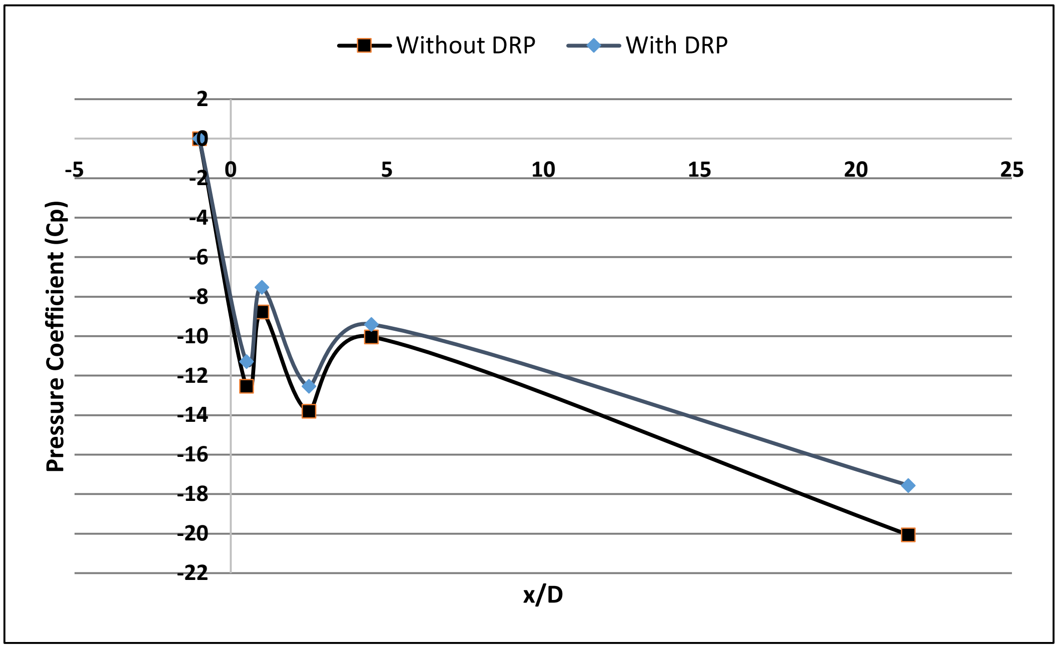

c) Double orifice with 2D spacing

Figure 4-17 Variation of pressure coefficient with normalized axial distance for the case of D_r = 0.63, Re= 3177 at 148ppm DRP; a) single orifice, b) double orifice with 1D spacing, c) double orifice with 2D spacing

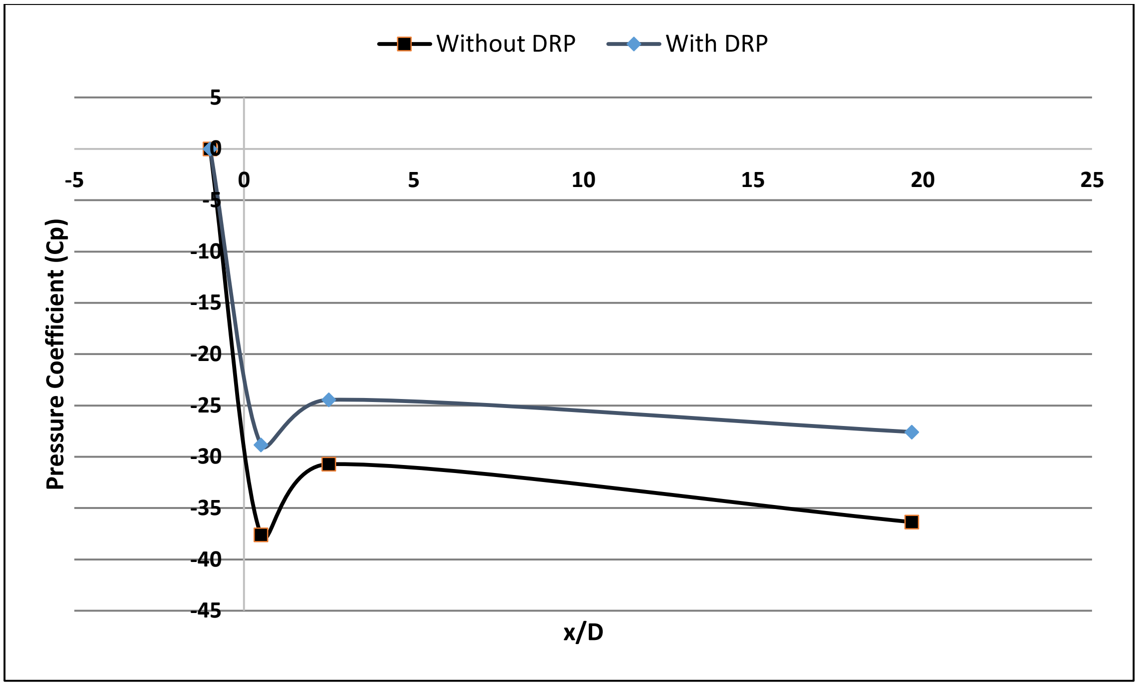

a) Single Orifice

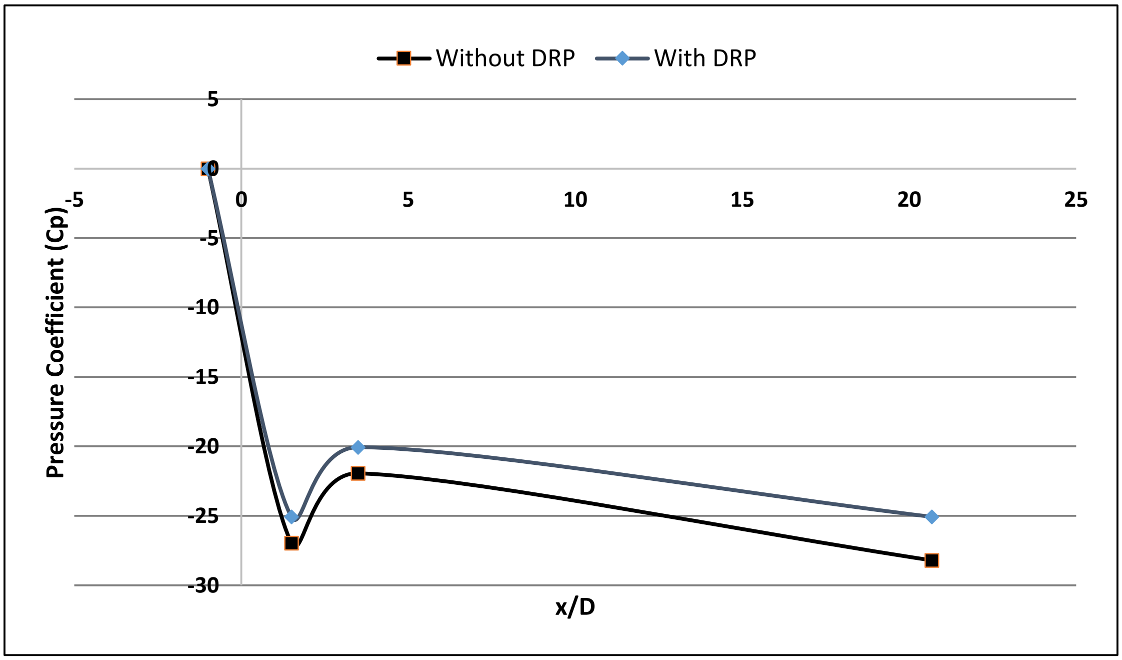

b) Double Orifice with 1D spacing

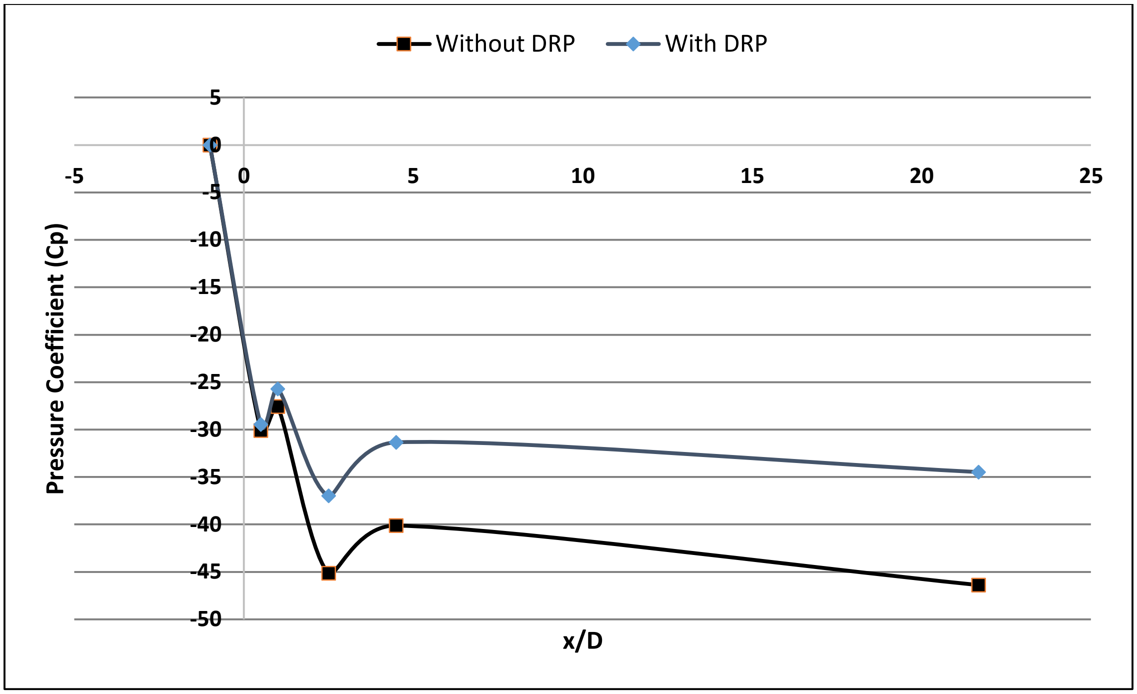

c) Double orifice with 2D spacing

Figure 4-18 Variation of pressure coefficient with normalized axial distance for the case of D_r = 0.5, Re= 3177 at 148ppm DRP; a) single orifice, b) double orifice with 1D spacing, c) double orifice with 2D spacing

4.1.4. Re=3972

Water Reynolds number in non-polymeric solution in this case was 3972 and the drag reducing polymer concentration in polymeric solution was 119ppm. Figure 4-19 and Figure 4-20 show the comparison of variation of pressure coefficient with normalized axial distance for 0.63 and 0.5 diameter ratio orifices at this Reynolds number respectively. 0.63 diameter ratio orifices experienced highest drag reduction at this flow rate. 35.7, 34.5, and 40.5% DR_T was observed for three configurations. Whereas 12, 4.5, and 31.4% DR_O was observed in corresponding three cases. 0.5 diameter ratio orifice showed 9.6, 19.5 and 14.6% DR_T for these three cases. Also, 10, 13.9 and 3% DR_O was observed in respective three arrangements.

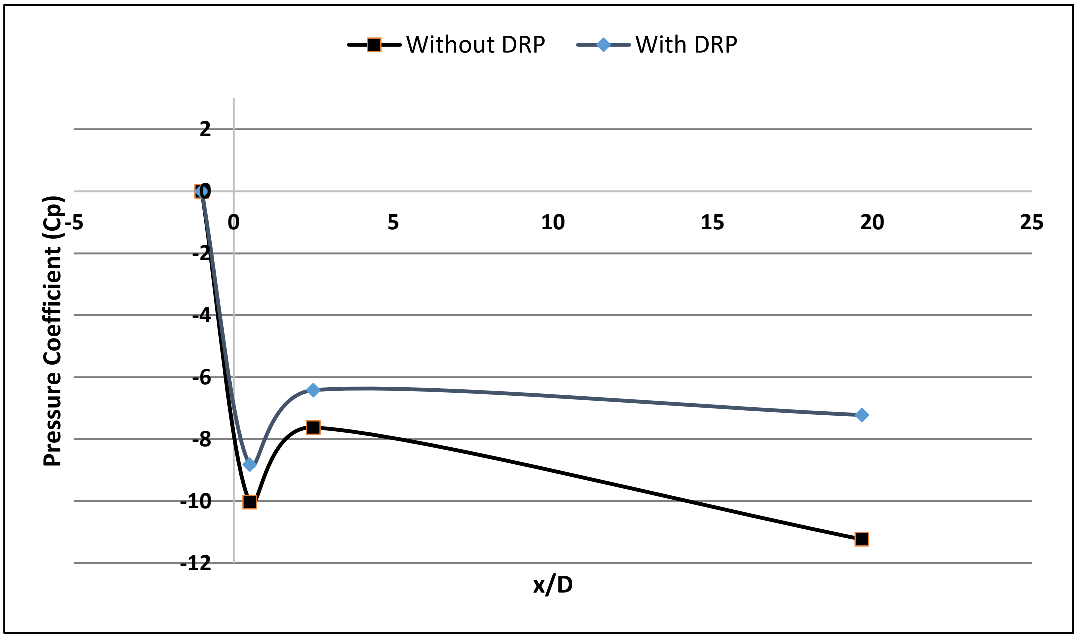

a) Single Orifice

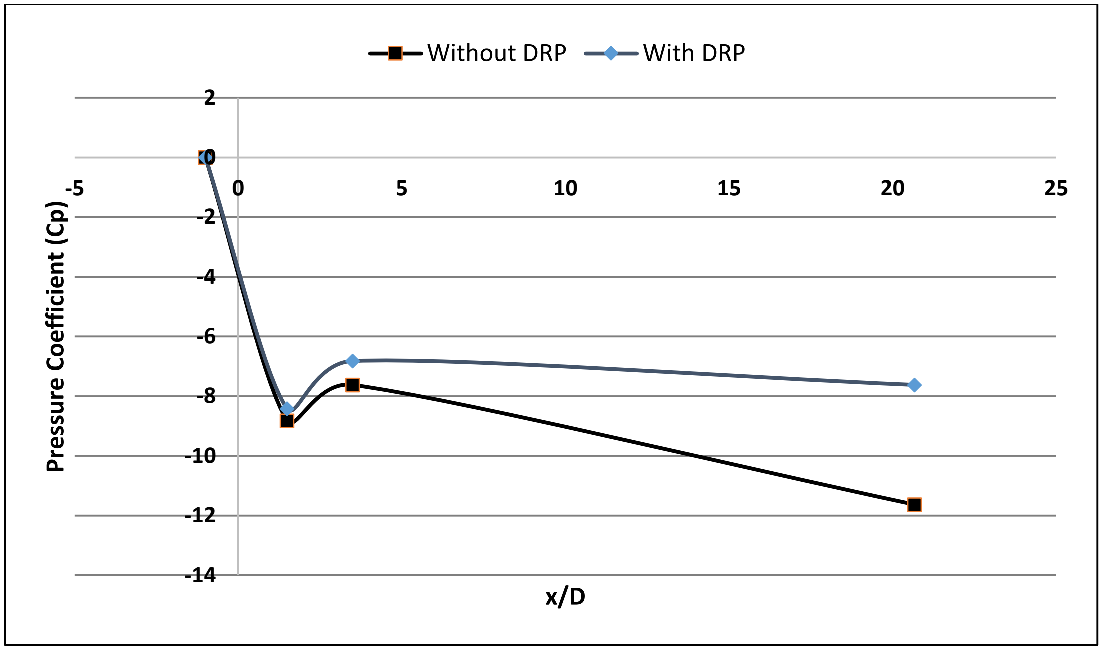

b) Double orifice with 1D spacing

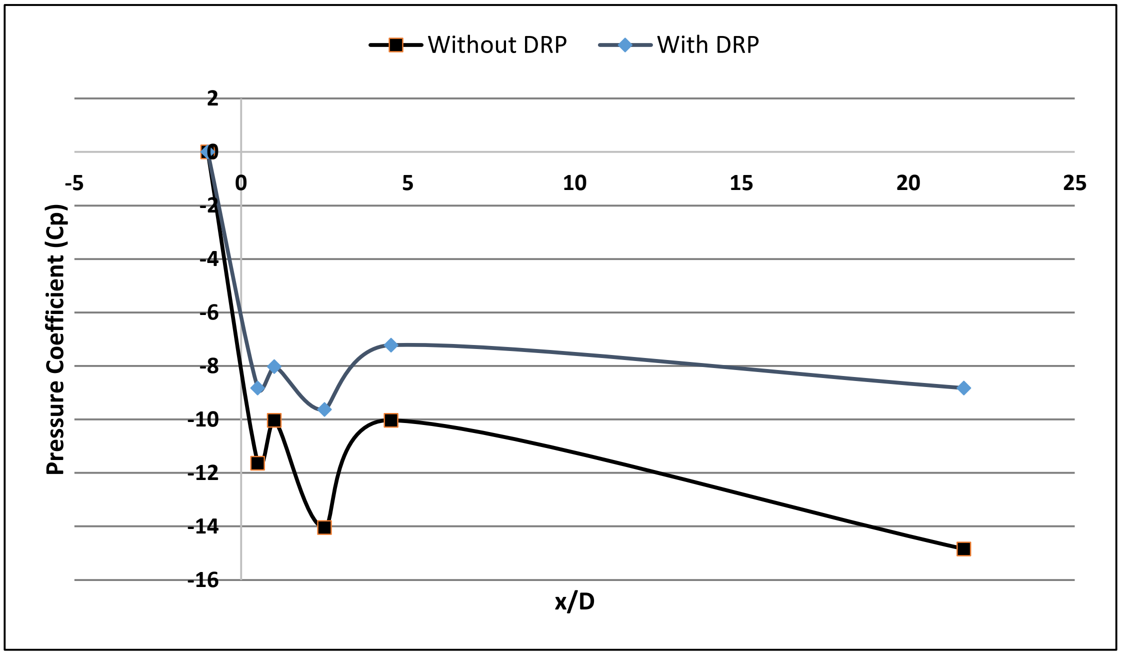

c) Single orifice with 2D spacing

Figure 4-19 Variation of pressure coefficient with normalized axial distance for the case of D_r = 0.63, Re= 3972 at 119ppm DRP; a) single orifice, b) double orifice with 1D spacing, c) double orifice with 2D spacing

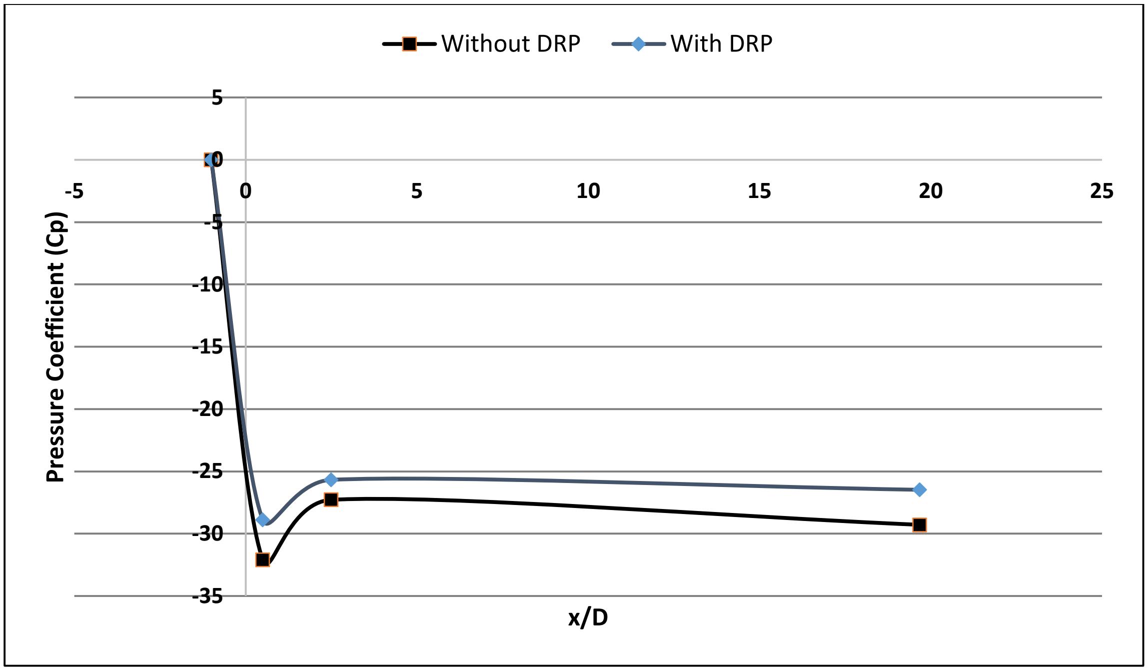

a) Single orifice

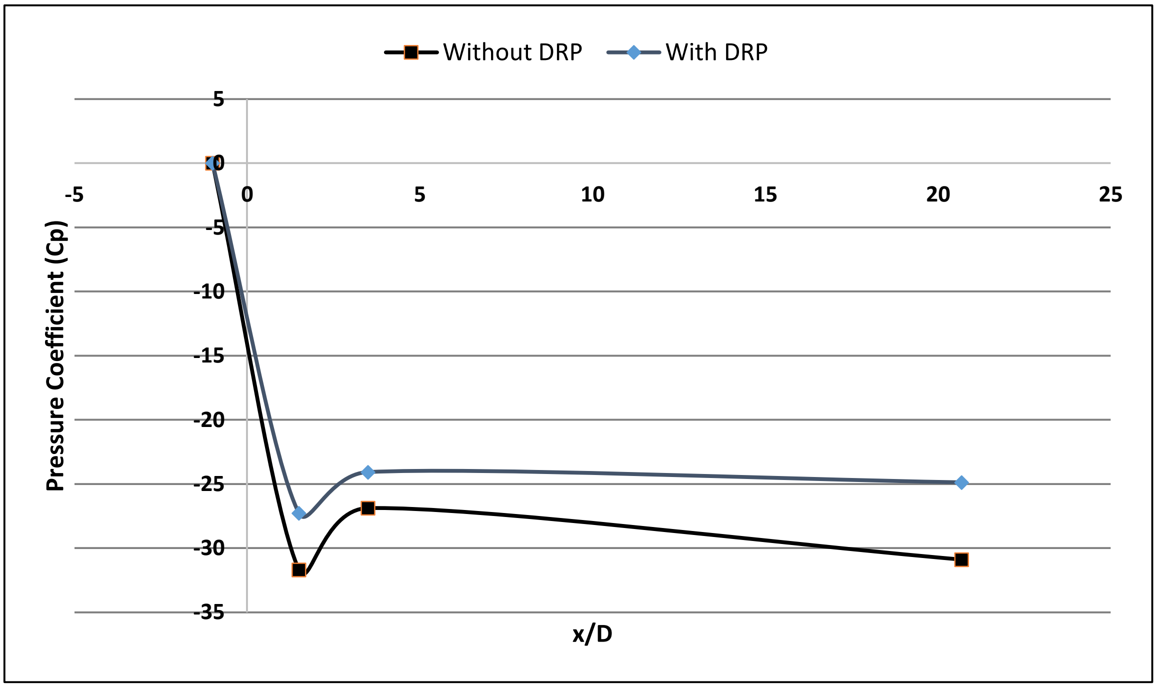

b) Double orifice with 1D spacing

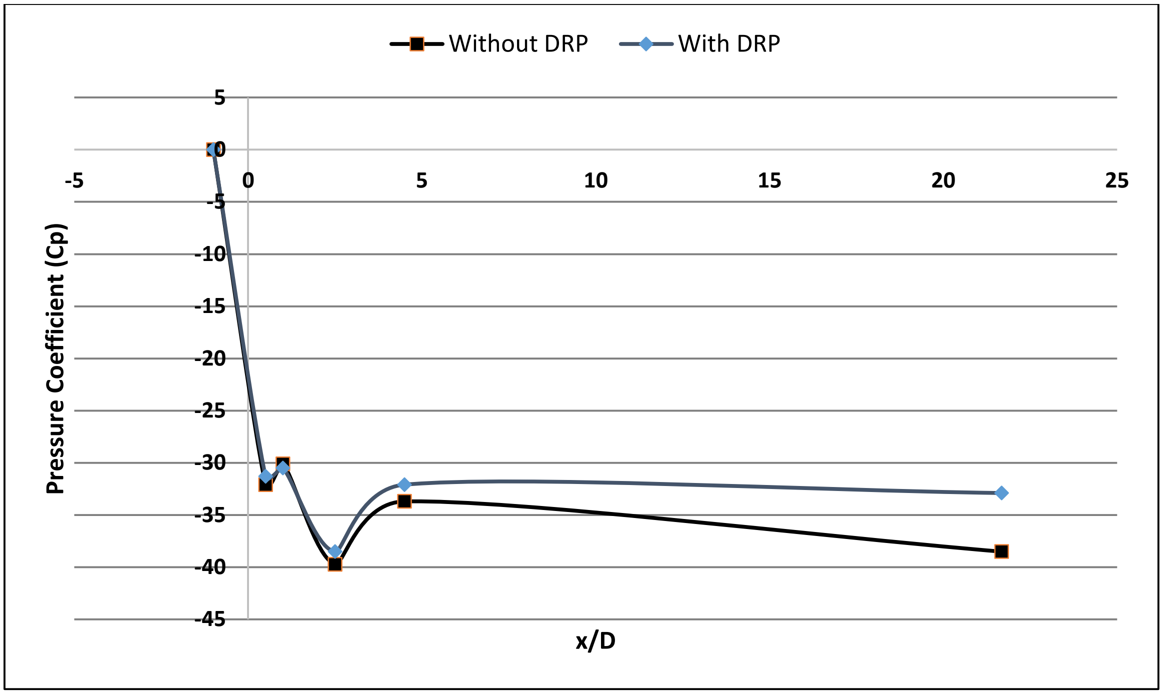

c) Double orifice with 2D spacing

Figure 4-20 Variation of pressure coefficient with normalized axial distance for the case of $D_r = 0.5$, Re= 3972 at 119ppm DRP; a) single orifice, b) double orifice with 1D spacing, c) double orifice with 2D spacing

4.1.5. Re=4369

The concentration of polymers in polymeric solution was kept at 108ppm in this case. Figure 4-21 and Figure 4-22 shows the pressure coefficient profiles for 0.63 and 0.5 diameter ratio orifices. 22.6, 17.2 and 17.9% DR_T was observed for the three cases of 0.63 diameter ratio orifice with 5.9, 6.9, and 20.9% DR_O. Whereas 13.8, 10.3, and 18.3% DR_T was found in 0.5 diameter ratio orifices along with 17.3, 6.8, 12.6 % DR_O across the orifices.

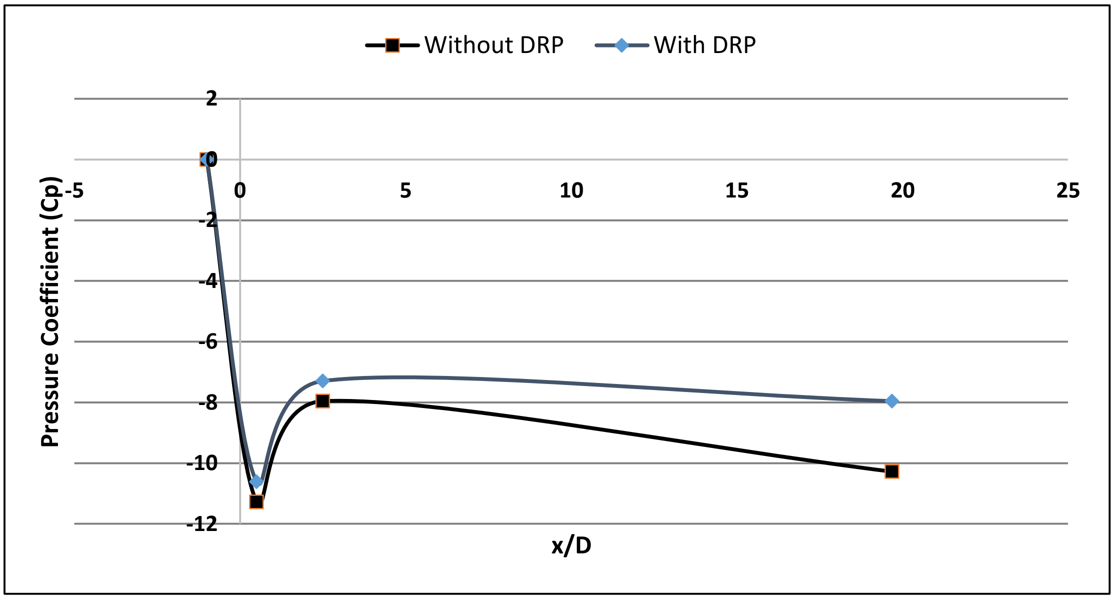

a) Single orifice

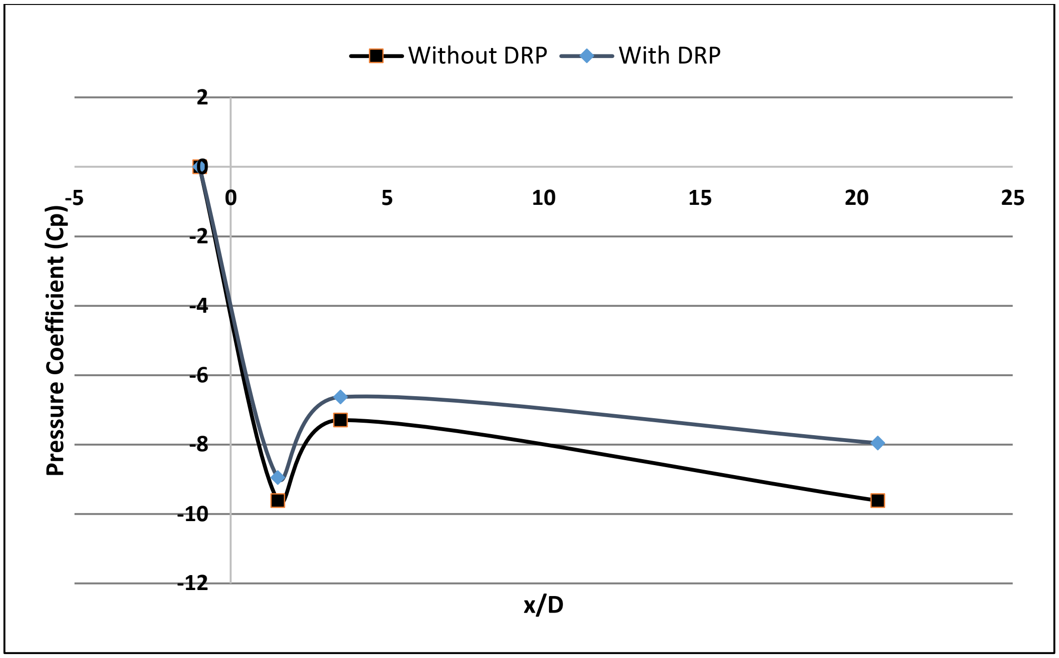

b) Double orifice with 1D spacing

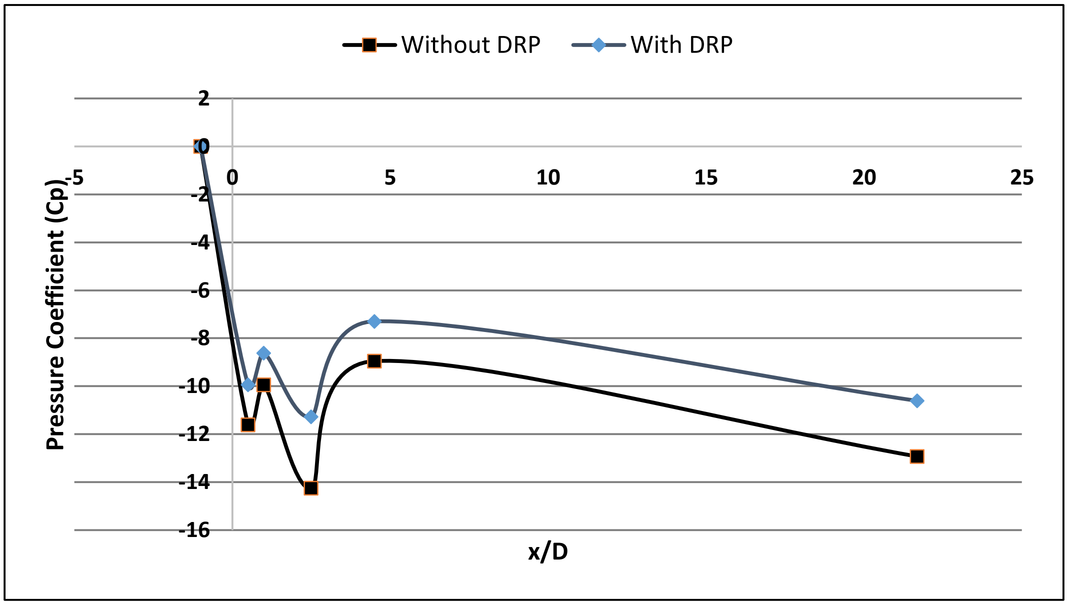

c) Double orifice with 2D spacing

Figure 4-21 Variation of pressure coefficient with normalized axial distance for the case of D_r = 0.63, Re= 4369 at 108ppm DRP; a) single orifice, b) double orifice with 1D spacing, c) double orifice with 2D spacing

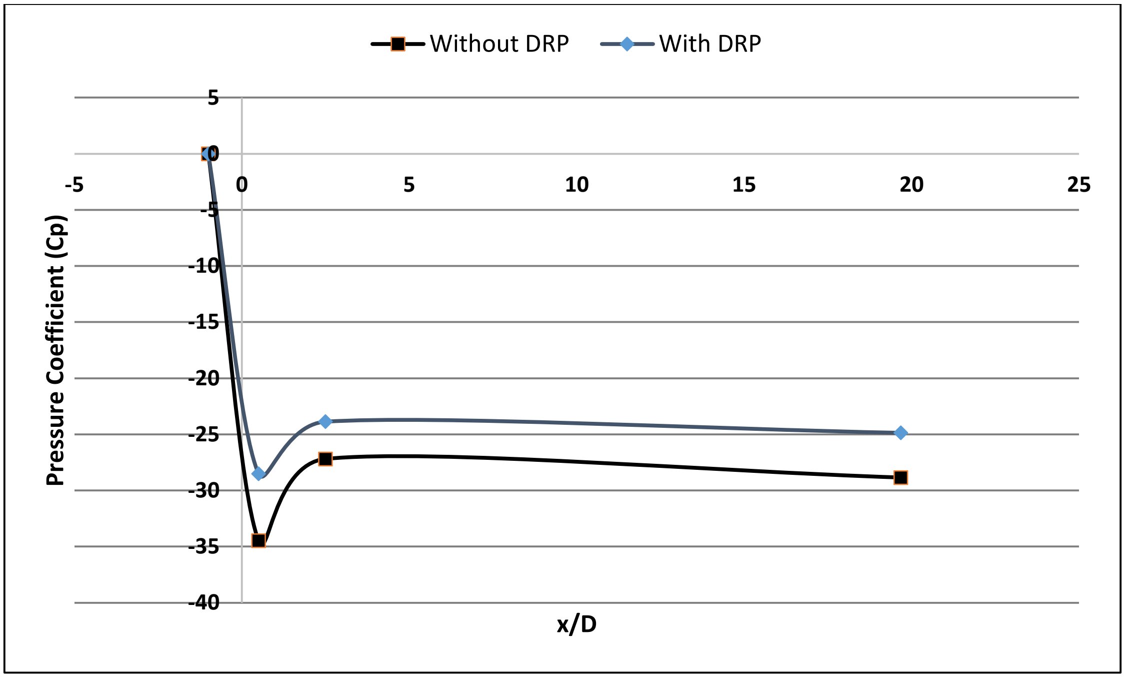

a) Single orifice

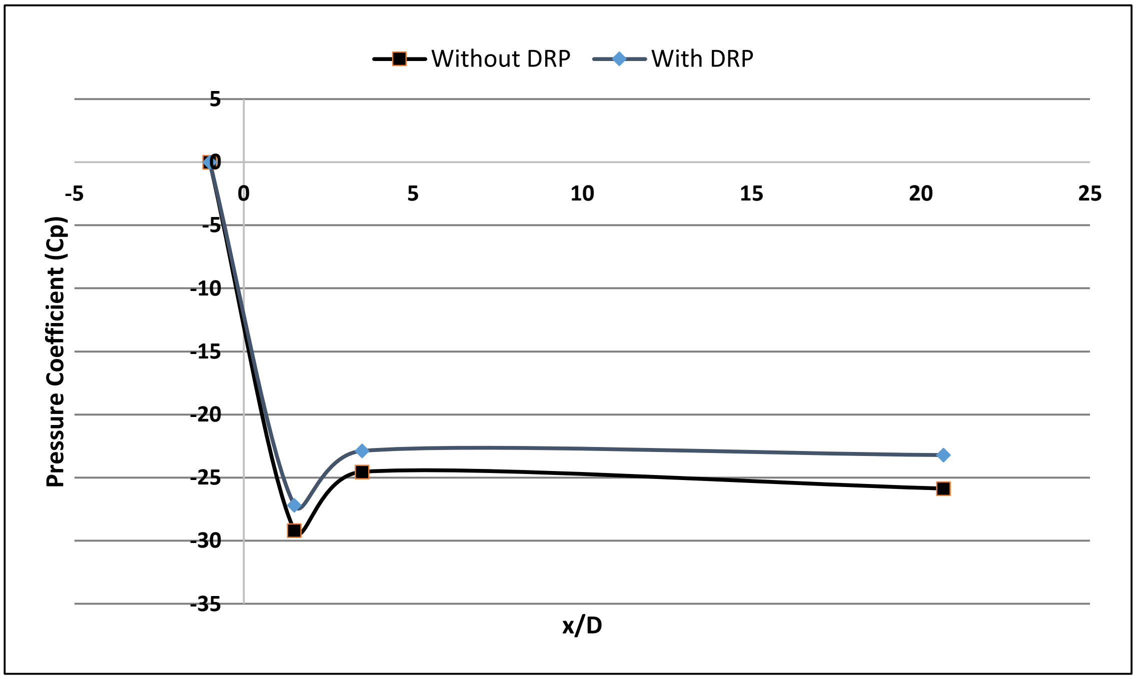

b) Double orifice with 1D spacing

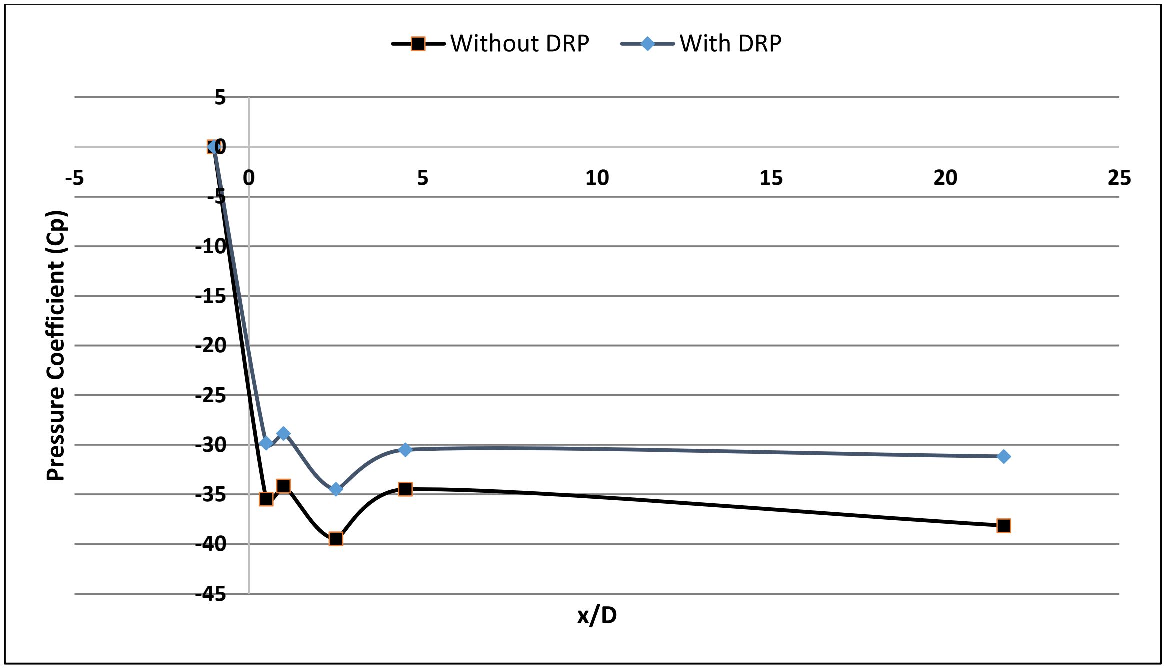

c) **Double orifice with 2D spacing**

Figure 4-22 Variation of pressure coefficient with normalized axial distance for the case of D_r = 0.5, Re= 4369 at 108ppm DRP; a) single orifice, b) double orifice with 1D spacing, c) double orifice with 2D spacing

4.1.6. Re=5362

The concentration of drag reducing polymers in polymeric solution was 89ppm in this case. Figure 4-23 and Figure 4-24 shows the pressure coefficient profiles of 0.63 and 0.5 diameter ratio orifices at this flow rate. 10, 9.3 and 9.8% DR_T was observed for the three cases of 0.63 diameter ratio orifice respectively having 8, 8.9 and 12.3% DR_O. 7.6, 12.3, and 12% DR_T was observed for corresponding cases in 0.5 diameter ratio orifices along with 10.3, 3.5, and 15.2 % DR_O respectively. Similar pressure drop in polymeric solution was observed in the work of Shima [40] through orifices having D_r = 0.562.

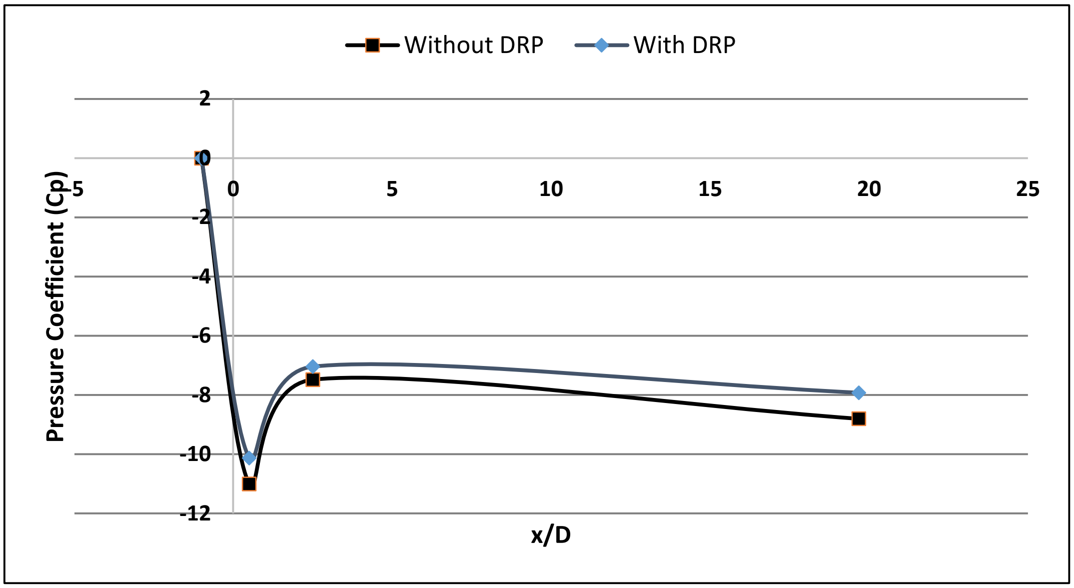

a) Single orifice

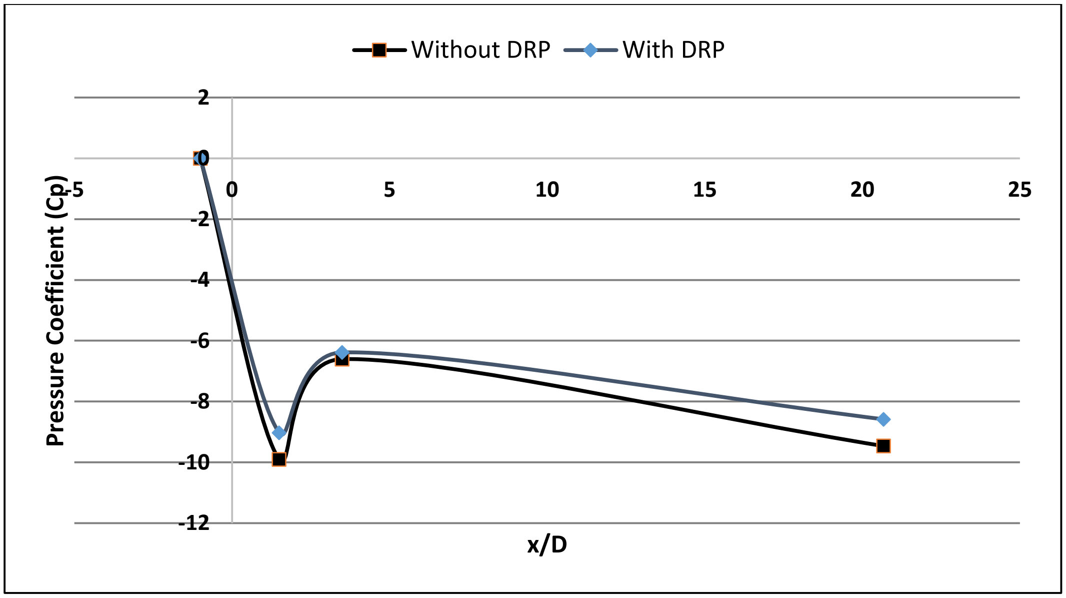

b) Double orifice with 1D spacing

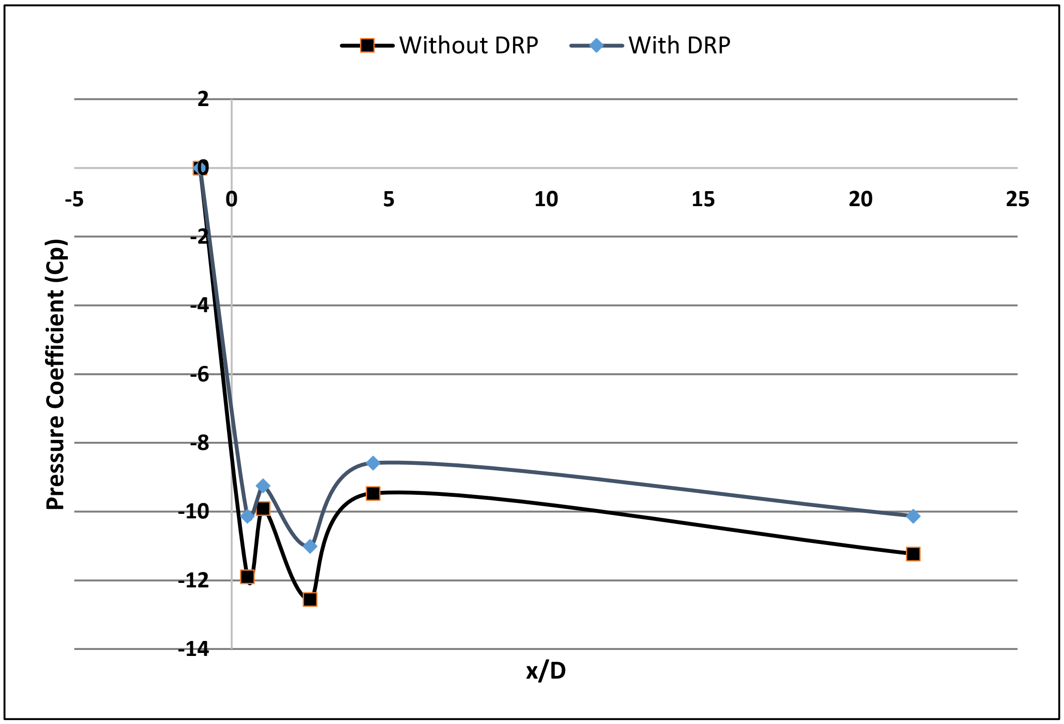

c) Double orifice with 2D spacing

Figure 4-23 Variation of pressure coefficient with normalized axial distance for the case of D_r = 0.63, Re= 5362 at 89ppm DRP; a) single orifice, b) double orifice with 1D spacing, c) double orifice with 2D spacing

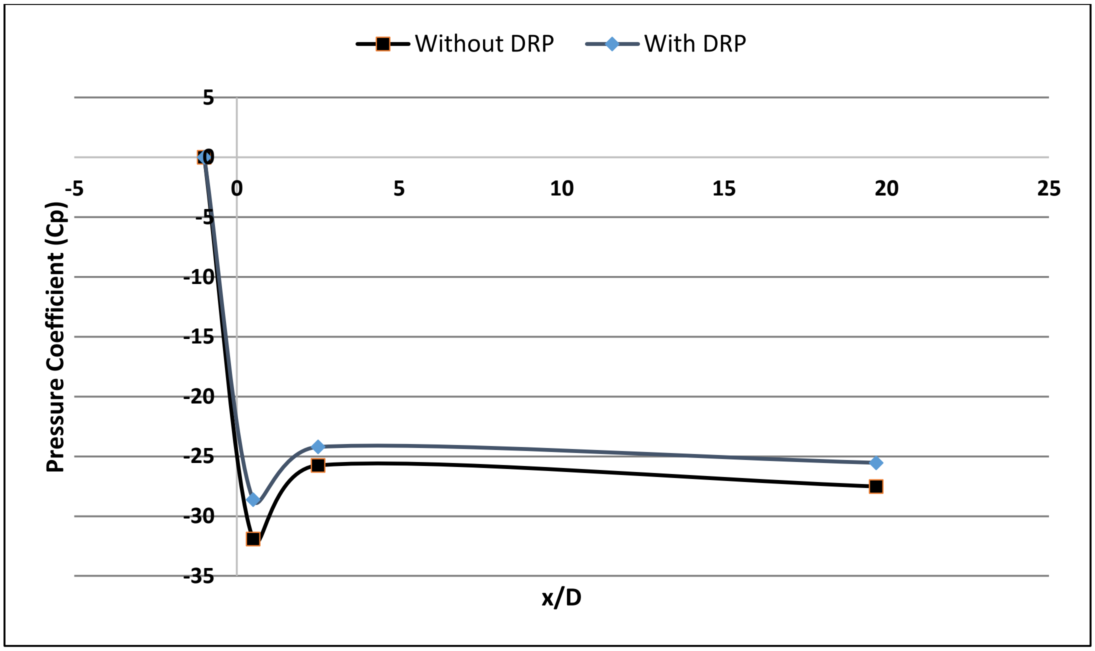

a) Single orifice

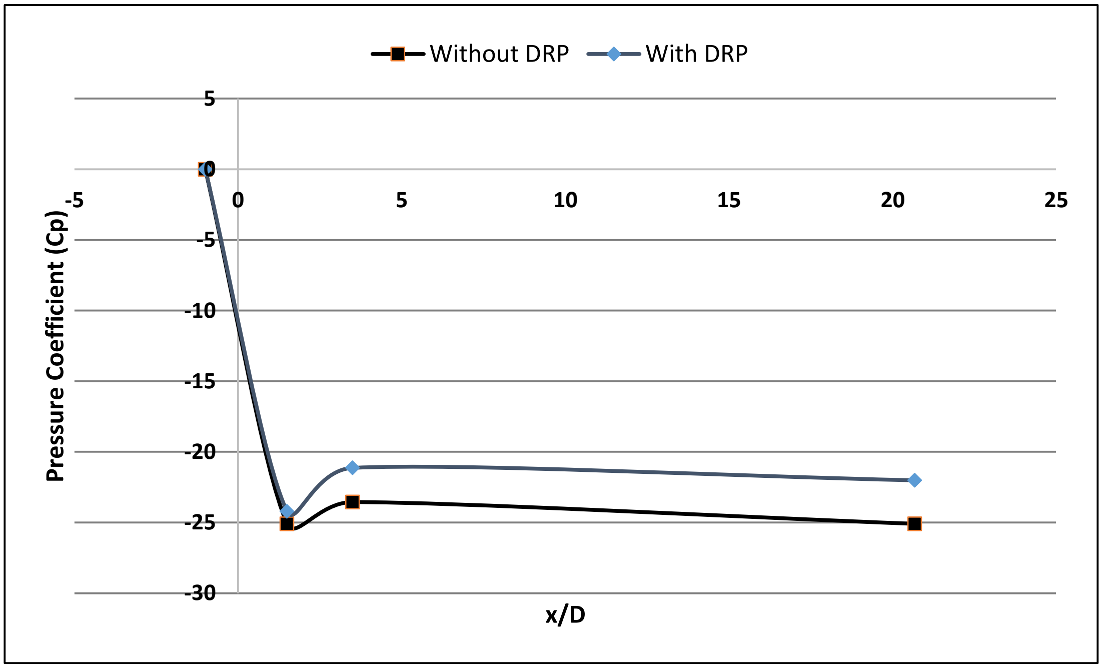

b) Double orifice with 1D spacing

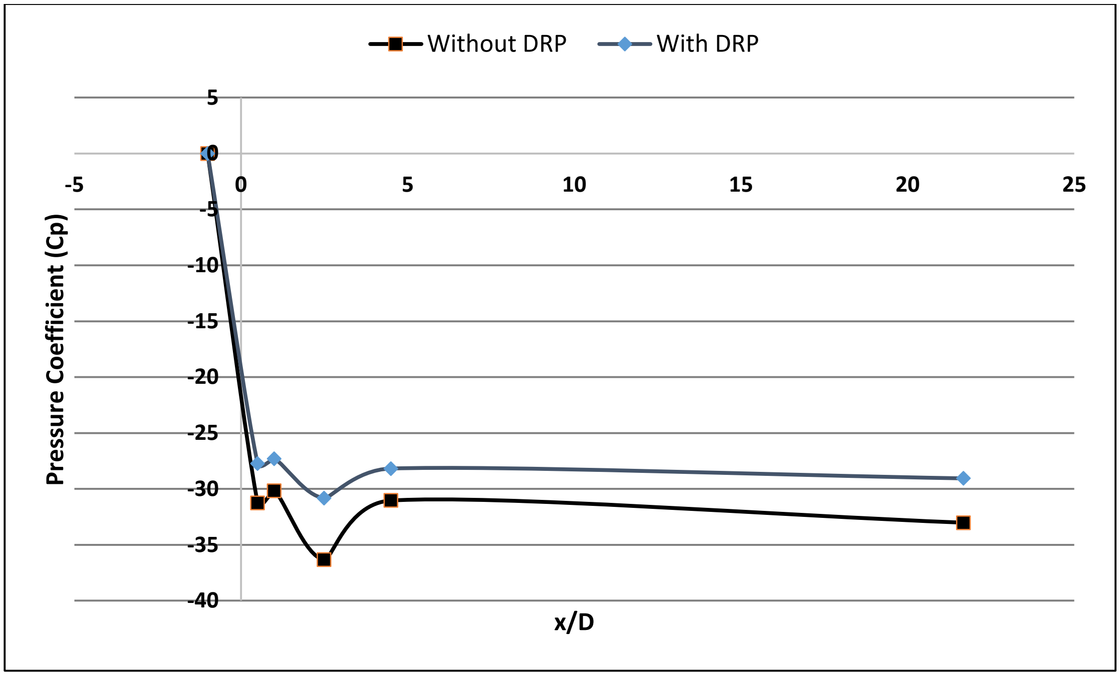

c) Double orifice with 2D spacing

Figure 4-24 Variation of pressure coefficient with normalized axial distance for the case of D_r = 0.5, Re= 5362 at 89ppm DRP; a) single orifice, b) double orifice with 1D spacing, c) double orifice with 2D spacing.

4.1.7. Re=5957

The concentration of drag reducing polymers in polymeric solution at this flow rate was maintained at 80ppm. Figure 4-25 and Figure 4-26 shows the pressure coefficient profiles of 0.63 and 0.5 diameter ratio orifices at this flow rate. 11.1, 7.5, and 18.6% DR_T was observed for D_r=0.63 orifice arrangements showing 5.3, 4.2, and 10.8% DR_O. 0.5 diameter ratio shows lesser DR_T of 2.8 and 4.8% for single and double orifice with 1D configuration, whereas double orifice with 2D spacing shows a greater DR_T of 10.6%. Similarly 3.3, 2, and 14.2% DR_O were found across these orifice arrangements.

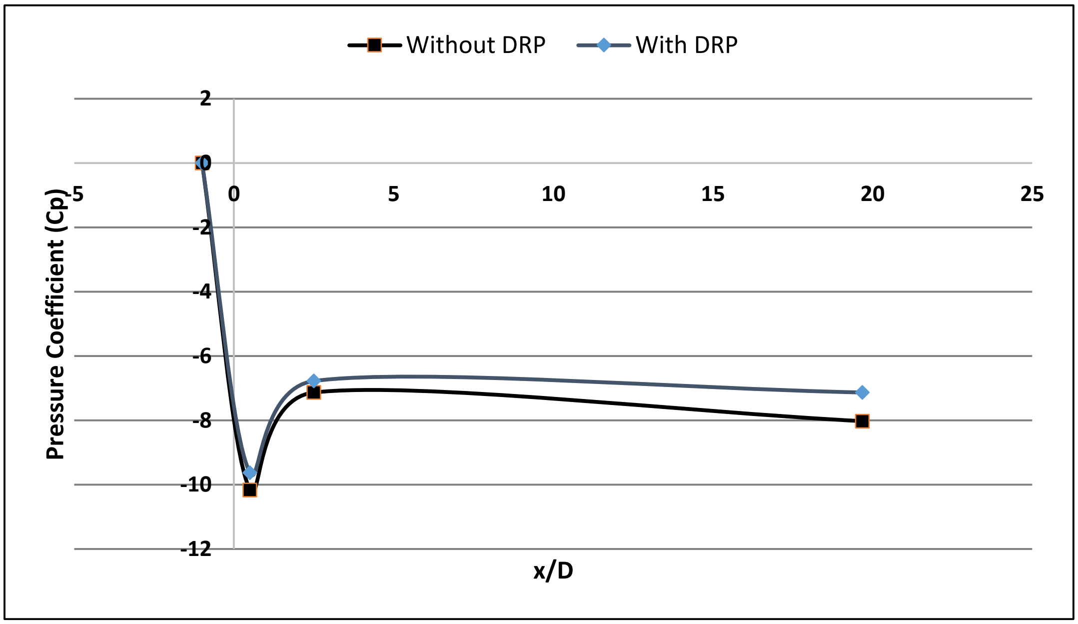

a) Single orifice

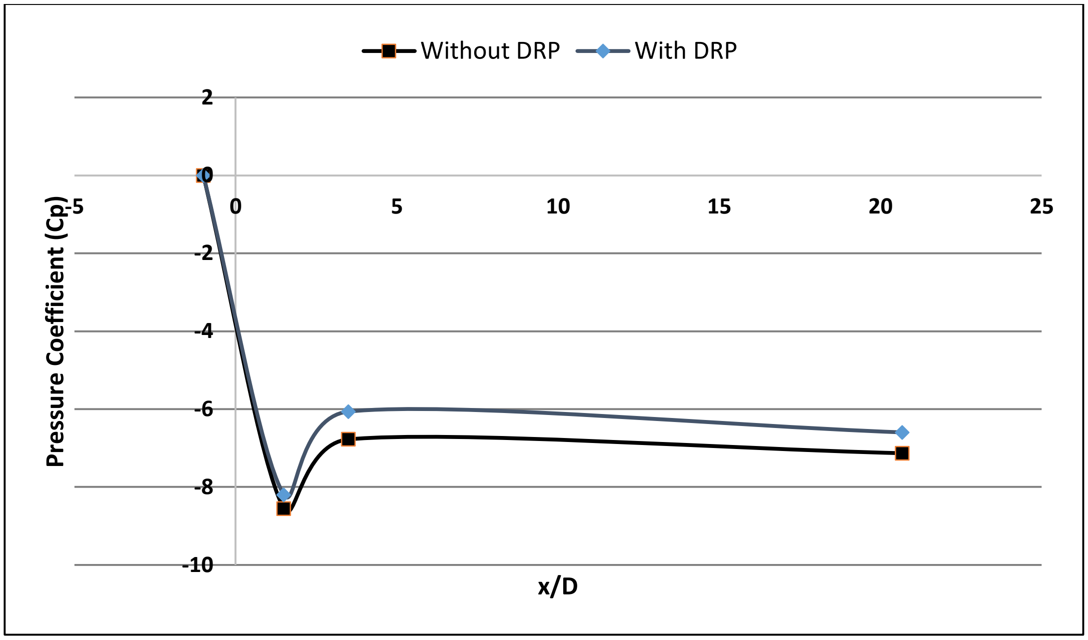

b) Double orifice with 1D spacing

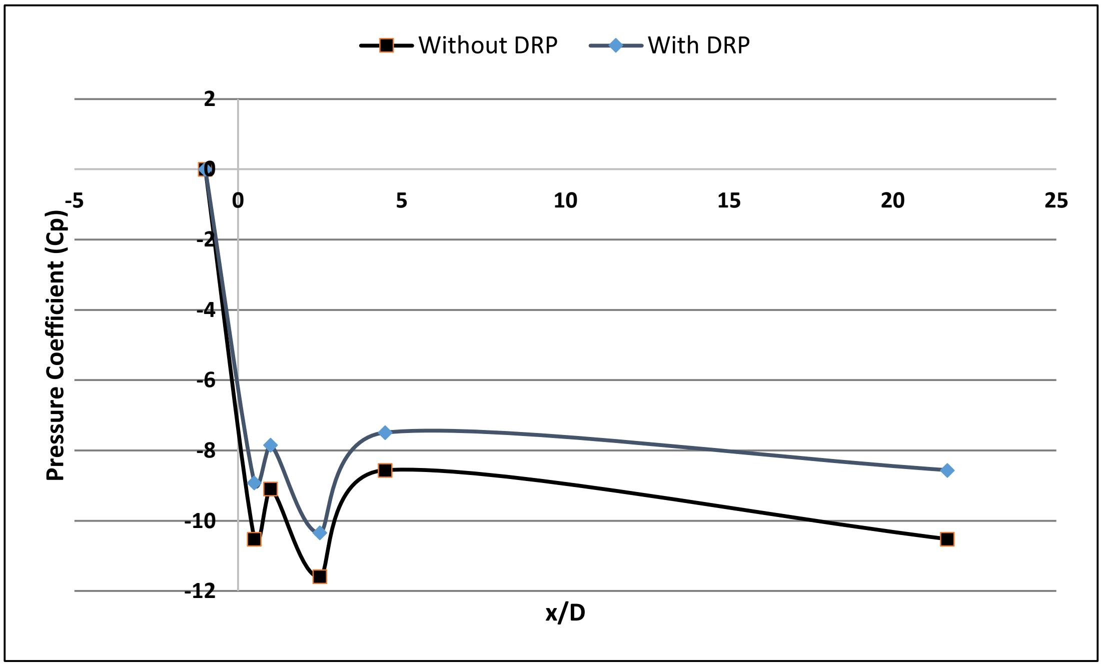

c) Double orifice with 2D spacing

Figure 4-25 Variation of pressure coefficient with normalized axial distance for the case of D_r = 0.63, Re= 5957 at 80ppm DRP; a) single orifice, b) double orifice with 1D spacing, c) double orifice with 2D spacing

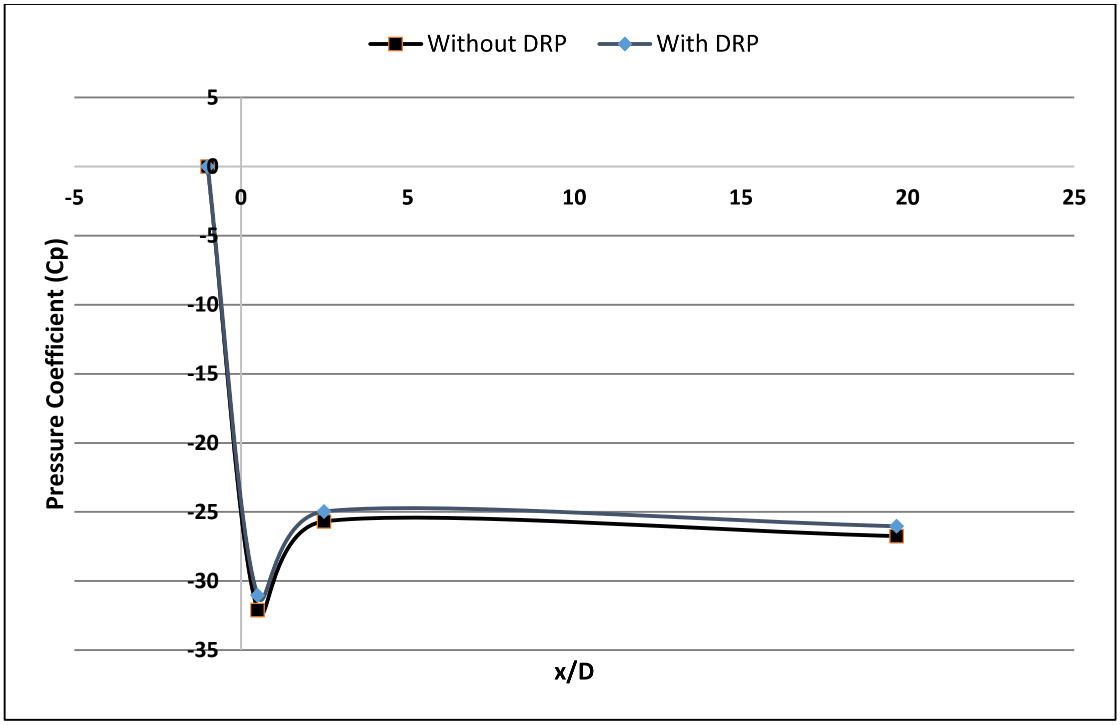

a) Single orifice

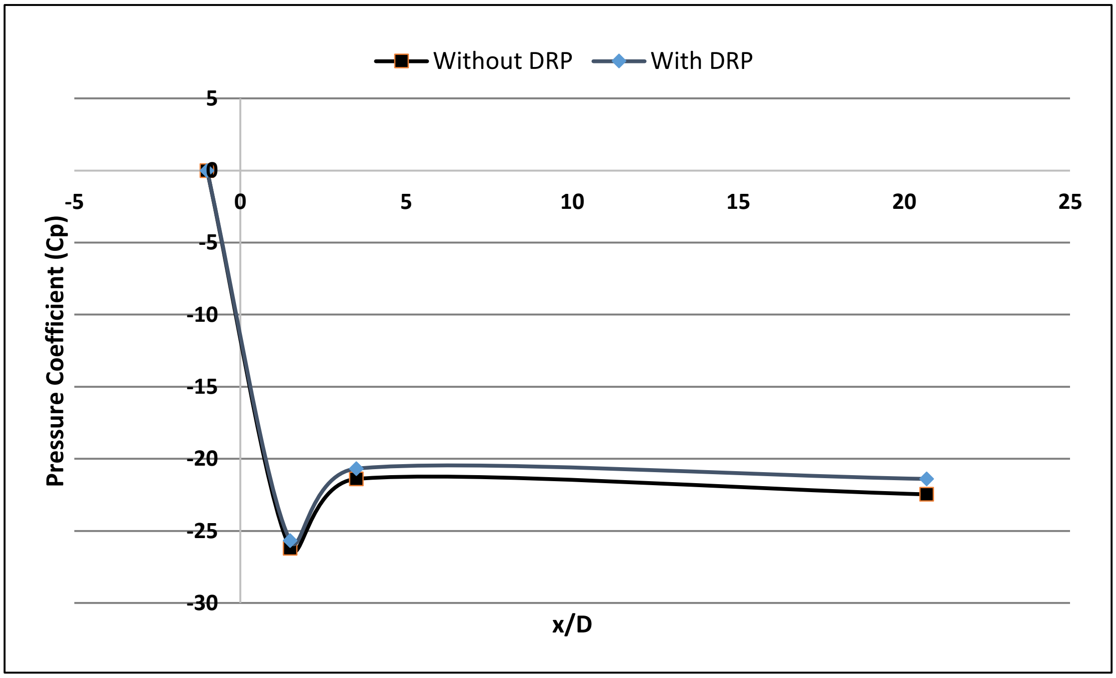

b) Double orifice with 1D spacing

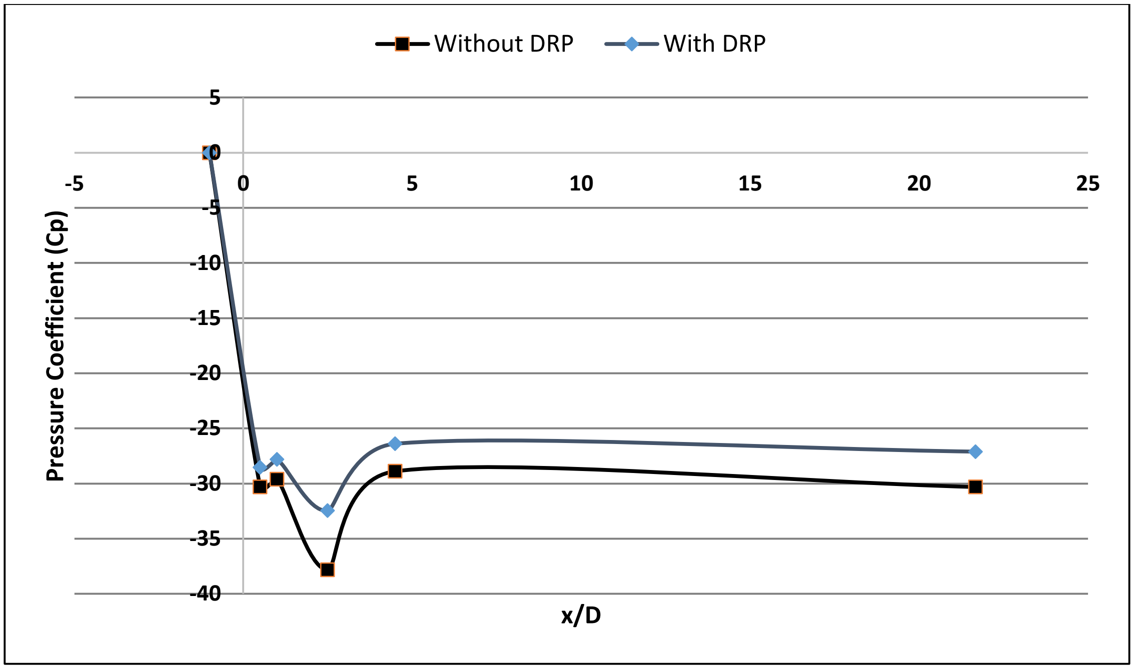

c) **Double orifice with 2D spacing**

Figure 4-26 Variation of pressure coefficient with normalized axial distance for the case of D_r = 0.5, Re= 5957 at 80ppm DRP; a) single orifice, b) double orifice with 1D spacing, c) double orifice with 2D spacing

4.1.8. Re=6951

The concentration of polymers in polymeric solution was maintained at 68ppm. Figure 4-27 and Figure 4-28 shows the pressure coefficient profiles of 0.63 and 0.5 orifices at this Reynolds number. 0.63 diameter ratio orifices show 20.8, 9.7, and 10.8% DR_T for the three arrangements of orifices along with 8.9, 0, and 7.7% DR_O respectively. 7.8, 6.6, and 4% DR_T were observed for corresponding cases of 0.5 diameter ratio orifice along with 6.5, 7.4 and 2.7% DR_O.

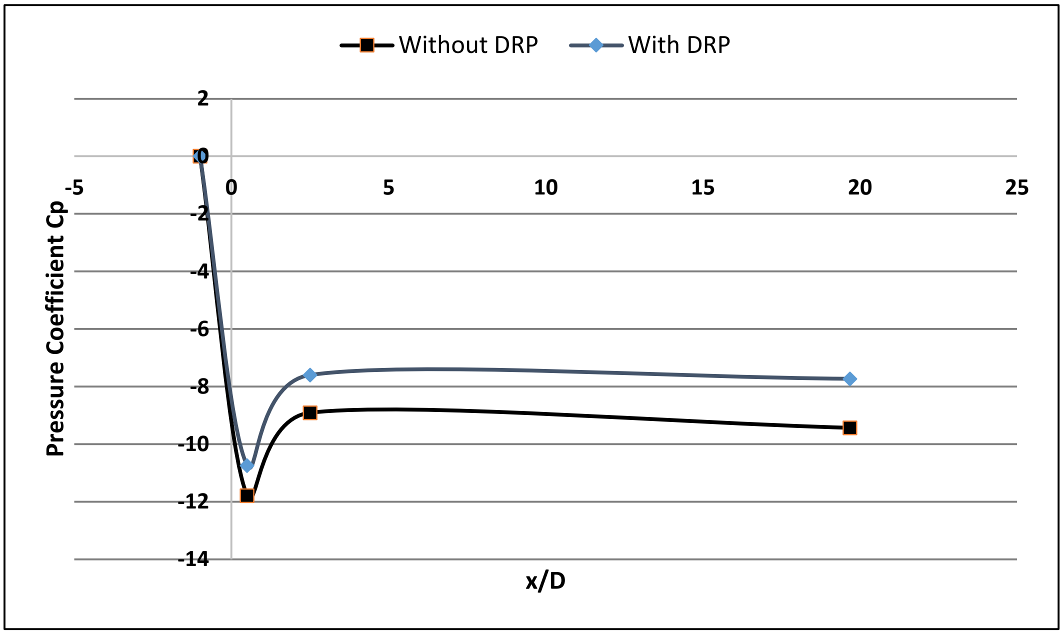

a) Single orifice

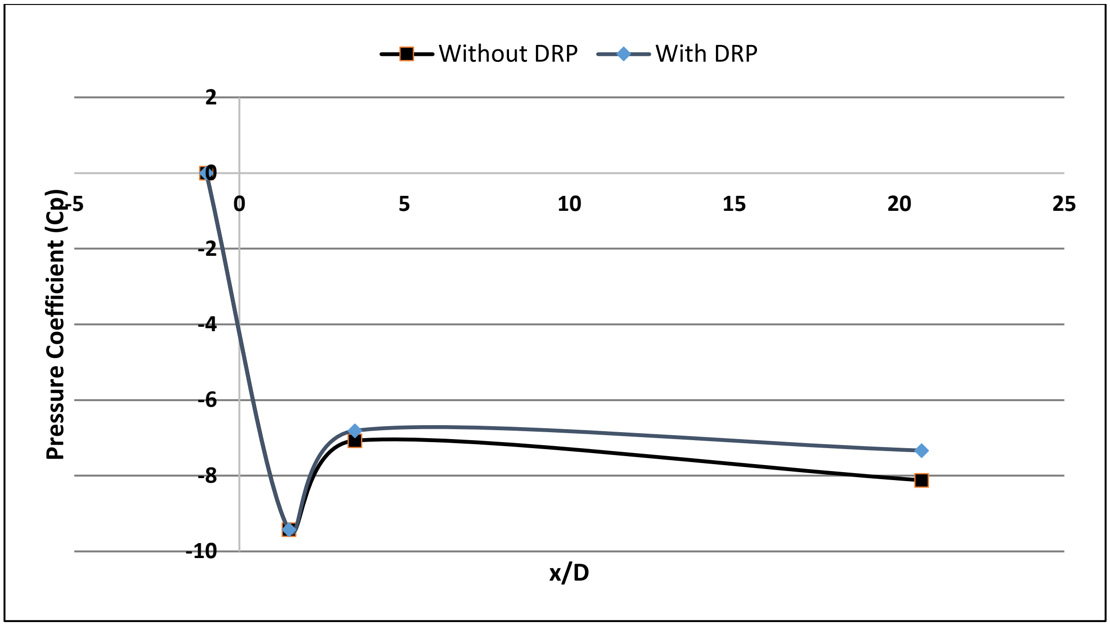

b) **Double orifice with 1D spacing**

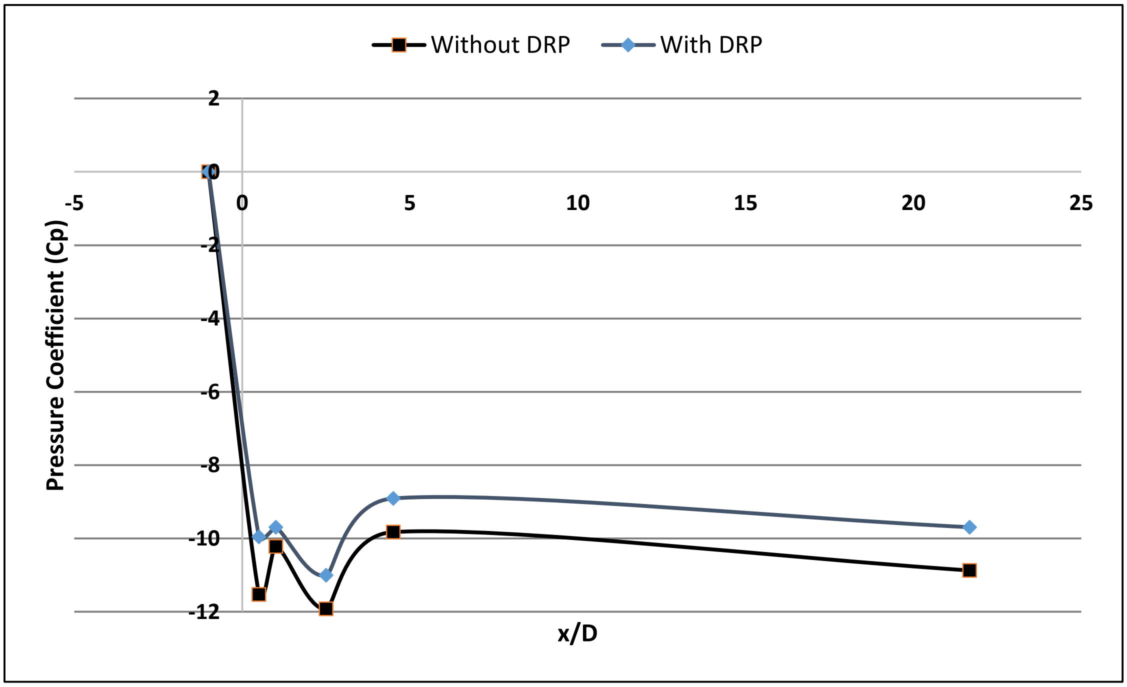

c) **Double orifice with 2D spacing**

Figure 4-27 Variation of pressure coefficient with normalized axial distance for the case of D_r = 0.63, Re= 6951 at 68ppm DRP; a) single orifice, b) double orifice with 1D spacing, c) double orifice with 2D spacing

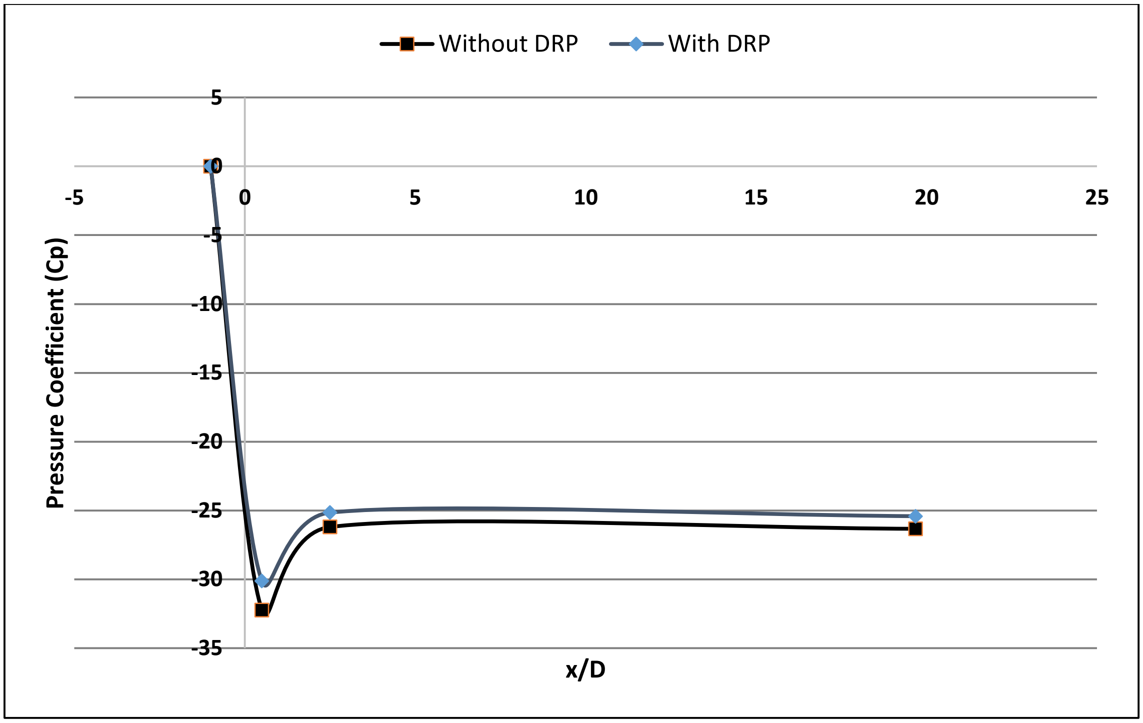

a) **Single orifice**

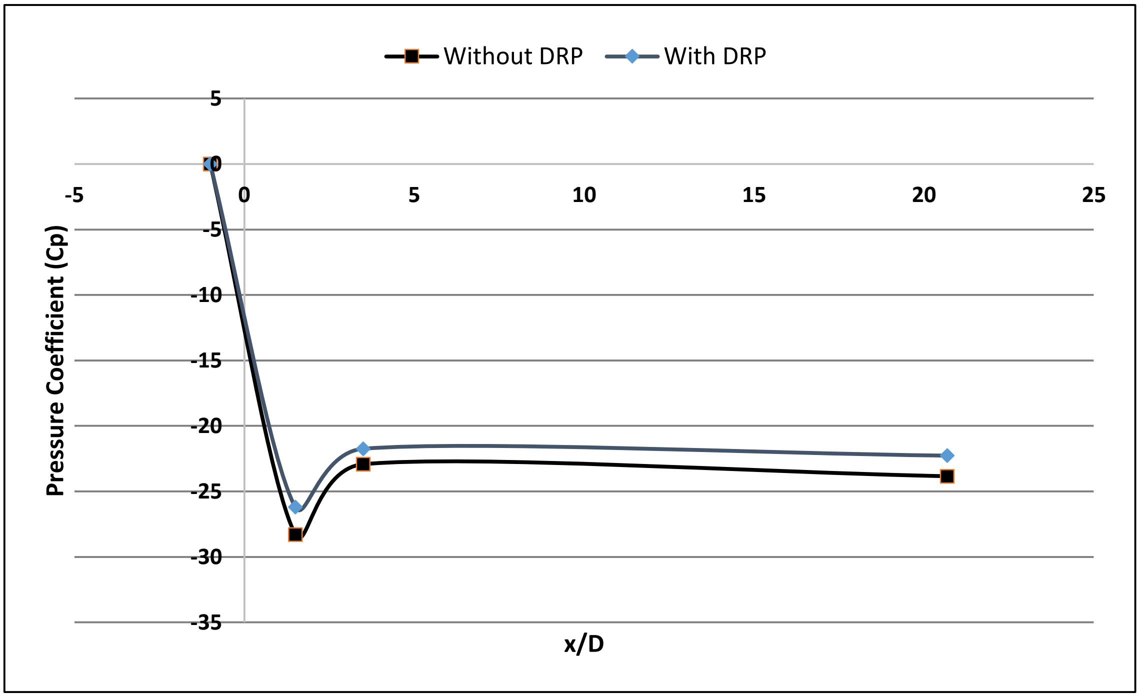

b) **Double orifice with 1D spacing**

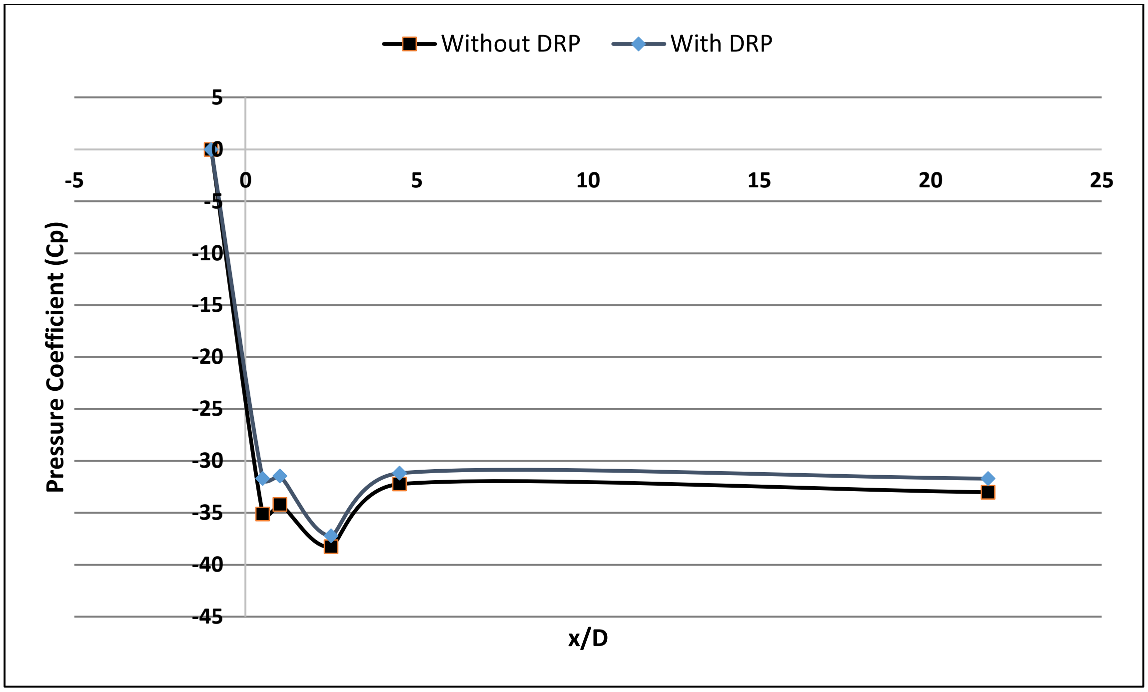

c) Double orifice with 2D spacing

Figure 4-28 Variation of pressure coefficient with normalized axial distance for the case of D_r = 0.5, Re= 6951 at 68ppm DRP; a) single orifice, b) double orifice with 1D spacing, c) double orifice with 2D spacing

4.1.9. Re=7944

The concentration of polymers in polymeric solution was kept at 60ppm for this flowrate. Figure 4-29 and Figure 4-30 shows the variation of pressure coefficient of 0.63 and 0.5 diameter ratio orifices at this Reynolds number. 5.1, 2.7, and 6.8% DR_T were observed for 0.63 diameter ratio single, double orifice with 1D spacing, and double orifice with 2D spacing. Similarly DR_O of 5.4, 0, and 1.67% were observed for the corresponding three arrangements. Whereas, 6.7, 3.1, and 4.6% are the corresponding DR_T for 0.5 diameter ratio orifices along with 6.5, 3.2, and 0% DR_O.

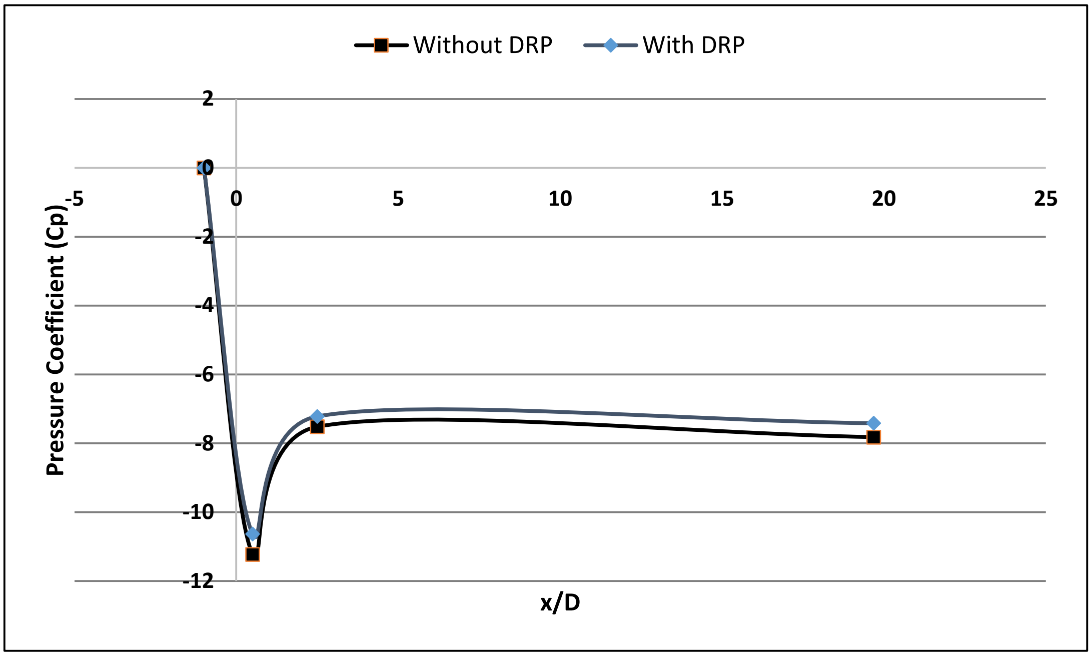

a) Single orifice

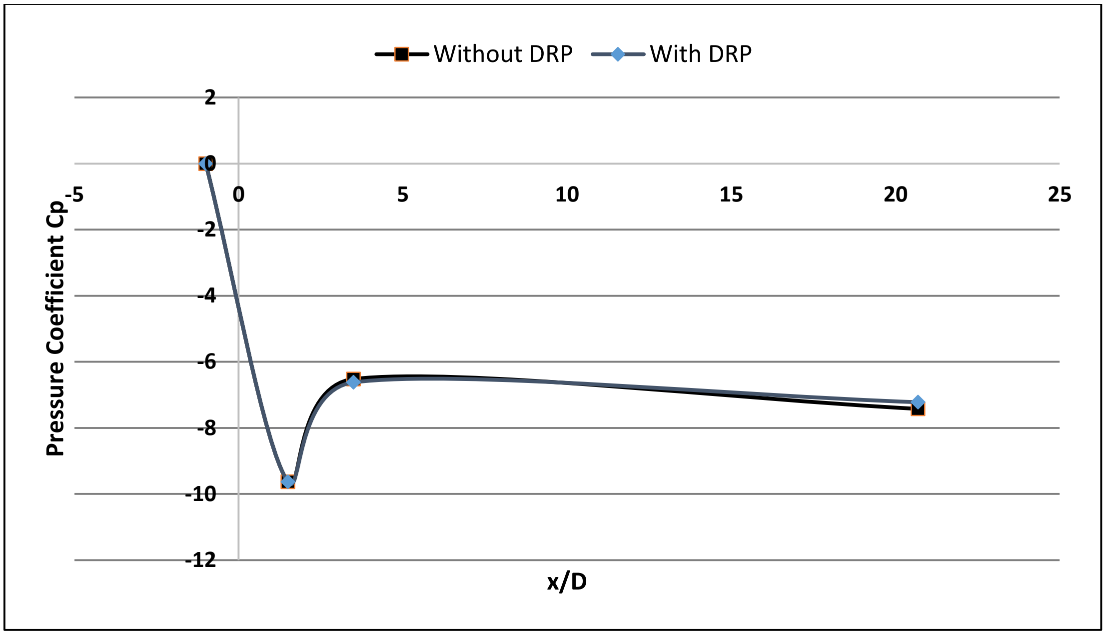

b) Double orifice with 1D spacing

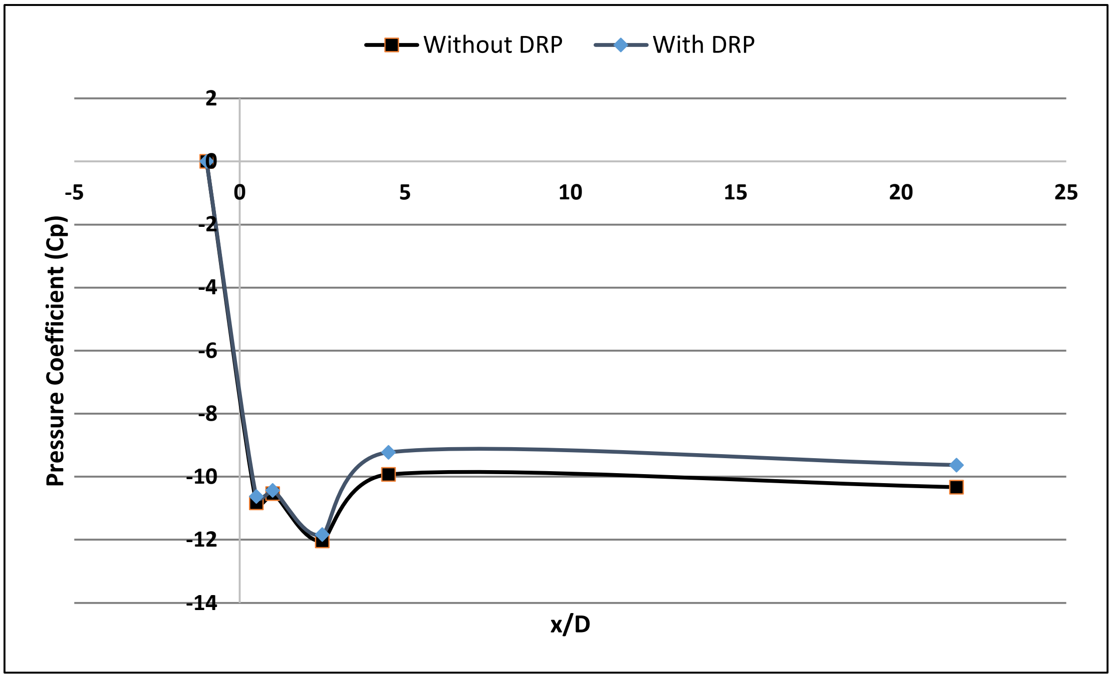

c) Double orifice with 2D spacing

Figure 4-29 Variation of pressure coefficient with normalized axial distance for the case of D_r = 0.63, Re= 7944 at 60ppm DRP; a) single orifice, b) double orifice with 1D spacing, c) double orifice with 2D spacing

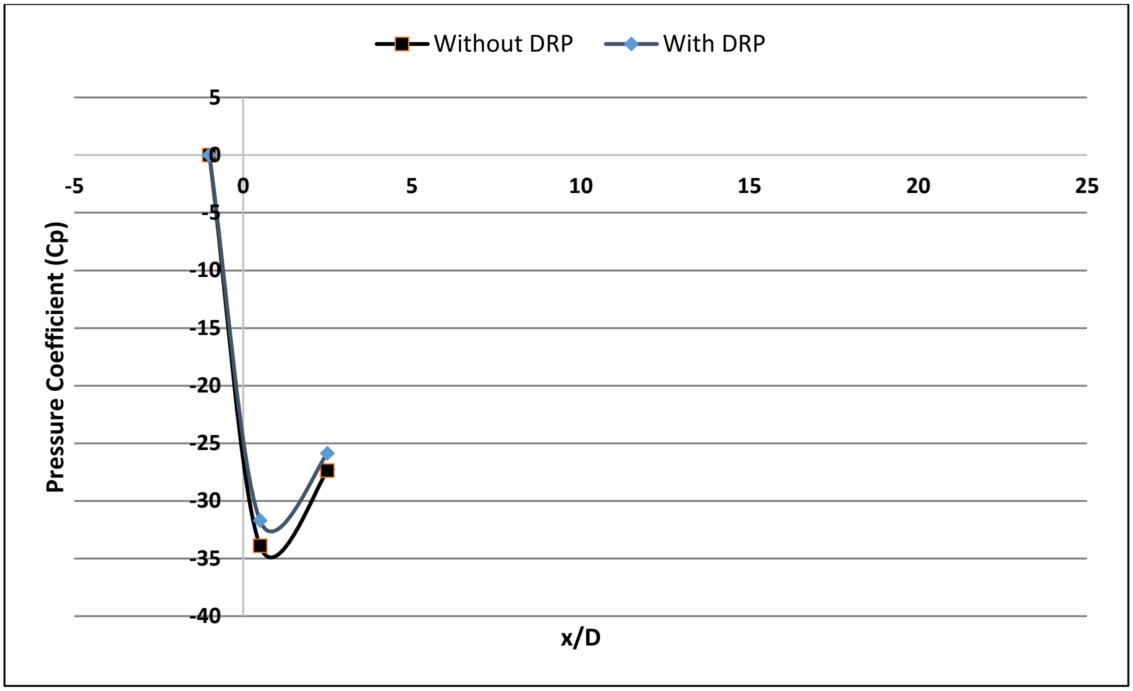

a) Single orifice

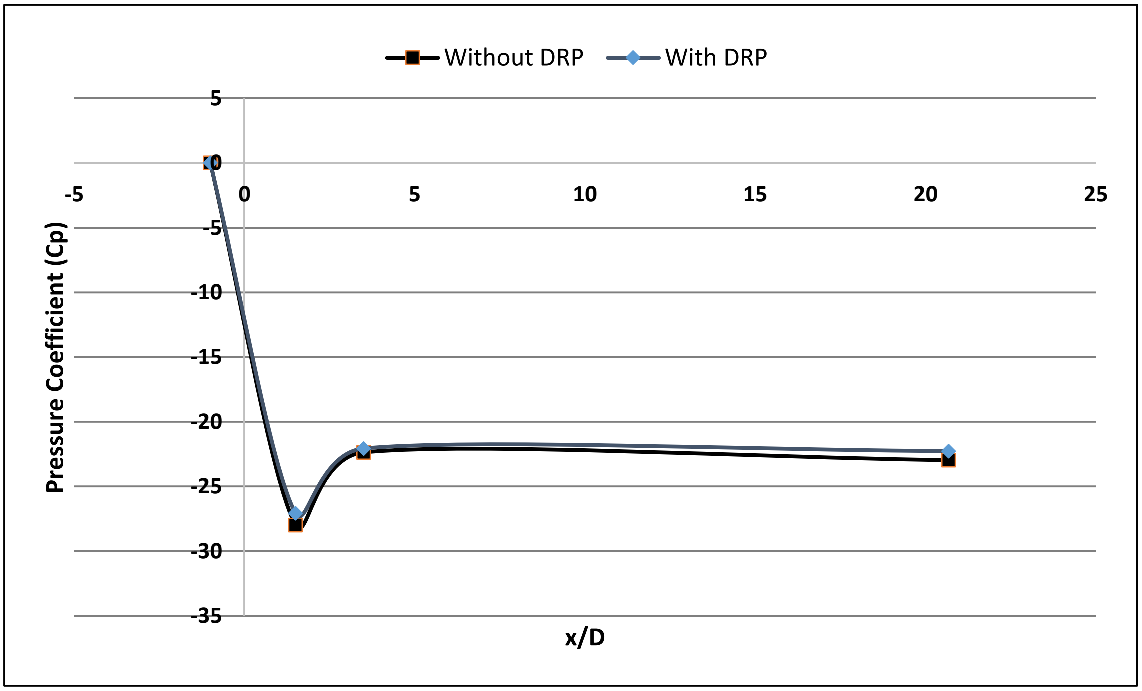

b) Double orifice with 1D spacing

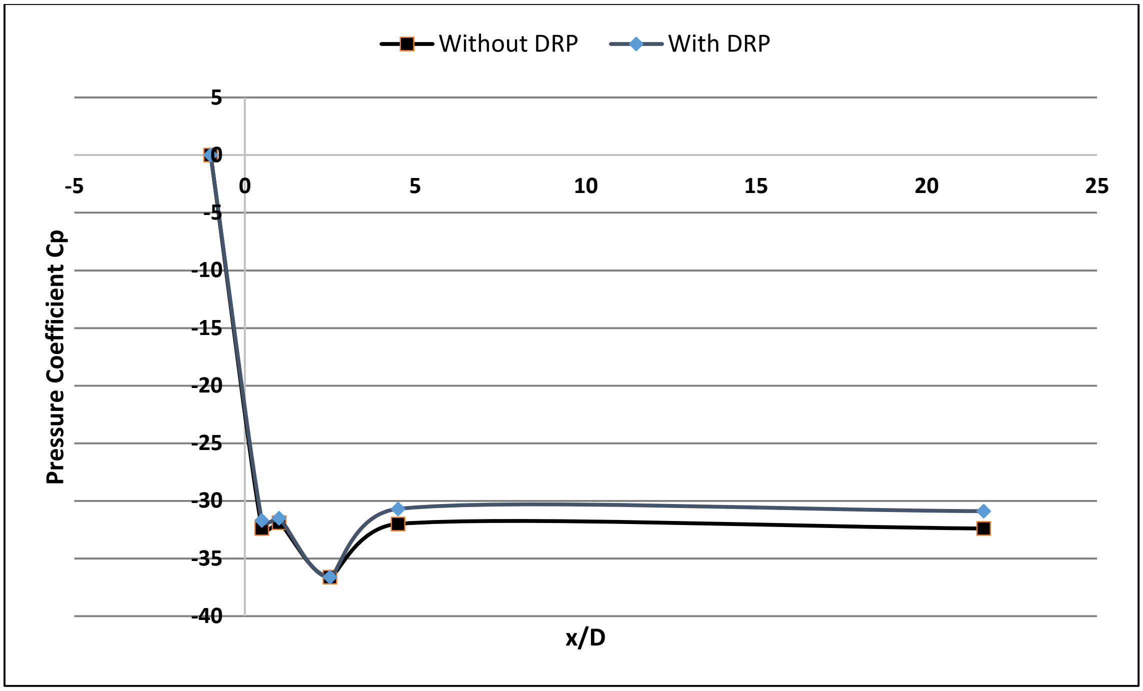

c) Double orifice with 2D spacing

Figure 4-30 Variation of pressure coefficient with normalized axial distance for the case of D_r = 0.5, Re= 7944 at 60ppm DRP; a) single orifice, b) double orifice with 1D spacing, c) double orifice with 2D spacing

4.1.10. Re=8937

The concentration of polymers in polymeric solution in this case was 53ppm. Figure 4-31 and Figure 4-32 shows the pressure coefficient profiles of 0.63 and 0.5 diameter ratio orifices for this case. DR_T of 3.2, 6.5, and 2.2% was observed in 0.63 diameter ratio orifices, along with 4.2, 0, and 0.6% DR_O while 5, 6.8 and 2.9% DR_T was observed for 0.5 diameter ratio orifices having 5.1, 5.3, and 0.83% DR_O respectively.

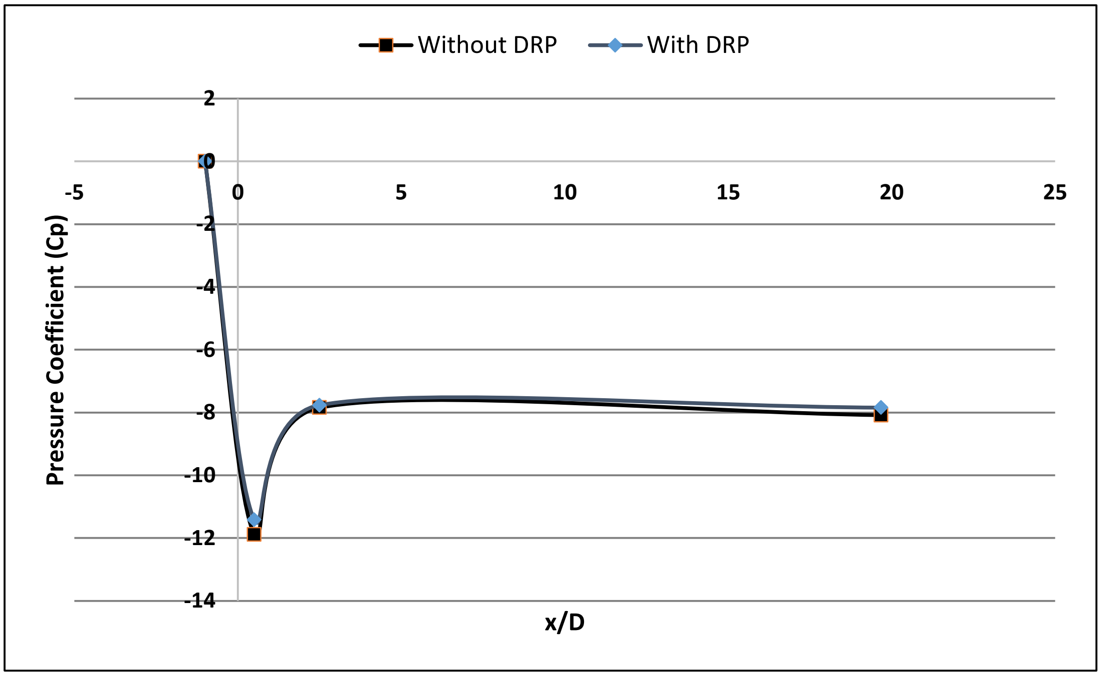

a) Single orifice

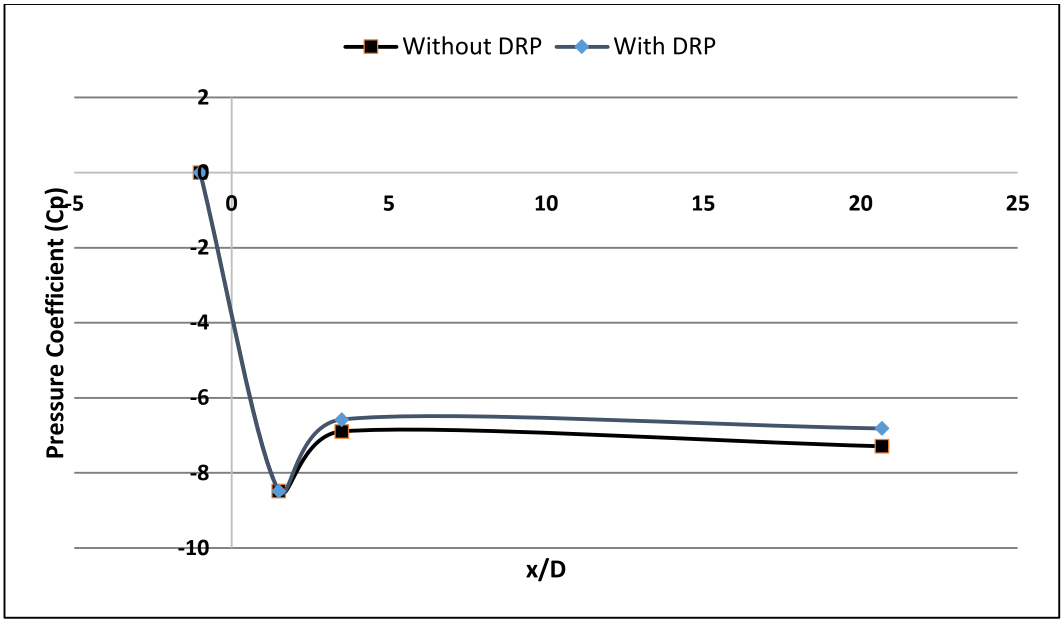

b) Double orifice with 1D spacing

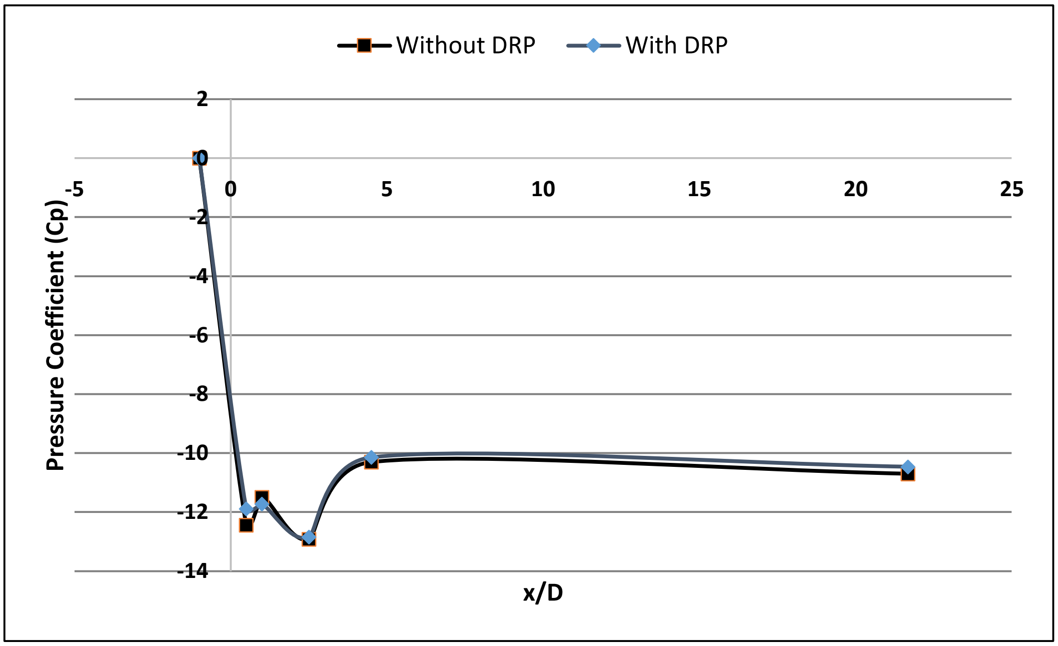

c) Double orifice with 2D spacing

Figure 4-31 Variation of pressure coefficient with normalized axial distance for the case of D_r = 0.63, Re= 8937 at 53ppm DRP; a) single orifice, b) double orifice with 1D spacing, c) double orifice with 2D spacing

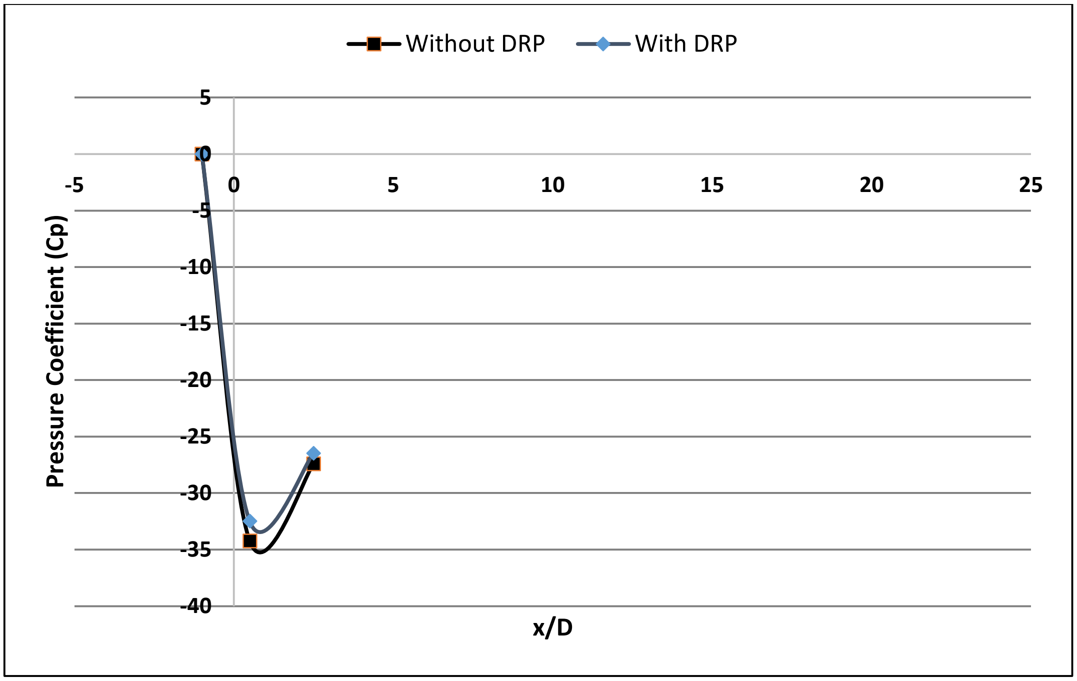

a) Single orifice

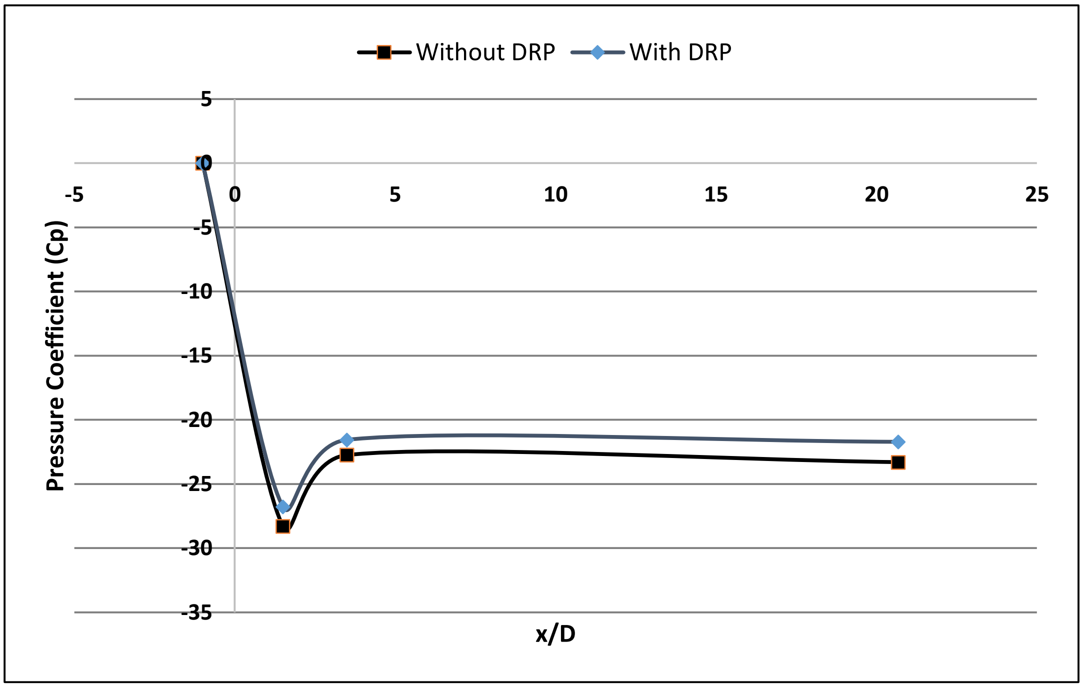

b) Double orifice with 1D spacing

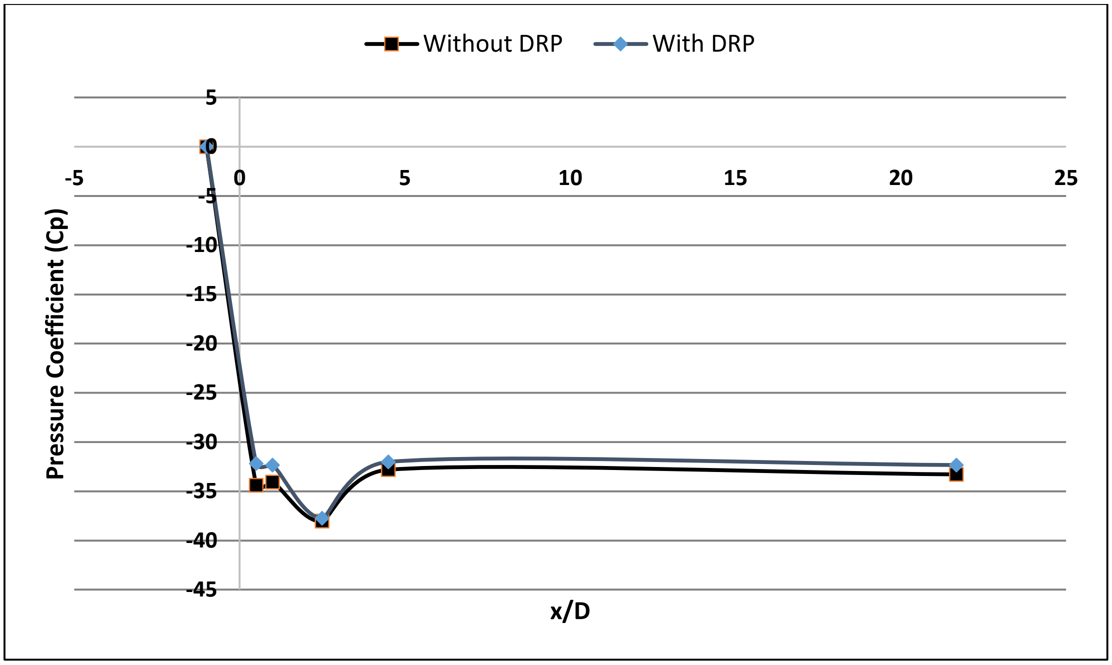

c) Double orifice with 2D spacing

Figure 4-32 Variation of pressure coefficient with normalized axial distance for the case of D_r = 0.5, Re= 8937 at 53ppm DRP; a) single orifice, b) double orifice with 1D spacing, c) double orifice with 2D spacing

4.1.11. Re=10128

The concentration of polymers in polymeric solution at this flow rate was 47ppm. Figure 4-33 and Figure 4-34 shows the pressure coefficient profiles for 0.63 and 0.5 diameter ratio orifices. 4.1, 2.5, and 2.9 % DR_T were observed in 0.63 diameter ratio orifice with 0, 0, and 0.48% DR_O. 4.3 and 1.1 % DR_T was observed for single and double orifice with 1D spacing respectively whereas 0% DR_T was seen for double orifice with 2D spacing along with 3, 0.65, and 0% DR_O in three arrangements of 0.5 diameter ratio orifices respectively.

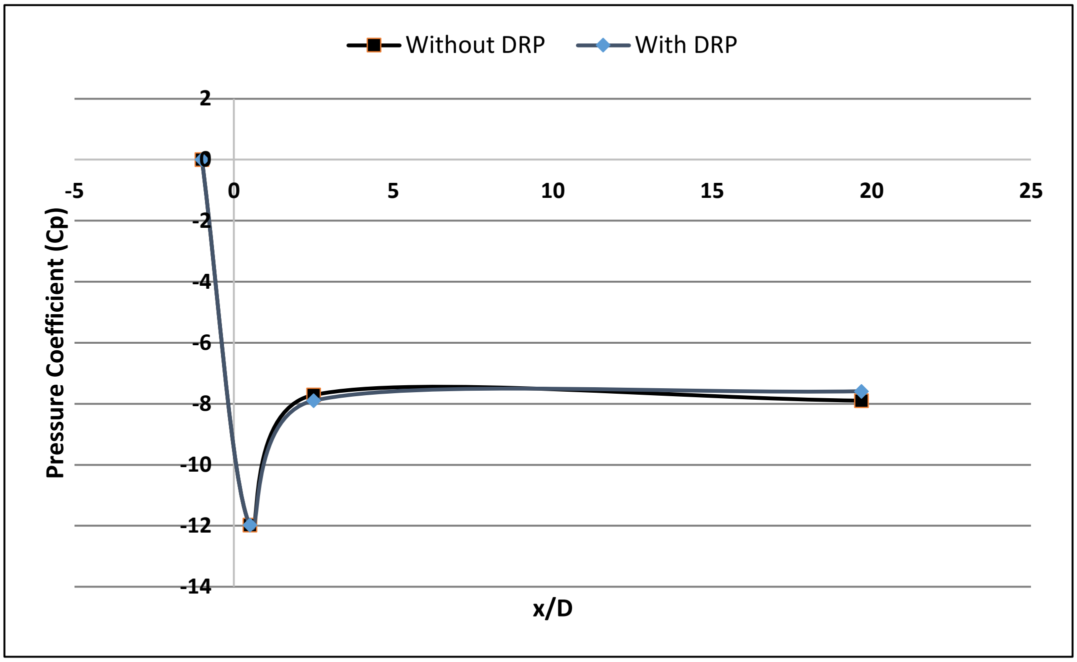

a) Single orifice

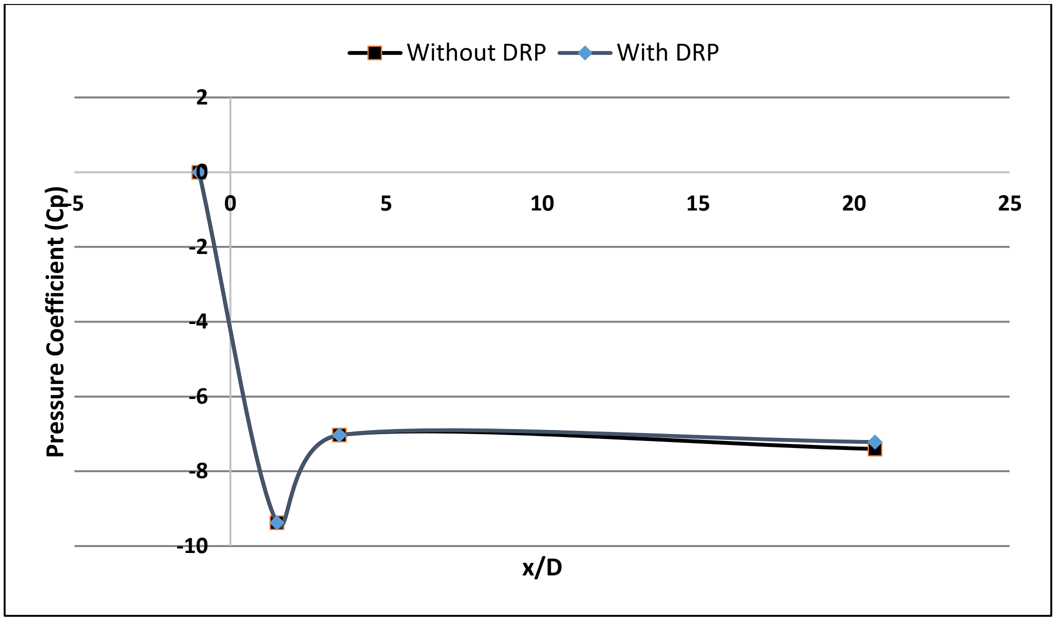

b) Double orifice with 1D spacing

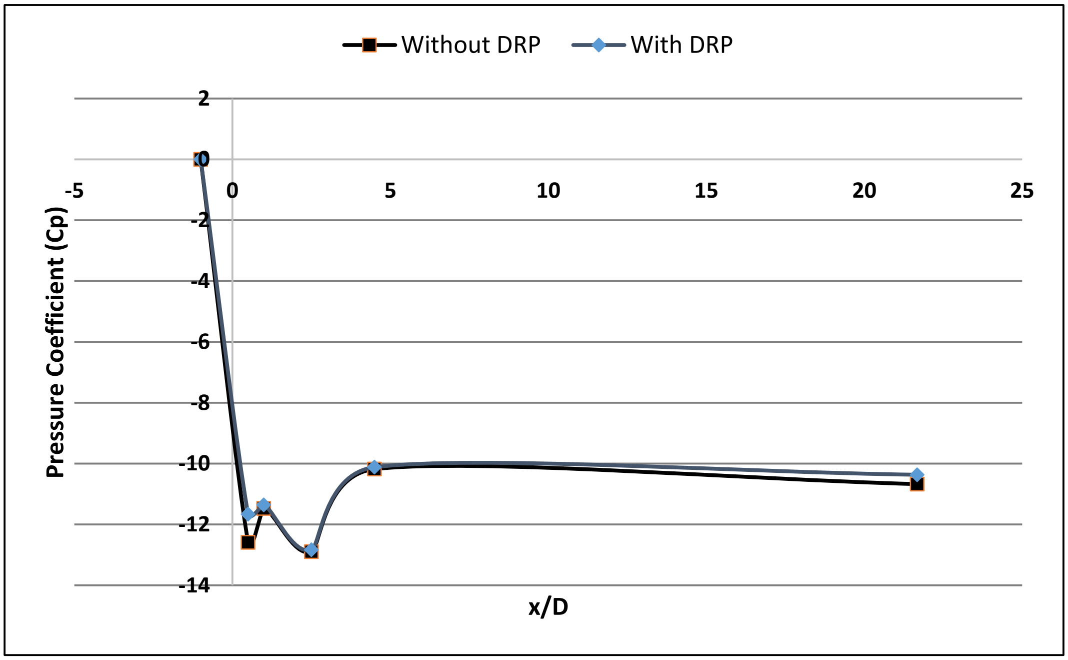

c) Double orifice with 2D spacing

Figure 4-33 Variation of pressure coefficient with normalized axial distance for the case of D_r = 0.63, Re= 10128 at 47ppm DRP; a) single orifice, b) double orifice with 1D spacing, c) double orifice with 2D spacing

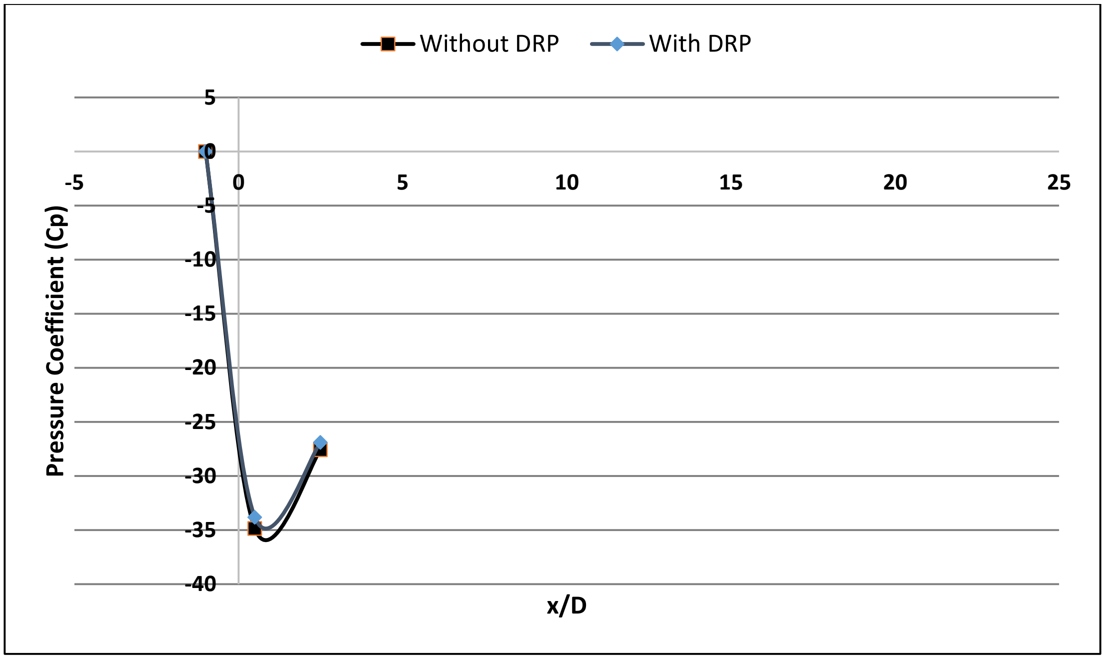

a) **Single orifice**

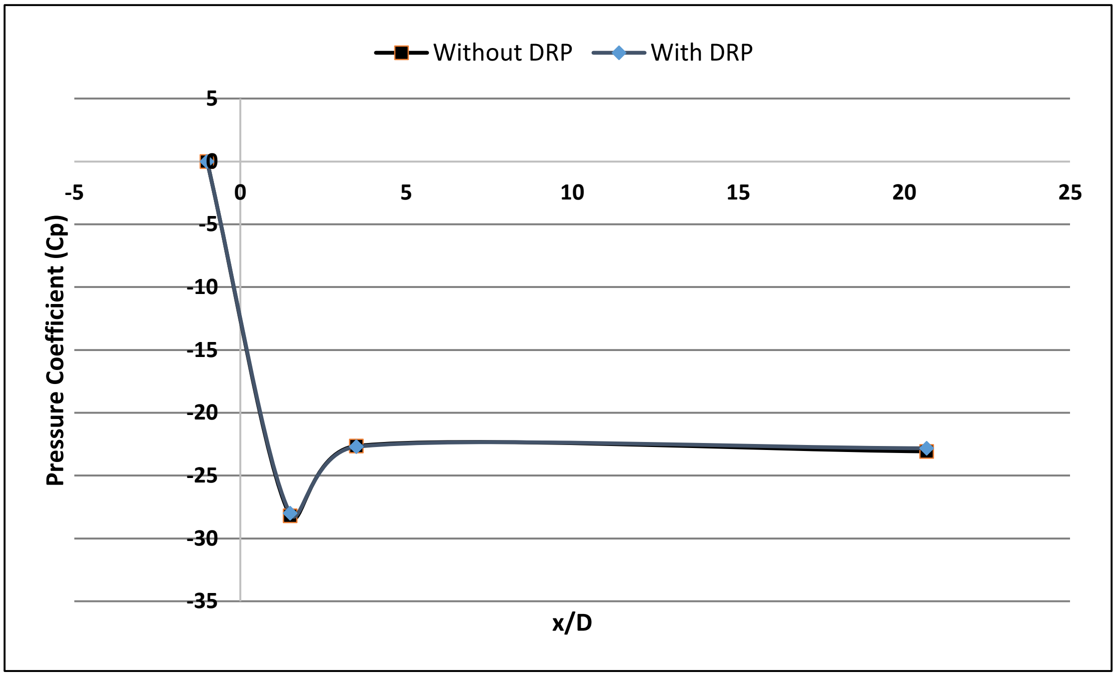

b) **Double orifice with 1D spacing**

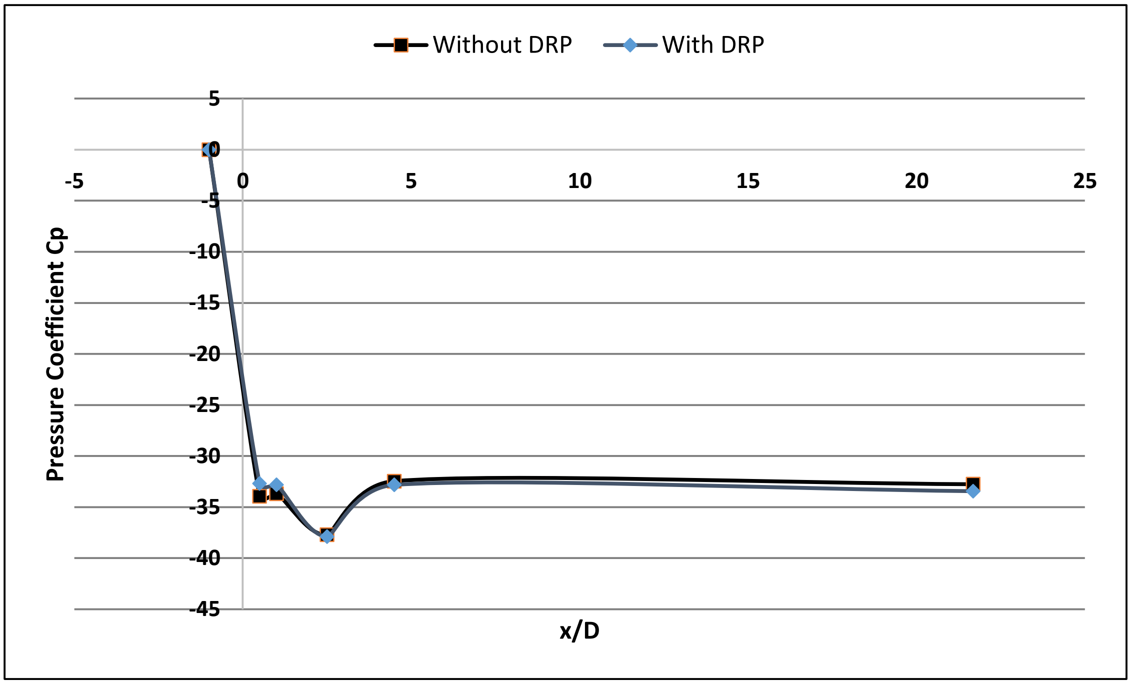

c) Double orifice with 2D spacing

Figure 4-34 Variation of pressure coefficient with normalized axial distance for the case of D_r = 0.5, Re= 10128 at 47ppm DRP; a) single orifice, b) double orifice with 1D spacing, c) double orifice with 2D spacing

4.1.12. Re=11915

The concentration of polymers in polymeric solution was kept at 40ppm for this case. Figure 4-35 and Figure 4-36 shows the pressure coefficient profiles at this Reynolds number for 0.63 and 0.5 diameter ratio orifices. 6.3, 7.7 and 1.2 % DR_T was observed for 0.63 orifices having 4, 5.4, and 6.7% DR_O whereas 6.8, 4.2 and 0% DR_T was observed for corresponding 0.5 diameter ratio orifices along with 5.8, 2.4, and 0% DR_O.

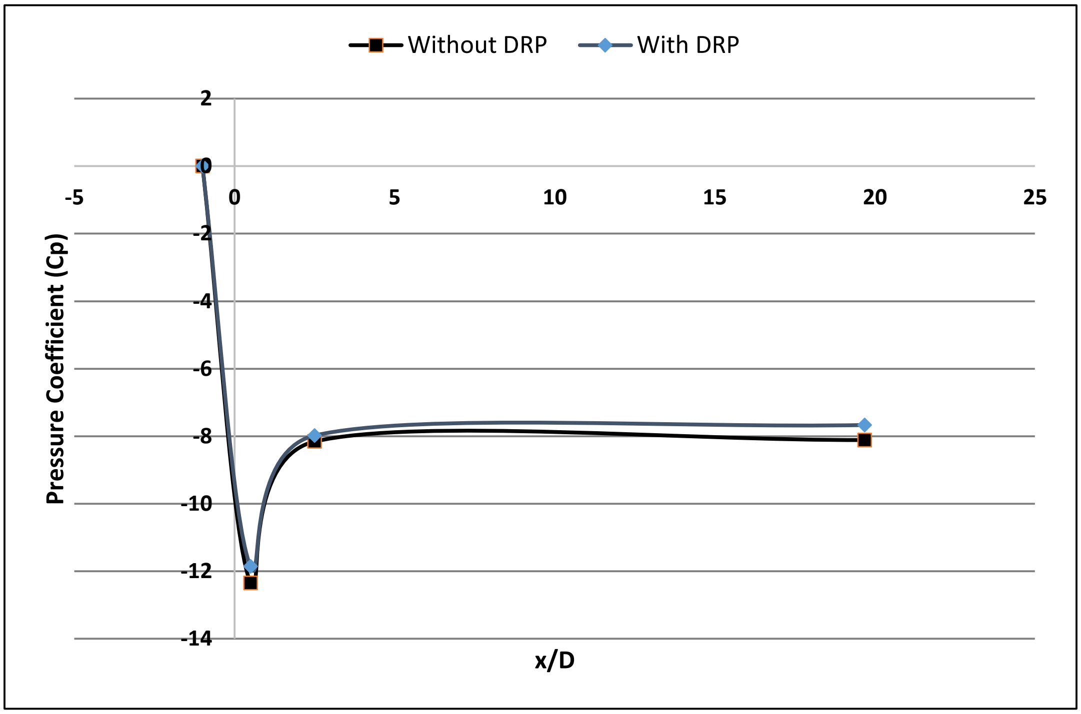

a) Single orifice

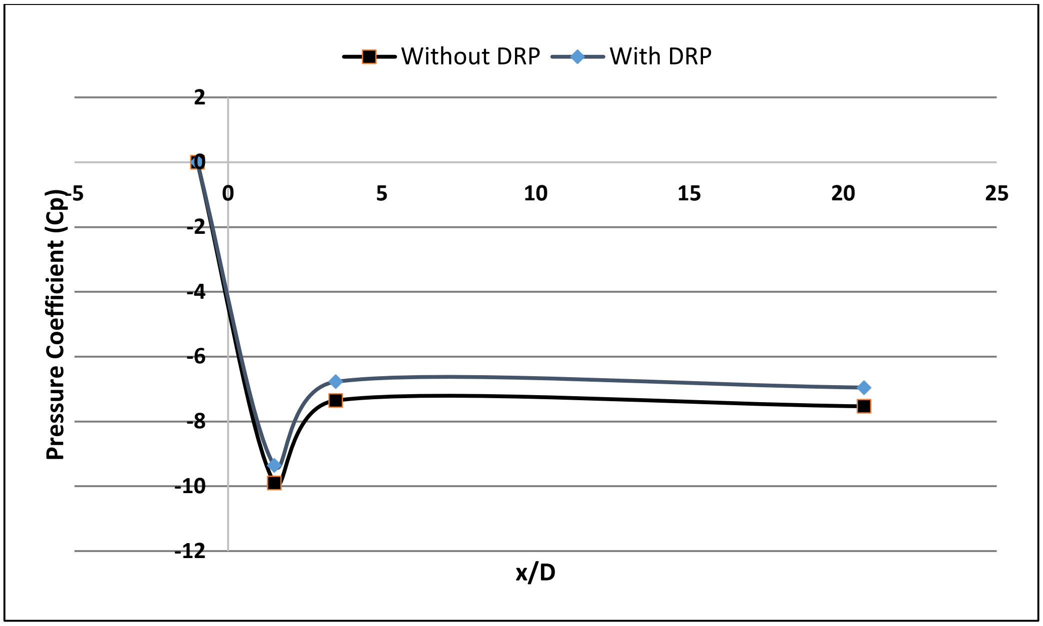

b) Double orifice with 1D spacing

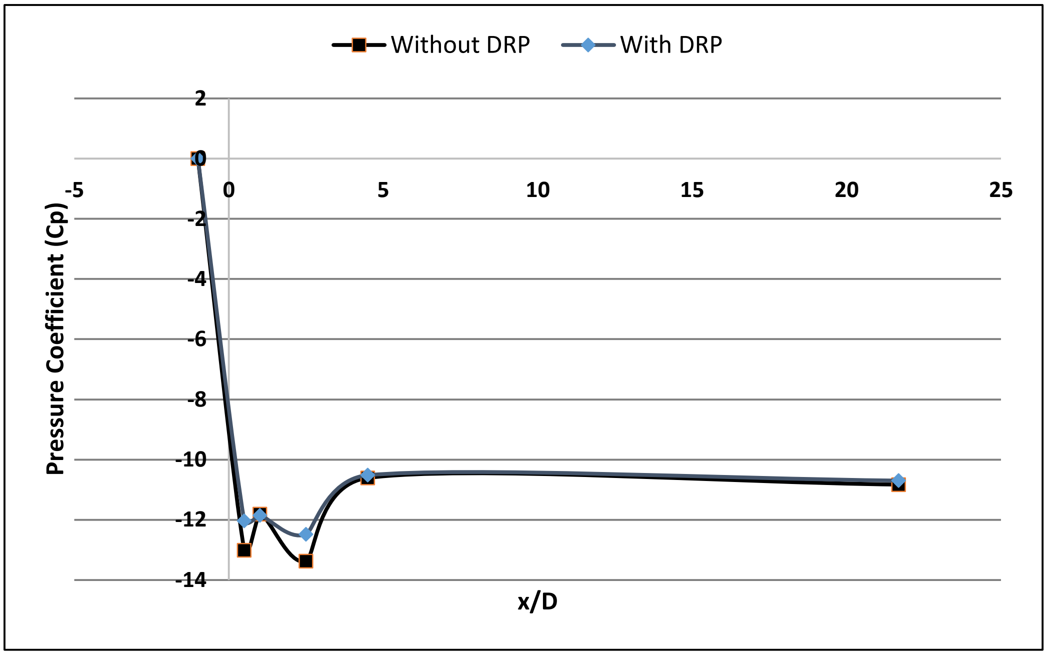

c) Double orifice with 2D spacing

Figure 4-35 Variation of pressure coefficient with normalized axial distance for the case of D_r = 0.63, Re= 11915 at 40ppm DRP; a) single orifice, b) double orifice with 1D spacing, c) double orifice with 2D spacing

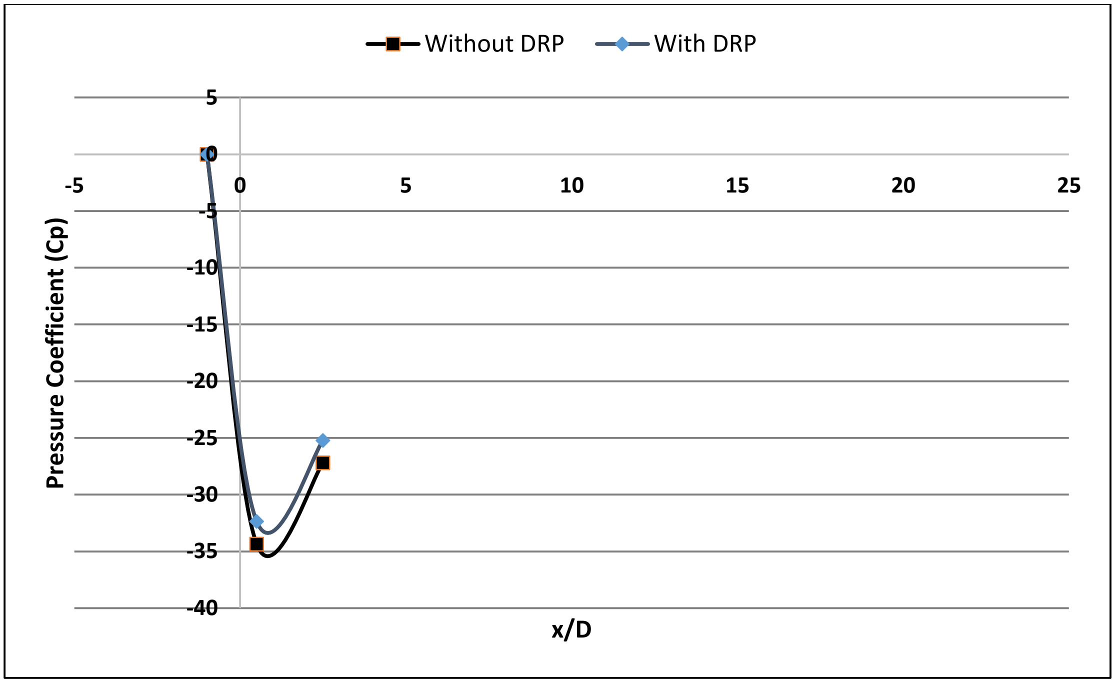

a) Single orifice

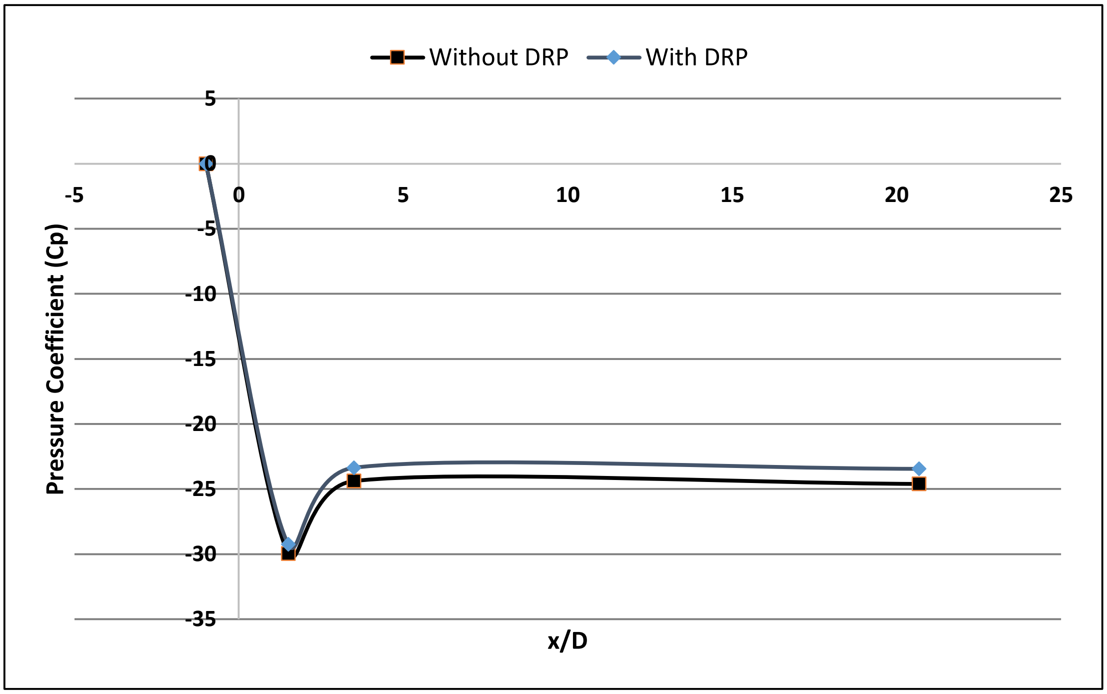

b) Double orifice with 1D spacing

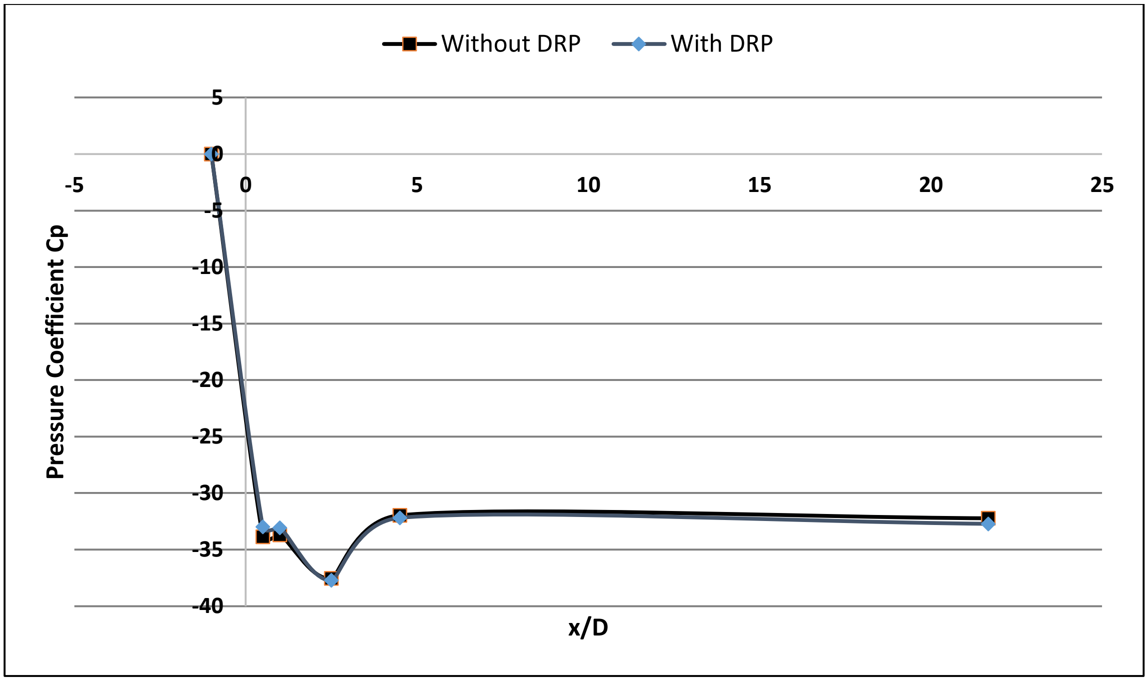

c) Double orifice with 2D spacing

Figure 4-36 Variation of pressure coefficient with normalized axial distance for the case of D_r = 0.5, Re= 11915 at 40ppm DRP; a) single orifice, b) double orifice with 1D spacing, c) double orifice with 2D spacing

Positive pressure gradient is observed in some cases in downstream of orifices which may be due to less number of ports installed. Hence in those cases, the last point has been intentionally removed. Another interesting finding of this experimental study is that the pressure drop was independent of the concentration of the drag reducing polymer as shown in Figure 4-37. The location of pressure taps are shown in Figure 3-8. The summary of experimental results of single phase pressure drop are presented in Table 4-2 and Table 4-3.

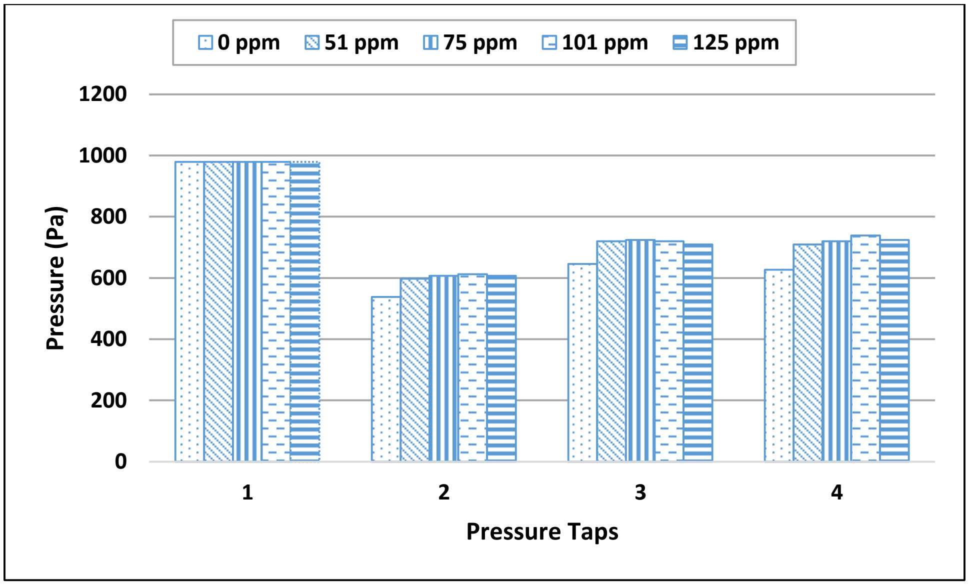

Figure 4-37 Effect of different concentration of DRP for single orifice having D_r = 0.63, Re= 8937

The random uncertainty ($S_{x}-$) of the Piezometric tubes for 'N' samples as calculated by eq. (4.5) and eq (4.6) was found to be 0.97%.

$$S_{x}- = \frac{S_x}{N} \tag{4.5}$$

$$S_x = \sqrt{\frac{\sum (X - \overline{X})^2}{N-1}} \tag{4.6}$$

Table 4-2 Summary of single phase pressure drop results for orifice having D_r=0.63

Diameter Ratio: 0.63													
Reynolds No.		**2383**	**2979**	**3177**	**3972**	**4369**	**5362**	**5957**	**6951**	**7944**	**8937**	**10128**	**11915**
DRP Concentration (ppm)		**196**	**158**	**148**	**119**	**108**	**89**	**80**	**68**	**60**	**53**	**47**	**40**
Single orifice	DR_T(%)	25	23.8	30.8	35.7	22.6	10	11.1	20.8	5.1	3.2	4.1	6.3
	DR_O(%)	9.1	6.7	5.3	12	5.9	8	5.3	8.9	5.4	4.2	0	4
Double orifice (1D spacing)	DR_T(%)	25	23.8	33.3	34.5	17.2	9.3	7.5	9.7	2.7	6.5	2.5	7.7
	DR_O(%)	10	21.4	17.6	4.5	6.9	8.9	4.2	0	0	0	0	5.4
Double orifice (2D spacing)	DR_T(%)	23.1	25	12.5	40.5	17.9	9.8	18.6	10.8	6.8	2.2	2.9	1.2
	DR_O(%)	18.8	4.7	9.1	31.4	20.9	12.3	10.8	7.7	1.67	0.6	0.48	6.7

Table 4-3 Summary of single phase pressure drop results for orifice having D_r=0.5

Diameter Ratio: 0.5													
Reynolds No.		**2383**	**2979**	**3177**	**3972**	**4369**	**5362**	**5957**	**6951**	**7944**	**8937**	**10128**	**11915**
DRP Concentration (ppm)		**196**	**158**	**148**	**119**	**108**	**89**	**80**	**68**	**60**	**53**	**47**	**40**
Single orifice	DR_T(%)	10.5	4.8	24.1	9.6	13.8	7.6	2.8	7.8	6.7	5	4.3	6.8
	DR_O(%)	6.3	2.4	23.3	10	17.3	10.3	3.3	6.5	6.5	5.1	3	5.8
Double orifice (1D spacing)	DR_T(%)	13.9	10	11.1	19.5	10.3	12.3	4.8	6.6	3.1	6.8	1.1	4.2
	DR_O(%)	6.9	5.3	7	13.9	6.8	3.5	2	7.4	3.2	5.3	0.65	2.4
Double orifice (2D spacing)	DR_T(%)	28.9	19	25.7	14.6	18.3	12	10.6	4	4.6	2.9	0	0
	DR_O(%)	17.1	12.1	18.1	3	12.6	15.2	14.2	2.7	0	0.83	0	0

Figure 4-38, Figure 4-39, and Figure 4-40 shows the variation of percentage total drag reduction (DR_T) at different Reynolds number for single orifice, double orifice with 1D spacing, and double orifice with 2D spacing having D_r=0.63 respectively. It is clear from these figures that total drag reduction is high at lower Reynolds number flows than at higher Reynolds number flows. Similar kind of behavior is observed for orifices having D_r=0.5 as shown in Figure 4-41, Figure 4-42, and Figure 4-43. Figure 4-44 shows the drag reduction (DR_O) across single orifice having D_r=0.63 at different Reynolds numbers. The DR_O for most of the cases remains between 4 to 12%. Figure 4-45 and Figure 4-46 represents DR_O across double orifice having same diameter ratio with 1D and 2D spacing respectively. The DR_O is greater at lower Reynolds number flows in both the cases. Orifices having D_r=0.5 showed similar trend of DR_O at different Reynolds numbers and in different arrangement of orifices as shown in Figure 4-47, Figure 4-48, and Figure 4-49. Drag reduction was also observed only in the low Reynolds numbers flows in the work of Takahiro et al. [45]

Figure 4-50 and Figure 4-51 shows the variation of total pressure drop for orifices having diameter ratio 0.63 without and with drag reducing polymer respectively. Whereas, Figure 4-52 and Figure 4-53 shows the variation of total pressure drop for orifices having diameter ratio 0.5 without and with drag reducing polymer respectively. It can be seen that double orifice with 1D spacing arrangement gives least pressure drop than single and double orifice with 2D spacing arrangement.

Figure 4-54 and Figure 4-55 shows the variation of pressure drop across orifices having diameter ratio 0.63 without and with drag reducing polymer respectively. Whereas, Figure 4-56 and Figure 4-57 shows the variation of pressure drop across orifices having diameter ratio 0.5 without and with drag reducing polymer respectively.

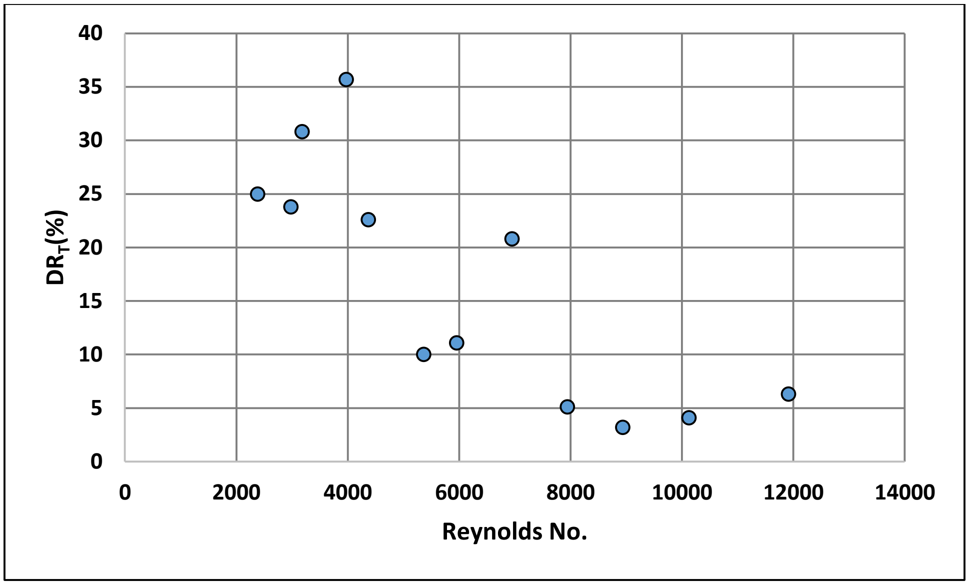

Figure 4-38 Variation of percentage total Drag Reduction (DR_T) at different Reynolds numbers for Single orifice having D_r=0.63

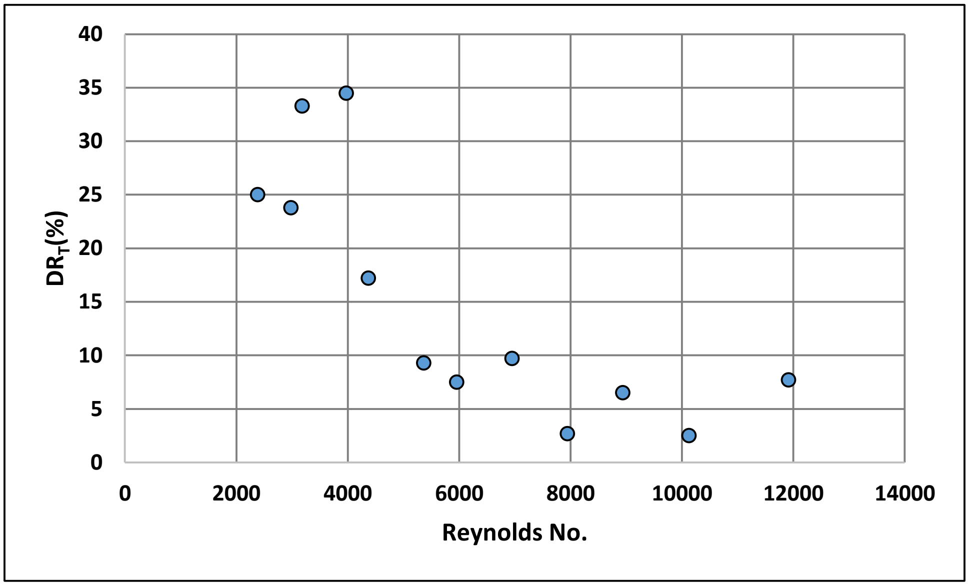

Figure 4-39 Variation of percentage total Drag Reduction (DR_T) at different Reynolds numbers for Double orifice with 1D spacing having D_r=0.63

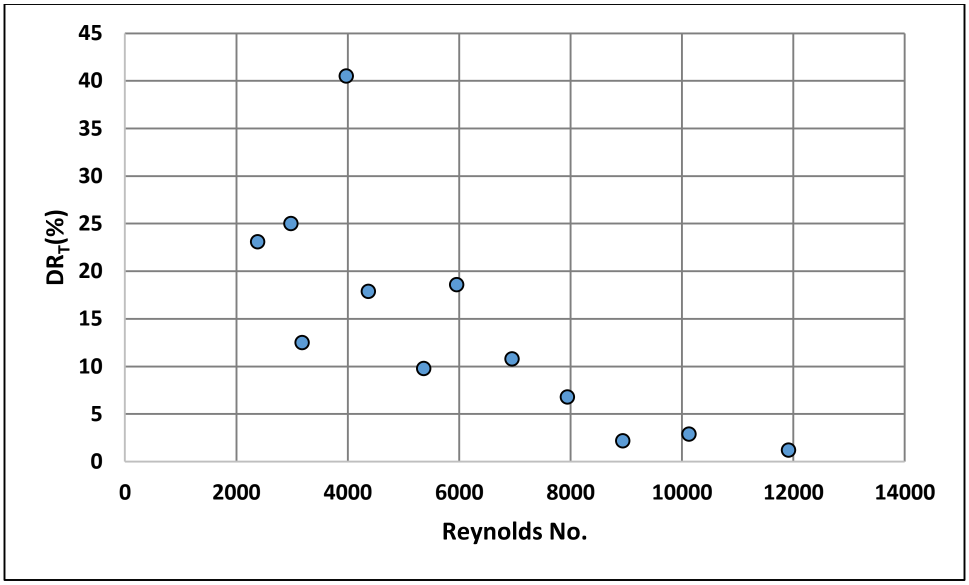

Figure 4-40 Variation of percentage total Drag Reduction (DR_T) at different Reynolds numbers for Double orifice with 2D spacing having D_r=0.63

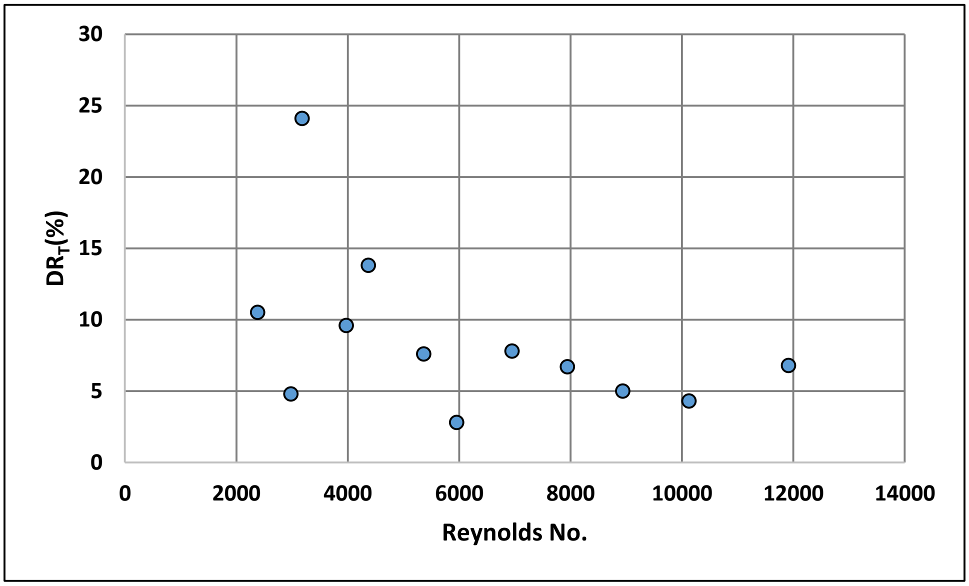

Figure 4-41 Variation of percentage total Drag Reduction (DR_T) at different Reynolds numbers for Single orifice having D_r=0.5

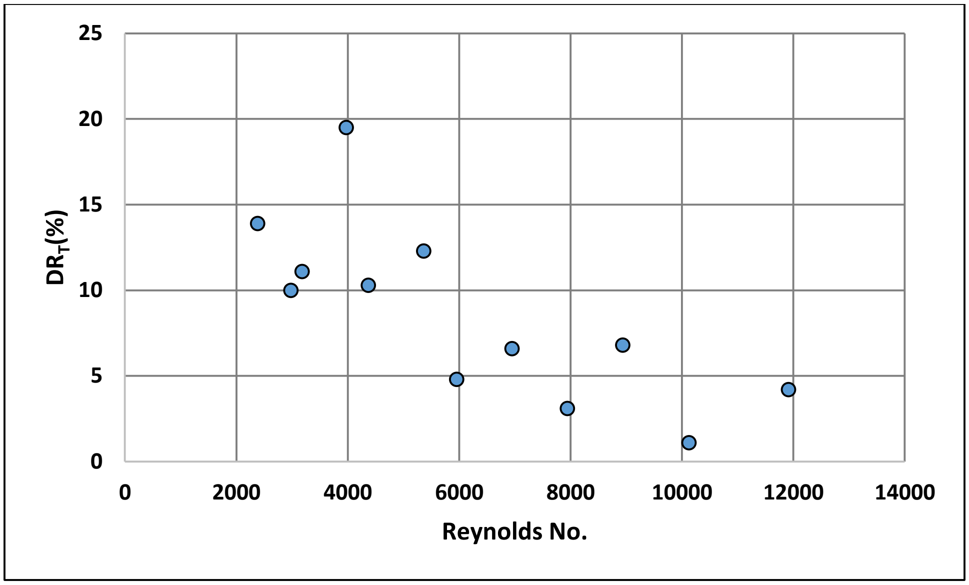

Figure 4-42 Variation of percentage total Drag Reduction (DR_T) at different Reynolds numbers for Double orifice with 1D spacing having D_r=0.5

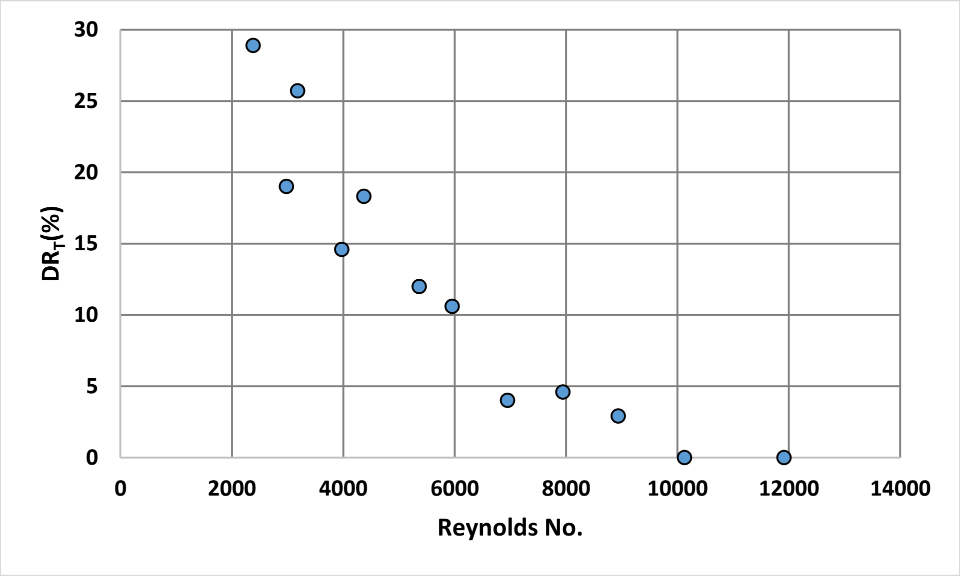

Figure 4-43 Variation of percentage Drag Reduction (DR_T) at different Reynolds numbers for Double orifice with 2D spacing having D_r=0.5

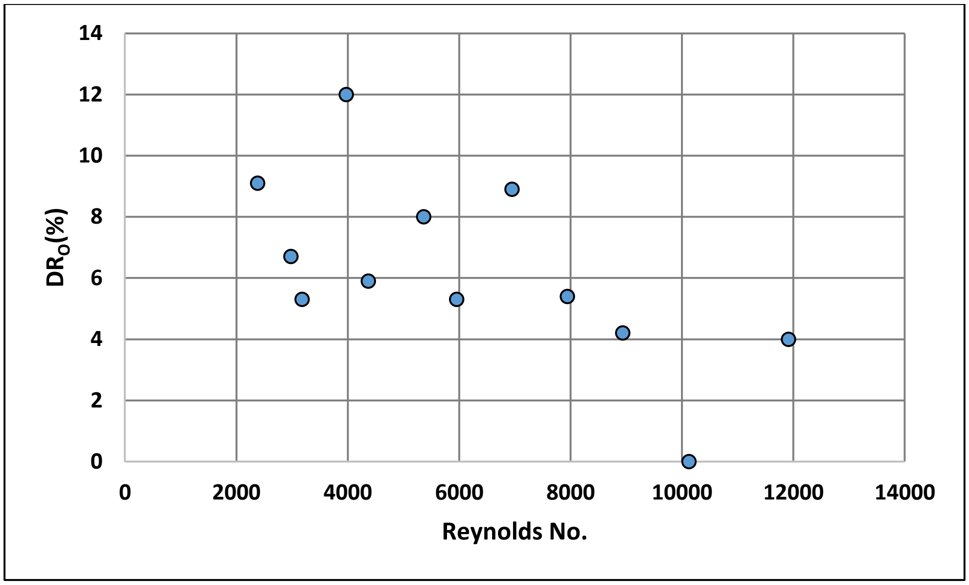

Figure 4-44 Variation of percentage Drag Reduction (DR$_O$) at different Reynolds numbers across Single orifice having D$_r$=0.63

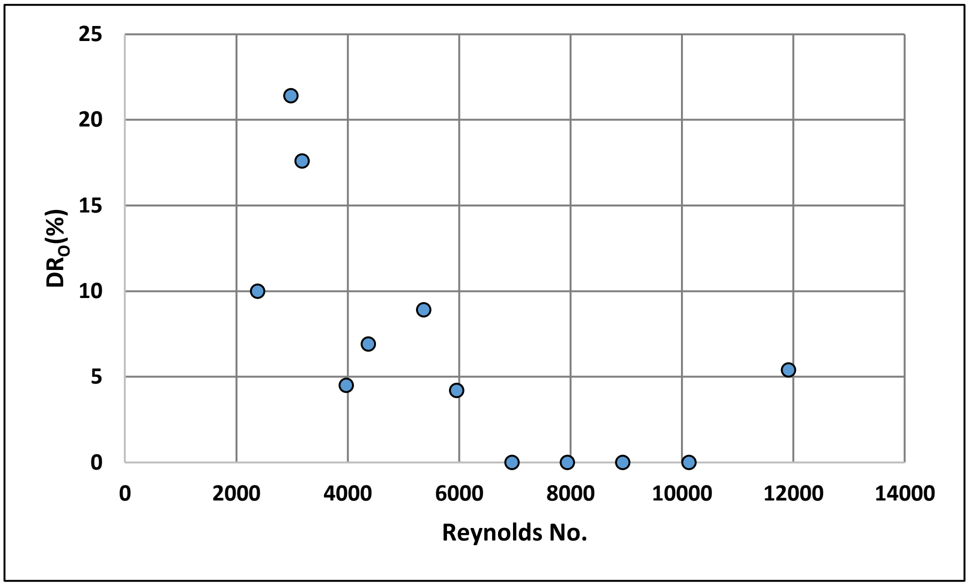

Figure 4-45 Variation of percentage Drag Reduction (DR$_O$) at different Reynolds numbers across Double orifice with 1D spacing having D$_r$=0.63

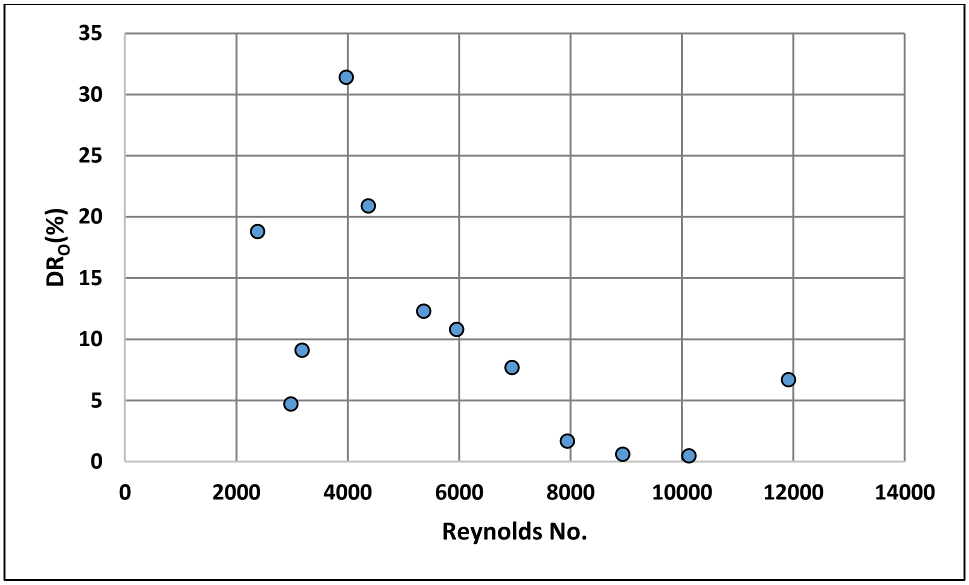

Figure 4-46 Variation of percentage Drag Reduction (DR_O) at different Reynolds numbers across Double orifice with 2D spacing having D_r=0.63

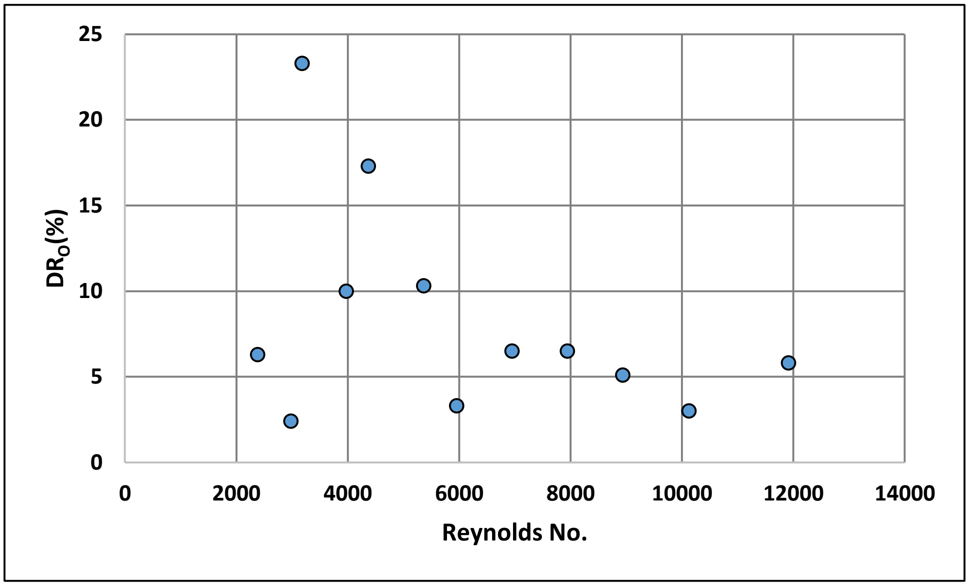

Figure 4-47 Variation of percentage Drag Reduction (DR_O) at different Reynolds numbers across Single orifice having D_r=0.5

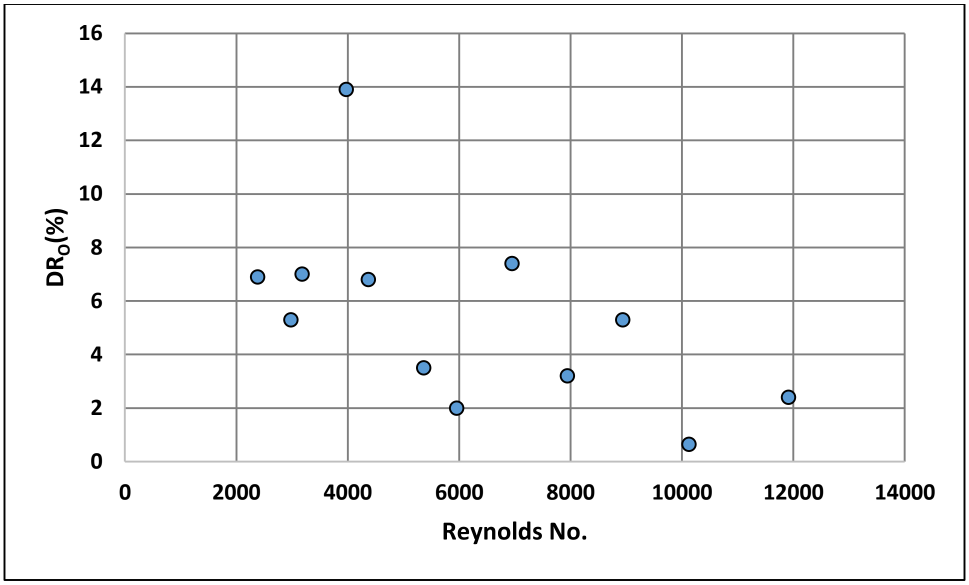

Figure 4-48 Variation of percentage drag Reduction (DR_O) at different Reynolds numbers across Double orifice with 1D spacing having D_r=0.5

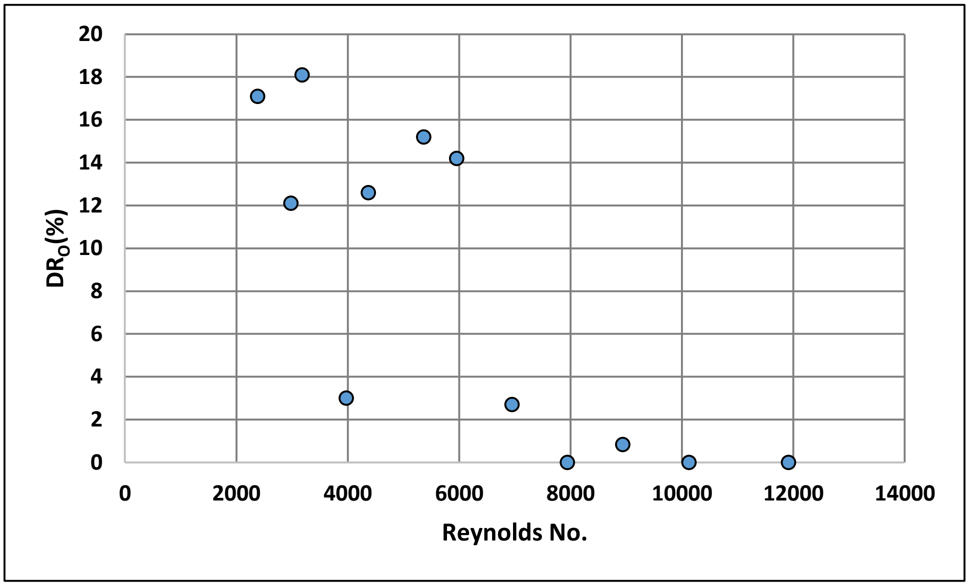

Figure 4-49 Variation of percentage Drag Reduction (DR_O) at different Reynolds numbers across Double orifice with 2D spacing having D_r=0.5

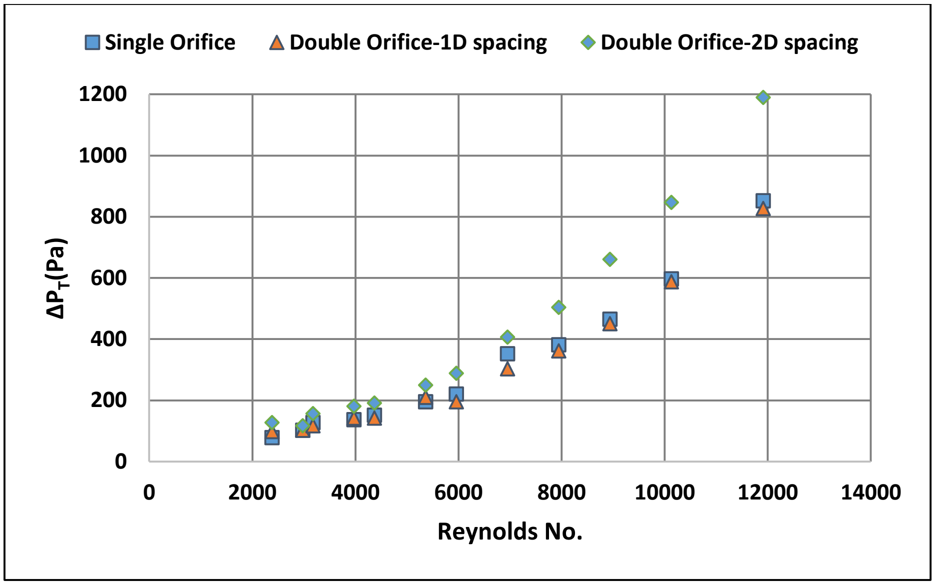

Figure 4-50 Variation of total static Pressure drop (ΔP_T) without DRP for orifices having D_r=0.63 at different Reynolds numbers

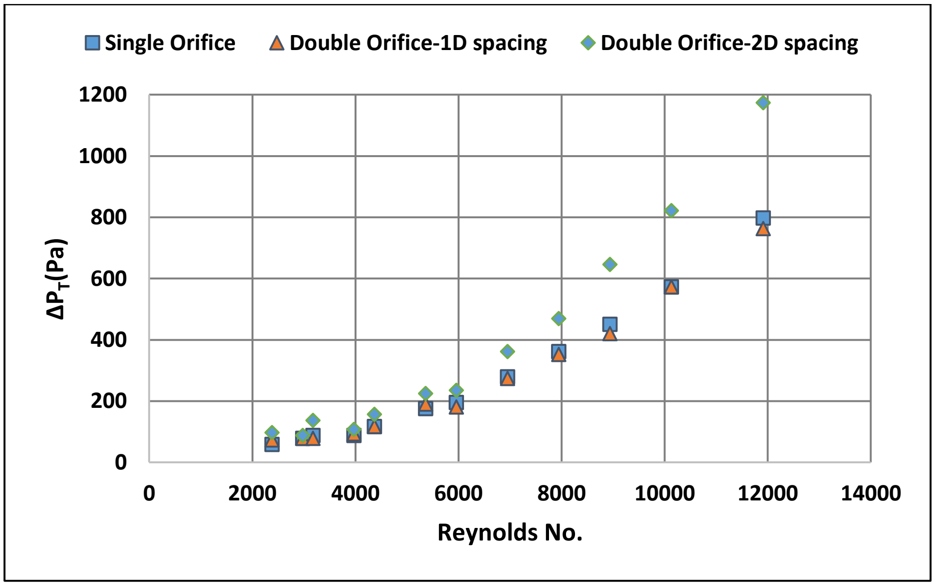

Figure 4-51 Variation of total static Pressure drop (ΔP_T) with DRP for orifices having D_r=0.63 at different Reynolds numbers

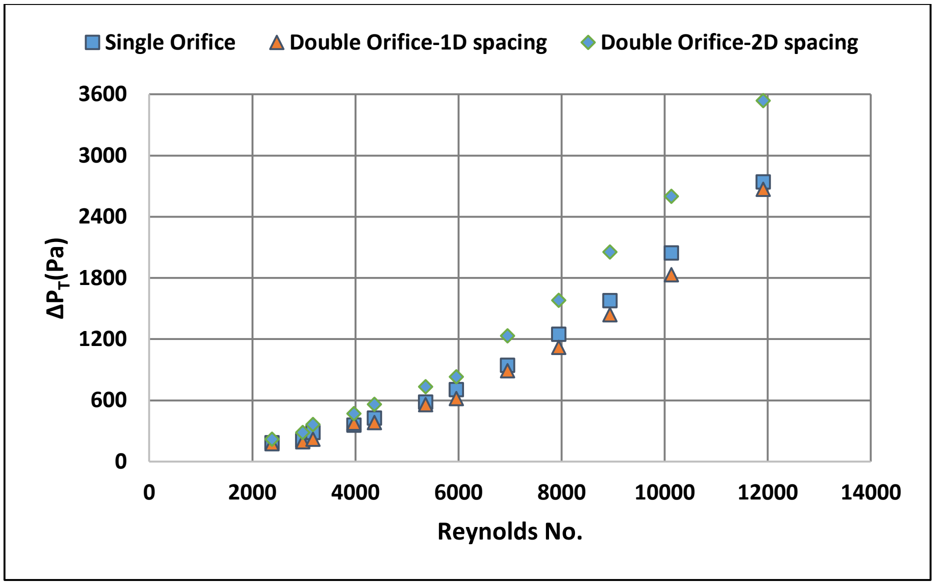

Figure 4-52 Variation of total static Pressure drop (ΔP_T) without DRP for orifices having D_r=0.5 at different Reynolds numbers

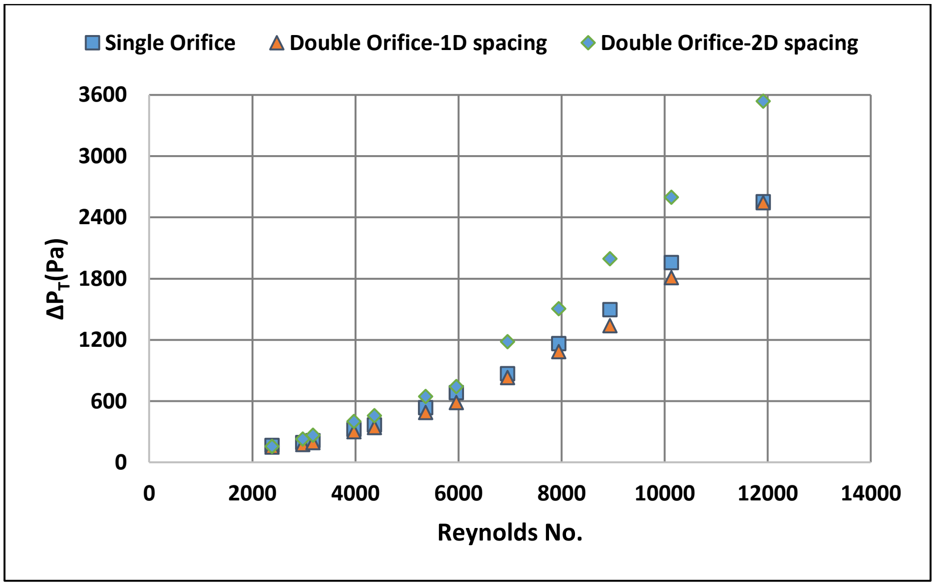

Figure 4-53 Variation of total static Pressure drop (ΔP_T) with DRP for orifices having D_r=0.5 at different Reynolds numbers

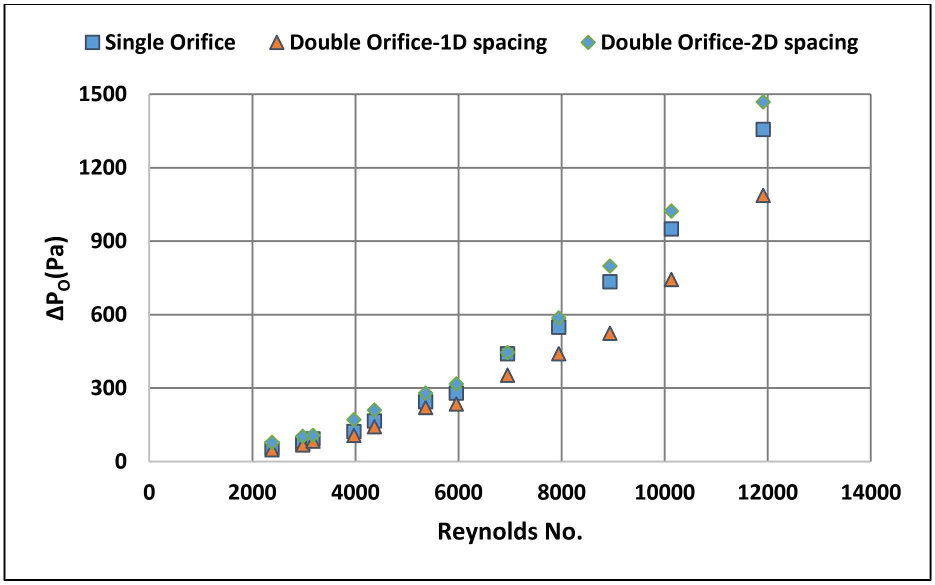

Figure 4-54 Variation of Pressure drop across orifices (ΔP_O) having D_r=0.63 without DRP at different Reynolds numbers

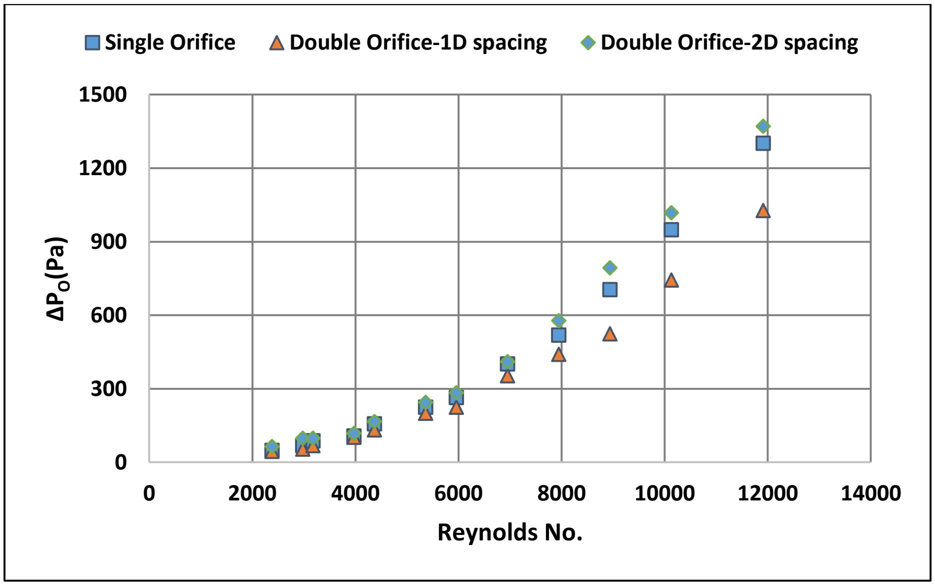

Figure 4-55 Variation of Pressure drop across orifices (ΔP_O) having D_r=0.63 with DRP at different Reynolds numbers

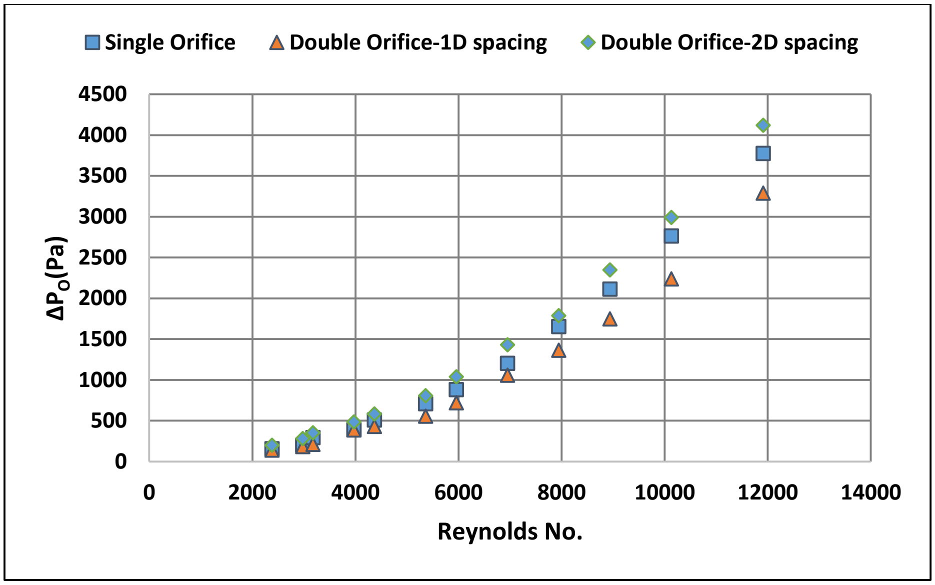

Figure 4-56 Variation of Pressure drop across orifices (ΔP_O) having D_r=0.5 without DRP at different Reynolds numbers

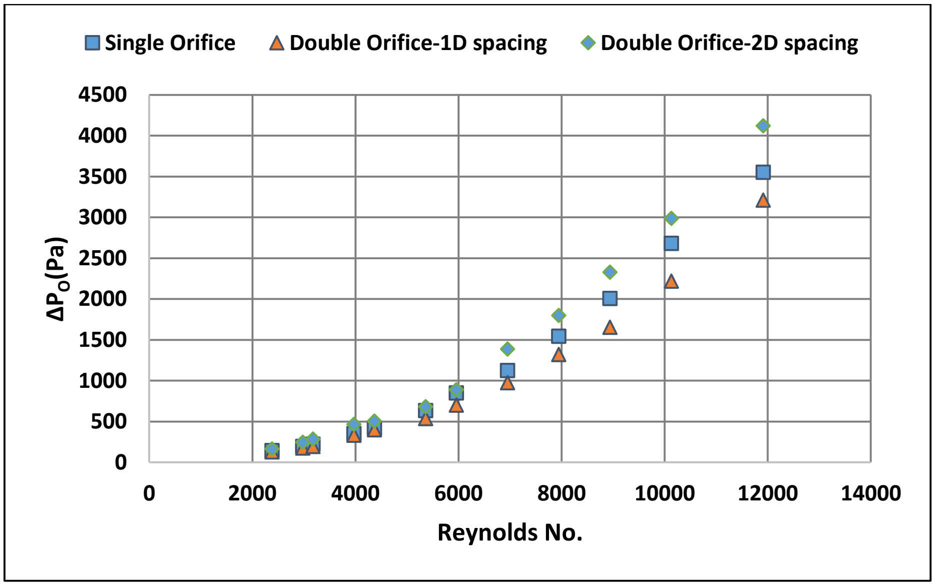

Figure 4-57 Variation of Pressure drop across orifices (ΔP_O) having D_r=0.5 with DRP at different Reynolds numbers

4.2. Two Phase Pressure Drop

Bubbly and slug flow were mainly observed at different water and air flow rates. Pressure reading were taken for 0.63 diameter ratio single orifice, double orifice with 1D spacing, and double orifice with 2D spacing. Drag reduction was found to occur in flows with drag reducing polymer. Double orifice with 1D spacing experienced lowest pressure drop, while double orifice with 2D spacing experienced largest pressure drop. Two phase pressure drop was quite greater than single phase pressure drop at corresponding liquid superficial Reynolds numbers. Similar increase in pressure drop in two phase flow through orifices has been previously reported in many papers such as in the work of Martha et.al. [33]

4.2.1. Bubbly Flow

In this case, the superficial water and air velocities were 0.437837 m/s and 0.164463 m/s respectively and the corresponding superficial water and air Reynolds nos. were 11121 and 258 respectively. Bubbly flow was observed before and after the orifice. The concentration of drag reducing polymers was maintained at 44ppm. Figure 4-58 shows the pressure profile for single orifice, double orifice with 1D spacing, and double orifice with 2D spacing for this flow regime. Total drag reduction (DR_T) of 9.1, 4.7, and 5.3% were observed for the respective three cases. 6.7, 2.9, and 7.7% drag reduction (DR_O) were also observed across these three arrangements.

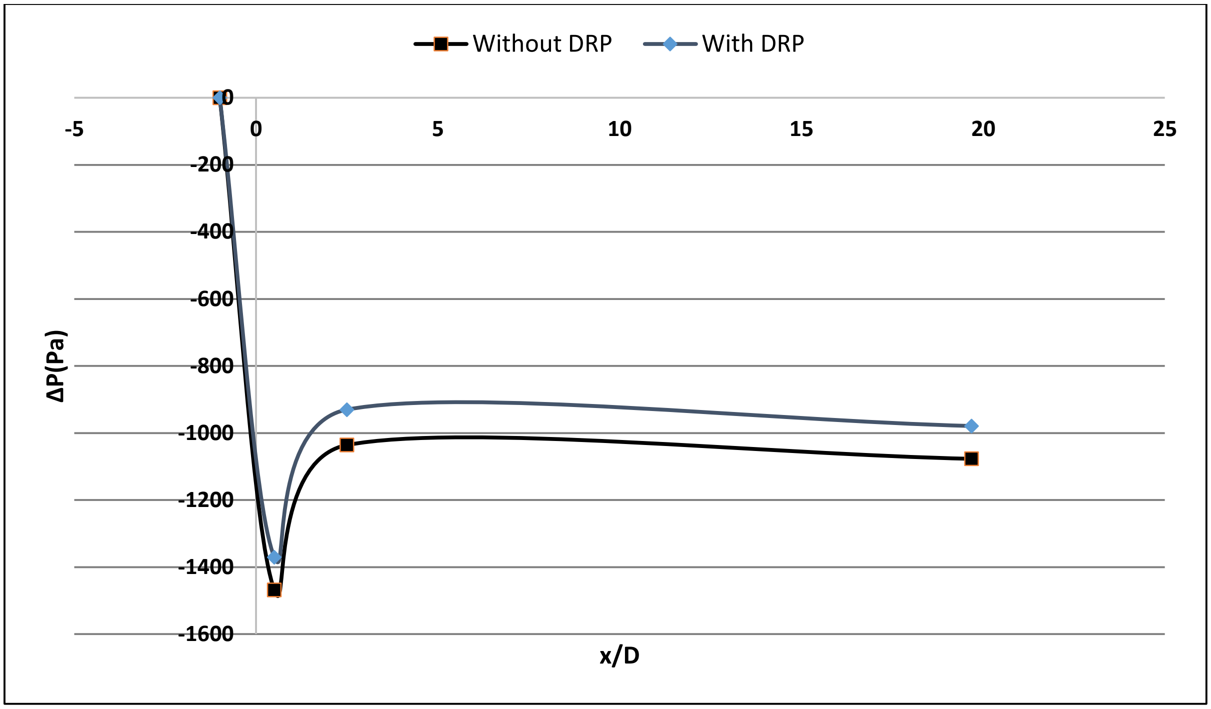

a) Single orifice

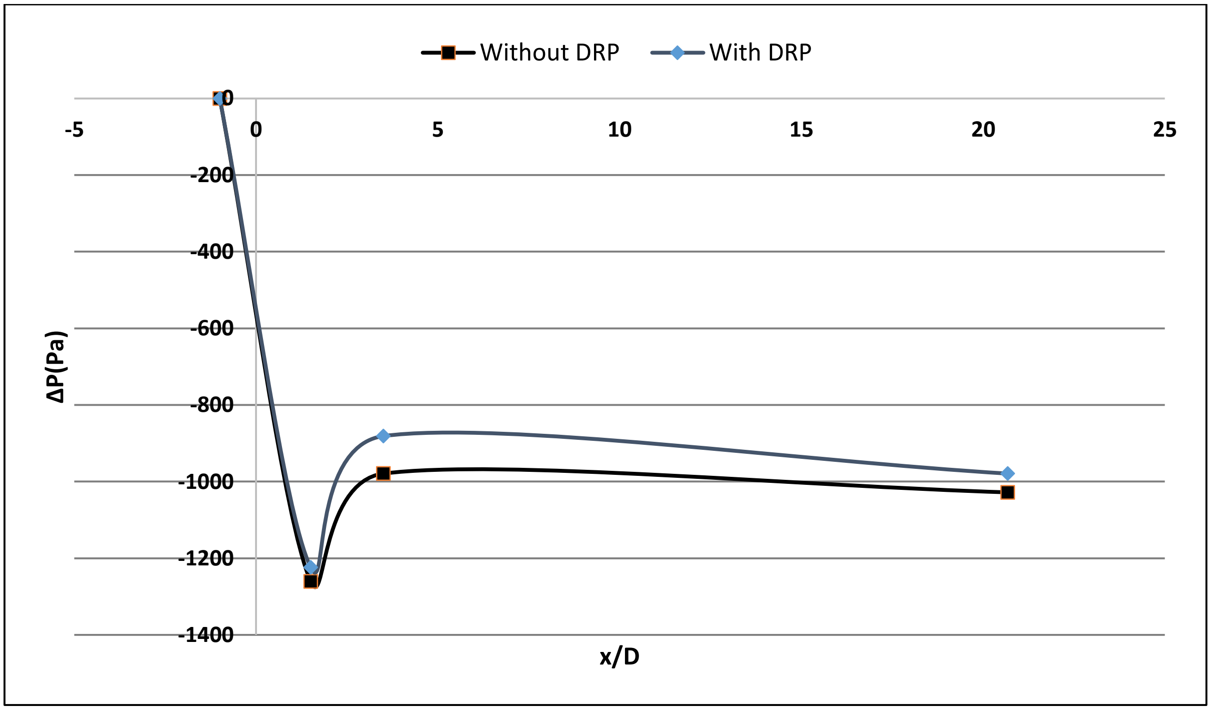

b) Double orifice with 1D spacing

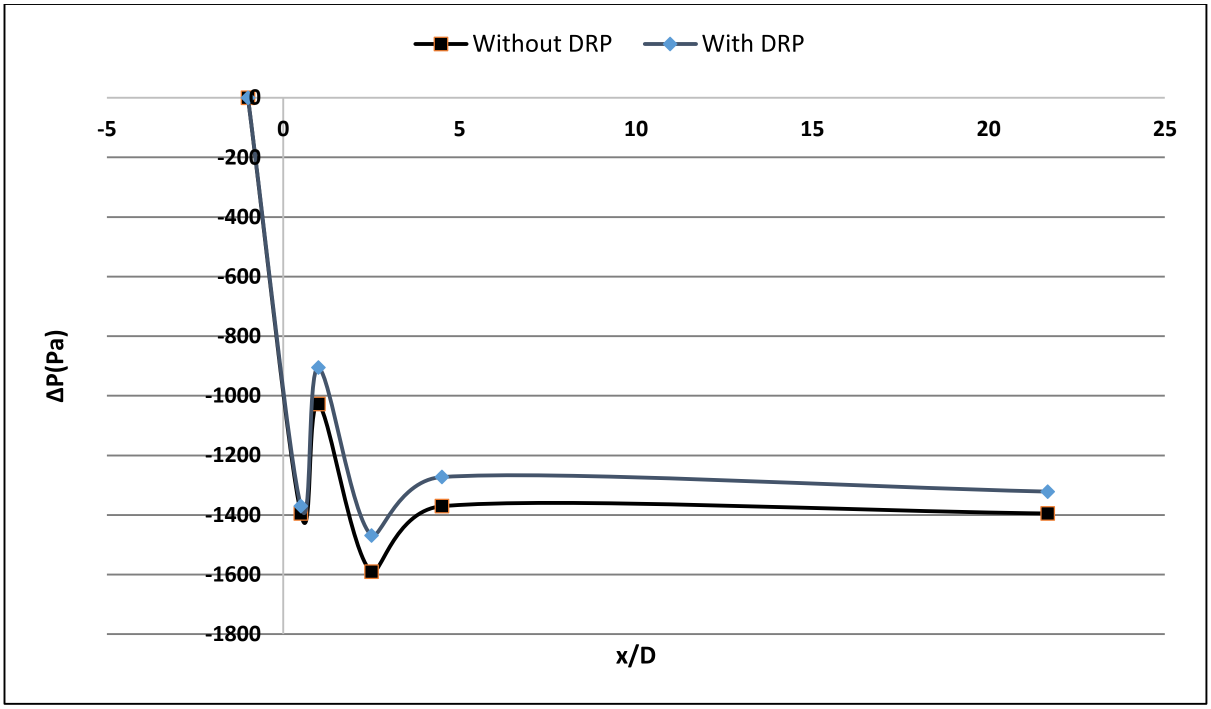

c) Double orifice with 2D spacing

Figure 4-58 Variation of static pressure difference with normalized axial distance of bubbly flow at 44ppm DRP; a) Single orifice, b) Double orifice with 1D spacing, c) Double orifice with 2D spacing

4.2.2. Slug Flow

Slug flow at two different water and air flow rates were observed. In first case, the superficial water and air velocities were 0.359652 m/s and 0.328926 m/s and the corresponding Reynolds nos. for water and air were 9135 and 516. The concentration of drag reducing polymers were kept at 53ppm. Figure 4-59 represents the pressure profile for this case for single orifice, double orifice with 1D spacing, and double orifice with 2D spacing. 7.1, 8.3, and 10.7% total drag reduction (DR_T) were achieved for the three arrangements of orifices. 3.1, 6.1, and 11.7% drag reductions (DR_O) were also observed across the respective three orifice arrangements.

In the other case, the superficial water and air velocities were 0.328378 m/s and 0.657853 m/s respectively and the corresponding Reynolds nos. were 8340 and 1032 respectively. The concentration of DRA was maintained at 58ppm in this case. 5.8, 8.9, and 7.2% DR_T were achieved in this case for single orifice, double orifice with 1D spacing, and double orifice with 2D spacing. Figure 4-60 shows the pressure drop profile for this flow regime. Also, 7.7, 3.8 and 6% DR_T were obtained for the respective three cases.

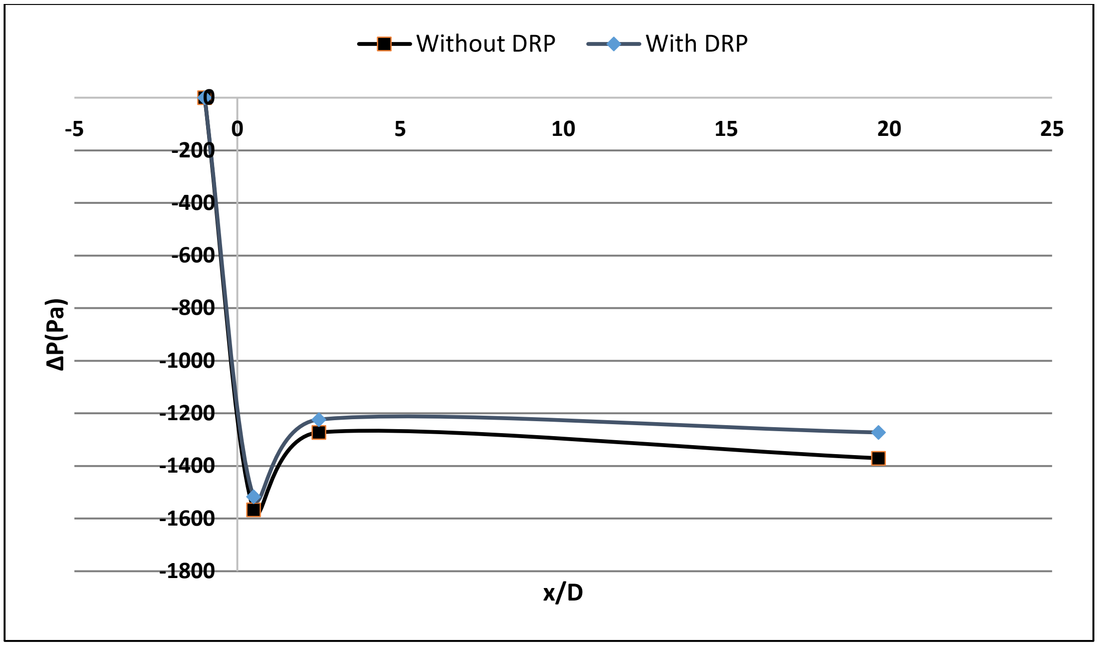

a) Single orifice

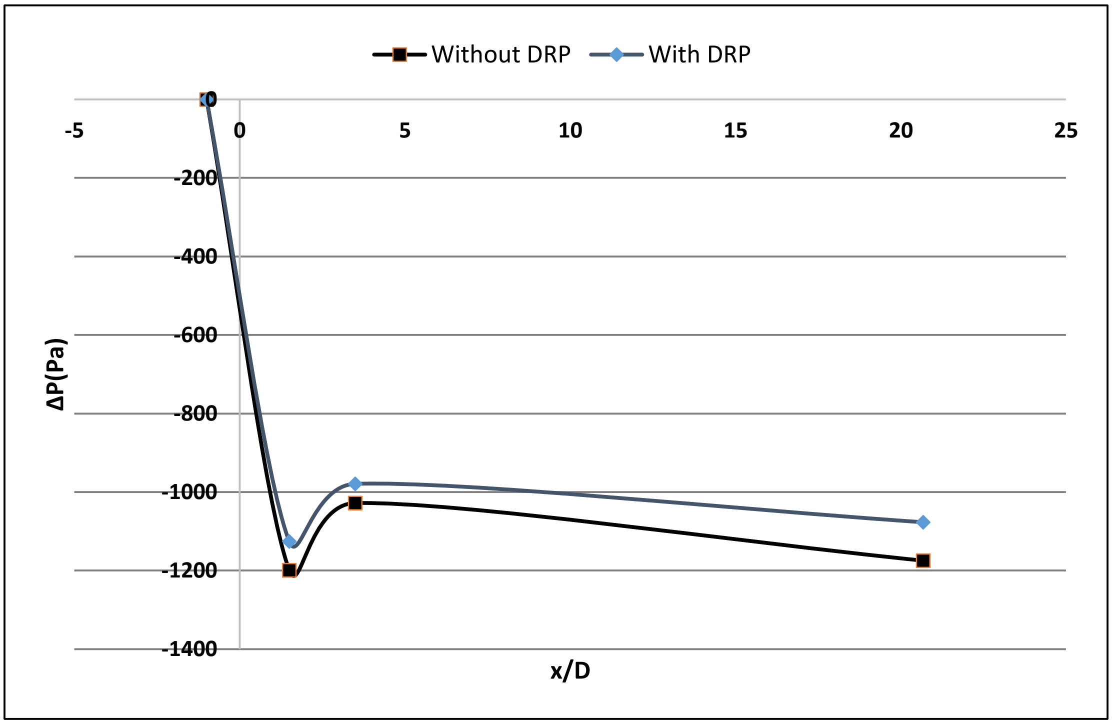

b) Double orifice with 1D spacing

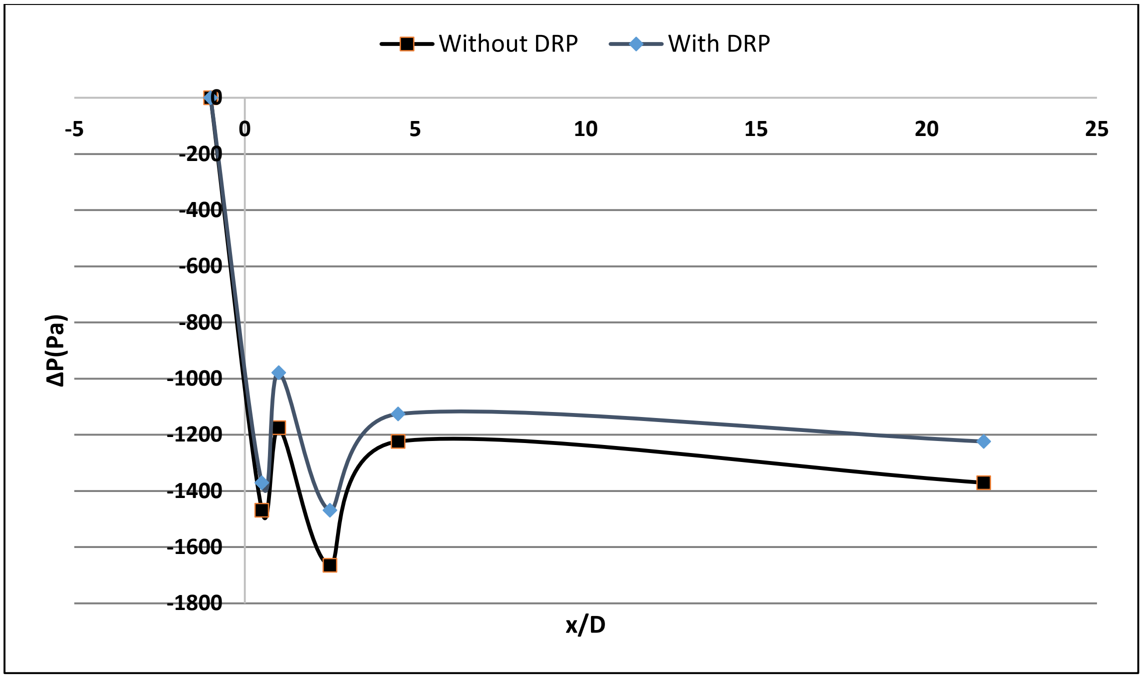

c) Double orifice with 2D spacing

Figure 4-59 Variation of static pressure difference with normalized axial distance for slug flow, liquid superficial Re= 9135 at 53ppm DRP; a) Single orifice, b) Double orifice with 1D spacing, c) Double orifice with 2D spacing.

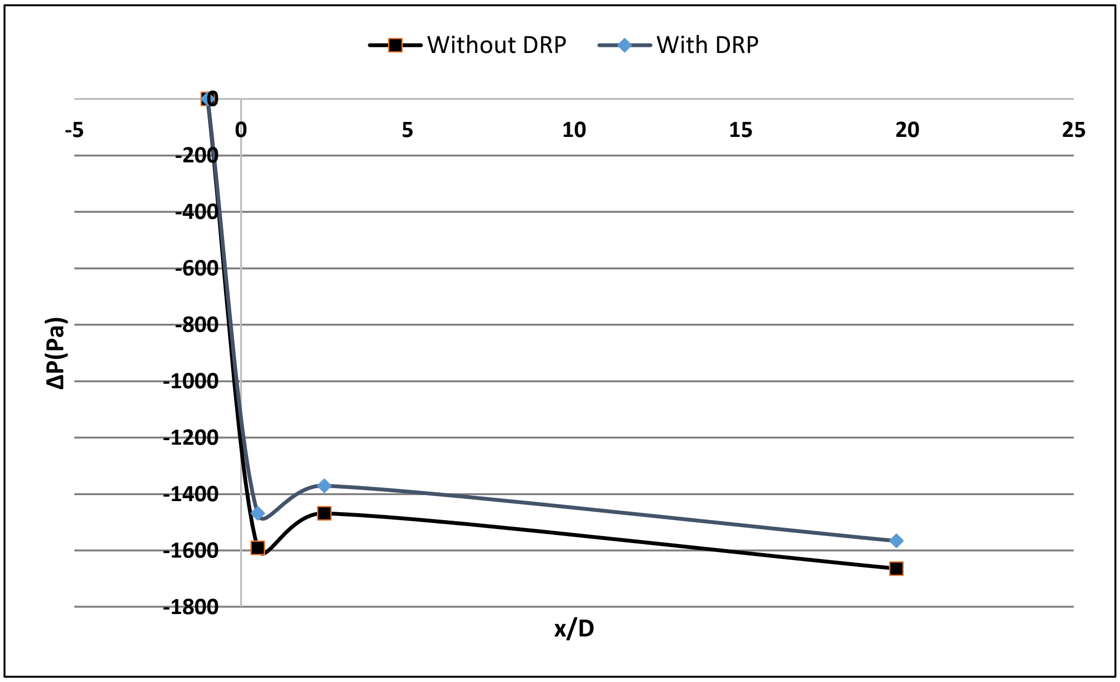

a) Single orifice

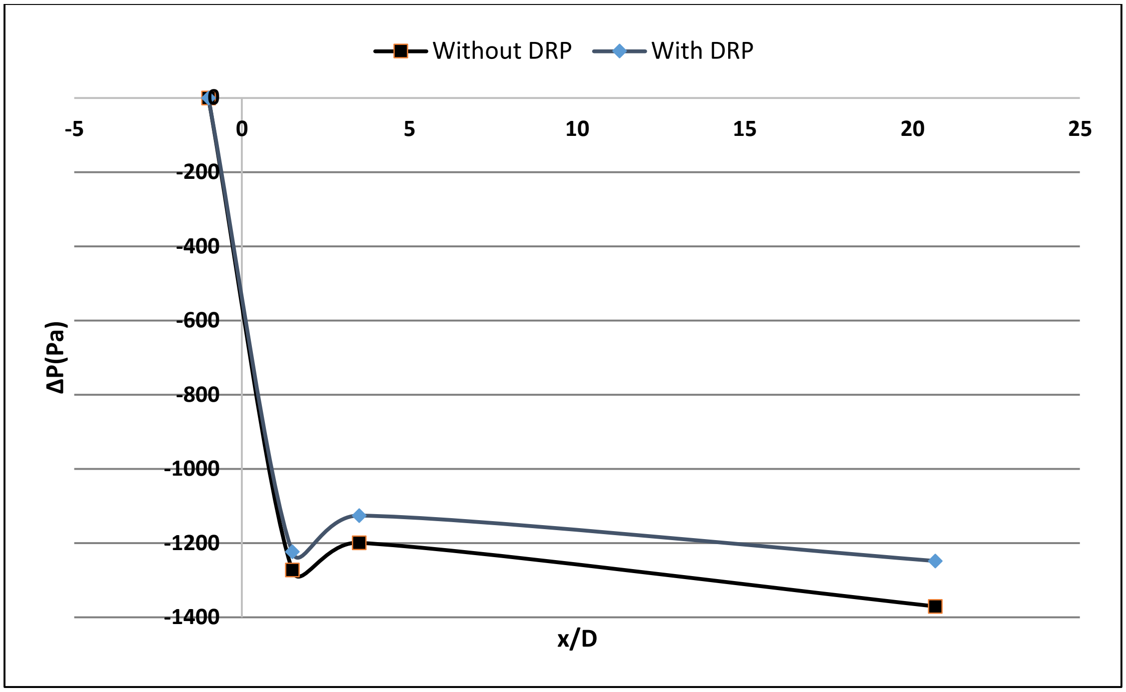

b) Double orifice with 1D spacing

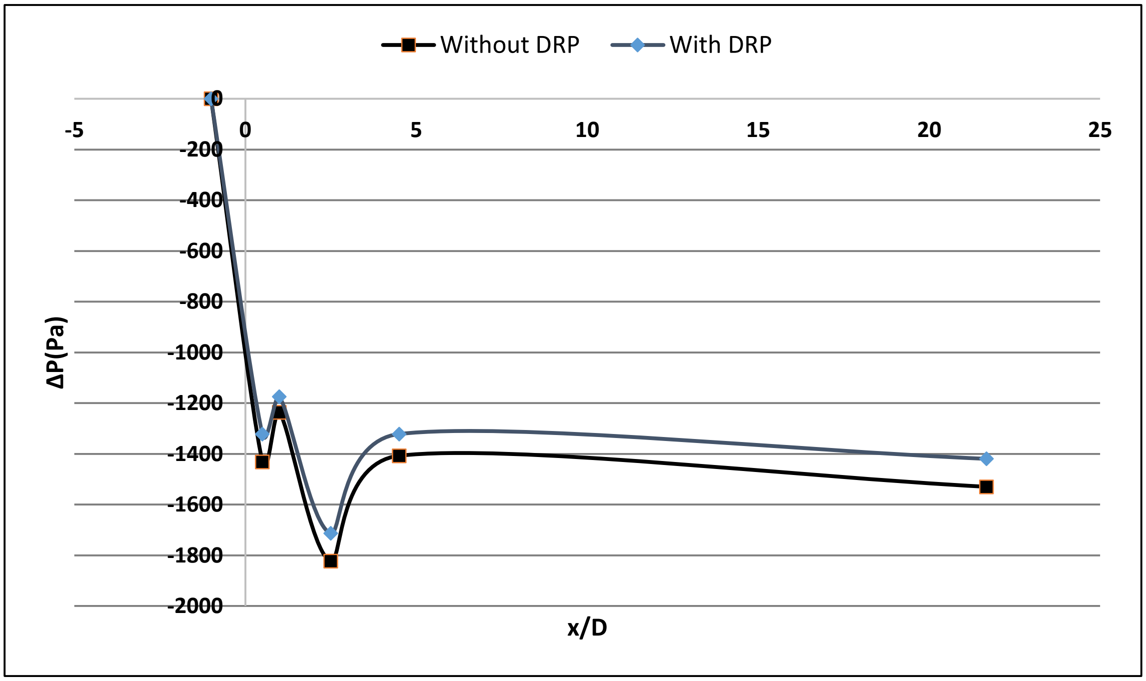

c) Double orifice with 2D spacing

Figure 4-60 Variation of static pressure difference with normalized axial distance for slug flow, liquid superficial Re= 8340 at 58ppm DRP; a) Single orifice, b) Double orifice with 1D spacing, c) Double orifice with 2D spacing.

Figure 4-61 shows the variation of percentage total drag reduction (DR_T) for single orifice, double orifice with 1D spacing and double orifice with 2D spacing at different superficial air Reynolds number respectively. Single orifice gave maximum total drag reduction in bubbly flow regime which was observed at lowest and highest Reynolds number of air and water respectively. Double orifice with 1D spacing showed maximum total drag reduction in slug flow regime where air Reynolds number is highest while double orifice with 2D spacing showed the maximum total drag reduction in case where slug flow was observed at moderate air and water flow rates.

Figure 4-62 shows the percentage drag reduction (DR_O) across single orifice, double orifice with 1D spacing, and double orifice with 2D spacing at different superficial air Reynolds numbers. It is shown that double orifice with 2D spacing gave highest pressure drag reductions across the orifices in most of the cases.

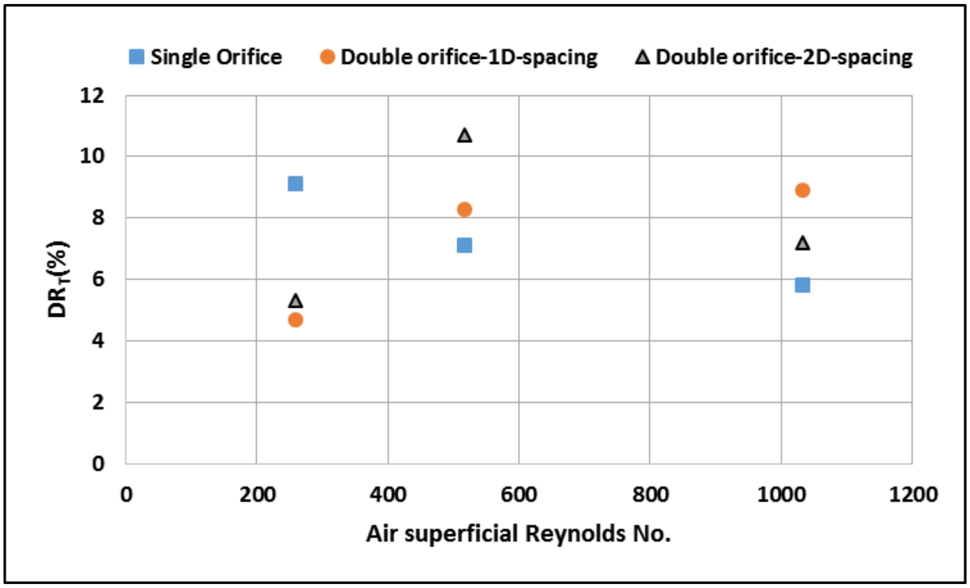

Figure 4-61 Variation of percentage total drag reduction (DR_T) at different Air superficial Reynolds numbers for orifices having D_r=0.63

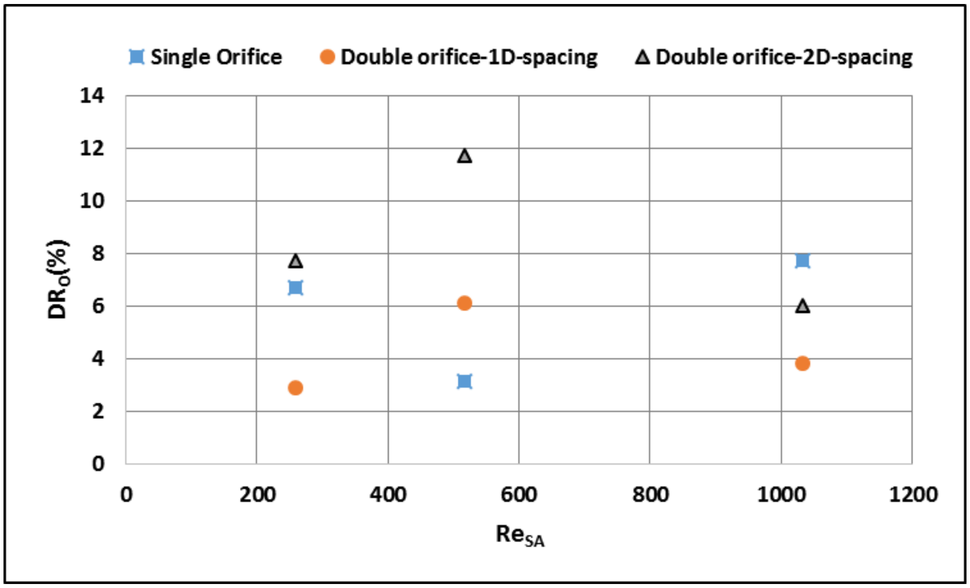

Figure 4-62 Variation of percentage drag reduction (DR_O) at different Air superficial Reynolds numbers across orifices having D_r=0.63

4.3. The Streamline Pattern

4.3.1. Re=3972

The frame rate and the exposure time were 1300fps and 430μs respectively for PIV recordings at this Reynolds number. Calibration width was 55mm and number of slides were 4000 approximately in each case. The streamline patterns for the representative flow rate at a Reynolds number of 3972 for single orifice D_r=0.63 is shown in Figure 4-63. The figure shows a comparison between the streamline patterns of flow without and with drag reducing polymer (DRP). It can be seen that the primary recirculation zone in the downstream side of the orifice is smaller in case of polymeric solution than in non-polymeric solution. Figure 4-64 displays the streamline patterns observed for single orifice having diameter ratio 0.5 with and without drag reducing polymer. The primary recirculation zone is smaller in case of flow with drag reducing polymer than in flow without drag reducing polymer. Also the reattachment length in case of polymeric solution is smaller than non-polymeric solution.

The streamline patterns in the spacing between two orifices in double orifice arrangement with 1D spacing and D_r=0.63 are shown in Figure 4-65. Two recirculation zones can be seen in flow without drag reducing polymer while the secondary recirculation zone is found to be diminished in flow with drag reducing polymer. The streamline pattern in the downstream of second orifice in the case of double orifice arrangement with 1D spacing is shown in Figure 4-66. Here also, the circulation zone in case of polymeric solution was found to be less than in non-polymeric solution.

Figure 4-67 and Figure 4-68 shows the streamline patterns in the spacing between the two orifices and the downstream of the second orifice respectively in case of double orifice configuration with 2D spacing. The recirculation zones were found to be smaller in polymeric solutions than in non-polymeric solutions.

Similar behavior of drag reducing agents behind the rectangular orifice was observed in the work of Takahiro et al. [45].

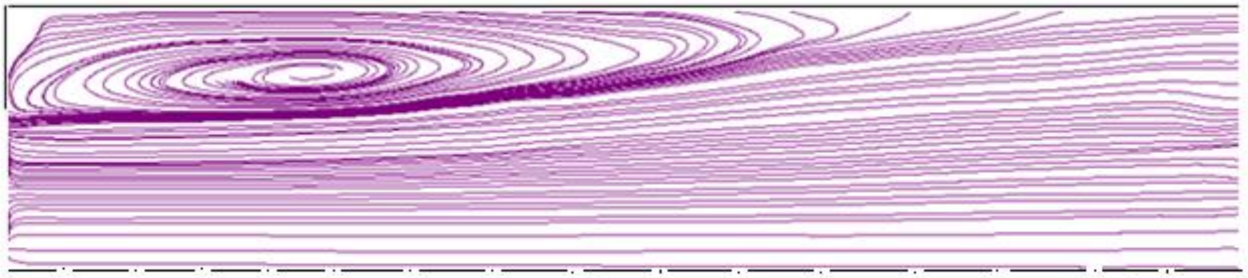

a) Without DRP

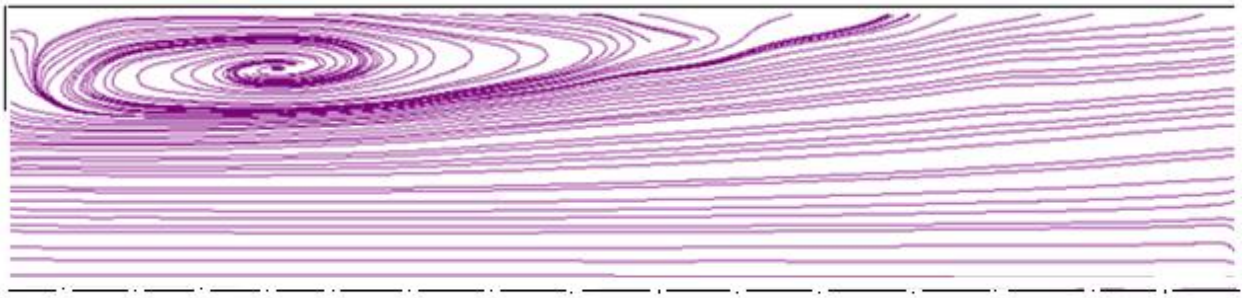

b) With DRP

Figure 4-63 Comparison of streamline patterns in downstream of single orifice at Re=3972, D_r=0.63; a) Without DRP, b) With 119 ppm DRP

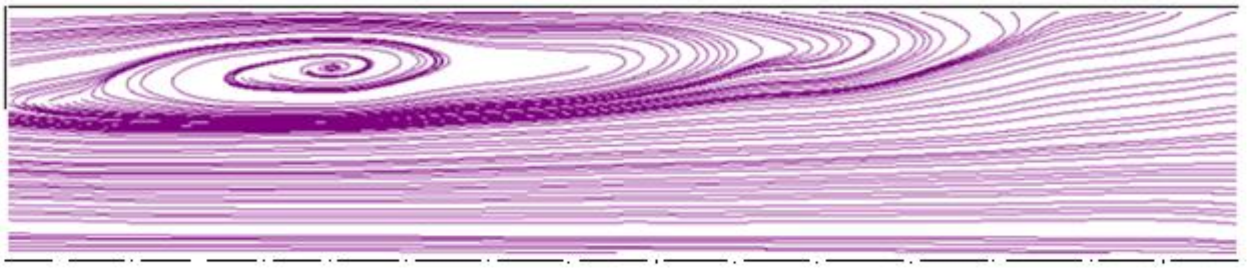

a) Without DRP

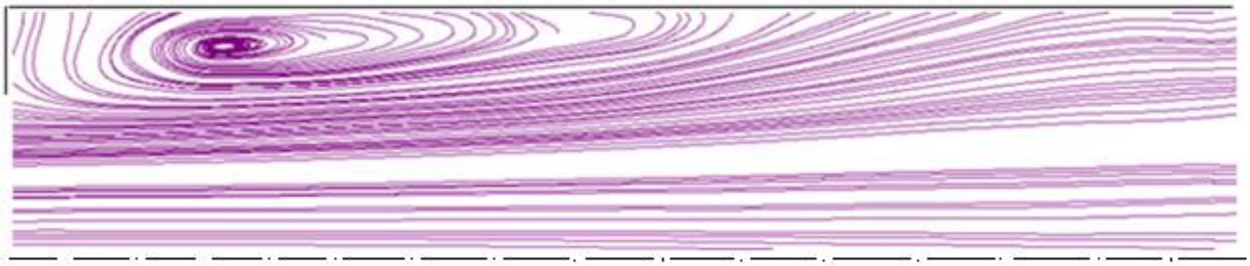

b) With DRP

Figure 4-64 Comparison of streamline patterns in downstream of single orifice at Re=3972, D_r=0.5; a) Without DRP, b) With 119 ppm DRP

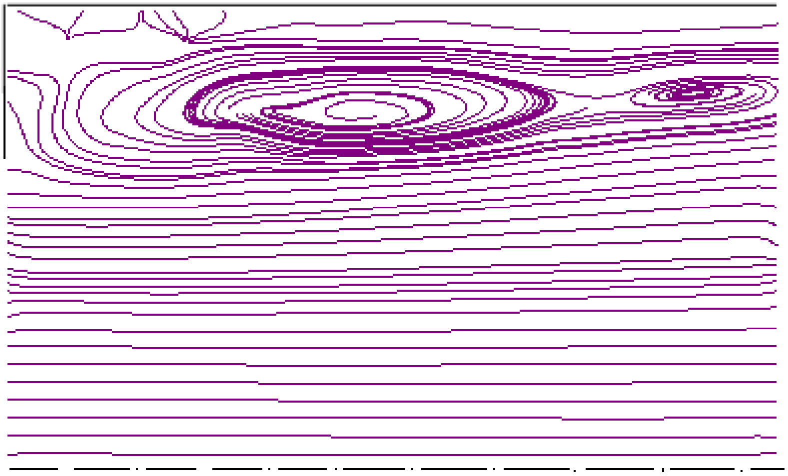

a) Without DRP

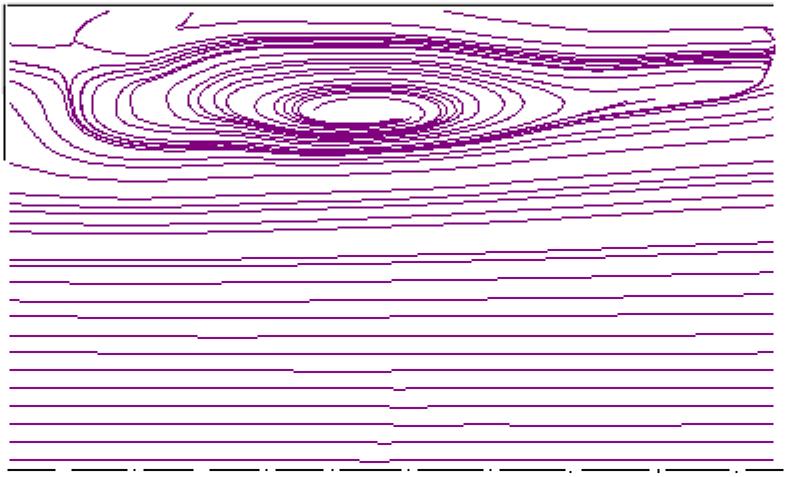

a) With DRP

Figure 4-65 Comparison of streamline patterns in the spacing between two orifices in double orifice arrangement with 1D spacing at Re=3972, D_r=0.63; a) Without DRP, b) With 119ppm DRP

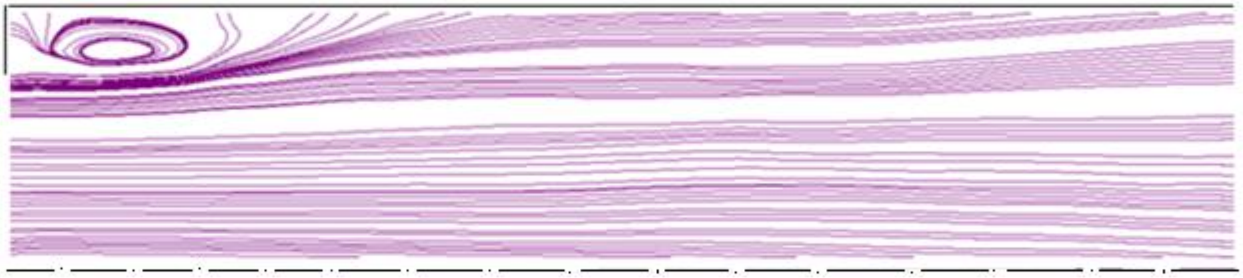

a) Without DRP

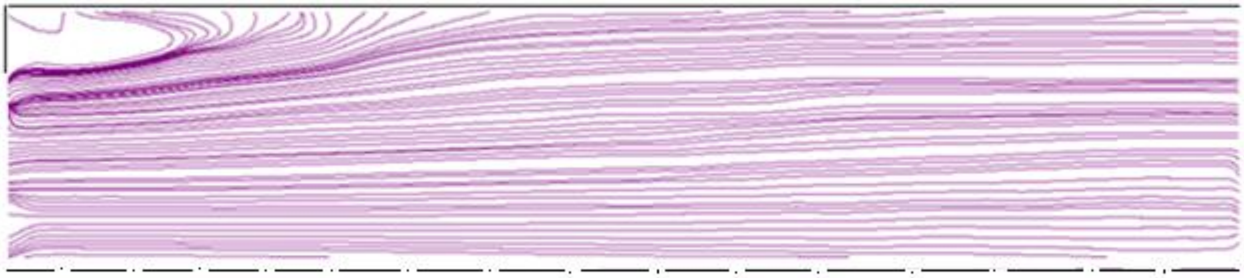

b) With DRP

Figure 4-66 Comparison of streamline patterns in the downstream of second orifice in double orifice arrangement with 1D spacing at Re=3972, D_r=0.63; a) Without DRP, b) With 119 ppm DRP

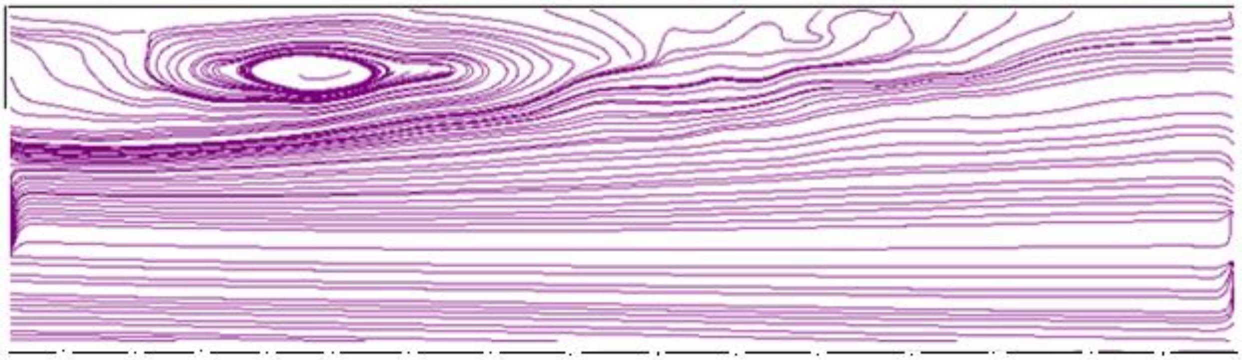

a) Without DRP

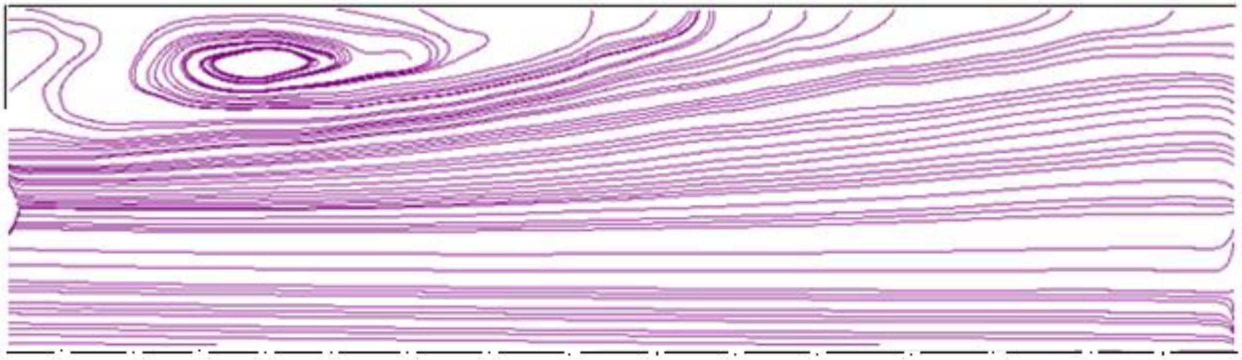

b) With DRP

Figure 4-67 Comparison of streamline patterns in the spacing between two orifices in double orifice arrangement with 2D spacing at Re=3972, D_r=0.63; a) Without DRP, b) With 119 ppm DRP

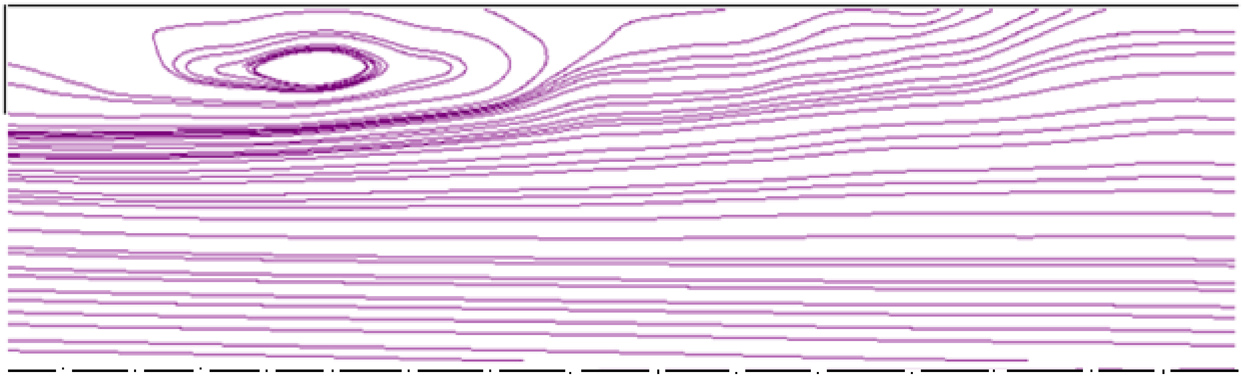

a) Without DRP

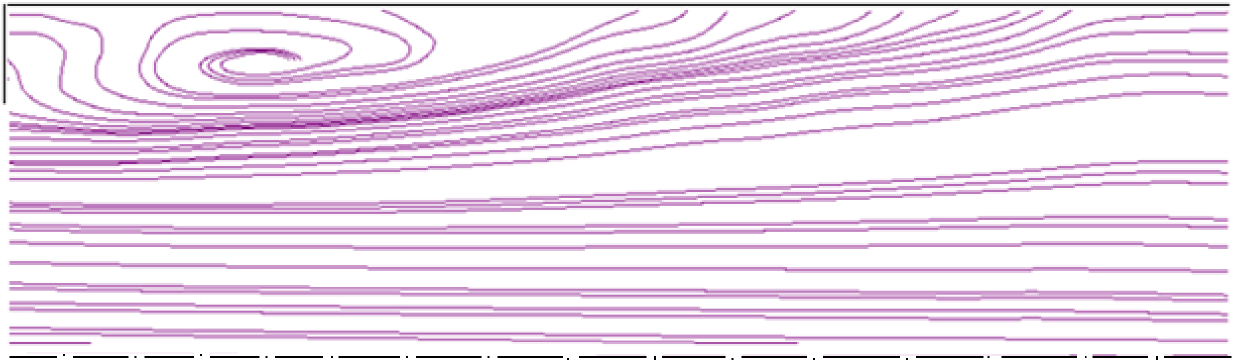

b) With DRP

Figure 4-68 Comparison of streamline patterns in the downstream of second orifice in double orifice arrangement with 2D spacing at Re=3972, D_r=0.63; a) Without DRP, b) With 119 ppm DRP

4.3.2. Re=5958

The frame rate and the exposure time were 2200fps and 300µs respectively at this Reynolds number for PIV recordings. Figure 4-69 shows the comparison between streamline patterns downstream of single orifice having diameter ratio 0.63 for flows with and without drag reducing polymer at the corresponding Reynolds number. The recirculation zones are similar however the recirculation zone in polymeric solution is comparatively smaller than in non-polymeric solutions. The reattachment point is approximately same in both the cases. Figure 4-70 shows the streamline patterns downstream of 0.5 diameter ratio orifice for the same case. The streamlines are similar to each other and the reattachment length is also the same.

Figure 4-71 shows the streamline patterns in the spacing between two orifices in double orifice arrangement with 1D spacing and D_r=0.63. Two recirculation zones are present in both the cases. However they are a bit smaller in case of polymeric solution. Figure 4-72 shows the streamline patterns in the downstream of second orifice in the case of double orifice arrangement with 1D spacing. The recirculation zone is comparatively smaller in case of polymeric solution.

Figure 4-73 and Figure 4-74 shows the streamline patterns in the spacing between the two orifices and the downstream of the second orifice respectively in case of double orifice arrangement with 2D spacing. The recirculation zones were found to be comparatively smaller in polymeric solutions than in non-polymeric solutions.

Flows with DRP showed comparatively smaller recirculation zones with smaller velocity values and smaller pressure drop through orifices than flow without DRP.

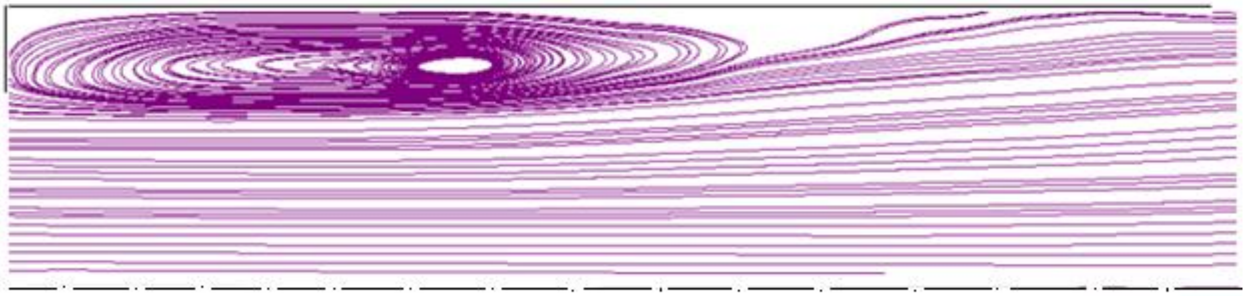

a) Without DRP

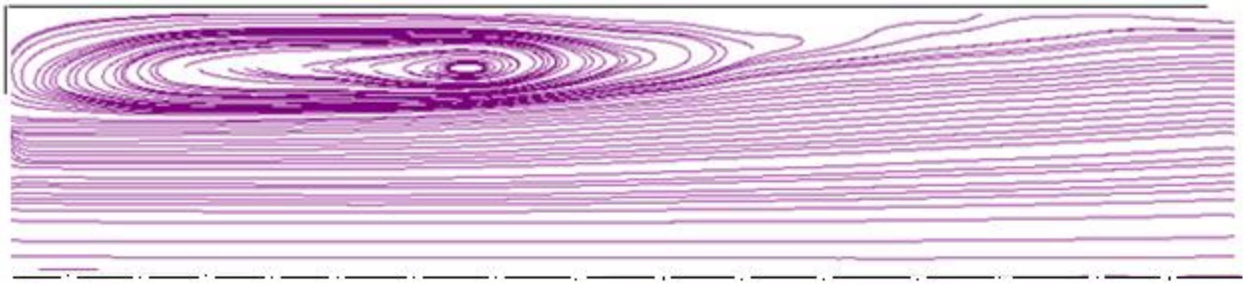

b) With DRP

Figure 4-69 Comparison of streamline patterns for single orifice at Re=5958, D_r=0.63; a) Without DRP, b) With 80 ppm DRP

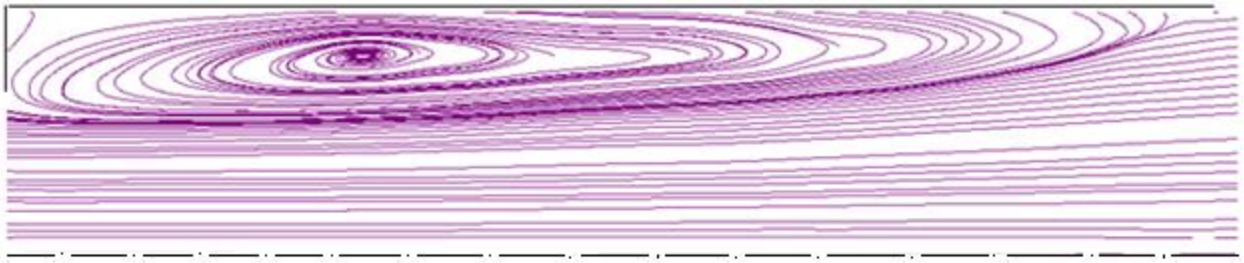

a) Without DRP

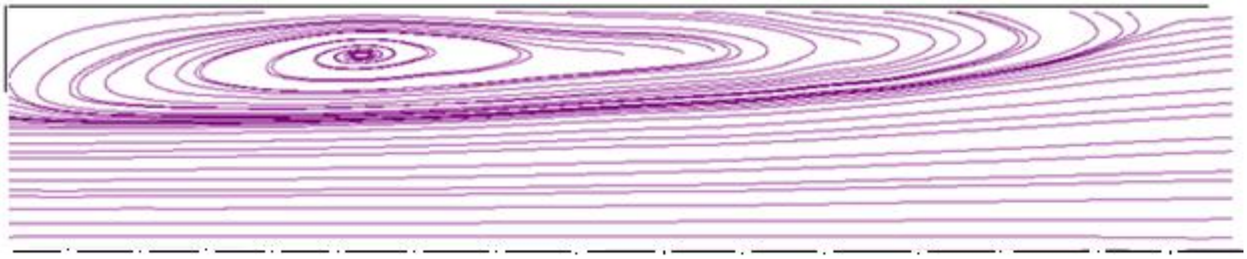

b) With DRP

Figure 4-70 Comparison of streamline patterns for single orifice at Re=5958, D_r=0.5; a) Without DRP, b) With 80 ppm DRP

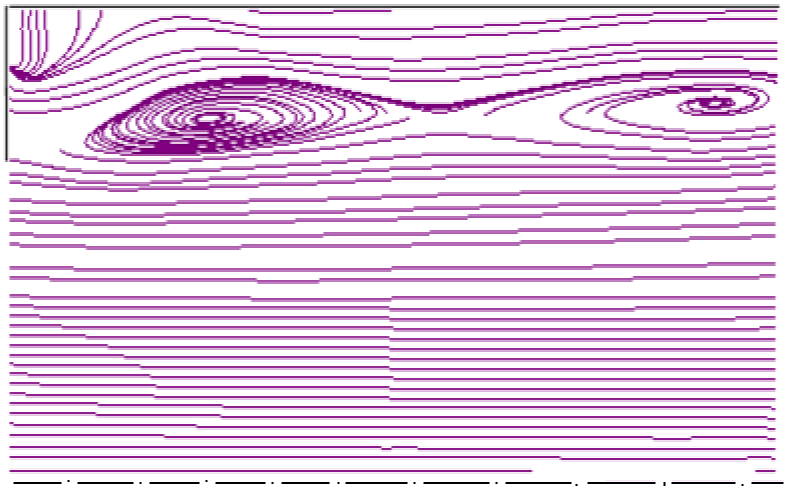

a) Without DRP

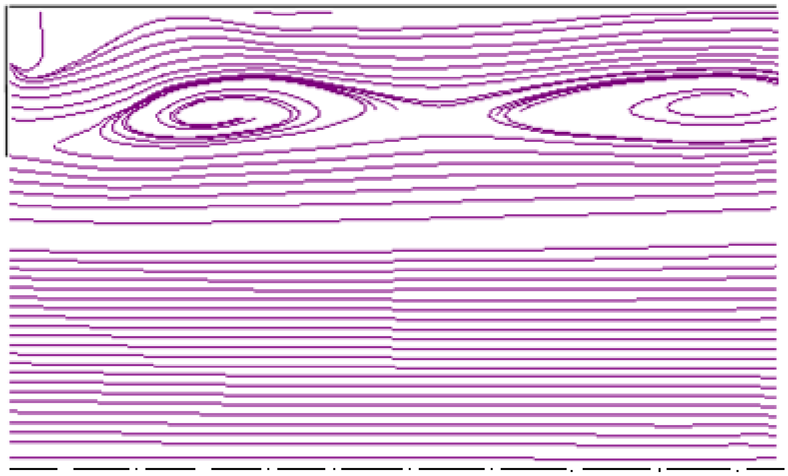

a) With DRP

Figure 4-71 Comparison of streamline patterns in the spacing between two orifices in double orifice arrangement with 1D spacing at Re=5958, D_r=0.63; a) Without DRP, b) With 80 ppm DRP

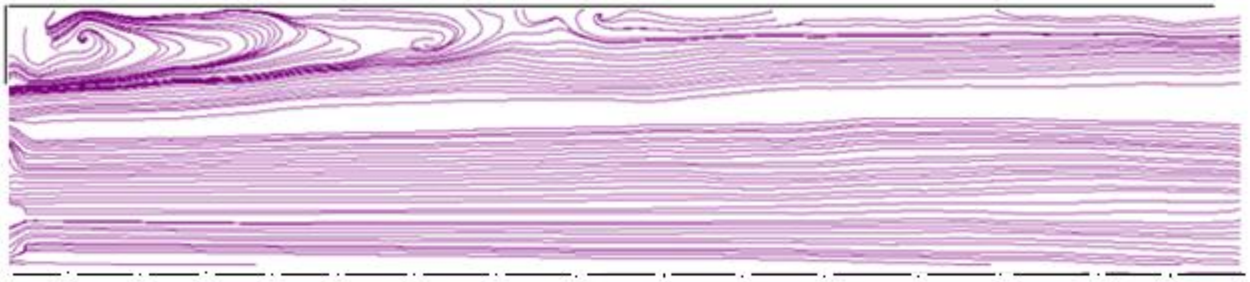

a) Without DRP

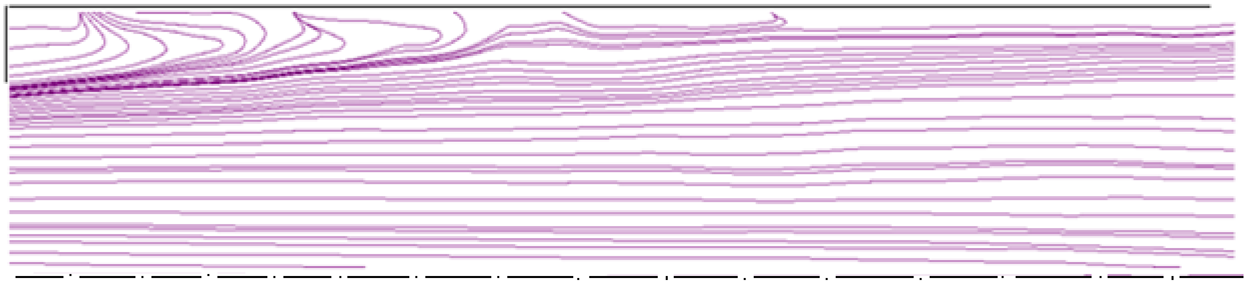

b) With DRP

Figure 4-72 Comparison of streamline patterns in the downstream of second orifice in double orifice arrangement with 1D spacing at Re=5958, D_r=0.63; a) Without DRP, b) With 80 ppm DRP

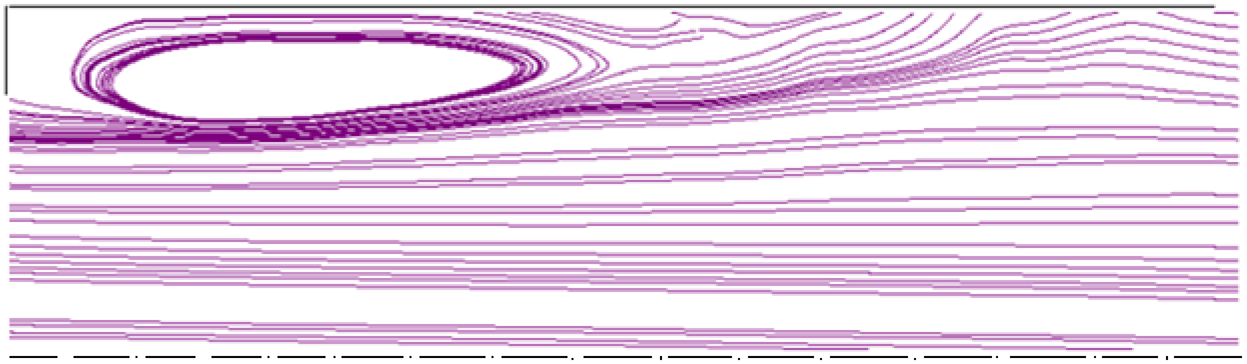

a) **Without DRPs**

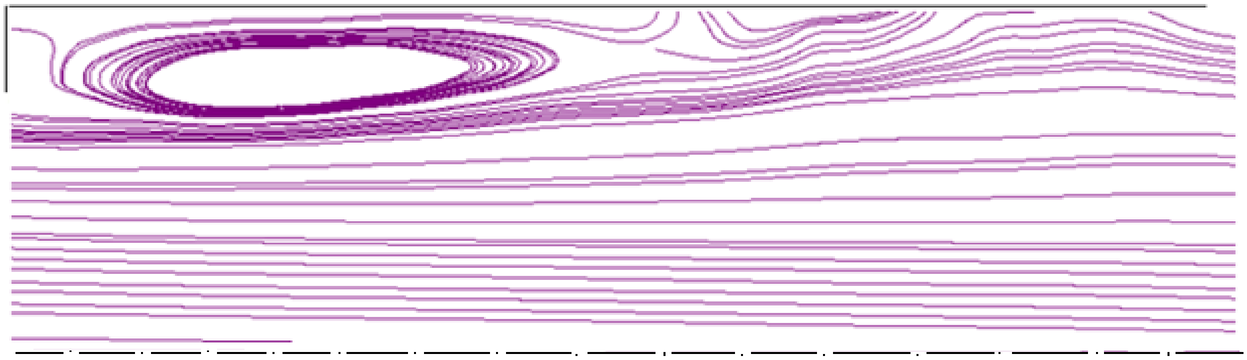

b) **With DRP**

Figure 4-73 Comparison of streamline patterns in the spacing between two orifices in double orifice arrangement with 2D spacing at Re=5958, D_r=0.63; a) Without DRP, b) With 80 ppm DRP

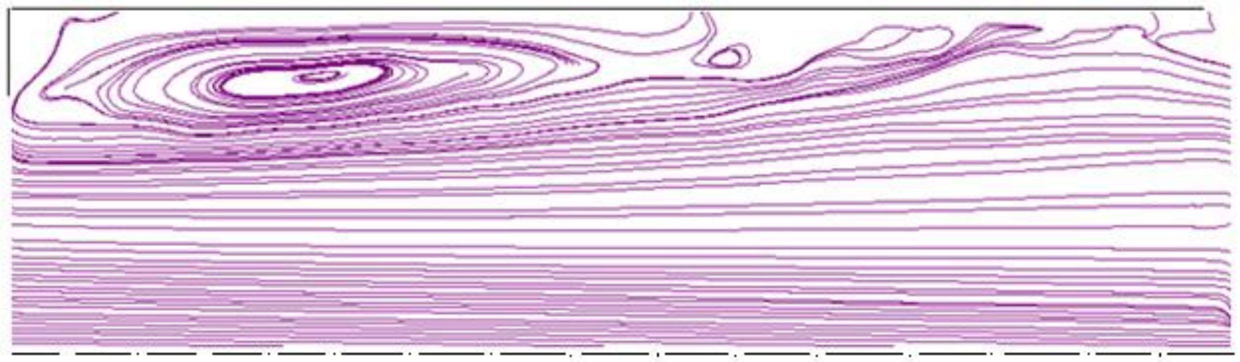

a) Without DRP

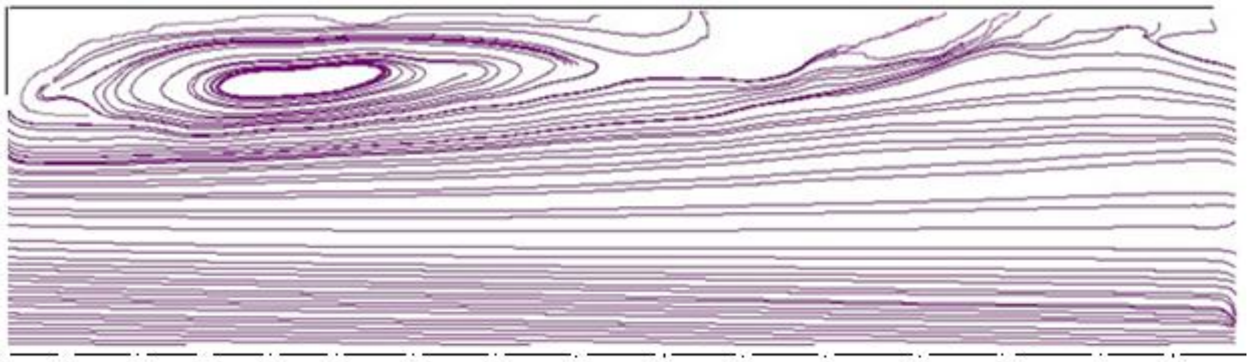

b) With DRP

Figure 4-74 Comparison of streamline patterns in the downstream of second orifice in double orifice arrangement with 2D spacing at Re=5958, D_r=0.63; a) Without DRP, b) With 80 ppm DRP

4.4. Velocity Profile

4.4.1. Re=3972

The axial velocity profiles determined at three different positions downstream of the orifice plate (x=0.5D, x=0.8D, and x=1.2D) for a single orifice with diameter ratio 0.63 at Reynolds number=3972 for flows with and without drag reducing polymer are shown in Figure 4-75. The ordinate and abscissa in the figure shows normalized axial velocity and normalized radial distance respectively. The maximum velocity in case of polymeric solution is less than non-polymeric solution. Both profiles show their maximum velocities at first axial location (x=0.5D) at the center of the pipe with a uniform velocity distribution up to radial distance of 0.2D. Then a rapid decrease of velocity occurs until reaching flow reversal near the wall. The flow reversal in case of polymeric solution is less than in non-polymeric solution. The flow reversal happens in the primary recirculation region near the wall behind the orifice as shown in Figure 4-63. As the recirculation zone in case of polymeric solution is lesser than in non-polymeric solution, hence the negative velocity is also less in polymeric solution. The velocity gradient in both the case is almost same. Similar kind of trend is observed at second (x=0.8D) and third (x=1.2D) axial locations. However the second axial location shows lower center line axial velocity than first location with smaller region of flow reversal. The third location shows smaller maximum velocity in the centerline with smaller reverse flow region and smaller velocity gradient at the orifice height. This means that flow is now getting the pipe flow characteristics as it is moving away from the orifice.

The axial velocity profiles for the same case through single orifice with diameter ratio 0.5 are presented in Figure 4-76. Here also the polymeric solution experiences smaller maximum velocities than non-polymeric solutions. Also the profiles are almost similar as that of 0.63 diameter ratio orifice. However the uniform velocity distribution at first axial location is much smaller than shown in Figure 4-75(a). The velocity gradient is higher in case of non-polymeric solution than in polymeric solution. Also reverse flow region is greater in non-polymeric solution than in polymeric solution.

The velocity profiles at three different axial locations (x=0.4D, x=0.5D, and x=1.2D) in the 1D spacing of double orifice configuration of D_r=0.63 at same Reynolds number for flow with and without drag reducing polymer are shown in Figure 4-77. It is shown in the figure that the centerline velocity is almost same at three locations representing small deceleration in the streamwise direction. The flow with drag reducing polymer shows relatively less peak velocity than flow without drag reducing polymer but the overall velocity profiles are almost the same. The axial velocity profiles determined at three different positions (x=0.5D, x=0.8D, and x=1.2D) downstream of the second orifice plate for same orifice configuration are shown in Figure 4-78. The flow with drag reducing polymer shows comparatively less peak velocity and velocity gradient than flow without drag reducing polymer.

The velocity profiles at the same axial locations (x=0.4D, x=0.5D, and x=1.2D) in the 2D spacing of double orifice configuration of D_r=0.63 at same Reynolds number for flow with and without drag reducing polymer are shown in Figure 4-79. Although flow with drag reducing polymer shows lesser peak velocities and recirculation zones than flow without drag reducing polymer but the overall profiles are quite similar. Similar kind of behavior of drag reducing polymer is observed downstream of the second orifice at three axial locations (x=0.5D, x=0.8D, and x=1.2D) as presented in Figure 4-80.

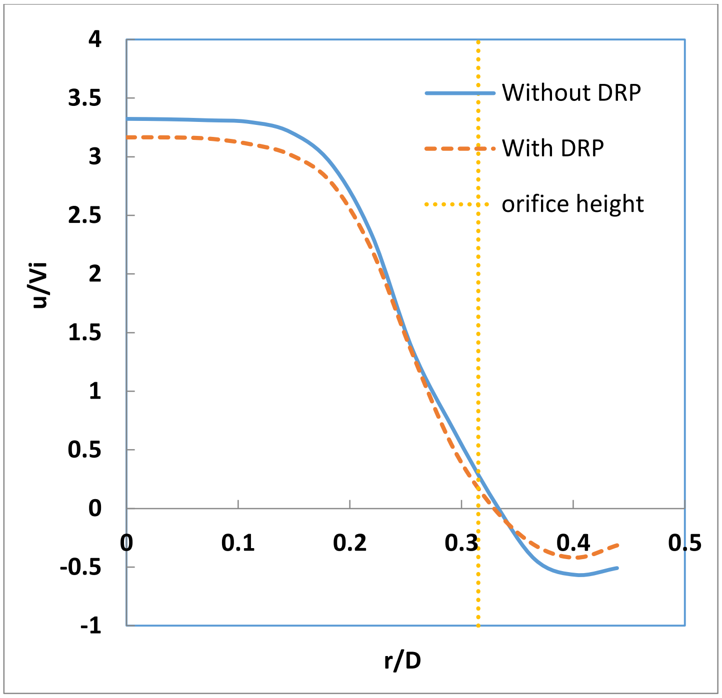
4
3.5
3
2.5
2
1.5
1
0.5
0
-0.5
-1
u/Vi
0
0.1
0.2
0.3
0.4
0.5
r/D
Without DRP
With DRP
orifice height

a) x= 0.5D

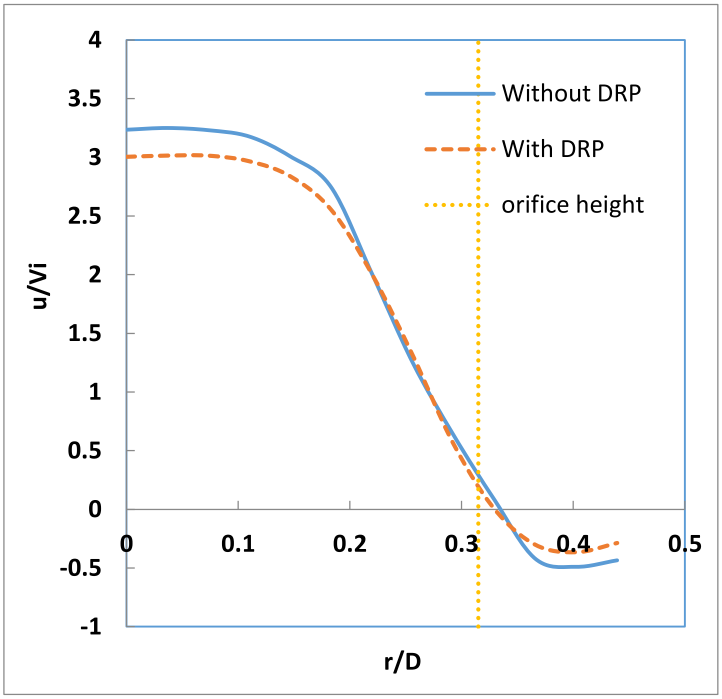
4
3.5
3
2.5
2
1.5
1
0.5
0
-0.5
-1
u/Vi
0
0.1
0.2
0.3
0.4
0.5
r/D
Without DRP
With DRP
orifice height

b) x=0.8D

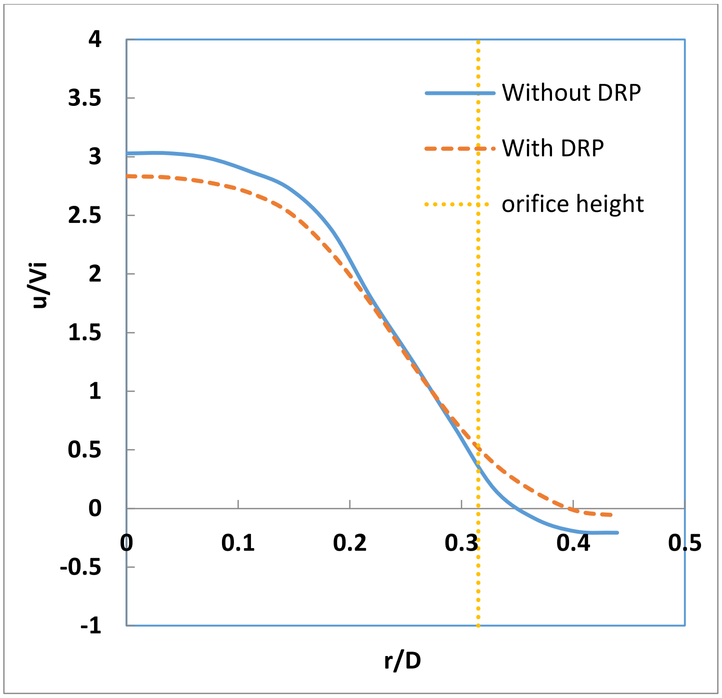

c) x=1.2D

Figure 4-75 Comparison of velocity profiles for single orifice at Re=3972 and 119ppm DRP, D_r=0.63; a) x=0.5D, b) x=0.8D, c) x=1.2D

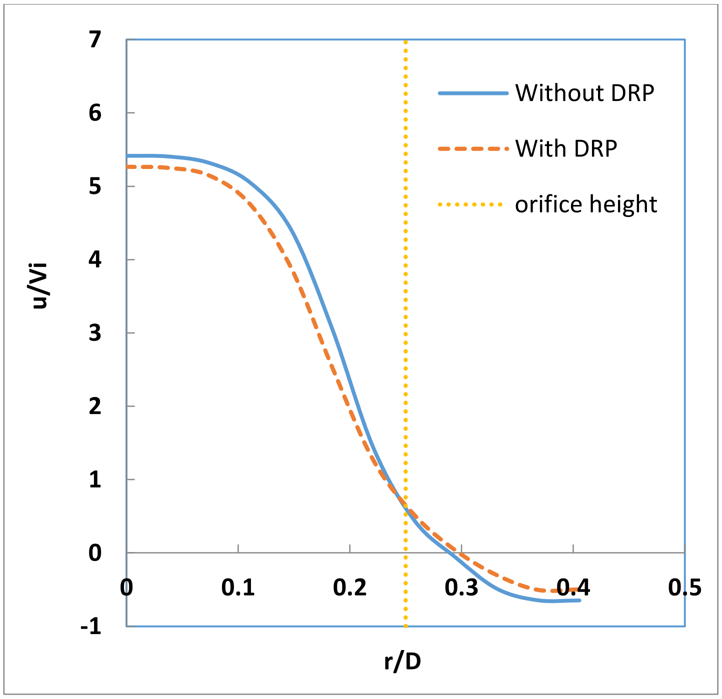

a) x=0.5D

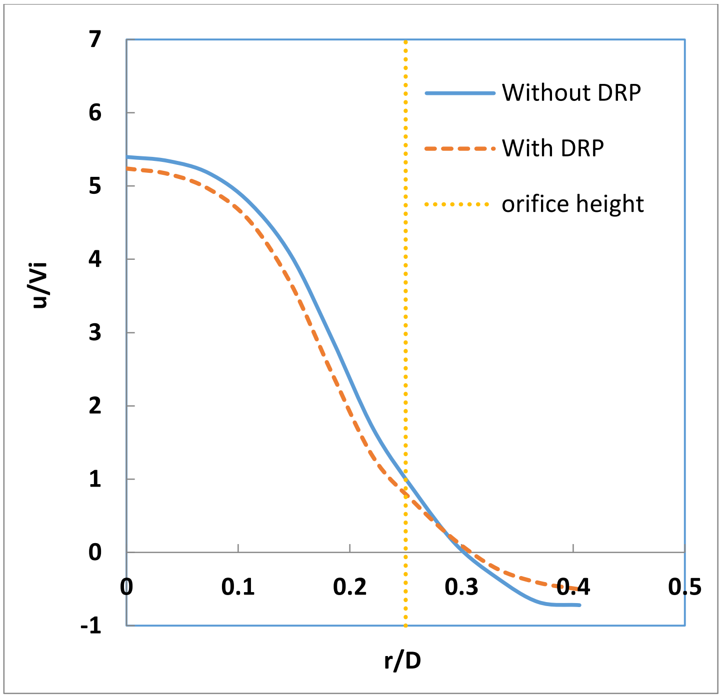

b) x=0.8D

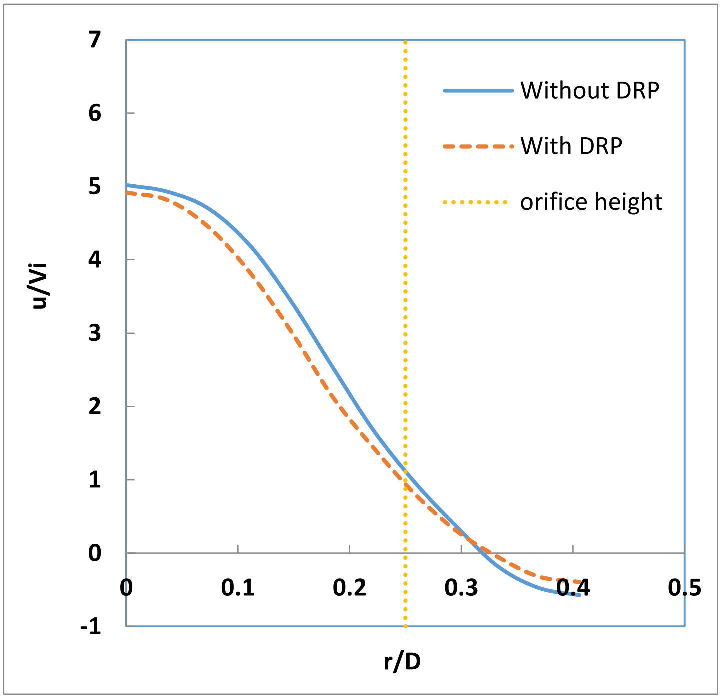

c) x=1.2D

Figure 4-76 Comparison of velocity profiles for single orifice at Re=3972 and 119ppm DRP, D_r=0.5; a) x=0.5D, b) x=0.8D, c) x=1.2D

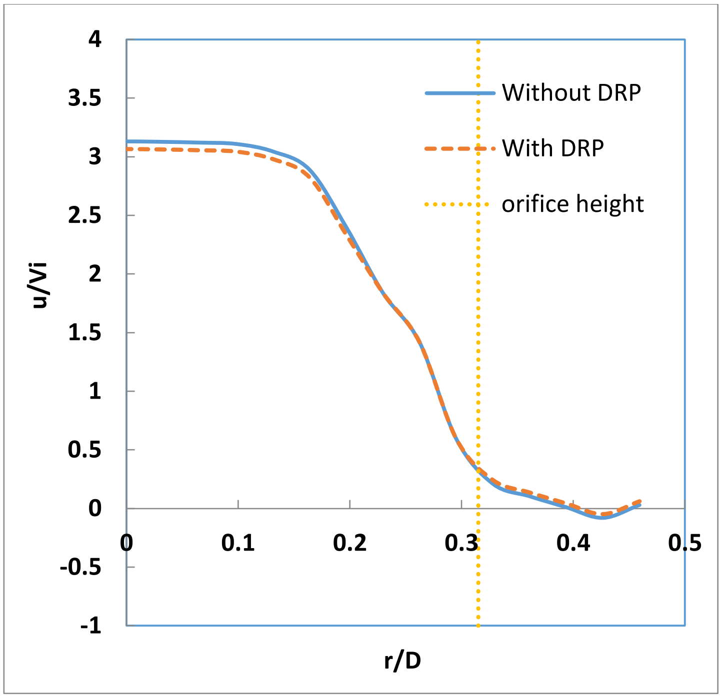

u/Vi
4
3.5
3
2.5
2
1.5
1
0.5
0
-0.5
-1
0
0.1
0.2
0.3
0.4
0.5
r/D
Without DRP
With DRP
orifice height

a) x=0.4D

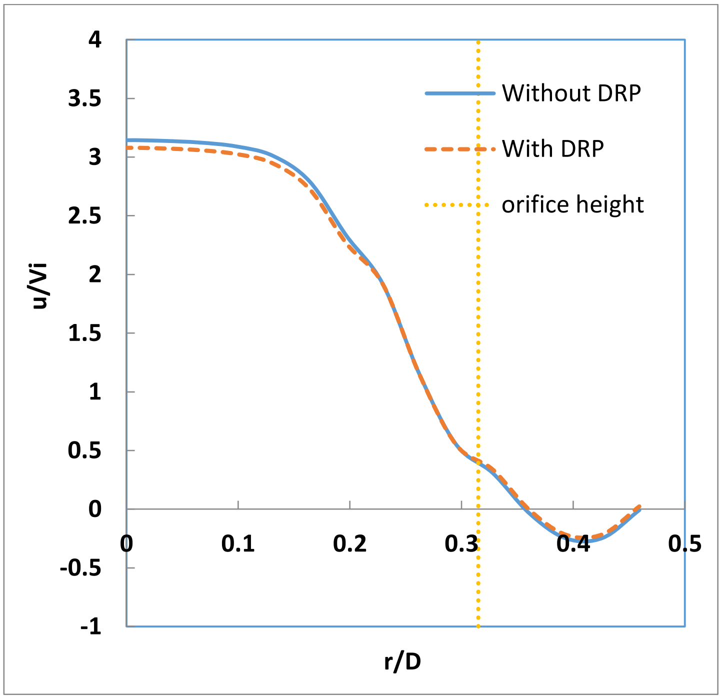

u/Vi
4
3.5
3
2.5
2
1.5
1
0.5
0
-0.5
-1
0
0.1
0.2
0.3
0.4
0.5
r/D
Without DRP
With DRP
orifice height

b) x=0.5D

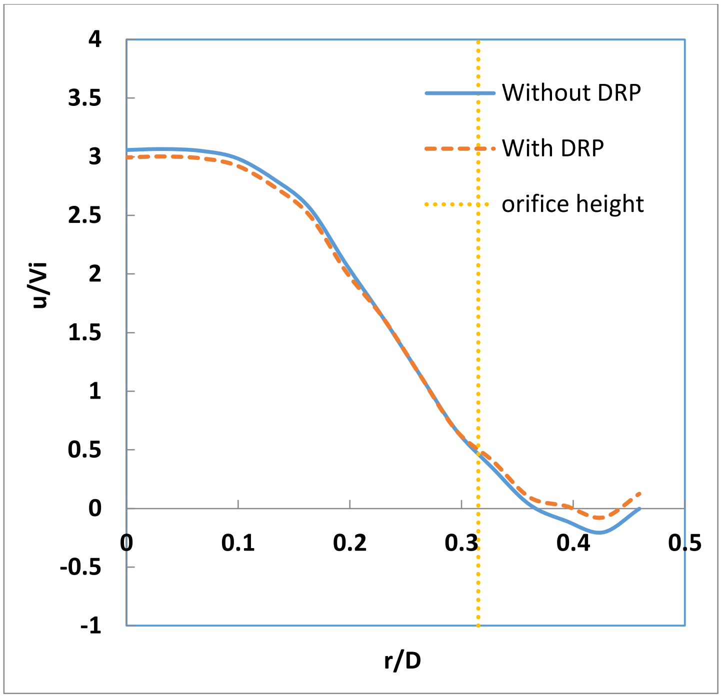

c) x=0.8D

Figure 4-77 Comparison of velocity profiles in the orifice spacing of double orifice arrangement with 1D spacing at Re=3972 and 119ppm DRP, D_r=0.63; a) x=0.4D, b) x=0.5D, c) x=0.8D

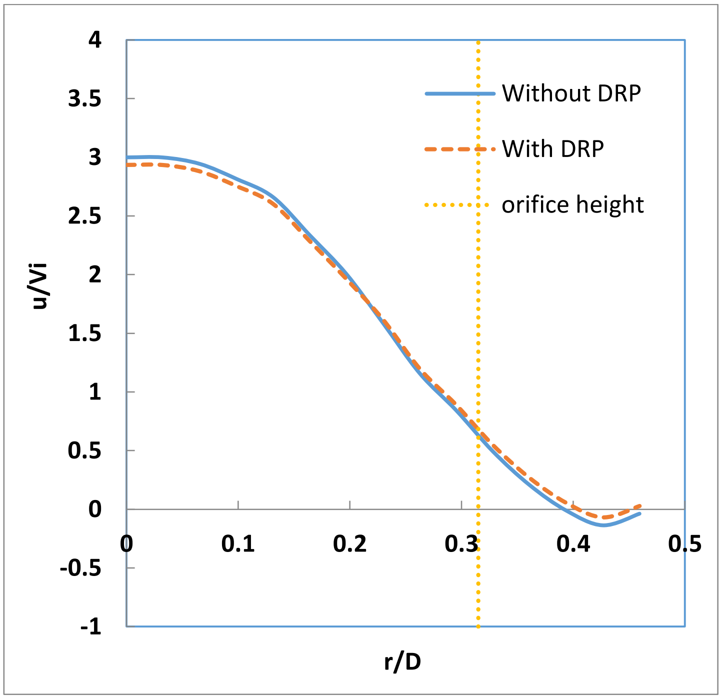

a) x=0.5D

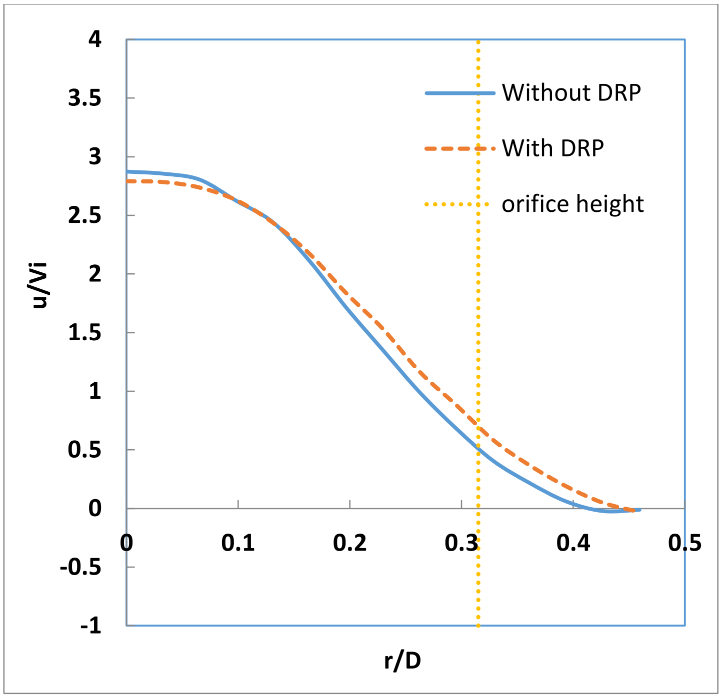

b) x=0.8D

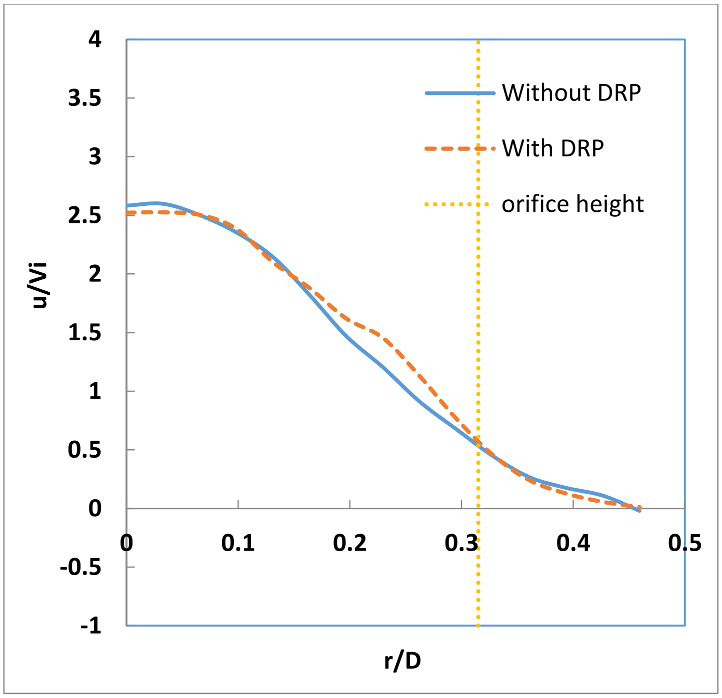

c) x=1.2D

Figure 4-78 Comparison of velocity profiles in the downstream of second orifice of double orifice arrangement with 1D spacing at Re=3972 and 119ppm DRP, D_r=0.63; a) x=0.5D, b) x=0.8D, c) x=1.2D

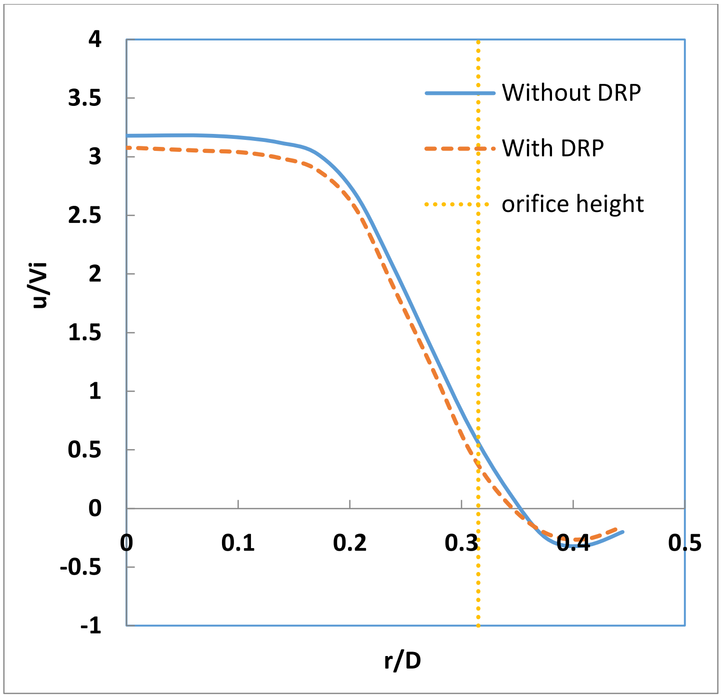
4
3.5
3
2.5
2
1.5
1
0.5
0
-0.5
-1
u/Vi
0
0.1
0.2
0.3
0.4
0.5
r/D
Without DRP
With DRP
orifice height

a) x=0.4D

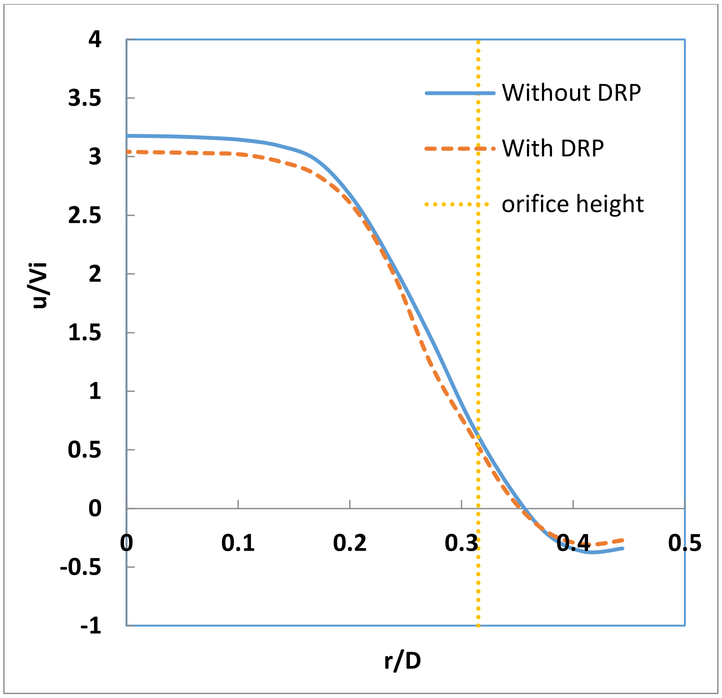
4
3.5
3
2.5
2
1.5
1
0.5
0
-0.5
-1
u/Vi
0
0.1
0.2
0.3
0.4
0.5
r/D
Without DRP
With DRP
orifice height

b) x=0.5D

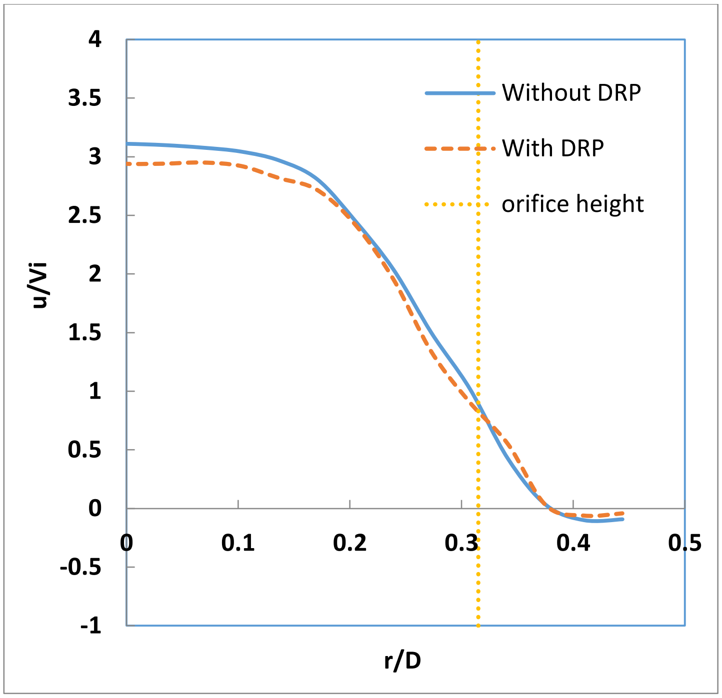

c) x=0.8D

Figure 4-79 Comparison of velocity profiles in the orifice spacing of double orifice arrangement with 2D spacing at Re=3972 and 119ppm DRP, D_r=0.63; a) x=0.4D, b) x=0.5D, c) x=0.8D

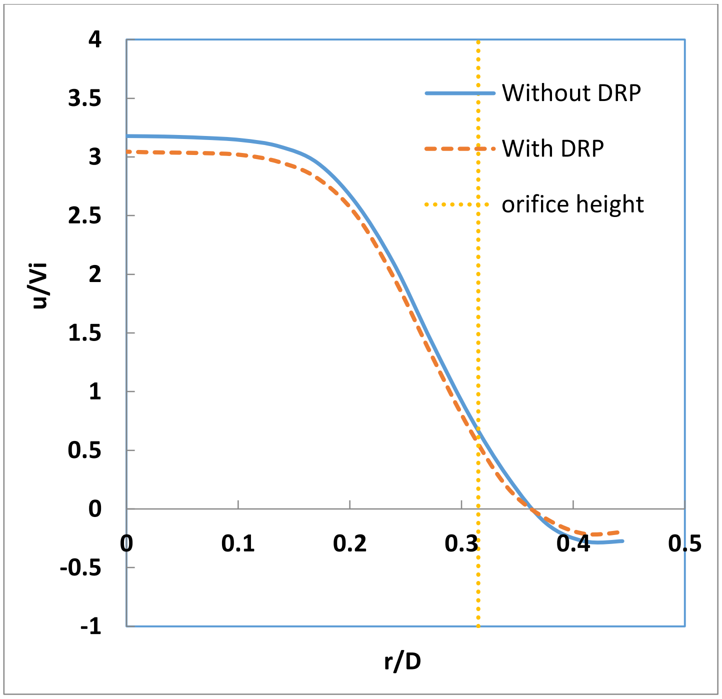

a) x=0.5D

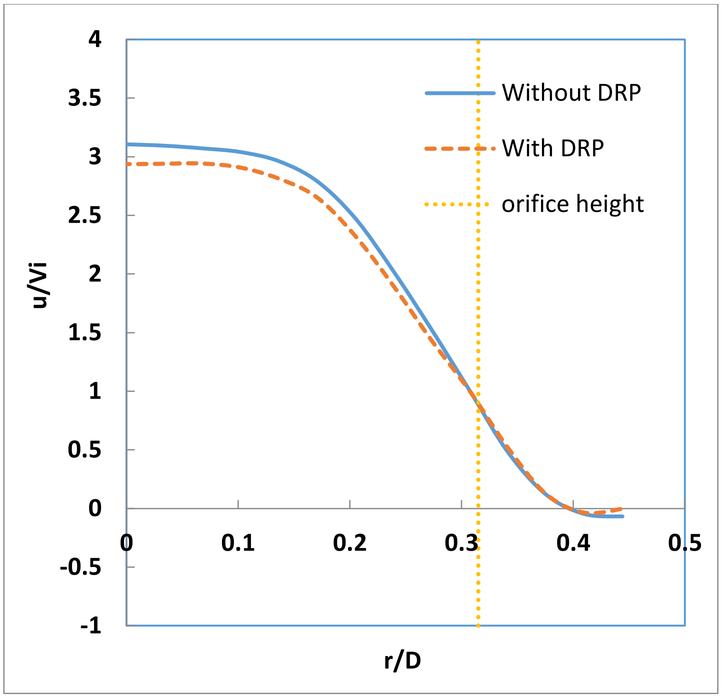

b) x=0.8D

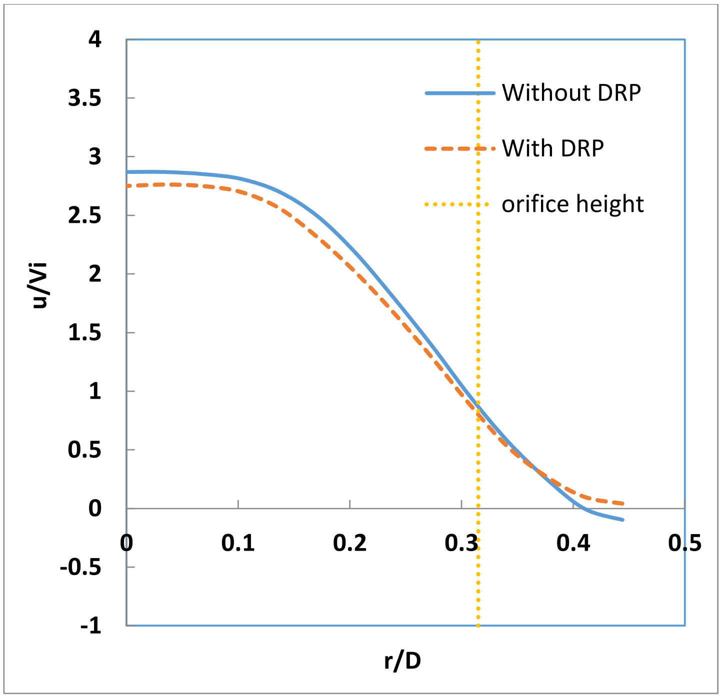

c) x=1.2D

Figure 4-80 Comparison of velocity profiles in the downstream of second orifice of double orifice arrangement with 2D spacing at Re=3972 and 119ppm DRP, D_r=0.63; a) x=0.5D, b) x=0.8D, c) x=1.2D

4.4.2. Re=5958

The axial velocity profiles determined at three different positions downstream of the orifice plate (x=0.5D, x=0.8D, and x=1.2D) for a single orifice with diameter ratio 0.63 at Re=5958 for flows with and without drag reducing polymer are shown in Figure 4-81. The profiles for two different flows are almost same at first axial location. At second axial location, the flow with drag reducing polymer shows a little less reverse flow than flow without drag reducing polymer. Similar trend is observed at third axial location.

Figure 4-82 shows the axial velocity profiles at same axial locations behind the single orifice at same Reynolds number for orifice plate having diameter ratio 0.5 with and without drag reducing polymer. The velocity profiles for the two cases are same at first and second axial locations. However the velocity values are lesser for polymeric solution as we move further downstream at the third axial location.

The velocity profiles at three different axial locations (x=0.4D, x=0.5D, and x=1.2D) in the 1D spacing of double orifice configuration of D_r=0.63 at same Reynolds number for flow with and without drag reducing polymer are shown in Figure 4-83. Flow with drag reducing polymer shows similar velocity profiles as that of flow without drag reducing polymer. The axial velocity profiles determined at three different positions (x=0.5D, x=0.8D, and x=1.2D) downstream of the second orifice plate for same orifice configuration at same Reynolds number are shown in Figure 4-84. At first axial location (x=0.5D), the peak velocities for the two cases are almost similar but the reverse velocity region is higher in case of flow without drag reducing polymer. At second axial location (x=0.8D), non-polymeric solution shows higher velocity gradient than polymeric solution. This difference decreases as we move away from the orifice plate at the third axial location (x=1.2D).

Figure 4-85 shows the velocity profiles at three different axial locations (x=0.4D, x=0.5D, and x=1.2D) in the 2D spacing of double orifice configuration of D_r=0.63 at same Reynolds number while Figure 4-86 shows the velocity profiles at three axial locations (x=0.5D, x=0.8D, and x=1.2D) behind the second orifice in the same orifice configuration and same Reynolds number for flow with and without drag reducing polymer. The flows with and without drag reducing polymer shows the similar velocity profiles behind first and second orifice at the corresponding locations.

We can conclude that drag reducing polymer has a unique effect on the flow behavior in each case. Their effect on flow characteristics is more prominent at lower Reynolds number flows. In short, influence of drag reducing polymer should be investigated separately in each case.

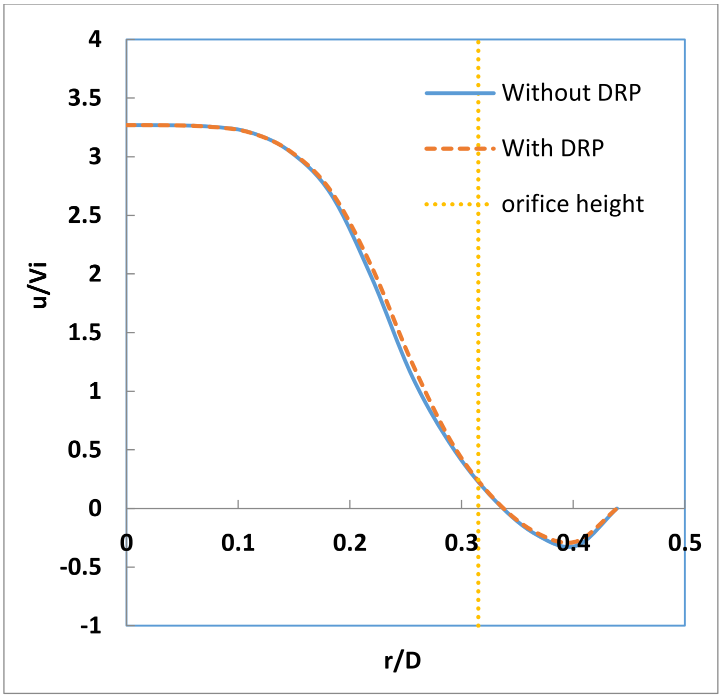
4
3.5
3
2.5
2
1.5
1
0.5
0
-0.5
-1
u/Vi
0
0.1
0.2
0.3
0.4
0.5
r/D
Without DRP
With DRP
orifice height

a) x=0.5D

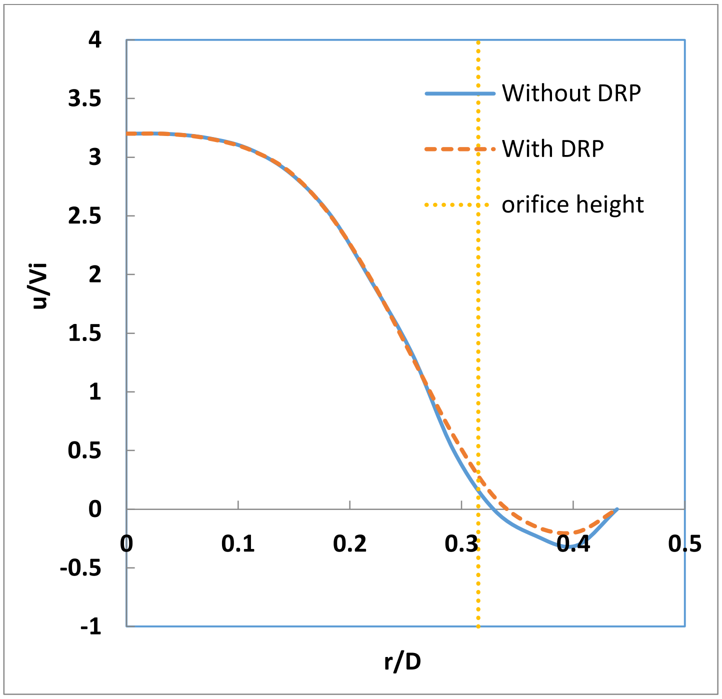
4
3.5
3
2.5
2
1.5
1
0.5
0
-0.5
-1
u/Vi
0
0.1
0.2
0.3
0.4
0.5
r/D
Without DRP
With DRP
orifice height

b) x=0.8D

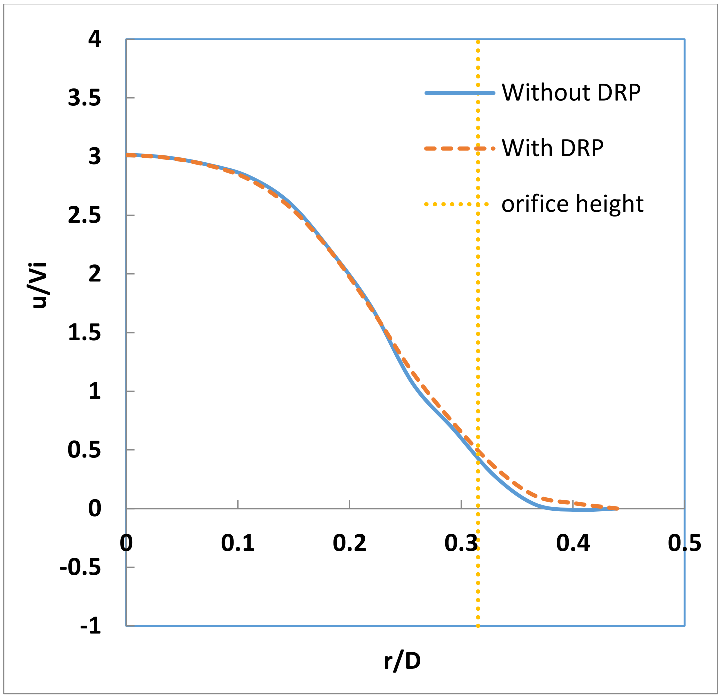

c) x=1.2D

Figure 4-81 Comparison of velocity profiles for single orifice at Re=5958 and 80ppm DRP, D_r=0.63; a) x=0.5D, b) x=0.8D, c) x=1.2D

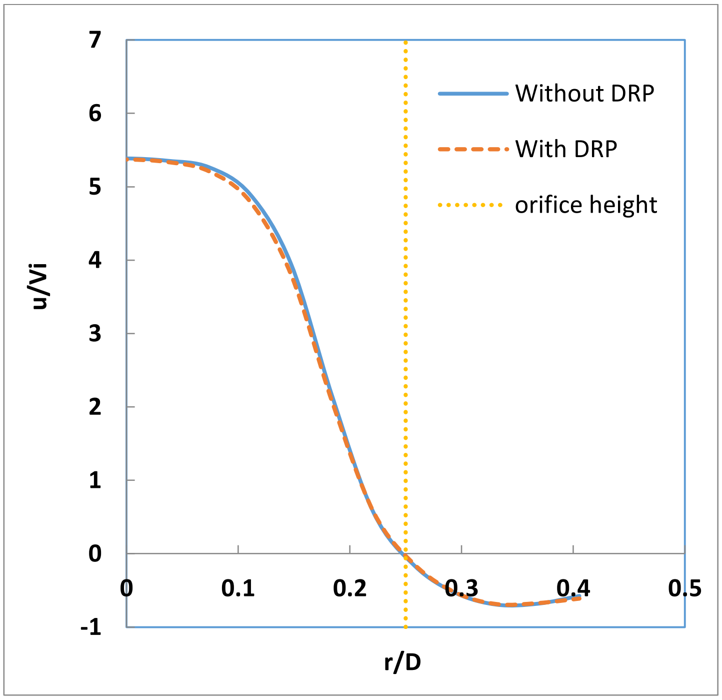

a) x=0.5D

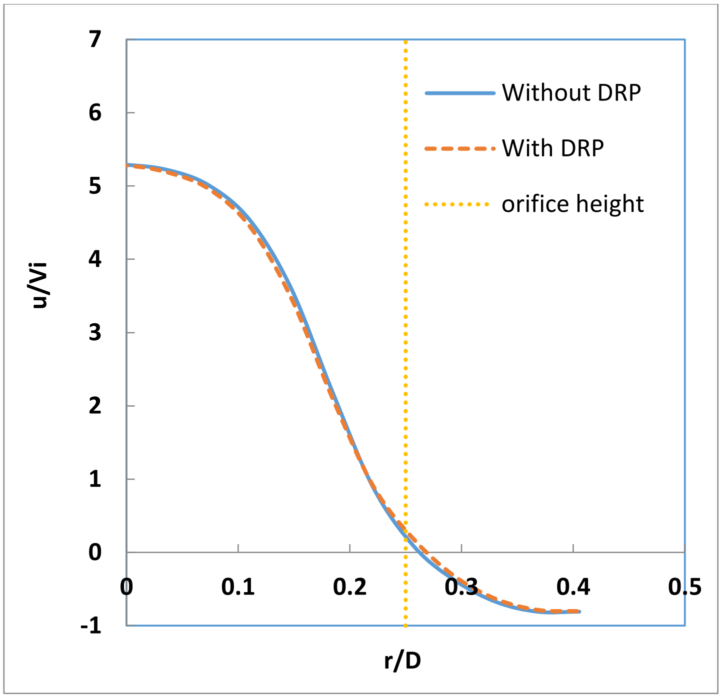

b) x=0.8D

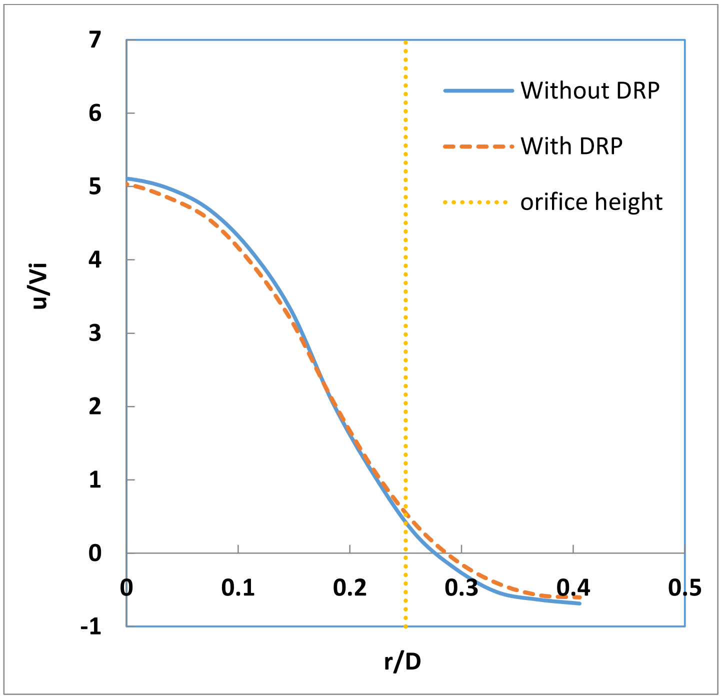

c) x=1.2D

Figure 4-82 Comparison of velocity profiles for single orifice at Re=5958 and 80ppm DRP, D_r=0.5; a) x=0.5D, b) x=0.8D, c) x=1.2D

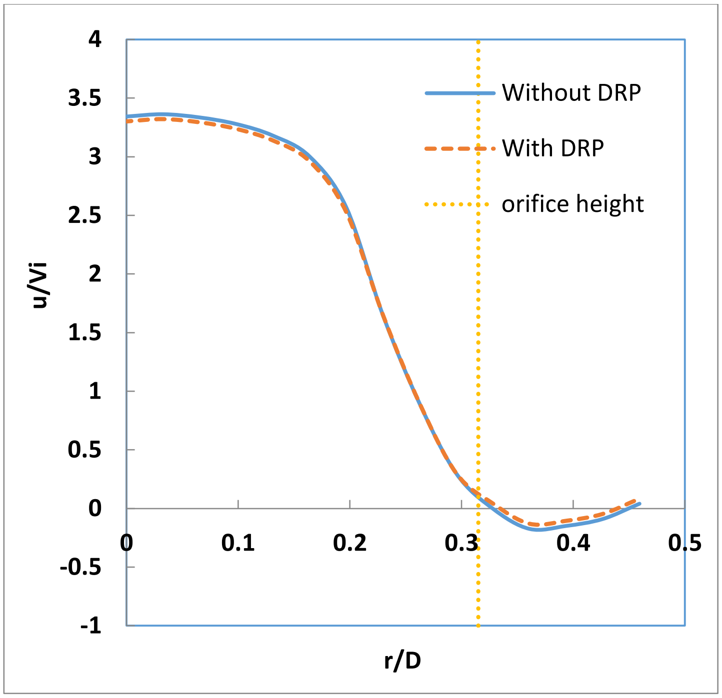
u/Vi
4
3.5
3
2.5
2
1.5
1
0.5
0
-0.5
-1
0
0.1
0.2
0.3
0.4
0.5
r/D
Without DRP
With DRP
orifice height

a) x=0.4D

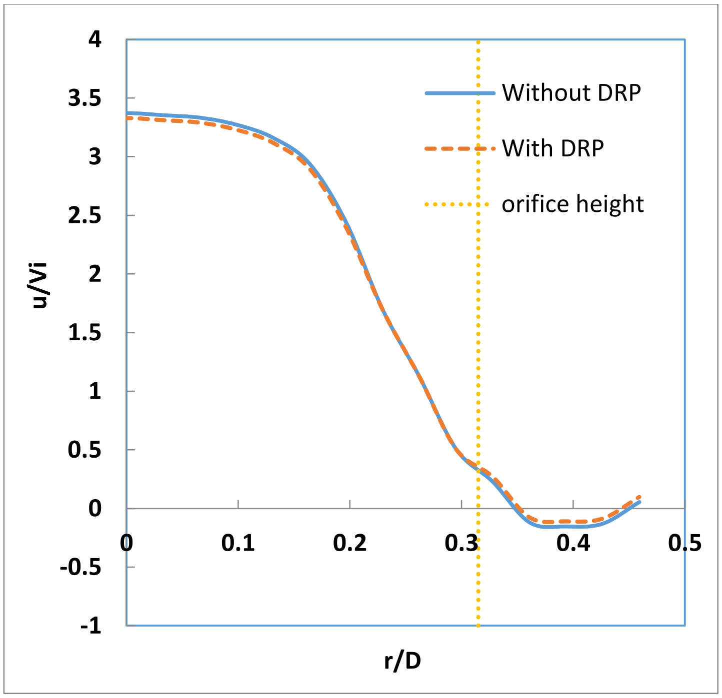
u/Vi
4
3.5
3
2.5
2
1.5
1
0.5
0
-0.5
-1
0
0.1
0.2
0.3
0.4
0.5
r/D
Without DRP
With DRP
orifice height

b) x=0.5D

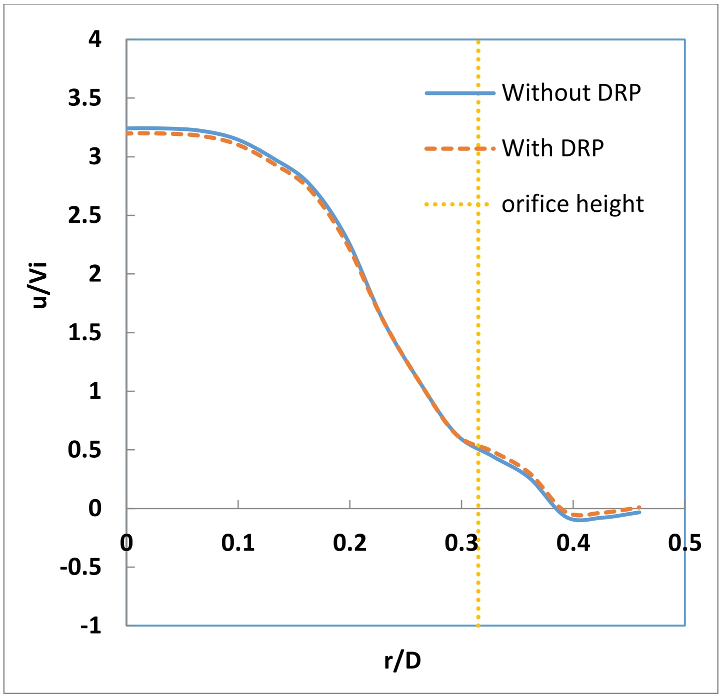

c) x=0.8D

Figure 4-83 Comparison of velocity profiles in the orifice spacing of double orifice arrangement with 1D spacing at Re=5958 and 80ppm DRP, D_r=0.63; a) x=0.4D, b) x=0.5D, c) x=0.8D

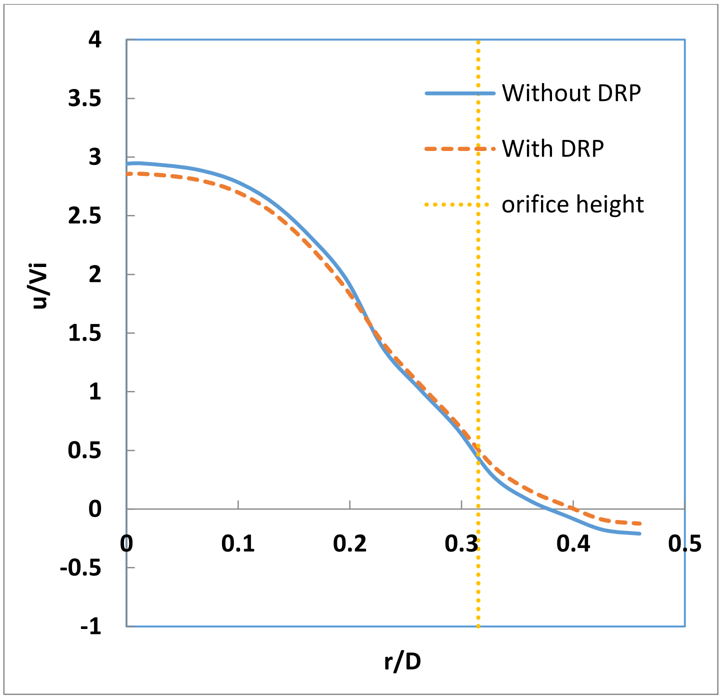

a) x=0.5D

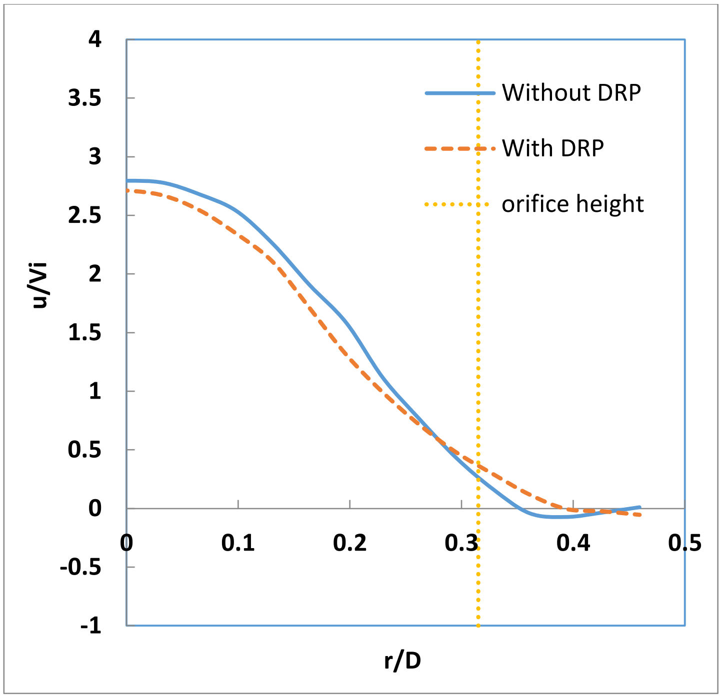

b) x=0.8D

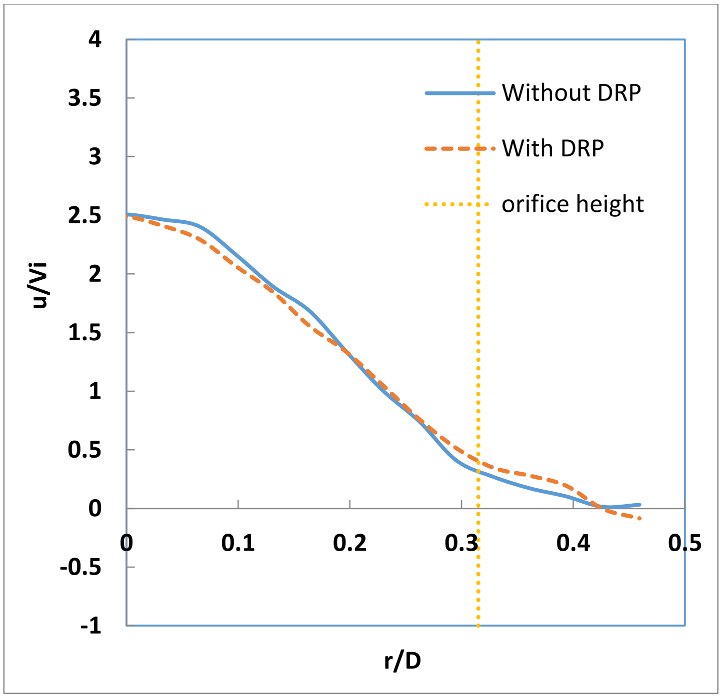

c) x=1.2D

Figure 4-84 Comparison of velocity profiles in the downstream of second orifice of double orifice arrangement with 1D spacing at Re=5958 and 80ppm DRP, D_r=0.63; a) x=0.5D, b) x=0.8D, c) x=1.2D

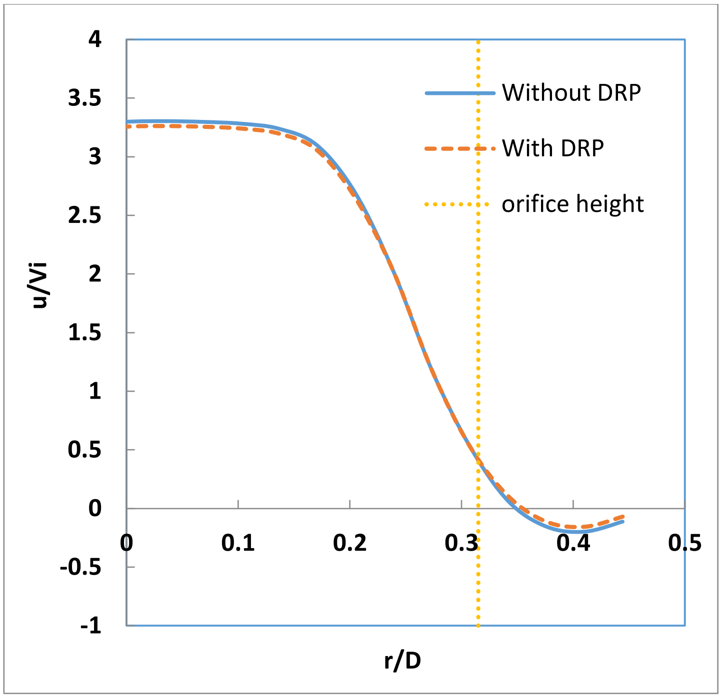
4
3.5
3
2.5
2
1.5
1
0.5
0
-0.5
-1
u/Vi
0
0.1
0.2
0.3
0.4
0.5
r/D
Without DRP
With DRP
orifice height

a) x=0.4D

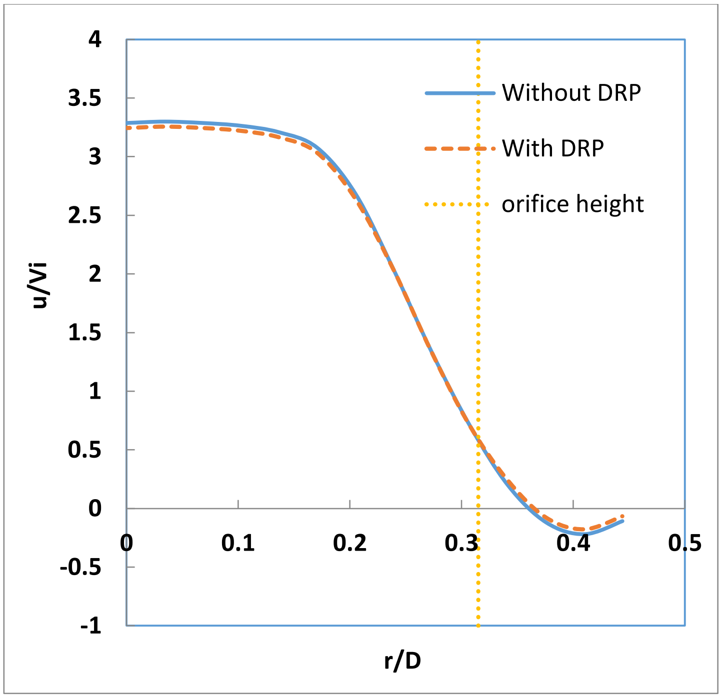
4
3.5
3
2.5
2
1.5
1
0.5
0
-0.5
-1
u/Vi
0
0.1
0.2
0.3
0.4
0.5
r/D
Without DRP
With DRP
orifice height

b) x=0.5D

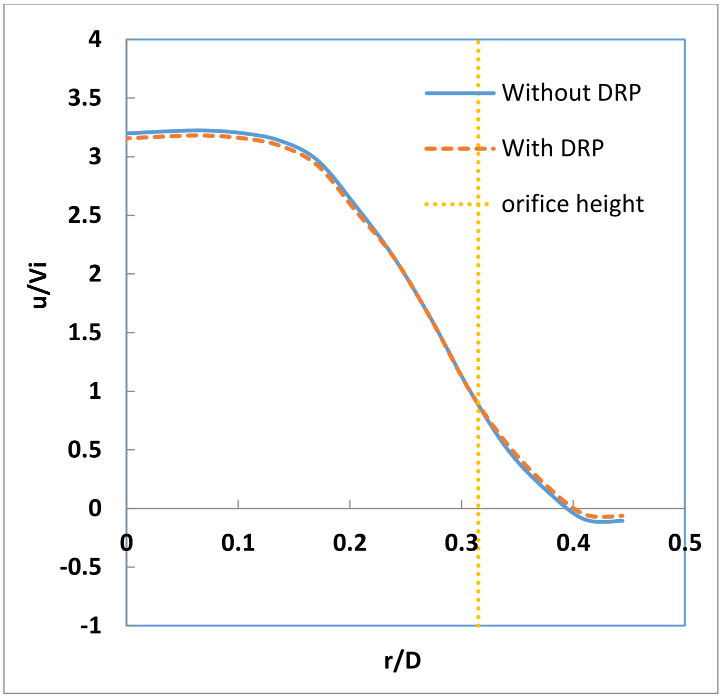

c) x=0.8D

Figure 4-85 Comparison of velocity profiles in the orifice spacing of double orifice arrangement with 2D spacing at Re=5958 and 80ppm DRP, D_r=0.63; a) x=0.4D, b) x=0.5D, c) x=0.8D

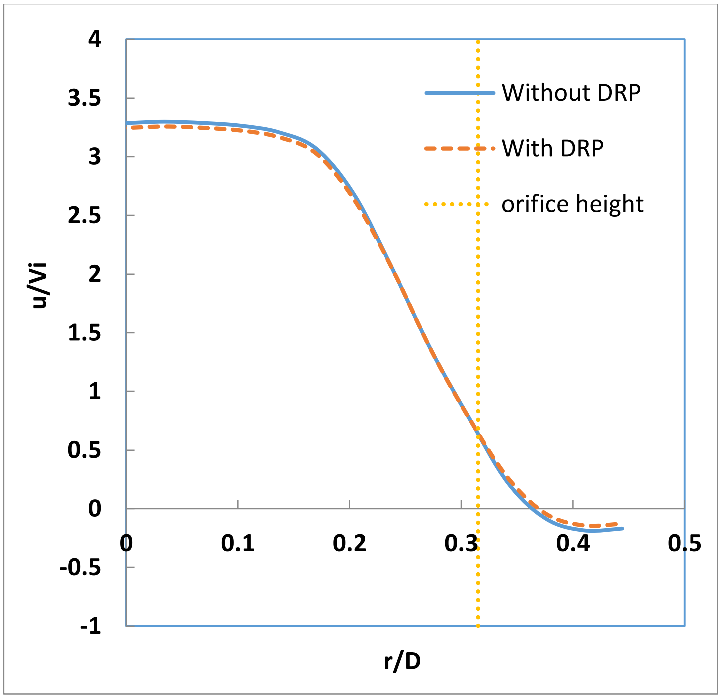

a) x=0.5D

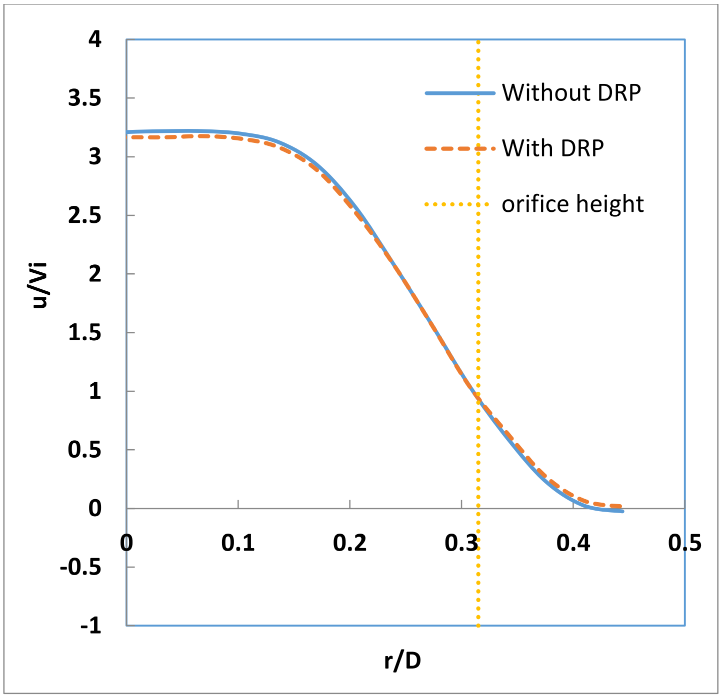

b) x=0.8D

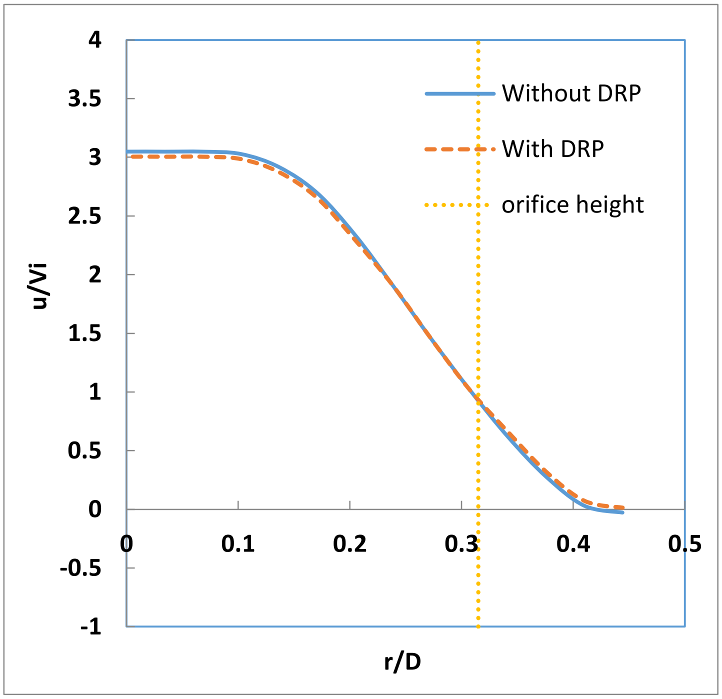

c) x=1.2D

Figure 4-86 Comparison of velocity profiles in the downstream of second orifice of double orifice arrangement with 2D spacing at Re=5958 and 80ppm DRP, D_r=0.63; a) x=0.5D, b) x=0.8D, c) x=1.2D

CHAPTER 5

CONCLUSIONS AND FUTURE RECOMMENDATIONS

5.1. Conclusions

The effect of drag reducing polymer (DRP) on flow characteristics in multiple orifice system has been examined experimentally by considering the effect of inlet flow velocity, orifice geometry, orifice spacing and concentration of DRP on the resulting flow structure. The Reynolds number 2300 to 12000 (based on average flow velocity), orifice spacing of one and two pipe diameter, orifice diameter ratios of 0.5 and 0.63 at different concentration of drag reducing polymer were considered. The water-soluble drag reducing polymer (DRP) used was ZETAG® 8165 which is a synthetic high molecular weight polyacrylamide. Pressure readings were taken with the help of piezometer tubes. Pressure drops for the case of flow with drag reducing polymers were less than the pressure drops in case of flow without drag reducing polymers. The percentage reduction in pressure drop was more in low Reynolds number flows than high Reynolds number flows. Two phase (air-water) flow was also studied for the case of 0.63 diameter ratio orifice and slight drag reduction was also observed in this case. Flow measurements and visualization were carried for the respective three orifice arrangements with Particle Image Velocimetry (PIV) technique. It was found that the recirculation zones were smaller in polymeric solutions than non-polymeric solution at low Reynolds number, similarly velocity values in polymeric solution were less than corresponding values in non-polymeric solutions. It is believed that addition of drag reducing polymer at low Reynolds number flows results in the suppression of Turbulent eddies and Reynolds stress behind the orifice.

5.2. Future Recommendations

The present study revealed that there are many characteristics of flow with drag reducing agents through orifice plates which need further detailed investigation. Other type of drag reducing agents like PEG (polyethylene glycol), and surfactants etc. should be studied and their behavior should be compared with flows without drag reducing agents through orifice. Also, in order to have accurate pressure readings especially for two-phase system, pressure transducers should be installed. Furthermore, time box and synchronizer can be added to the current PIV setup to get more accurate recordings.

REFERENCES

[1] B. Toms, "Some Observation on the Flow of linear Polymer Solutions Through Straight," in *Proc. First Intern. Congr. on Rheology*, 1948.

[2] [Online]. Available: http://flo-quest.com/activeingr.php.

[3] D.Chisolm, "Two-phase flow in Pipelines and Heat Exchangers," *Longman Group Edition, London,* 1983.

[4] S. K. Mammatha K. Roul, "Single-Phase and Two-Phase Flow through thin and thick orifices in horizontal pipes," *Journal of Fluids Engineering,* vol. 134, September 2012.

[5] R. C. Baker, Flow Measurement Handbook: Industrial Designs, Operating Principles,Performance and Applications, Cambridge University Press, Sep 29, 2005.

[6] O. Baker, "Simultaneous Flow of Oil and Gas," *Oil and Gas J.,* no. 53, p. 185, 1954.

[7] J.M.Mandhane, G.A.Gregory and A. Aziz, "A Flow Pattern Map for Gas-Liquid flowing horizontal pipes.," *Int. J. Multphase Flow,* no. 1, pp. 537 -553, 1974.

[8] Y. Taitel and A.E.Dukler, "A Model for Predicting Flow Regime Transitions in Horizontal and Near Horizontal Gas-Liquid Flow," *AIChE J,* no. 22, pp. 47-55, 1976.

[9] P.Y.Lin and T. Hanratty, "Effect of Pipe Diameter on Flow Patterns for air-water flow in Horizontal Pipes," *Int. J. Multiphase Flow,* no. 13, pp. 549-563, 1987.

[10] W. Jepson and R. Taylor, "Slug Flow and Its Transition in Large Diameter Horizontal Pipes," *Int. J. Multphase Flow,* vol. 19, no. 3, pp. 411-420, 1993.

[11] E. J. Greskovich and A. L. Shrier, "Drag reduction in two-phase flow," *Industrial & Engineering Chemistry Fundamentals,* vol. 10, pp. 646-648, 1971.

[12] R. Rosehart, D. Scott and E. Rhodes, " Gas-liqud slug flow with drag-reducing polymer solutions," *AIChE Journal,* vol. 18, pp. 744-750, 1972.

[13] N. D. Sylvester and J. P. Brill, "Drag reduction in two-phase annular-mist flow of air and water," *AIChE Journal,* vol. 22, pp. 615-617, 1976.

[14] A. Al-Sarkhi and T. Hanratty, "Effect of drag-reducing polymers on annular gas–liquid flow in a horizontal pipe," *International journal of multiphase flow,* vol. 27, pp. 1151-1162, 2001.

[15] A. Al-Sarkhi and T. Hanratty, "Effect of pipe diameter on the performance of drag-reducing polymers in annular gas-liquid flows," *Chemical Engineering Research and Design,* vol. 79, pp. 402-408, 2001.

[16] A. Soleimani, A. Al-Sarkhi and T. J. Hanratty, "Effect of drag-reducing polymers on pseudo-slugs—interfacial drag and transition to slug flow," *International journal of multiphase flow,* vol. 28, pp. 1911-1927, 2002.

[17] S. Baik and T. J. Hanratty, "Effects of a drag reducing polymer on stratified gas-liquid flow in a large diameter horizontal pipe," *International journal of multiphase flow,* vol. 29, pp. 1749-1757, 2003.

[18] A. Al-Sarkhi and A. Soleimani, "Effect of drag reducing polymers on two-phase gas–liquid flows in a horizontal pipe," *Chemical Engineering Research and Design,* vol. 82, pp. 1583-1588, 2004.

[19] A. Al-Sarkhi and Abu-Nada, "Effect of drag reducing polymer on annular flow patterns of air and water in a small horizontal pipeline," in *Twelfth International Conference on Multiphase Production Technology*, Barcelona, Spain., 25–27 May 2005.

[20] A. Al-Sarkhi, E. Abu-Nada and M. Batayneh, "Effect of drag reducing polymer on air–water annular flow in an inclined pipe," *International journal of multiphase flow,* vol. 32, pp. 926-934, 2006.

[21] R. Wilkens and D. Thomas, "Multiphase drag reduction: Effect of eliminating slugs," *International journal of multiphase flow,* vol. 33, pp. 134-146, 2007.

[22] R. Fernandes, B. Fleck, T. Heidrick, L. Torres and M. Rodriguez, "Experimental Study of DRA for Vertical Two-Phase Annular Flow," *Journal of energy resources technology* , vol. 131, p. 023002, 2009.

[23] N. Sylvester, R. Dowling and J. Brill, "Drag reduction in cocurrent horizontal natural gas-hexane pipe flow," *Polymer Engineering & Science,* vol. 20, pp. 485-492, 1980.

[24] F. C. Johansen, "Flow through Pipe Orifices at Low Reynolds Numbers," *Proceedings of the Royal Society of London, Series A, Containing Papers of a Mathematical and Physical Character,* vol. 126(801), pp. 231-245, 1930.

[25] F. W. Medaugh and G. D. Johnson, "Investigation of the Discharge and Coefficients of Small Circular Orifices," *Civil Engineering,* vol. 10(7), pp. 422-424, 1940.

[26] S. H. Alvi, K. Sridharan and N. S. Lakshmana Rao, "Loss Characteristics of Orifices and Nozzles," *ASME Journal of Fluids Engineering,* vol. 100(3), pp. 299-307, 1978.

[27] B. Sahin and H. Ceyhan, "Numerical and Experimental Analysis of Laminar Flow through Square-Edged Orifice with Variable Thickness," *Transactions of the Institute of Measurement and Control,* vol. 18(4), pp. 166-174, 1996.

[28] T. Hasegawa, M. Suganuma and H. Watanabe, "Anomaly of Excess Pressure Drops of the Flow through Very Small Orifices," *Physics of Fluids,* vol. 9(1), pp. 1-3, 1997.

[29] G. K. Morris, S. V. Garimella and J. A. Fitzgerald, "Flow-Field Prediction in Submerged and Confined Jet Impingement Using the Reynolds Stress Model," *ASME Journal of Electronic Packaging,* vol. 121(4), pp. 255-262, 1999.

[30] L. M. Mincks, "Pressure Drop Characteristics of Viscous Fluid Flow across Orifices," Ames, 2002.

[31] O. Mustafa, "Flow Characteristics around Orifice using PIV Technique," Adana, 2010.

[32] A. A. Abdulrazaq, "Investigation of Flow and Erosion characteristics through a set of restricting orifices," ME dept, KFUPM, Dhahran, 2015.

[33] S. Martha, C. G. Dionysius and L. Laurence, "Effect of Flow-Obstruction Geometry on Pressure Drops in Horizontal Air-Water flow.," *Int Journal of Multiphase Flow,* vol. 9, no. 1, pp. 73-85, 1983.

[34] H. Zhang, S. Lu and G. Yu, "An Investigation of Two-Phase Flow Measurement with orifices for Low-quality mixtures," *lnt Journal of Multiphase Flow,* vol. 18, no. 1, pp. 149-155, 1991.

[35] M. Fossa and G. Guglielmini, "Pressure drop and void fraction profiles during horizontal flow through thin and thick orifices," *Experimental Thermal and Fluid Science,* vol. 26, p. 513–523, 2002.

[36] S. Arun Kumar, B. Tapan Kumar and D. Sudip Kumar, "Pressure Losses in Orifices for the Flow of Gas-Non-Newtonian Liquids," *The Canadian Journal of Chemical Engineering,* vol. 77, June 1999.

[37] L. G. O. Jorge, J. C. Passos, R. Verschaeren and C. V. D. Geld, "Mass flow rate measurements in gas–liquid flows by means of a venturi or orifice plate coupled to a void fraction sensor," *Experimental Thermal and Fluid Science,* vol. 33, pp. 253-260, 2009.

[38] C. Alimonti, G. Falcone and O. Bello, "Two-phase flow characteristics in multiple orifice valves," *Experimental Thermal and Fluid Science,* vol. 34, p. 1324–1333, 2010.

[39] K. R. Manmatha and S. K. Dash, "Single-Phase and Two-Phase Flow Through Thin and Thick Orifices in Horizontal Pipes," *Journal of Fluids Engineering,* vol. 134, Sep 2012.

[40] S. Nobuyuki, "Loss and Discharge characteristics of a flow of polymer solutions through pipe orifices.," *Bulletin of JSME,* vol. 27, March 1984.

[41] H. Tomiichi, U. Akiomi and N. Takatsune, "Huge reduction in pressure drop of water, glycerol/water mixture, and aqueous solution of polyethylene oxide in high speed flows through micro-orifices," *Physics of Fluids,* vol. 21, 2009.

[42] U. Akiomi, H. Tomiichi and N. Takatsune, "Drag reduction for liquid flow through micro-apertures," *Journal of Non-Newtonian Fluid Mechanics,* vol. 165, p. 1516–1524, 2010.

[43] U. Akiomi, H. Tomiichi, K. Shouta, K. Masato, U. Hiroshige and N. Takatsune, "Flow Properties of Several Types of Liquid Flows through Micro-Orifices," *Journal of Fluid Science and Technology,* vol. 6, 2011.

[44] U. Akiomi, H. Tomiichi, N. Takatsune and N. Toshiyuki, "Flow properties of nanobubble mixtures passing through micro-orifices," *International Journal of Heat and Fluid Flow* , vol. 40, pp. 106-115, 2013.

[45] T. Takahiro, M. Motozawa, D. Tsurumi and Y. Kawaguchi, "PIV and DNS analyses of viscoelastic turbulent flows behind a rectangular orifice," *International Journal of Heat and Fluid Flow,* vol. 41, pp. 66-79, 2003.

[46] M. Al-Yarri, A. Al-Sarkhi, I.A.Hussein and B.Abu-Sharkh, "Effect of Drag Reducing Polymers on surfactant-stabilized water-oil emulsions flow," *Experimental Thermal and Fluid Sciences,* vol. 51, pp. 319-331, Nov 2013.

[47] R. Adrian, "Particle-imaging techniques for experimental fluid mechanics.," *Annu Rev Fluid Mech.,* vol. 23, pp. 261-304, 1991.

[48] M. Raffel, C. Willert, S. Wereley and J.Kompenhans, "Particle Image Velcimetry," *Curr.Sci,* vol. 79, pp. 51-60, 2007.

[49] R. Keane and R. Adrian, "Optimization of particle image velocimeters," *Opt. Methods Flow Particle Diagnostics,* vol. 68, pp. 139-159, 1989.

[50] Y. Agrawal, L.Talbot and K.Gong, "Laser anemometer study of flow development in curved circular pipes," *Journal of Fluid Mechanics,* 2006.

APPENDIX

SINGLE PHASE PRESSURE DROP READINGS

Diameter Ratio: 0.63, Without Polymers													
Reynolds No.		**2383**	**2979**	**3177**	**3972**	**4369**	**5362**	**5957**	**6951**	**7944**	**8937**	**10128**	**11915**
Single orifice	P1(cm)	7.5	12.45	14.8	9.1	10.75	22	17.4	19.4	12.15	16.5	21.5	30.9
	P2(cm)	6.95	11.7	13.85	7.85	9.05	19.5	14.85	14.9	6.55	9	11.8	17.05
	P3(cm)	7.05	11.8	14	8.15	9.55	20.3	15.7	16	8.4	11.55	15.25	21.75
	P4(cm)	6.7	11.4	13.5	7.7	9.2	20	15.45	15.8	8.25	11.75	15.1	21.8
Double orifice (1D)	P1(cm)	6.6	11.1	12.7	19	7.15	11	13.4	19	9.25	12.1	15.7	22.45
	P2(cm)	6.1	10.4	11.85	17.9	5.7	8.75	11	15.4	4.75	6.75	8.1	11.35
	P3(cm)	6.15	10.6	12.05	18.05	6.05	9.5	11.5	16.3	6	7.75	10	14.2
	P4(cm)	5.6	10.05	11.5	17.55	5.7	8.85	11.4	15.9	5.55	7.2	9.7	14
Double orifice (2D)	P1(cm)	11	16.9	18.8	8.8	10.25	16.4	19.45	9.9	13.3	17.25	16	22.6
	P2(cm)	10.2	16.05	17.8	7.35	8.5	13.7	16.5	5.5	7.9	9.4	5.8	8
	P3(cm)	10.35	16.2	18.1	7.55	8.75	14.15	16.9	6	8.05	10	6.7	9.35
	P4(cm)	10.2	15.85	17.7	7.05	8.1	13.55	16.2	5.35	7.3	9.1	5.55	7.6
	P5(cm)	10.35	16	18	7.55	8.9	14.25	17.05	6.15	8.35	10.75	7.75	10.7
	P6(cm)	9.7	15.7	17.2	6.95	8.3	13.85	16.5	5.75	8.15	10.5	7.35	10.45

Diameter Ratio: 0.63, With Polymers													
Reynolds No.		**2383**	**2979**	**3177**	**3972**	**4369**	**5362**	**5957**	**6951**	**7944**	**8937**	**10128**	**11915**
Polymer ppm		**196**	**158**	**148**	**119**	**108**	**89**	**80**	**68**	**60**	**53**	**47**	**40**
Single orifice	P1(cm)	7.3	11.45	7.7	11.5	7.5	11	7.5	10.9	14.7	14.9	15.05	17.7
	P2(cm)	6.8	10.75	6.8	10.4	5.9	8.7	5	6.8	9.4	7.7	5.35	4.4
	P3(cm)	7	10.85	7	10.7	6.4	9.4	5.9	8	11.1	10	8.65	8.75
	P4(cm)	6.7	10.65	6.8	10.6	6.3	9.2	5.8	8.05	11	9.9	8.9	9.1
Double orifice (1D)	P1(cm)	8.05	12.3	14	21.7	7.3	11.4	13.45	9	12	9.15	11.9	16.2
	P2(cm)	7.6	11.75	13.3	20.65	5.95	9.35	11.15	5.4	7.2	3.8	4.3	5.7
	P3(cm)	7.65	11.9	13.5	20.85	6.3	9.95	11.75	6.4	8.6	5	6.2	8.6
	P4(cm)	7.3	11.5	13.2	20.75	6.1	9.45	11.6	6.2	8.4	4.85	6.05	8.4
Double orifice (2D)	P1(cm)	10.9	17.5	8.5	7.6	9.4	9.2	11.4	10.5	15.3	13.3	13.5	18.9
	P2(cm)	10.4	16.7	7.6	6.5	7.9	6.9	8.9	6.7	10	5.8	4.05	5.4
	P3(cm)	10.5	16.8	7.9	6.6	8.1	7.1	9.2	6.8	10.1	5.9	4.3	5.6
	P4(cm)	10.25	16.5	7.5	6.4	7.7	6.7	8.5	6.3	9.4	5.2	3.1	4.9
	P5(cm)	10.4	16.8	7.75	6.7	8.3	7.25	9.3	7.1	10.7	6.9	5.3	7.1
	P6(cm)	9.9	16.6	7.1	6.5	7.8	6.9	9	6.8	10.5	6.7	5.1	6.9

Diameter Ratio: 0.5, Without Polymers													
Reynolds No.		**2383**	**2979**	**3177**	**3972**	**4369**	**5362**	**5957**	**6951**	**7944**	**8937**	**10128**	**11915**
Single orifice	P1(cm)	6.2	9.75	11.85	18.3	23	11.9	14.7	20.95	28.35	36.55	35.1	48.5
	P2(cm)	4.6	7.7	8.85	14.3	17.8	4.65	5.7	8.65	11.45	14.95	6.85	9.95
	P3(cm)	4.8	8.05	9.4	14.9	18.9	6.05	7.5	10.95	14.7	19.25	12.75	18
	P4(cm)	4.3	7.65	8.95	14.65	18.65	5.65	7.2	10.9	15.6	20.45	14.2	20.5
Double orifice (1D)	P1(cm)	7.1	11.3	12.85	21.7	25.8	11.5	13.5	19.8	25.95	22.35	28.75	35.7
	P2(cm)	5.65	9.4	10.7	17.75	21.4	5.8	6.15	9	12	4.5	5.9	2.1
	P3(cm)	5.8	9.75	11.1	18.35	22.1	6.15	7.5	11.05	14.8	8	10.4	8.35
	P4(cm)	5.3	9.3	10.6	17.85	21.9	5.8	7.2	10.7	14.5	7.65	10.05	8.45
Double orifice (2D)	P1(cm)	8.25	12.7	14.6	23.4	11.5	17.1	21	31.05	21.9	27	33.4	45.1
	P2(cm)	6.6	10.6	12.2	19.4	6.15	10	12.5	17.65	5.75	5.3	5.9	7.1
	P3(cm)	6.8	10.85	12.4	19.65	6.35	10.25	12.7	18	6	5.5	6.1	7.3
	P4(cm)	6.2	9.8	11	18.45	5.55	8.85	10.4	16.45	3.65	3	2.85	3
	P5(cm)	6.55	10.2	11.4	19.2	6.3	10.05	12.9	18.75	5.95	6.3	7.1	9.25
	P6(cm)	6	9.8	10.9	18.6	5.75	9.6	12.5	18.45	5.75	6	6.85	8.95

Diameter Ratio: 0.5, With Polymers													
Reynolds No.		**2383**	**2979**	**3177**	**3972**	**4369**	**5362**	**5957**	**6951**	**7944**	**8937**	**10128**	**11915**
Polymer ppm		**196**	**158**	**148**	**119**	**108**	**89**	**80**	**68**	**60**	**53**	**47**	**40**
Single orifice	P1(cm)	12	8.9	9.6	15.7	9.4	12	15.5	17.3	19.9	25.5	31.7	42
	P2(cm)	10.5	6.9	7.3	12.1	5.1	5.5	6.8	5.8	4.1	5	4.3	5.7
	P3(cm)	10.7	7.3	7.65	12.5	5.8	6.5	8.5	7.6	7	8.8	9.9	13.7
	P4(cm)	10.3	6.9	7.4	12.4	5.65	6.2	8.2	8	8	10.2	11.7	15.9
Double orifice (1D)	P1(cm)	6.9	11.5	13.4	9	8.8	10.5	11.7	14.4	17	19.9	26.4	38.1
	P2(cm)	5.55	9.7	11.4	5.6	4.7	5	4.5	4.4	3.5	3	3.7	5.3
	P3(cm)	5.65	10	11.8	6	5.35	5.7	5.9	6.1	6	6.3	8	11.9
	P4(cm)	5.35	9.7	11.4	5.9	5.3	5.5	5.7	5.9	5.9	6.2	7.9	12.1
Double orifice (2D)	P1(cm)	12.4	19.45	10.25	16.5	18.8	16.2	19.7	18.9	21.9	27.2	34.9	48.1
	P2(cm)	11.3	17.4	7.9	12.6	14.3	9.9	11.7	6.8	6.1	6.9	8.4	11.1
	P3(cm)	11.5	17.5	8.2	12.7	14.45	10	11.9	6.9	6.2	6.8	8.3	11
	P4(cm)	10.7	16.9	7.3	11.7	13.6	9.2	10.6	4.7	3.5	3.4	2.9	3.1
	P5(cm)	11.1	17.3	7.75	12.5	14.2	9.8	12.3	7	6.6	7	7.7	10.9
	P6(cm)	10.8	17.1	7.5	12.4	14.1	9.6	12.1	6.8	6.5	6.8	7.5	10.8

TWO-PHASE PRESSURE DROP READINGS

Diameter Ratio: 0.63, Without Polymers				
Air Re		**260**	**516**	**1032**
Water Re		**11121**	**9135**	**8340**
Single orifice	P1(cm)	22	22	26
	P2(cm)	7	6	9.75
	P3(cm)	11.42	9	11
	P4(cm)	11	8	9
Double orifice (1D)	P1(cm)	24	22	25
	P2(cm)	11.13	9.75	12
	P3(cm)	14	11.5	12.75
	P4(cm)	13.5	10	11
Double orifice (2D)	P1(cm)	26.25	23	26.63
	P2(cm)	12	8	12
	P3(cm)	15.75	11	14
	P4(cm)	10	6	8
	P5(cm)	12.25	10.5	12.25
	P6(cm)	12	9	11

Diameter Ratio: 0.63, With Polymers				
Air Re		**260**	**516**	**1032**
Water Re		**10723**	**8738**	**7944**
PPM		**44**	**53**	**58**
Single orifice	P1(cm)	21	23	26
	P2(cm)	7	7.5	11
	P3(cm)	11.5	10.5	12
	P4(cm)	11	10	10
Double orifice (1D)	P1(cm)	23	22	25.5
	P2(cm)	10.5	10.5	13
	P3(cm)	14	12	14
	P4(cm)	13	11	12.75
Double orifice (2D)	P1(cm)	27	24	26.5
	P2(cm)	13	10	13
	P3(cm)	17.75	14	14.5
	P4(cm)	12	9	9
	P5(cm)	14	12.5	13
	P6(cm)	13.5	11.5	12

VITAE

Name : Baqir Muhammad

Nationality : Pakistani

Date of Birth : 05-Nov-1991

Email : baqirmalik_5@yahoo.com

Address : Rawalpindi, Pakistan.

ACADEMIC BACKGROUND

University of Engineering and Technology, Taxila, Pakistan.
Bachelors of Science in Mechanical Engineering. 2013

RESEARCH

Technology landscaping of a Robot for in-service corrosion coupon Installation and Retrieval
Investigation of argon purging time for welding stainless steel pipes.
Drag Reduction and Heat Transfer in Drag Reducing Polymeric Solutions

PUBLICATIONS

M. Baqir, A.Z. Khan, “Spatial Comparative Analysis of Parabolic Trough Collectors and Photovoltaic Systems in Saudi Arabia”, World Journal of Engineering (Under Review)

MEMBERSHIPS

Registered Engineer with Pakistan Engineering Council

COMPUTER SKILLS

Microsoft Office Suite, AUTOCAD, MATLAB, ANSYS